A METHOD FOR MEASURING HUMAN FOOT SHAPE DURING RUNNING STANCE

by

Robert Blenkinsopp

A Doctoral Thesis

Submitted in partial fulfilment of the requirements for the award of
Doctor of Philosophy of Loughborough University.

March 2015

CERTIFICATE OF ORIGINALITY

This is to certify that I am responsible for the work submitted in this thesis, that the original work is my own except as specified in acknowledgements or in footnotes and neither the thesis nor the original work contained therein has been submitted to this or any institution for a degree.

Signed ……………………………………………………………………

Date ……………………………………………………………………

Abstract

Knowledge of the three dimensional shape of the human foot is important in the design of shoes to facilitate correct fit. Currently only the static shape of the foot is considered despite the fact that the foot undergoes changes in its shape, particularly in athletic pursuits, due to associated movements and loadings. Attempts, presented in research, have been made to measure dynamic foot shape. However, to date, measurements have been limited in detail as well as restricted to walking gait, as a result of the method. The work of this thesis aimed to develop a methodology that would be capable of measuring the three dimensional shape of the human foot during the stance phase of gait, in locomotion speeds associated with running.

A novel method has been developed that employs digital image correlation (DIC): a non-contact, passive, optical measurement technology that is capable of measuring the three dimensional shape of a surface as it moves, using photogrammetric principles. The DIC technology is also able to associate shape measurements made between discrete stages and therefore allow deformation measurements to be derived, both for the surface and measurements derived from it. A validation of GOM ARAMIS, the preferred system in which the technology was embodied, was conducted, which included the calibration of both shape and surface deformation measurements, the latter via a methodology incorporating novel material measures. Shape measurements from an individual system were calibrated to within ±0.1mm and to within ±0.5%strain for surface deformations.

The dynamic shape measurement method employed six camera pair systems to enable all foot surfaces to be imaged throughout stance and therefore allow measurements of the full foot to be made, using DIC. As part of the methodology development, alignment of individual measurements to form a single composite measurement, the referencing of measurements and the interpolation of gaps in surface measurements has been addressed. The developed method also incorporates the capability to measure kinematics without the need for additional hardware by using the same images captured for DIC and measures kinetics via an instrumented force platform.

Measurement results were presented for multiple measurements of a single subject based on a set of metrics defined to characterise foot shape, which included absolute and relative cross sectional areas, perimeters, volumes and surface deformations. A set of base measurements: surfaces and kinematic point's positions, of two additional subjects were also conducted in an attempt to demonstrate the methodology beyond a single subject.

An investigation into the repeatability and reproducibility of measurements derived using the methodology was carried out to assess the influence of particular process variables on measurement variations within and between test sessions. Tests were conducted using the same raw image data to remove the subject

variability from the analysis. In measurement repeatability assessment, only the surface interpolation variable would vary between tests, as all other process variables remained constant meaning only shape measurements were affected, in which extremely low variations were found (CV<0.1%). In reproducibility the greatest contribution to measurement variation was made by the marker placement and reference variables with the cumulative effect of shape and kinematics found to be within ±8% (CV) and ±2.5° respectively.

The method created in this research greatly improves the capabilities for the measurement of foot shape during gait, particularly where locomotion velocity exceeds that associated with walking. The methodology has the potential to be applied in a number of research areas related to the measurement of dynamic foot morphology and understanding the change in foot shape during the stance phase of gait. Furthermore, the capability for the measurement of kinetics and kinematics concurrently to dynamic shape measurements also allows the potential for wider applications in understanding the drivers for human foot shape change and potential relationships to injury.

A novel method for calibrating digital image correlation measurements for large deformations has also been developed as part of the work of this research work.

Publication Arising from this Work

Blenkinsopp, R, Harland, A, Price, D, Lucas, T, Roberts, J. (2012): "A Method to Measure Dynamic Dorsal Foot Surface Shape and Deformation During Linear Running Using Digital Image Correlation". Procedia Eng Vol. 34 Pg 266-271.

Acknowledgements

"Today is the greatest day of my life…

….I woke up".

Maurice H Fallon, Grandad.

Contents

1. Introduction

Along with apparel and equipment, athletic footwear is one of the three dominant segments within the sporting goods market. In 2010, in the USA, athletic footwear made up $12.6 billion of the total market value of $74 billion (SGMA, 2011). In an industry that is predicted to grow globally to $266 billion by 2017 (Lucintel, 2012), footwear products are integral to a sports business and hence there is competition in footwear innovation between the leading sports brands each vying for a larger market share.

When partaking in different sports the user requirements for the shoe will change, resulting in a need for different shoes both within and between sports. This has been exploited by sports goods manufacturers who often offer a varied range of shoe types based on different sports and the associated customer requirements for each. Despite the multiple different shoe types available, the overarching manufacturing process involved in creating a shoe remains relatively consistent.

A key component in the manufacture of any shoe is the shoe last, an object that acts as a basic foot shape around which material components are constructed to create the shoe. The last is fundamental to the manufacture of the shoe as its shape will influence not only the overall style and design of the shoe but also fit and comfort (A. Luximon & Luximon, 2009). Although the three dimensional shape of a shoe last does not typically resemble the human foot, lasts are still informed by human foot shape; namely length and girth measurements, which in a mass manufacturing scenario, will be aimed at creating a foot shape representative of the population or (more likely) target consumer. Historically, the measurement of human foot shape has been conducted manually. However, in more recent years the advent and development of scanning technology has enabled similar measurements to be measured automatically in addition to allowing more detailed foot shape measurements to be made, to inform last design.

The measurement of human foot shape and associated methods for shape measurement have to date, been almost exclusively performed when the foot is stationary. However, the foot is a complex structure, which changes shape during the movements and loadings associated with human locomotion. This is particularly prevalent in sporting activities such as running where the foot can experience multi-axial loads of multiple body weights during stance (Cavanagh & Lafortune, 1980).

Studies have shown that improper fitting of shoes can be related to foot problems (Milner, 2010), yet, at present, only static shape is considered in the design of both shoes and lasts. Consideration of the dynamic foot shape has the potential to inform shoe and last design to improve the function and fit of shoes, especially in sporting activities, where changes in the foot shape are likely to be at their greatest. Dynamic foot shape methods to date, due to the infancy of the field, are extremely limited in the measurement

capabilities and the locomotion speeds that can be accommodated. A method has yet to be fully developed that enables measurement of the human foot shape during running. Once this has been established the analysis can be developed and implementation of the dynamic foot shape measurements can be taken up.

1.1. Objectives

The aim of this research therefore was to develop a methodology that is capable of measuring the shape of the human foot at multiple stages throughout the stance phase of running. The objectives required to achieve this aim were as follows:

OBJ_1 - Understand the function of the foot, how it moves during the stance phase of gait and the causes of change in foot shape.

OBJ_2 - Identify existing methods and technologies for measurement of human body morphology, for the foot in particular.

OBJ_3 - Establish the measurement requirements of the methodology.

OBJ_4 - Select an appropriate technology to make dynamic foot shape measurements.

OBJ_5 - Validate a measurement system in which the selected technology is embodied.

OBJ_6 - Understand how measurements are affected by changing measurement system parameters.

OBJ_7 - Develop a method to measure full foot shape surfaces and associated measurements outlined in the methodology requirements.

OBJ_8 - Demonstrate the developed methodology for foot shape and associated measurements.

OBJ_9 - Understand the repeatability and reproducibility of the developed measurement methodology.

1.2. Thesis Overview

This thesis documents the development of a methodology for the measurement of human foot shape during running stance. Following this introductory chapter, Chapter 2 gives an introduction to the topics relevant to the research carried out. It outlines the relevant human anatomy involved in human locomotion, as well as the measurement of the human running gait through kinematics and kinetics. Existing research conducted in the measurement of human body shape with an emphasis on human foot shape is reviewed.

Chapter 3 describes the measurement methodology requirements before Chapter 4 outlines the identification and selection of a measurement technology from which a method can be developed for measurement of human foot shape. An overview of the principles for the selected technology is outlined as well as the measurement system used within the developed method. A validation of the measurement system for use within a method is carried out and the areas for further investigation identified.

Chapter 5 reports the calibration of shape and surface deformation measurements using the selected measurement system to establish measurement accuracy. This includes the development of material measures for shape and surface deformation as well as an investigation into the effect of user controlled components of the methodology on measurement accuracy.

Chapter 6 reports the development of the methodology for measurement of foot shape during running stance. It outlines the data capture and data analysis stages required to create a virtual foot shape, which can then be analysed appropriately. The concurrent measurement of kinematics and kinetics as part of the methodology is also presented and associated steps to achieve a measurement discussed. Potential measurement capabilities of the method are also discussed.

Chapter 7 demonstrates the application of the developed methodology, presenting shape, kinetic and kinematic results for multiple trials of a subject. An overview of measurements from different subjects is also presented.

Chapter 8 details the results from an investigation into the repeatability and reproducibility of the developed measurement methodology and establishes the effect of particular methodological variables on shape, surface deformation and biomechanical measurements.

Chapter 9 provides conclusions to the work presented in this thesis, reviewing whether research aims and objectives have been met, as well as discussing the novelty and implications of the work. This is followed by a discussion into the potential future work following this research.

2. Literature Review

The review of the current literature attempted to address OBJ_1 and OBJ_2 outlined in §1.1. The purpose of the review was to provide a knowledge base for research activities as well as outlining the current work in the measurement of dynamic body morphology that would assist in directing research activities and ensuring novelty.

2.1. The Functional Anatomy of the Foot and Ankle

In attempting to devise a method for measuring the dynamic shape of the foot, it was necessary to understand the basic anatomy that forms the three dimensional foot shape. This has been approached firstly by outlining the anatomical components: bones and muscles followed by the structures and joints formed within the foot, which govern its movement. As most of the information presented in this section is widely accepted within the academic community, the purpose is not to perform a critical review, but to instead provide a knowledge base for the research work that will be conducted.

2.1.1. Bones of the Human Foot

The foot is an integral mechanical component of the lower extremity necessary for smooth and stable gait (Sammarco *et al.*, 2001). It serves two functions: support and propulsion (Floyd, 2006). The foot is a highly complex structure comprised of 26 bones, which collectively form an arch shape. In addition, there are numerous intrinsic muscles and more than 100 ligaments. As a result of its unique qualities the foot can be rigid or flexible, allowing it to be adjusted to different ground conditions or varying speeds of locomotion, in addition to acting as a structurally supporting platform to attenuate repetitive loads of multiples of body weight in magnitude resulting from ground contact (Hamill, 2003; Sammarco *et al.*, 2001). The bones of the foot and lower leg that articulate to form the ankle and foot joints that will be discussed in the following sections are depicted in Figure 2-1.

2.1.2. Muscles of the Foot and Ankle

There are 23 muscles acting on the ankle and the foot, 12 originating outside the foot and 11 inside. The intrinsic muscles of the foot follow the primitive limb pattern of dorsal extensors and plantar flexors (Gray, 2004). They can be grouped into four layers and are responsible for either moving the toes or for supporting the arches of the foot (Van de Graaf, 1998). The extrinsic muscles of the ankle and foot can generally be grouped according to location and function; plantar flexors in the posterior, dorsal flexors in the anterior with evertors and invertors located laterally and medially respectably (Floyd, 2006).
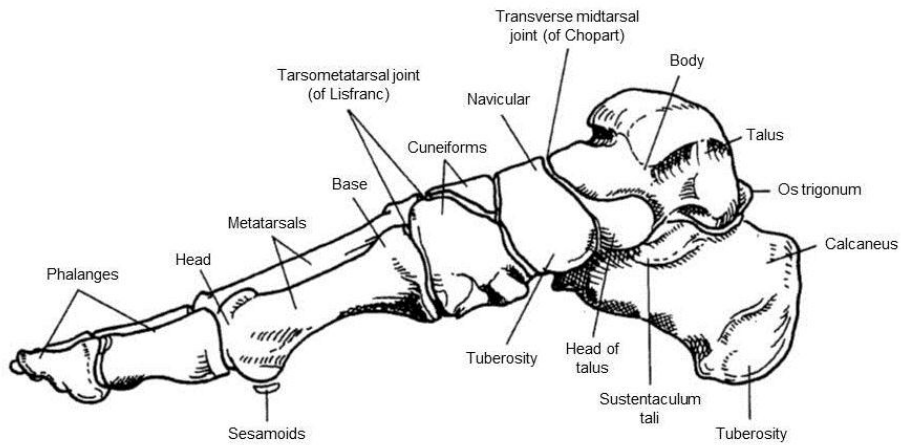
MEDIAL VIEW
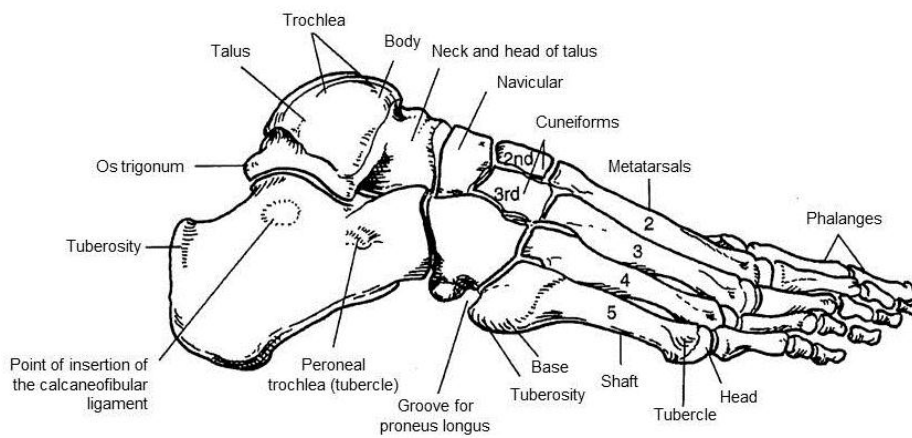
LATERAL VIEW
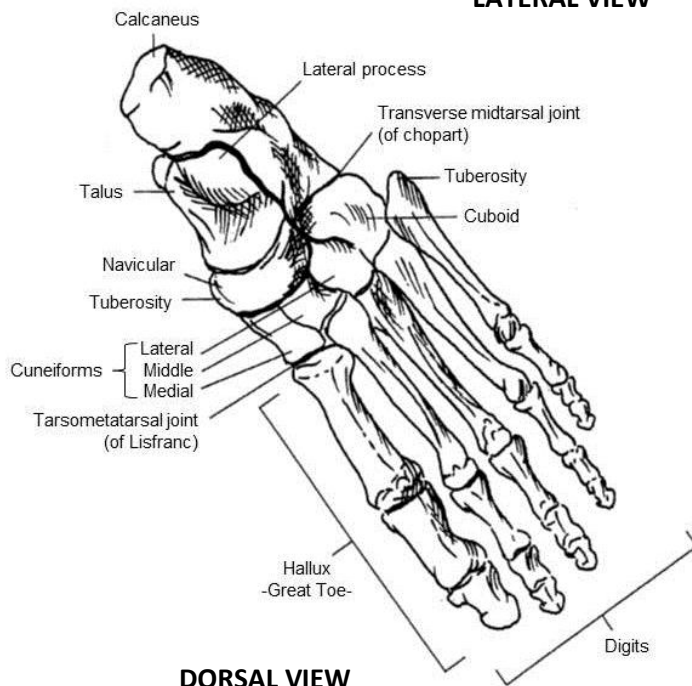
DORSAL VIEW
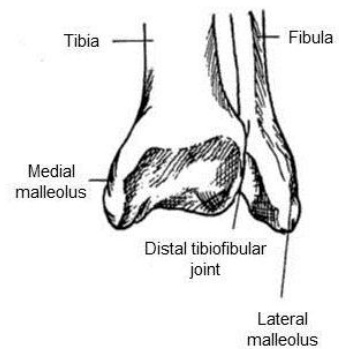
TIBIOFIBULAR ARTICULATION

Figure 2-1 – Medial, Lateral and Dorsal views of the foot and ankle bones (Sammarco & Hockenbury, 2001)

The posterior compartment is divided into deep and superficial compartments. The superficial compartment includes the plantaris and the gastrocnemius and soleus, the latter two collectively known as the triceps surae, more commonly known as the calf muscle (Floyd, 2006). The deep compartment consists of four muscles: the flexor hallucis longus, flexor digitorum longus, tibalis posterior and the popliteus. The former three contribute to plantar flexion and inversion and the latter to plantar flexion only (Floyd, 2006). Those muscles located on the anterior aspect are dorsal flexors consisting of the tibalis anterior, peroneus tertius, extensor digitorum longus and extensor hallucis longus.

2.1.3. Arches of the Foot

The tarsals and metatarsals of the foot form three arches, shown in Figure 2-2, two running longitudinally and one running transversely across the foot. These arches are not rigid, instead yielding under loading and spring back when the load is removed (Van de Graaf & Fox, 1995).

The lateral longitudinal arch is formed by the calcaneus, cuboid and fourth and fifth metatarsals. This arch can play a support role by bearing some of the weight during locomotion as it is lower than the medial arch and can make contact with the ground (Hamill & Knutzen, 2003).

The medial longitudinal arch is located on the medial side of the foot extending from the calcaneus bone to the talus, the navicular, the three cuneiforms and the distal ends of the three medial metatarsals. It is much more flexible and mobile than the lateral arch, playing a significant role in shock absorption; although very adjustable it does not make contact with the ground in normal feet, however, it does elongate rapidly after initial heel contact through to full foot contact with the ground (Hamill & Knutzen, 2003).
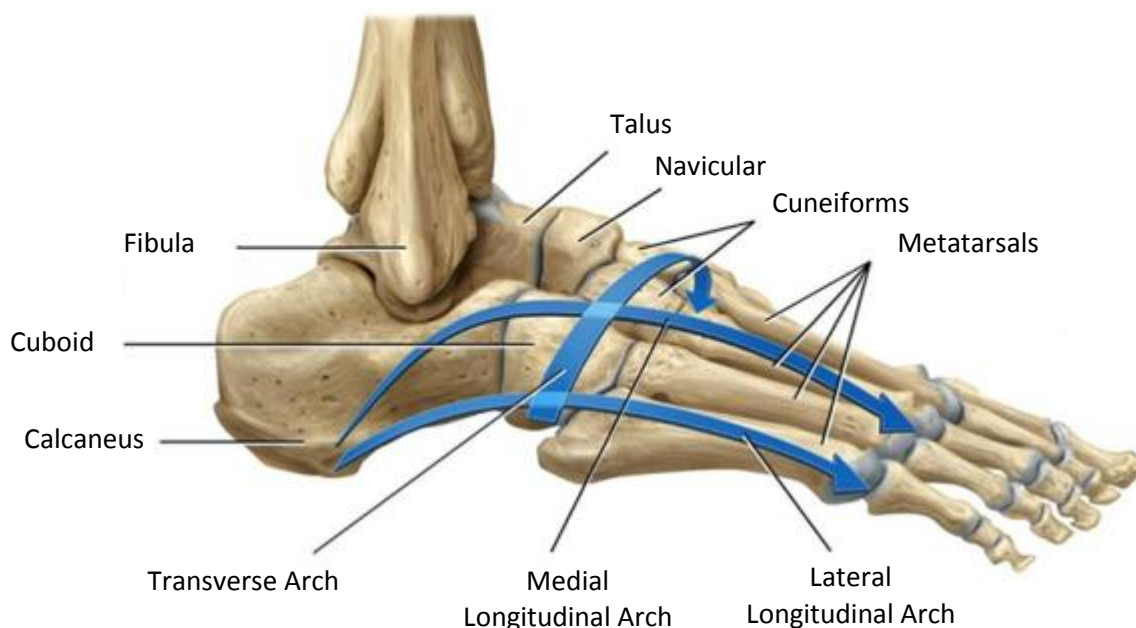
Figure 2-2 - Lateral View of Longitudinal and Transverse Foot Arches

2.1.4. Joints of the Foot and Ankle

The motion of the foot occurs on three cardinal planes and axes. As shown in Figure 2-3 plantarflexion and dorsiflexion occur in the sagittal plane, abduction and adduction occur in the transverse plane and inversion and eversion occur in the frontal plane.
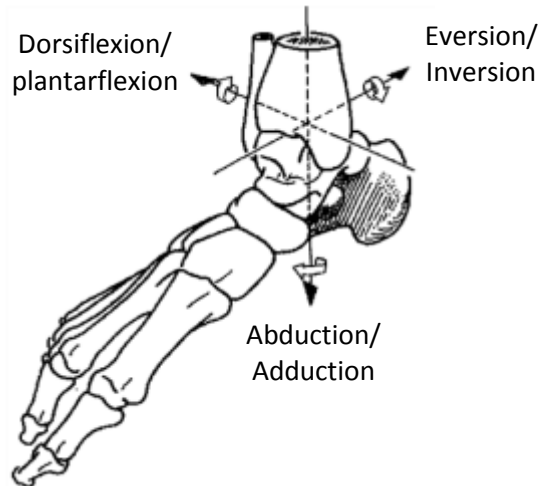
Figure 2-3 - Axes of Motion in the Foot and Ankle (Adapted from: Sammarco et al. (2001))

2.1.4.1. The Ankle Joint

The lower leg, comprised of the tibia and fibula bones, connects the foot with the rest of the body. The ankle joint, technically known as the talocrural joint, is the proximal joint of the foot made by the articulation of the talus in the rearfoot and the distal tibia and distal fibula. In clinical interpretations the ankle axis are often detailed, including separate axis for plantarflexion and dorsiflexion (Hicks, 1953). However it is extremely difficult to determine the ankle joint axes around which the actual rotation movements occur (Nigg & Hintermann, 2002; Van den bogert et al, 1994), consequently the ankle joint is commonly approximated as a hinge joint, with a transverse axis of rotation normal to the sagittal plane, passing through the centre of the lateral malleolus at the distal fibula, as demonstrated by Scott and Winter (1991).

The ankle joint allows approximately 50° of plantar flexion and between 15° and 20° of dorsiflexion from the neutral axis (Floyd, 2006). An improved range of dorsiflexion is enabled during knee flexion as a result of reduced tension in the biarticular gastrocnemius muscle (calf muscle), located behind the tibia and fibula.

2.1.4.2. The Subtalar Joint

Moving distally from the talocrural joint is the subtalar joint (STJ), also known as the talocalcaneal joint, consisting of the articulation between the talus and the calcaneus bones, the two largest weight bearing bones in the foot that form the hind foot. The articulation of the two bones occurs at three sites: anteriorly,

posteriorly and medially as a result of the concave surface of the talus and the convex surface of the calcaneus (Dugan & Bhat, 2005).

The axis of the subtalar joint runs through the sagittal, frontal and transverse planes of the foot, approximately 42° from the horizontal in the sagittal plane and approximately 16° from the midline of the foot (Manter, 1941), which enables complex tri-planar motions to occur (Dugan & Bhat, 2005), limited by the ligaments supporting the talus (Hamill & Knutzen, 2003). These tri-planar movements at the subtalar joint are called pronation and supination, however confusingly they can also be referred to clinically as subtalar inversion and eversion (Sammarco & Hockenbury, 2001).

Pronation is a combination of eversion, dorsiflexion and abduction while supination is a combination of plantarflexion, inversion and adduction (Hamill *et al.*, 2003) occurring in the sagittal, transverse and frontal planes respectively. One must be careful in the proper use of the terms "pronation" and "supination" as they are a combination of movements within the three cardinal body planes and are often used wrongly to represent "eversion" and "inversion" respectively (B. Nigg & Hintermann, 2002).

The primary function of the subtalar joint is to absorb the rotation of the lower extremity during the support phase of gait (Hamill & Knutzen, 2003) this is achieved by transforming tibial rotation into forefoot pronation and supination (Sammarco & Hockenbury, 2001). This is enabled by the oblique axis of the joint, working as a mitred hinge arrangement (Mann, 1993), transforming internal lower extremity rotation into forefoot pronation at ground contact, so that the forefoot is flexible to absorb shock and uneven ground surfaces, and external rotation into forefoot supination so the foot is a rigid lever for propulsion.
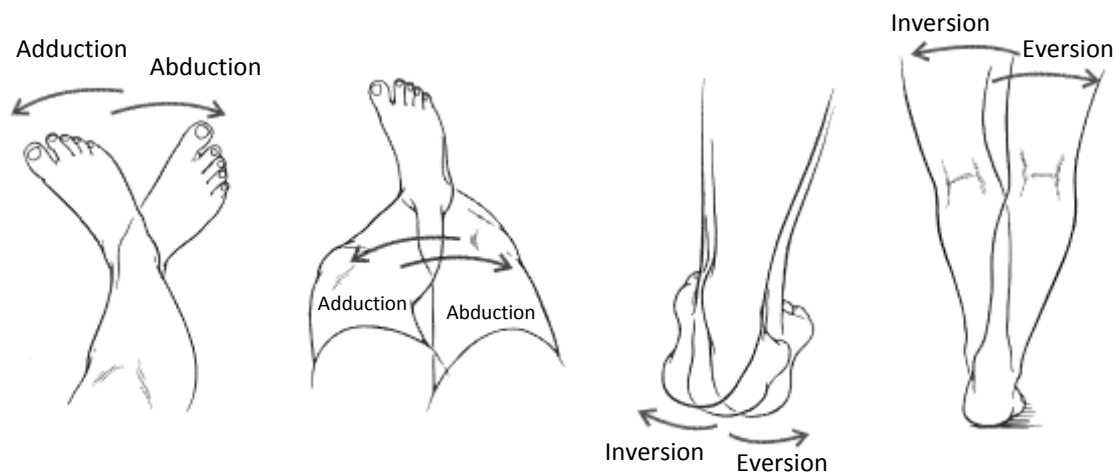
Figure 2-4 - Subtalar Movement Differences in the Open and Closed Chain System, (Adapted From Hamill and Knutzen (2003).

When the foot is off the ground it is moving on a fixed tibia and the subtalar movement to create pronation is produced by calcaneal eversion, abduction and dorsiflexion in the open chain (Scott & Winter, 1991) and

supination is created by a combination of calcaneal inversion, adduction and plantarflexion. In a weight bearing closed system, much of the pronation and supination is produced by the weight of the body acting on the talus (Hamill & Knutzen, 2003) hence, due to the constraining of the calcaneus, the talus moves on the calcaneus instead of the reverse, as observed in an open chain system. An illustration of the differences between subtalar movements in open and closed chain systems are shown in Figure 2-4.

The movement of the calcaneus has been found to be consistent regardless of whether it is weight bearing or not (Hamill & Knutzen, 2003) thus making calcaneus inversion and eversion measurements the most useful in determining subtalar motion. Measuring calcaneus eversion through measurement of rearfoot eversion is assumed to be an accurate predictor of pronation and supination (Ferrandis *et al.*, 1994).

2.1.4.3.   Transverse Tarsal Joints

The transverse tarsal joint, also known as the midtarsal joint and often referred to as Chopart's joint, consists of two joints: on the lateral side of the foot, the calcaneocuboid joint, consisting of the articulation between the calcaneus and the cuboid bone, and the talonavicular joint on the medial side consisting of the articulation between the talus and navicular bone.

Inversion and eversion occur along the longitudinal axis of the joint (Manter, 1941), the combination with the subtalar and the midtarsal joint allow approximately 20-30° of inversion and 5-15° of eversion (Floyd, 2006; Sammarco & Hockenbury, 2001).

The interrelation of the transverse tarsal joints and the subtalar joint produce either foot flexibility during pronation or foot rigidity during supination (Elftman, 1960). Flexibility is achieved as a result of the major axis of the two joints being parallel, 'unlocking' the forefoot joints (James *et al.*, 1978) during midstance after which the joint's major axis are convergent 'locking' the forefoot joints creating rigidity during propulsion.

2.1.4.4.   Tarsometatarsal Joints

The tarsometatarsal joints are the joints between the three cuneiform bones and cuboid and the five metatarsal bones, collectively known as the Lisfranc's joint. Although these joints produce little motion (Sammarco & Hockenbury, 2001), the lateral side does allow more movement than the medial side, as shown in an 'in vitro' study by Ouzonian and Shereff (1989) to determine midfoot motion, this allows varied load distribution between the metatarsal heads of the forefoot (Kapanji, 1970) during standing and locomotion.

2.1.4.5.   Forefoot Joints

The forefoot is comprised of the metatarsals and the phalanges, which function to maintain the transverse metatarsal arch, the medial longitudinal arch and the flexibility in the first metatarsal (Hamill & Knutzen,

2003). The phalanges join the metatarsal to form the metatarsophalangeal joints (MPJ), classified as condyloid-type joints (Floyd, 2006). Each toe in the forefoot has three phalanges, except the great toe (or hallux) which has two; the joints between the phalanges distal from the MPJ are called the interphalangeal joints. In the hallux there is one interphalangeal joint, whereas two exist, proximal and distal, in the lesser four toes.

According to Floyd (2006) at the great toe, in the MPJ, there is approximately 45° of flexion and 70° of extension in the sagittal plane with the interphalangeal joint capable of flexing from 0° of full extension to 90° of flexion. The MPJ of the lesser four toes allow approximately 40° of flexion and 40° of extension, the proximal interphalangeal joints in the lesser toes flex from 0° of extension to 35° of flexion and the distal interphalangeal joints flex from 30° of extension to 60° of flexion (Floyd, 2006).

2.2. Biomechanics of Human Locomotion

The shape of the foot is determined by the alignment of the underlying anatomical structures which are continuously altered by the foot's movement during locomotion as external forces associated with stance act upon the foot. Having outlined the underlying anatomy of the human foot, the structures and joints created and the independent movement capabilities of those joints, it was necessary to establish how the foot moves as a whole system during the stance phase of gait to facilitate support and propulsion. It was also necessary to understand the external loadings experienced during those movements, which would contribute to the foot's morphology and its change in shape during stance. From a basic viewpoint, aspiring to measure something as it moves, also meant that it was necessary to understand what that movement would be, to inform future methodology development.

2.2.1. The Human Gait

Bipedal locomotion, generally referred to as gait, is a functional task requiring complex interactions and coordination of major joints in the lower extremity of the human body. Gait is a cyclic activity which can be decomposed into two phases: a stance phase and a swing phase, the purpose of which is to efficiently translate the body's centre of mass in the overall direction of locomotion (Novacheck, 1998; Barr *et al.*, 2001). A full gait cycle can be defined by the occurrence of a specific gait event by one limb through to the same event, occurring once the limb has passed through the two phases of gait; stance and swing. Figure 2-5 shows a schematic of the sequence of the walking gait cycle.

IC: Initial contact, LR: Loading response, MST: Midstance, TST: Terminal Stance, PS: Preswing,

ISW: Initial Swing, MSW: Midswing, TSW: Terminal Swing
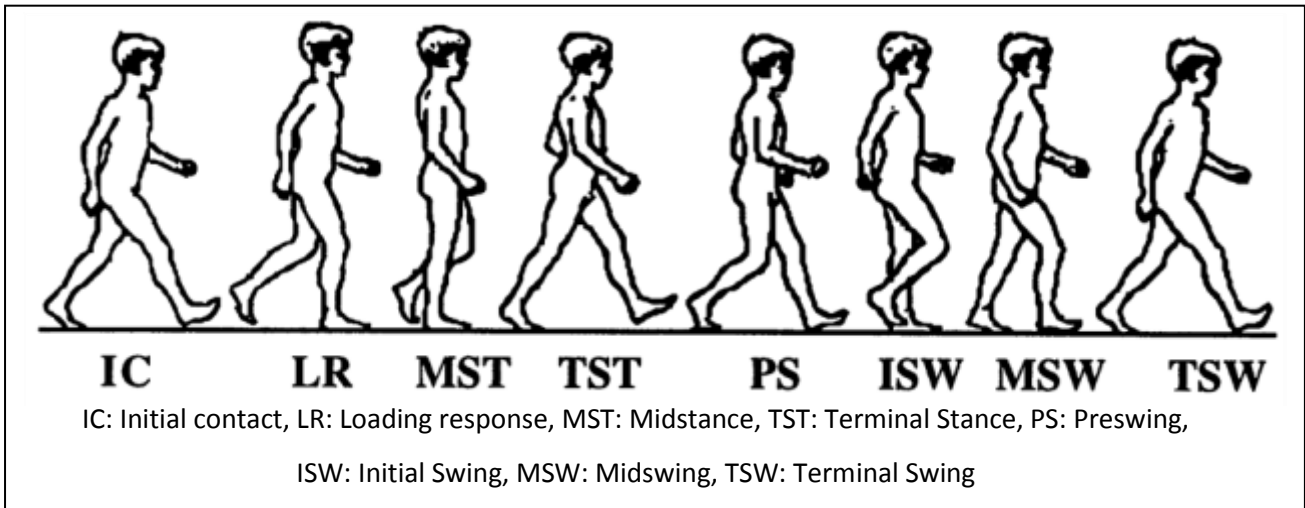
Figure 2-5 - The Walking Gait Cycle (Novacheck, 1998)

As outlined in Figure 2-5, the two phases of gait can be further broken down into further sub phases. Stance can be decomposed to six events or periods (Barr *et al.*, 2001): initial contact; the foot comes into contact with the ground, loading response; the sole of the foot comes into contact with the floor and the weight of the body is accepted onto the supporting limb, midstance; the period during which the tibia rotates over the stationary foot in direction of locomotion, terminal stance; period during which the weight of the body is transferred from the hind and midfoot regions onto the forefoot, pre-swing; during which a rapid unloading of the limb takes place - in walking this weight is transferred to the contralateral limb, and finally toe off; the point at which the foot breaks contact with the ground, demarcating the beginning of the swing phase. The swing phase is separated into three sub phases (Barr *et al.*, 2001); initial swing, midswing and terminal swing, also depicted in Figure 2-5.

2.2.1.1. Walking Gait

During walking, the stance phase is sufficiently long enough temporally, that it exceeds 50% of the entire gait cycle. As a result there are periods during which both feet are in contact with the ground, generally referred to as double limb support, occurring twice during the cycle: at the beginning and the end of the stance phase.

Figure 2-6 depicts the temporal sequence of walking gait; the shaded coloured regions indicate the periods in which the corresponding foot is in contact with the ground, overlapping white regions show the periods of double limb support.
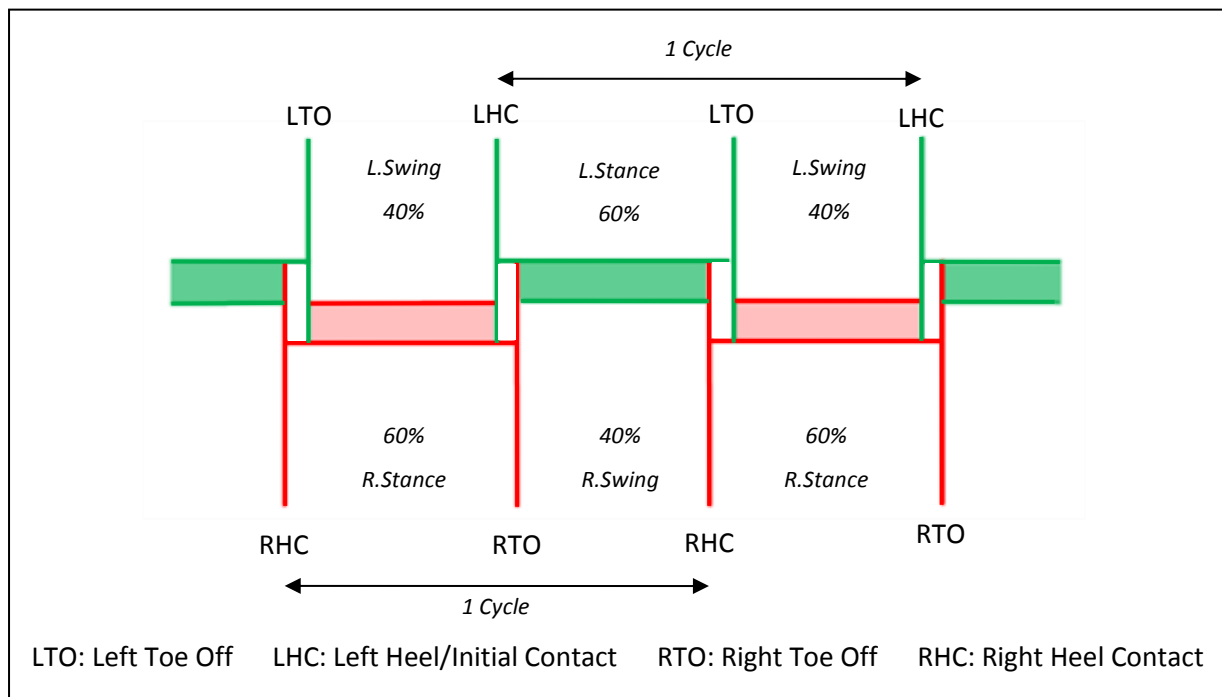
Figure 2-6 - Schematic Diagram Showing Temporal Sequence of Walking Gait, Right Foot (Red), Left Foot (Green) (Adapted From Barr and Backus (2001))

2.2.1.2. Running Gait

In running, the stance phase is shorter and hence does not exceed 50% of the gait cycle, the result is that there are no periods of double limb support, instead there are periods when neither foot is in contact with the ground. This is referred to as double float, occurring twice in the cycle, at the beginning and at the end of the swing phase.

Figure 2-7 depicts the temporal sequence of running gait highlighting the regions of double float. The transition from walking to running locomotion is characterised by the change from double limb support to double float.

As locomotion speed increases; the gait cycle time shortens, the amount of time spent in the stance phase of gait decreases, the time spent in swing increases and the time of double float lengthens (Dugan & Bhat, 2005; Novacheck, 1998). Running is considered to be a gait speed exceeding approximately 3.3 m·s^{-1} (Sammarco & Hockenbury, 2001). At submaximal running velocities, generally speaking there are three types of 'running style' based on the strike pattern of the foot during the stance phase of gait: rearfoot, forefoot and midfoot. According to Lieberman (2012), in rearfoot running, the heel impacts with the ground first, whereas in forefoot running the foot first impacts in the metatarsophalangeal joint (MPJ) region also referred to as the 'ball of the foot'. In midfoot running, the ball of the foot and the heel impact simultaneously. These definitions can be applied by observing the foot impact in an appropriate manner, usually high speed video footage. There are other methods of classifying foot strike, for example using

centre of pressure (COP) at initial impact relative to shoe length (Cavanagh & Lafortune, 1980), however it has been highlighted that the index proposed is arbitrary with respect to the foot's anatomy (Lieberman, 2012).
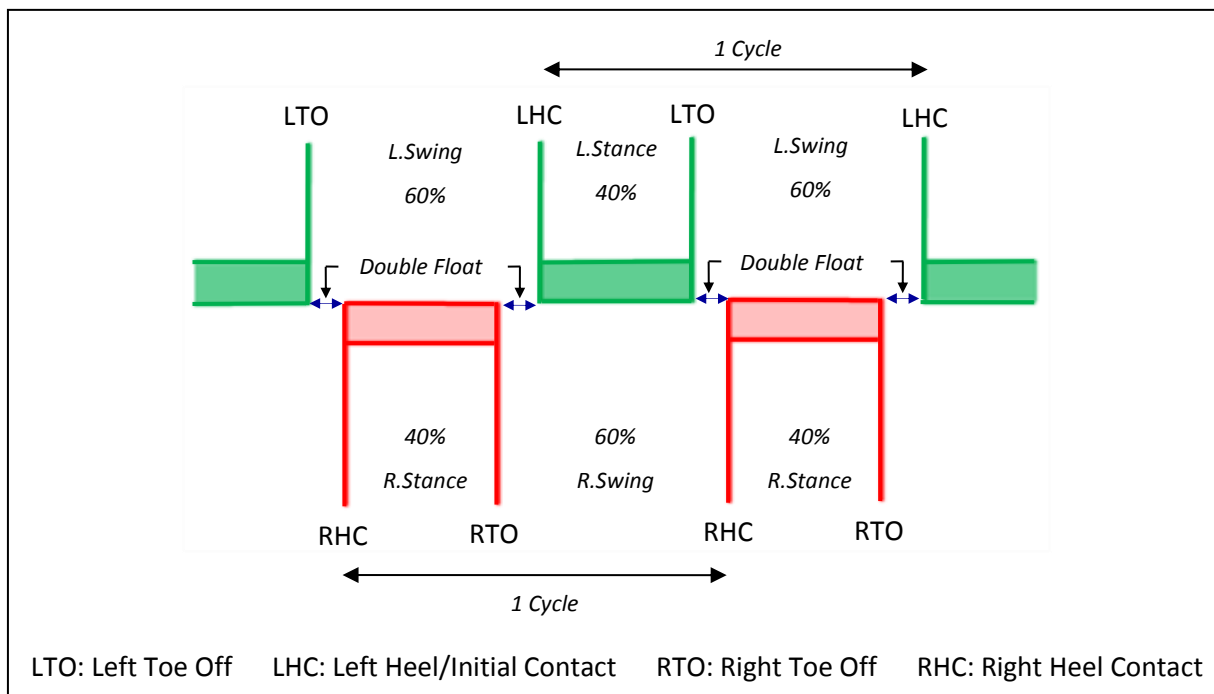
Figure 2-7 - Schematic Diagram Showing Temporal Sequence of Running Gait at 3.2m/s, Right Foot (Red), Left Foot (Green) (Adapted From Adapted From Barr And Backus, (2001)

Rearfoot running styles are generally associated with running in a shod condition, although midfoot and forefoot running styles are adopted, it is to a lesser extent (Hasegawa, Yamauchi, & Kraemew, 2007). Forefoot running styles are generally associated with running in a barefoot condition (without shoe/ with minimalist shoe).

2.2.2. Kinematics of Running

Kinematics is a branch of mechanics that attempts to describe the temporal and spatial components of motion of an object without consideration of the causes leading to the motion. Displacement, velocity and acceleration of body segments, whether absolute or relative are the principle measurements of interest within kinematics, although dependent on study, centre of mass of the body can also be of interest.

Running kinematics describe the way the whole, or parts, of the body move in space. In the lower extremity chain, movement of any component will influence every aspect within it; for example a certain foot position or movement will influence the position or movement at the knee or hip (Hamill & Knutzen, 2003), this effect has been linked to various injuries in the lower extremity within literature (Edington *et al.*, 1990).

Kinematic measurements can be used as a tool to enable the effect of particular variable interventions to be identified (K. Williams, 2000); they can also be used as a measure of repeatability or reproducibility.

2.2.2.1. Whole Body Kinematics

The distance and time between successive contacts of the same foot with the ground are known as stride length and stride time (Cavanagh, 1987), the inverse of the latter is often referred to as stride rate (K. Williams, 2000) or stride frequency (Cavanagh & Kram, 1990). One must be careful not to be confused with step time and step rate, which are measurements of successive contacts of opposite feet , which also links to cadence(defined as number of steps per unit time) (Dugan & Bhat, 2005).

Running velocity is the product of stride length and stride rate (K. Williams, 2000), so in order to run faster one must increase stride rate (or cadence) or increase the length of each stride. Stride length (Cavanagh & Kram, 1990; Luthanen & Komi, 1977) and stride rate (K. Williams, 2000) increase linearly over running speeds of between 2.5m·s^{-1} and 6 m·s^{-1}, however at faster speeds, (>8m·s^{-1}) the rate of increase of stride length reduces and begins to level off (Dillman, 1975).

2.2.2.2. Kinematics of the Foot and Ankle

Sagittal Plane Kinematics

Early kinematic research was limited due to methods and technologies available to measure three dimensional positions of markers placed on the human body. These methods were generally limited to 2D tracking of markers using high speed video footage and digitisation techniques. For this reason, the focus of lower extremity kinematic research was for measurements in the sagittal plane, as the greatest joint excursions occur in this anatomical plane during running. Studies focussing specifically on the foot and ankle considered the movements of the rearfoot in the frontal plane as these measurements were used to approximate foot pronation and supination motions.

Typical sagittal plane kinematics for the ankle joint, throughout a running cycle at four different speeds are presented in Figure 2-8, which show the variation in movement patterns as a result of runner velocity and can be used to describe the overall movement of the foot and ankle during running.

At foot impact, the foot is typically in a dorsiflexed position, after which a period of rapid plantarflexion is experienced, as a result of the torque produced at the heel at the initial contact (Snel *et al.*, 1985). After the rapid plantarflexion, there is then an extended period of dorsiflexion reaching a maximum at midstance followed by steady plantarflexion through to toe off, with a maximum attained shortly after toe off. Figure 2-8 shows that at faster running speeds the foot is plantarflexed at impact and hence, the ankle tends to enter the proceeding dorsiflexion phase straight away.
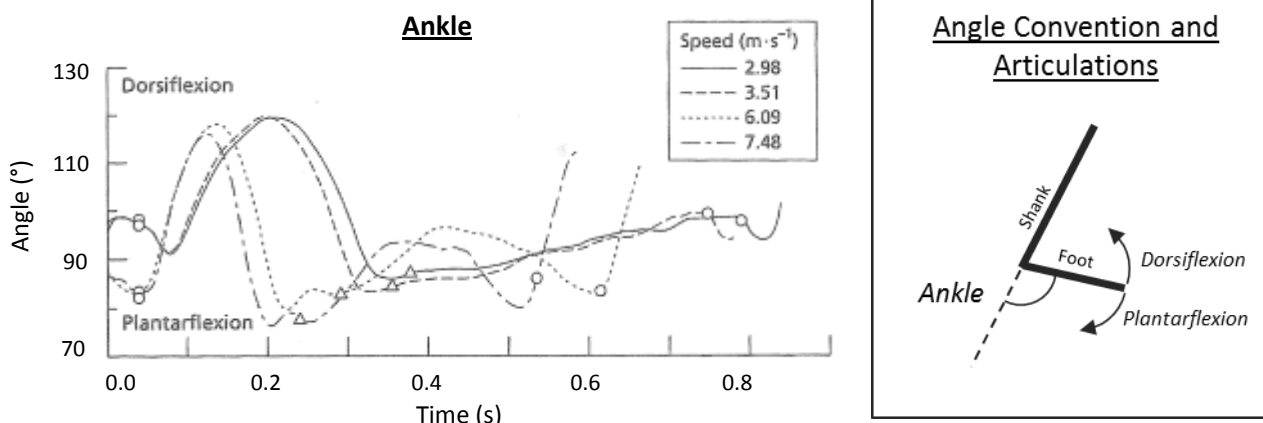
Figure 2-8 –Kinematics of the ankle joint in the sagittal plane at different running speeds (Adapted from Williams, 2000)

Taunton *et al.* (1985) measured 10° ankle dorsiflexion to the shank at foot contact in comparison to walking when the foot is in a 'neutral' position at approximately 90° to the shank. Generally, 20° to 25° of plantarflexion is used in running gait with approximately 10° of dorsiflexion required for efficient gait (Brown & Yavarsky, 1987; Hamill & Knutzen, 2003), however studies in running by Nilsson *et al.* (1985) and Williams (K. Williams, 1980) measured maximum dorsiflexion to be 17.5° and 25° respectively, whilst Mclay *et al.* measured 17.9°(±7°) plantarflexion and 19.4°(±7°) dorsiflexion in basketball players, showing how much dorsiflexion is in fact appears to be used.

Frontal Plane Kinematics

During the gait cycle at heel strike, the foot makes contact with the ground in a slightly supinated position after which the foot then begins to immediately pronate accompanying internal rotation of both the tibia and femur (Donatelli, 1987). Pronation continues for approximately 70% of the support phase, reaching a maximum at approximately 35-45% of the stance phase (Hamill *et al.*, 2003) which is approximately when the centre of gravity passes over the weight bearing foot (James *et al.*, 1978). Once the foot is flat in the stance phase the lower extremity begins to rotate externally, which is transmitted to the talus, as the foot is 'fixed' to the ground; this external rotation causes the foot to begin to supinate through to toe off.

A normal amount of pronation provides a means of decreasing peak forces by attenuation over a longer period of time (Hreljac *et al.*, 2000) however pronation must end before midstance to allow the foot to become rigid for push off (Subotnick, 1985). It has been speculated by a number of authors, in a number of studies and reviews, that excessive or compensatory pronation of the foot is a contributing factor to several common overuse injuries including: Achilles tendinitis, tibial stress syndrome (shin splints), plantar fasciitis, iliotibial band friction syndrome and patella femoral pain syndrome (PFPS). However, to date conclusive clinical and epidemiological evidence is yet to be presented in literature (Reinschmidt & Nigg, 2000).

Despite the inconclusive link, numerous research studies have attempted to measure the foot pronation and supination during running and the effects of particular interventions. Kinematic studies measuring the foot

and ankle kinematics specifically, commonly direct attention to measurement of calcaneal eversion and inversion in the frontal plane (transverse body plane). This measurement facilitates a reliable approximation of pronation and supination occurring at the subtalar joint (Clarke *et al.*, 1983) as it is the most independent component of the pronation/supination movement and the simplest to measure (Ferrandis *et al.*, 1994).

Pronation   **Neutral**   **Supination**
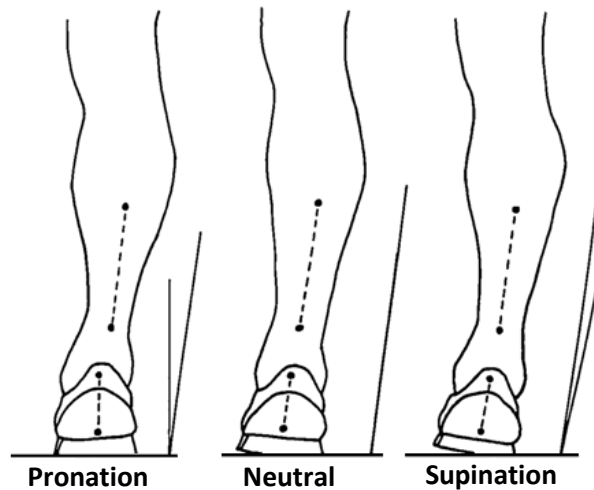
Figure 2-9 - Pronation and supination movements definitions from rearfoot angle measurements projected onto the frontal plane (adapted from Clarke et al 1983)

Early studies carried out employed 2D methods via imaging of the lower limb from a posterior view, with measurement of skin markers placed on the shank and rearfoot, as shown in Figure 2-9, projected onto the frontal plane to allow angular measurements to be made (Figure 2-10). The 2D method has been used by a number of authors to measure the effect of various interventions on pronation (Clarke *et al.*, 1983b; McNair & Marshall, 1994; B. Nigg et al., 1987; Perry et al., 1995). Care is advised in the interpretation of results, as the measurement is derived from point projections meaning 2D methods are susceptible to error, especially in the latter stages of stance when large out of plane rotations occur (Soutas-Little & Beavis, 1987).
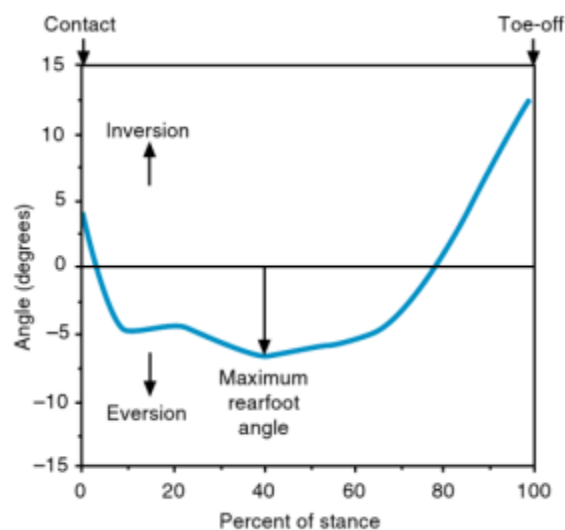
Figure 2-10 - Typical rearfoot angle curve during stance for heel toe running (from McGinnis (2005))

The error associated with 2D measurements, along with improvement in measurement techniques, has resulted in a movement to 3D methods for measuring rearfoot kinematics. These have been implemented in a number of studies, in which some replicate the marker placements on the calcaneal as seen in 2D studies (Butler *et al.*, 2006) whist others have alternatively defined the calcaneal eversion from a rearfoot eversion as part of a multi segment foot model (Eslami *et al.*, 2007).

Eslami *et al.* (2007) measured a mean maximum rearfoot eversion (pronation) value of 8.8° (±2.3) in barefoot measurements, increasing to 9° (±4.1) in the shod condition. In Butler's (2006) study, comparing the influence of shoe and foot arch types for a set of measures that included rearfoot eversion, for a cushioned shoe, average excursion and peak values of 8.0° (±3.0) and 9.7° (±2.6) were measured respectively.

2D rearfoot kinematic measurement methods were extended by Stacoff et al. (1989). The authors argued that previous investigations had not accounted for the influence of the forefoot on calcaneal eversion and therefore markers were placed on the first and fifth metatarsals to measure the forefoot angle from which a torsional angle between rear and forefoot was derived. Results from their study showed that increased stiffness of the foot (through shoe introduction), decreased the torsional movement between the rearfoot and forefoot and significantly increased pronation (calcaneal eversion). Subsequent 3D studies have demonstrated that joints distal to the rearfoot can influence the kinematic coupling at the ankle-complex joint and that forefoot sagittal and transverse planar movements are strongly coupled with rearfoot frontal plane motion in rear and forefoot strike conditions (Pohl & Buckley, 2008).

Multi Segment Kinematic Analysis

The advent of advanced three dimensional point measurement systems such as VICON (Oxford Metrics, Oxford) and Qualisys (Gothenburg, Sweden) has enabled more detailed kinematic measurements to be made more accurately in all three anatomical planes, as well as enabling the improvement of the kinematic models, from which more comprehensive kinematic measurements are derived. Multi segment kinematic analysis has been applied in clinical gait studies and is beginning to become more prevalent in sports biomechanics research to describe movements of the lower extremity, especially the foot and ankle complex in more detail.

Measurements have been achieved through the implementation of kinematic models that enable the relative movement of a differing numbers of 'segments', defined anatomically in a selection of ways via the application of reflective markers applied to the body, that intend to simplify the complex anatomical structure of the bones in the lower extremity. A marker set must enable sufficient marker visibility, where possible avoid marker occlusions during movement, and define the appropriate segments as well as allowing

natural movement. Some models only consider segments and joints distal to the knee, whilst others include definition of segments that enable analysis of the knee and hip joint also.

Wolf *et al.* (2009) employed a model with five defined segments: pelvis, thigh, shank, rearfoot, midfoot, defined from 47 markers, to investigate kinematic repeatability of a runner. This comprehensive model is not only capable of ankle and foot joint measurements, but also of hip and knee measurements. Carson *et al.* (2001) proposed a model that represented the lower extremity distal of the knee via four segments: tibia, hindfoot, forefoot and hallux. This model, also known as the Oxford Foot Model has been employed multiple times in published studies for running, for example by Morio et al (2009) to compare shod and barefoot kinematics. A similar four segment model (distal of the knee joint) was presented by Leardini (2007), which modelled the three foot segments slightly differently, defining calcaneus, midfoot and metatarsals. This model also has the potential to simplify the foot into a single segment as well as measuring hallux rotations in the transverse and sagittal plane.

Other lower extremity and foot models do exist, and models can be adapted when appropriate to the need of an investigator or the measurement metrics required.

2.2.3. Kinetics of Running

Kinetics is the branch of mechanics concerned with the forces that cause motions of bodies. In running, kinetics generally refers to the analysis of the ground reaction force (GRF) and the mechanical derivatives of the lower extremity joints. GRF kinetic data can be combined with kinematic data to estimate joint reaction forces and net muscle moments of each of the joints in the lower extremity using inverse dynamics.

2.2.3.1. Ground Reaction Forces

The ground reaction force (GRF) is the force, in accordance with Newton's third law, equal in magnitude and opposite in direction to the force applied to the ground by the foot during the stance phase of gait. Like other contact forces it is actually a distributed force that acts over a contact surface. It should be noted that all segments of the body contribute to the total body acceleration and is not entirely attributable to action of the lower extremity, although it does make a significant contribution in running (Miller, 1990).

When analysing GRF in running, the resultant GRF can be decomposed into three orthogonal components: a vertical force component, an anteroposterior force component and a mediolateral force component, acting along axes F_z, F_y and F_x respectively, with corresponding moments M_z, M_y and M_x (Figure 2-11). It is important to remember that these are three components of a single force that changes in magnitude and direction and point of application throughout the course of support. The point of application of the GRF is defined using spatial co-ordinates a_x and a_y in the transverse plane, with a location at a representative centre of pressure (CoP).
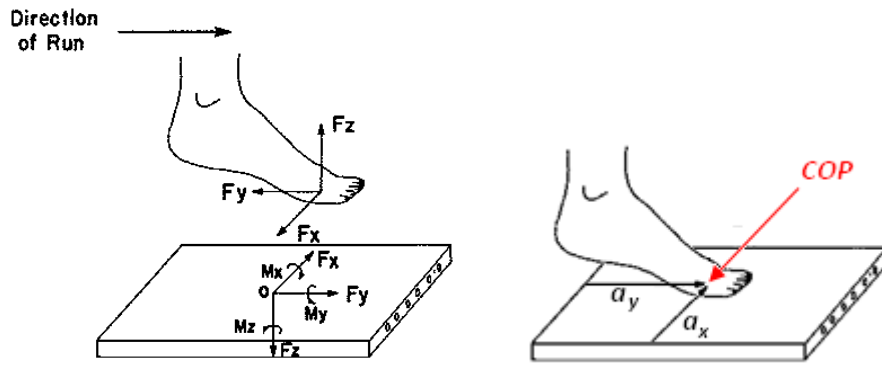
Figure 2-11 - Ground Reaction Force Vectors and Moments and COP Measurement (Adapted From Cavanagh And Lafortune, 1980)

Vertical GRF Component

The vertical component of GRF has the largest magnitude of the three components of GRF. It is generally a bimodal shape for rear and midfoot strikers featuring two distinct peaks as shown in Figure 2-12. The first 'high frequency' impact peak can be referred to as the passive peak or impact force peak with the second 'low frequency' impact peak referred to as the active force peak (Nigg, 1983). Active and passive are used to describe the state of muscular activity; in the impact peak there is little dependence on muscular activity, whereas in the active peak there is dependence as the muscles assist in the acceleration of the body off the ground.
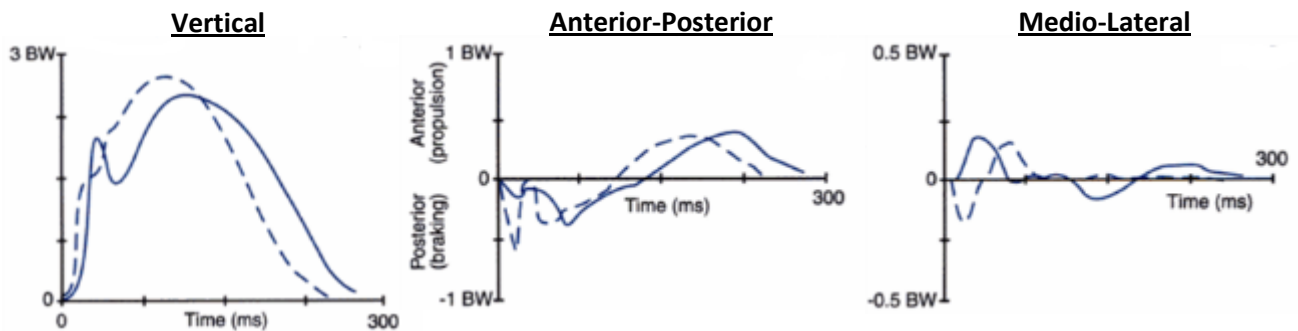
Figure 2-12 - Typical vertical, anterior-posterior and medio-lateral ground reaction forces for rearfoot (solid line) and forefoot (dashed line) running styles (from Williams (1985))

Cavanagh and Lafortune (1980) measured GRF for 17 subjects both male and female running at an average speed of 4.5 m·s^{-1}, reporting mean vertical GRF for rearfoot runners of 2.2 Body Weights (BW) (s.d.=0.4) at the passive impact peak and 2.8 BW (s.d.=0.3) at the active force peak. The impact peak occurred at 23ms (s.d.=0.3) with the more slowly rising active force peak occurring 83ms (s.d.=8ms) after initial contact.

In a re-examination of preceding literature for heel striker runners, running at a range of speeds Munro *et al.* (1987) reported ranges for peak values; impact force peak occurring between 6-17% and active force peak occurring between 35-50% of total stance period. This was in agreement with Cavanagh and Lafortune (1980) as well as with previous studies by Clarke *et al.* (1983d) and Hamill *et al.* (1983).

19

Studies in the literature have established a positive correlation between vertical GRF component and running speed. Munro *et al.* (1987) reported an increase of impact force peak magnitude from 1.6BW at 3.0 ms^{-1} to 2.3BW at 5.0 m·s^{-1} with an active force peak magnitude increasing from 2.5BW at 3 m·s^{-1} to 2.8BW at 5 m·s^{-1}. Hamill *et al.* (1983) reported force in newtons per kg of body mass, showing an increase from 20.64 N·kg^{-1} to 30.69 N·kg^{-1} in impact force peak values between 4 and 6 m·s^{-1} and an increase from 27.53 to 29.75 in active force peak values for the same speed differences. Nigg *et al.* (1987a) studied 14 male runners running at four velocities between 3 and 6 m·s^{-1}, they presented what appeared to be a linear increase in impact force peak, from 1.33kN at 3 m·s^{-1} to 2.17kN at 6 m·s^{-1} in running velocity; they also noted a fairly linear decrease in occurrence time for impact force peak also. For active force peak the authors observed a significant increase from 1.86kN to for 3 m·s^{-1}to 2.26kN for 6 m·s^{-1} running velocity.

Anteroposterior GRF Component

The anteroposterior GRF component is directly related to the horizontal acceleration of the total body's centre of mass during the support phase of gait. It consists of two distinct phases (Figure 2-12); an initial phase in which GRF direction opposes forward movement, termed braking, and the latter phase in which force is consistent with the direction of motion, termed propulsion (Munro *et al.*, 1987). If the braking component is larger than the propulsive component then the runner's velocity will decrease; conversely greater propulsion than braking will result in an increase in runner velocity. Differences between positive and negative will only occur if accelerating or decelerating; when running at a constant velocity the values should be approximately equal.

Cavanagh and Lafortune (1980) presented mean anteroposterior force components in their study with subjects running at a constant average velocity of 4.5 m·s^{-1}, with peaks of approximately 0.43BW (S.D. 0.05). They also showed that for a midfoot striker there is a double peaked braking phase of equal magnitude before the latter propulsive phase.

Mediolateral GRF Component

Mediolateral ground reaction forces indicate how the centre of mass of the body transfers from side to side during the stance phase. The mediolateral GRF component, which acts perpendicular to the direction of motion, is relatively small in magnitude in comparison to vertical and anteroposterior forces (Figure 2-12) and hence is generally characterised by high variability in both magnitude and profile. Miller (1990) refers to studies (Cavanagh *et al.*, 1980; Hamill *et al.*, 1983) where subjects were running at comparable speeds, that agree that the component magnitude falls within the region of between 0.1 to 0.2BW.

Because GRF is a measurement of the acceleration of the total body centre of gravity and not the foot, it is not appropriate to attempt to distinguish foot pronation and supination movements from mediolateral GRF components (Miller, 1990). Likewise attempts to measure changes in mediolateral GRF as a result of changes

of shoe type or introduction of bracing or orthotics would be flawed as a result of the inherent variability of the component (Munro *et al.*, 1987).

2.2.4. Influence of a Shoe on Running Biomechanics

From a biomechanical perspective there are two principal roles performed by a sport shoe: to prevent excessive load acting on structures of the human body and related injuries and to improve performance (B. Nigg & Segesser, 1992). Speculation that reduction of excessive impact forces and/or pronation reduces frequency of running injuries has resulted in running shoe designs incorporating features that reduce excessive pronation, through 'pronation control' systems and reduce excessive impact forces, through 'cushioning' systems (B. Nigg & Segesser, 1992; Reinschmidt, Van Den Bogert, et al., 1997).

2.2.4.1. Shoe Influence on GRFs

Vertical GRFs

The protection against overloading through the attenuation of impact forces experienced in running is one of the most important aspects of construction and selection of a running shoe. It has been shown that the vertical force impact peak (VFIP) is significantly reduced in shod conditions in comparison to barefoot running (Clarke *et al.*, 1983; Komi *et al.*, 1987) and that time to VFIP, VFIP minimum, time to VFIP minimum, vertical force active peak (VFAP), time to VFAP and overall contact time are also significantly increased (Clarke *et al.*, 1983; De Wit *et al.*, 2000). However, other studies have shown an opposite relationship for VFIP values. Divert et al. (2005) reported significantly lower VFIP values for barefoot running in comparison to shod. He and his co-workers speculated that increased running durations for measurements (≈3minutes) led the runner to reduce the high mechanical stress occurring at the heel, by switching to a forefoot running technique, whereas in shorter testing periods with limited number of steps, runners are able to sustain and then maintain high impact peaks.

Clarke et al. (1983b), showed that there was no measured difference in the magnitude of VFIP in shoes of differing midsole hardness, however time to is VFIP significantly decreased with increasing shoe hardness, which was in agreement with observations in an earlier study (Clarke *et al.*, 1983a). The increased time to VFIP is explained by the relatively lower spring constant of the softer material causing greater deflection for the same force; hence the advantageous situation occurs whereby although the same force is applied to the musculoskeletal system it is at a reduced rate. Nigg *et al.* (1988) showed in their study that VFIP could be influenced as a result of midsole hardness and heel flare.

Anteroposterior and Mediolateral GRFs

The comparison of anteroposterior and mediolateral GRFs in shod and barefoot running is limited in the literature as vertical GRFs are the intended component to be influenced by the shoe. Anteroposterior GRFs

have been shown to have significantly lower propulsive peaks in shod running when compared with barefoot (Divert et al., 2005), a result of the interactions occurring between the shoe and ground, which can be influenced via shoe sole materials and design. The high intra subject variability of medio-lateral force measurements has made assessment difficult (Divert et al., 2005), however, peak lateral forces have been shown to be significantly decreased in the shod condition versus barefoot and the timing of peak lateral forces significantly increased (Morley et al., 2010).

2.2.4.2.   Shoe Influence on Frontal Plane Kinematics

Studies have shown that when running in a shod condition in a 'normal' running shoe, compared to barefoot, the maximum rearfoot eversion angle (representing pronation) and time to maximum eversion significantly increase (Morley et al., 2010) however the converse has also been measured in relation to eversion angle (Bates *et al.*, 1978). Care should be taken when interpreting results as markers on the shoe can overestimate the actual movement of the foot within it (Reinschmidt *et al.*, 1997), which may explain the discrepancies between studies. As well as timing and magnitude of the rearfoot eversion angle, in the shod condition, studies have shown the stance duration and rearfoot inversion angle at contact increase significantly and that the rearfoot eversion movement starts later and ends sooner within the stance phase (Bates et al., 1978; Schuette *et al.*, 2013).

Focussed investigations have been conducted to measure the effect of particular shoe design features on a runner's kinematics in the frontal plane. These have included the midsole hardness (Clarke, Frederick, & Hamill, 1983a; Hamill, Bates, & Holt, 1992; Maclean, Davis, & Hamill, 2009), heel flare and height (Clarke *et al.*, 1983a; B. Nigg & Morlock, 1987; Reinschmidt & Nigg, 2000), shoe stiffness (Stacoff et al., 1989) and the shoe upper (Ferrandis, 1994).

2.3.   Human Foot Shape and Last Design

The shoe last: an aid model in the industrial shoe making process, is a reproduction of the approximate shape of the human foot (A. Luximon & Luximon, 2013) and is normally manufactured from either wood, high density polyethylene (HDPE) or aluminium. There are many types of shoe last used in different shoe industries (Pivečka & Laure, 1995) although the most simple is a solid last, an example of which is shown in Figure 2-13. The last determines the internal space of a shoe, which must correspond the human foot, knowledge of human foot shape is a therefore prerequisite to optimise shoe fit (Krauss *et al.*, 2010).

Figure 2-13 – A solid shoe last manufactured from HDPE

The two main shoe-last design guidelines are the AKA640-WMS and the Chinese system, however each country has its own guides for sizing and grading (A. Luximon & Luximon, 2009). The last design begins with the bottom pattern, which uses foot length (L_f) and foot width (W_f) to derive last measurements such as last width, length and bottom length (Figure 2-14) taking into account allowances for shoe features.

M_1 -   1st Metatarsal Head

M_0 - 1st Metatarsal Head Floor Contact

P_1 - 5th Metatarsal Head

P_0 - 5th Metatarsal Head Floor Contact

r_a -   Toe Allowance

r_h -   Heel Allowance

Foot Length (L_f) = OA

Foot Width (W_f) = $MM_1 + PP_1$

Foot Print Width (W_{fp}) = $MM_0 + PP_0$

Last length (L_L) = $OA + r_h + r_a$

Last Bottom Length (L_{LB}) = $OA + r_a$

Last Width (W_L) – intermediate of W_f and W_{fp}
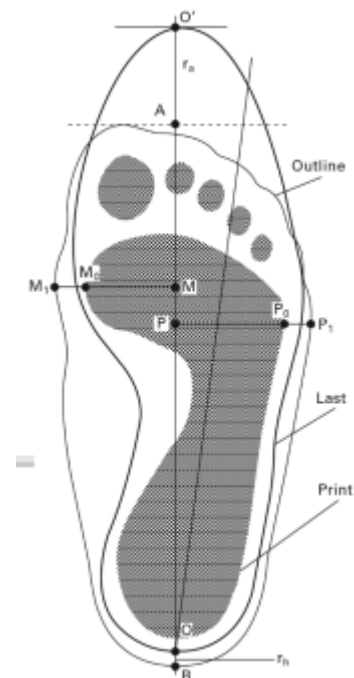
Figure 2-14 – Dimensional relationship between the foot and the shoe last (Y. Luximon & Luximon, 2013)

23

As well as linear length and breadth measurements, foot girths (circumferences) can also be utilised in the shoe last design such as ball girth, waist girth and instep girth (Figure 2-15) as well as heel girth and ankle girth depending on shoe type (Y. Luximon & Luximon, 2013).

Waist Girth
Instep Girth
Ball Girth

Waist Girth
Instep Girth
Ball Girth

(a)

(b)
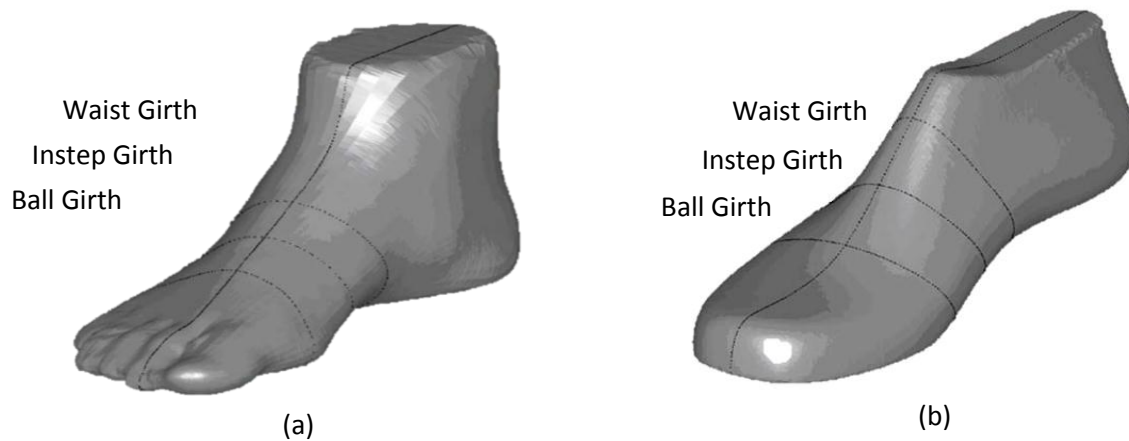
Figure 2-15 – Waist, instep and ball girths measured on (a) the foot and (b) on a shoe last (Wang, 2010)

Dimensions of the shoe last relative to the foot are dependent upon the shoe type and design, the upper materials employed and the desired shoe fit. Although it is advised that last design considers the changing foot dimensions as a result of movement and loading (Y. Luximon & Luximon, 2013) there is no hard and fast rule to convert three dimensional foot shape measurements into a last design, as design decisions are based on a number of factors related to the shoe. Last design can therefore be an iterative process whereby adaptations are made to the last from feedback from shoe prototyping and user wear trials.

Shoe lasts for mass manufacture are generally designed in a single size and then graded to create intermediate size variations (Mitchell *et al.*, 1995). The grading progressively enlarges or reduces the dimensions of the last via one of three approaches: arithmetic (a constant value), geometric (a constant percentage of an individual dimension) or proportional (the same percentage for all dimensions) (Y. Luximon & Luximon, 2013).

2.4. Measuring Human Foot Shape

2.4.1. Overview

The measurement of human body shape has been of interest to people for centuries, with the ability to describe the human body being critical in industries and fields such as clothing, ergonomics, industrial design and architecture. The movement to mass production of products in the nineteenth century, especially in fashion based industries such as clothing and footwear sparked considerable efforts into understanding the human body form; so a discrete set of products to 'fit' a broad population could be produced. In more recent years the improvement in and development of new technologies has brought about the potential for measurements to further improve products related to body shape.

2.4.2. Shape Measurement Technologies

A three dimensional surface can be represented by an array of points with known Cartesian co-ordinates (x,y,z) and then a mathematical model formulated to describe the surface shape based on these points. The ultimate goal therefore of 3D shape measurement techniques is to determine Cartesian co-ordinates of a surface (Su & Zhang, 2010). In a dynamic application, the Cartesian co-ordinates vary with time, from which other quantities such as shape displacement and deformation can be derived.

Methods to facilitate three dimensional shape measurements fall into one of two categories; contact and non-contact with each of these having a number of sub categories. As the names suggest, the former involves physically touching an objects to retrieve shape information e.g. with an instrument or a probe, whereas the latter obtains object information without making physical contact, e.g. through imaging or scanning. The focus in this review will be on non-contact technologies.

The majority of non-contact measurement technologies and methods are capable of measuring an object's external shape only, although technologies such as magnetic resonance imaging (MRI) and x-ray computed topography (CT), used extensively in medical applications, have the capability of measuring internal shape features. Many commercially available non-contact shape measurement systems employ some form of imaging technology from which three dimensional shape is reconstructed. The development of imaging technologies over the last ten to fifteen years, especially in the digital field, has enabled the improvement of measurement resolutions and accuracies for shape measurement systems (Daanen & Ter Haar, 2013).

Although a number of non-contact shape measurement technologies exist, the main four technologies used within systems for human body measurements will be outlined here, namely: laser scanning, structured light, stereo-photogrammetry and millimetre wave measurement, three of which employ some form of imaging and stereo vision in the method.

Laser scanning is an active technique where one or more laser lines are projected onto a body's surface, the light of which is scattered and then imaged by one or more cameras/sensors positioned at a fixed angle. Using triangulation the spatial co-ordinates of points along the laser line on the object surface can be calculated using trigonometric principles (Azernikov & Fischer, 2008; Ji & Leu, 1989). Static and handheld laser scanning devices are available commercially, operating in both the visible and infra-red ranges of the light spectrum. Measurements are reliant on the appropriate laser scattering and therefore surface properties such as reflectiveness and roughness can impact results.

Structured light methodologies measure three-dimensional geometry by projecting a light pattern onto a surface. The projected pattern, which can consist of any light pattern (Daanen & Ter Haar, 2013), although dots or stripes are generally used, is geometrically distorted by the object's shape. Once projected, the surface and pattern is imaged by cameras placed at a known position relative to the pattern projector. The three dimensional position of points on the surface, defined by the projected pattern, can be calculated using correlation techniques to match points between projected image and camera. As with laser scanning, triangulation calculations are used to determine the three dimensional position of a point. Resolution of measurements can be improved by adjusting separation and quality of pattern features, or/and employing a phase shift which moves the projected pattern across the surface whilst being imaged. Structured light measurements can be made much faster than laser scanning, allowing in specific setups, measurement of dynamic shape (Kimura *et al.*, 2008; Schmeltzpfenning et al., 2010; Zhang & Huang, 2006).

Stereo-photogrammetry is a stereo vision approach, like laser scanning and structured light, however instead of a camera-projector or camera-laser scan pairing; stereo photogrammetry is a passive technique that employs two cameras, viewing the same surface. 3D surface data is extracted from the images from each camera using features or patterns on the surface of interest. Correspondence of surface features between images is achieved using a stereo matching technique, such as cross correlation (Kimura *et al.*, 2009). Stereo-photogrammetry can also be implemented as an active system, where surface features are provided by a structured light projection. The projected pattern is then imaged by the stereo camera pair. In both scenarios the calculation of surface points in three dimensions is enabled by defining a common world coordinate system for the cameras, thereby providing the basis for relating image locations in all cameras to a common 3D position (Sutton *et al.*, 2009).

Millimetre wave (mmW) technology is not an image based method. It harnesses waves in the 'extremely high frequency' radio spectrum band, with wavelengths between 1 and 10 mm. Active scanners measure the reflection patterns of waves projected onto human body to evaluate shape, whereas passive scanners measure mmW emitted by the human skin itself (Daanen & Ter Haar, 2013). mmW's can pass through certain mediums unaffected, such as clothing material, however they cannot pass through human skin, for

this reason active mmW scanners have been employed in security applications, for example at airports to identify concealed weapons.

The discussed measurements technologies enable capture of full field surface data in the form of dense point clouds, from which discrete measurements describing body shape can be drawn. It is of course possible to make particular anthropometric measurements manually using appropriate tools (e.g. callipers or tape measures), however these methods are generally time consuming, have a reduced measurement resolution and are more prone to operator error.

2.4.3. Static Foot Morphology

Quantitative description of the human foot shape is important for a number of applications relating to ergonomic design of footwear, orthotics and insoles and clinical assessments (Telfer & Woodburn, 2010). In shoe design, proper fit is arguably the most important aspect of the design, in order to prevent the foot sliding inside of or out of the shoe (Krauss *et al.*, 2010). Adequate fit is achieved by matching the internal shoe cavity with the shape of the foot, allowing the shoe to support the foot in its physiological function (Hawes *et al.*, 1994). Understandably, shoe fit can be optimised with knowledge of the shape of the foot. However, foot shape is complicated due to the fact that numerous factors are associated with foot morphology, including biological variance, age, body mass index, parity and sex (Krauss *et al.*, 2010), each of which, theoretically, should be taken into account to enable proper design of shoes.

The majority of research in foot morphology has been conducted via measurement of the human foot shape in a static position; this position is usually standing, using technologies discussed in §2.4.2. Attempts to characterise foot shape has been made via the application of linear and cross sectional measures derived from full field measurements (Hong *et al.*, 2011; Jimenez-Ormeno *et al.*, 2013; Krauss et *et al.*, 2008; Mauch *et al.*, 2009; Xiong *et al.*, 2009).

These methodologies have enabled comparison of foot shape between male and females (Hong *et al.*, 2011; Luo *et al.*, 2009), loading conditions (Xiong *et al.*, 2009), body weight and foot growth patterns (Jimenez-Ormeno *et al.*, 2013) and measurement methodology (Witana *et al.*, 2006). Static foot scan data has also been used to compare the suitability of male shoe lasts for female feet (Krauss *et al.*, 2010), as well in attempts to classify foot shape in adults (Krauss *et al.*, 2008) and children (Mauch *et al.*, 2009).

Furthermore, like anatomical joint alignment, foot morphology has an important effect on the relationship between the ground reaction force and the axes of rotation of the ankle, knee and lower extremity as well as the corresponding forces developed on these structures (Murphy, *et al.*, 2003). A number of studies have attempted to link foot morphology to runner injury; however, most have generally focused on basic arch
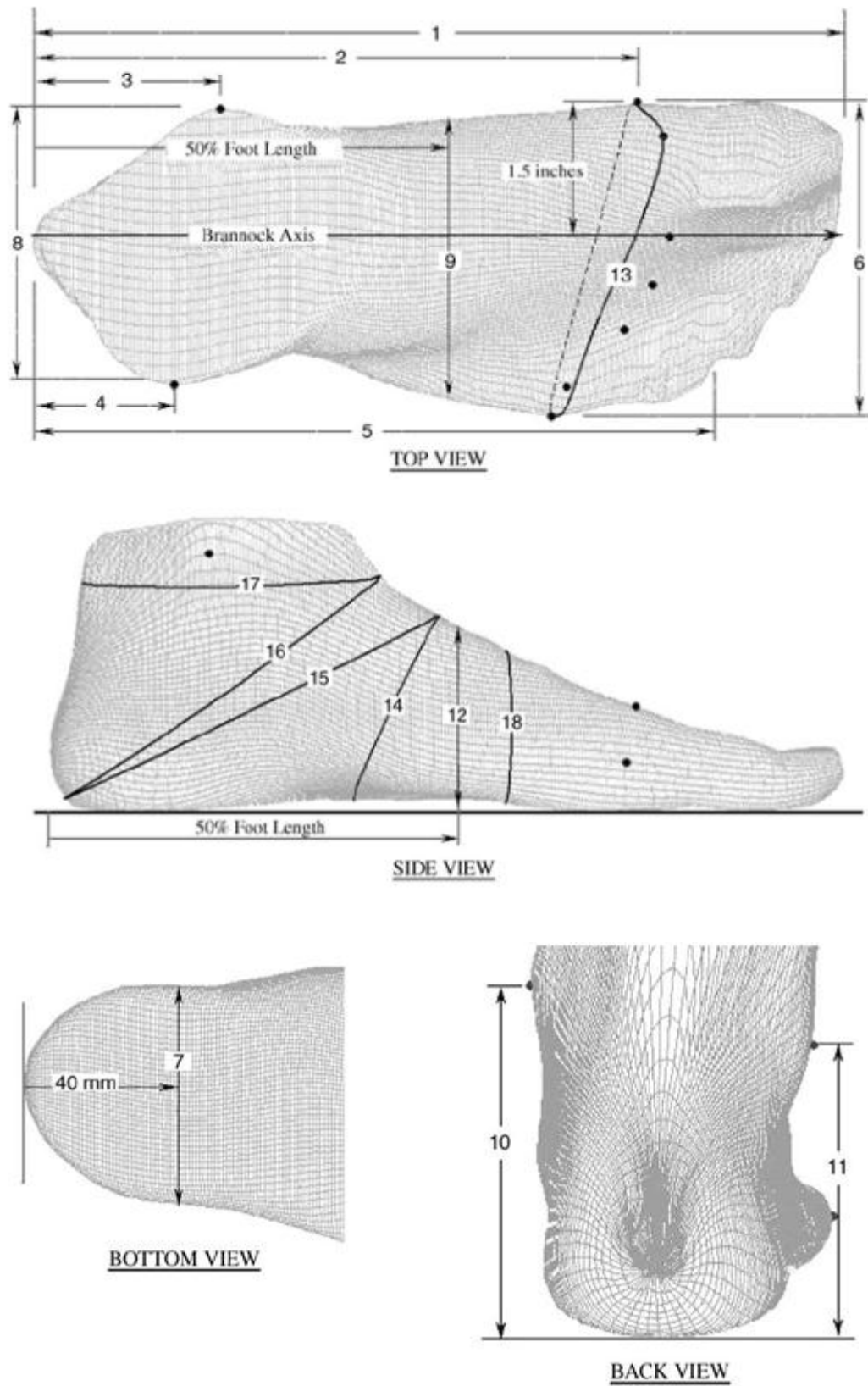
Figure 2-16 - Dimensioning of a Static Foot Scan (from Witana et al. 2006)

No.	Dimension Name	Measurement Type	Definition
1	Foot length	Length	Distance along Brannock axis from pternion to the tip of the longest toe.
2	Arch length		Distance along Brannock axis from pternion to most medially prominent point on the 1st metatarsal head.
3	Heel to medial malleolus		Length from pternion to the most medially protruding point of the medial malleolus measured along the Brannock axis
4	Heel to lateral malleolus		Length from pternion to the most laterally protruding point of the lateral malleolus measured along the Brannock axis
5	Heel to fifth toe		The distance along the Brannock axis from pternion to the anterior 5th toe tip
6	Foot width	Width	Maximum horizontal breadth across the foot-perpendicular to the Brannock axis in the region in front of the most laterally prominent point on the fifth metatarsal head
7	Heel width		Breadth of the heel 40 mm forward of the pternion
8	Bimalleolar width		Distance between the medially protruding on the medial malleolus and the most laterally protruding point on the lateral malleolus measured along a line perpendicular to the Brannock axis
9	Mid-foot width		Maximum horizontal breadth, across the foot perpendicular to the Brannock axis at 50% of foot lengths from the pternion
10	Medial malleolus height	Height	Vertical distance from the floor to the most prominent point on the medial malleolus
11	Lateral malleolus height		Vertical distance from the floor to the most prominent point on the lateral malleolus
12	Height at 50% foot length		Maximum height of the vertical cross-section at 50% of foot length from the pternion
13	Ball girth	Cross-section/girth	Circumference of foot, as if measured with a tape touching the medial margin of the head of the 1st metatarsal bone, top of the 1st metatarsal bone and lateral margin of the head of the 5th metatarsal.
14	Instep girth		Smallest girth over middle cuneiform prominence
15	Long heel girth		The girth from instep point around back heel point
16	Short heel girth		Minimum girth around back heel point and dorsal foot surface
17	Ankle girth		Horizontal girth at the foot and leg intersection
18	Waist girth		Circumference at the approximate centre of the metatarsal, measured in a vertical place, perpendicular to the Brannock axis.

Table 2-1 -Foot dimensioning definitions (from Witana et al. (2006))

measures with conflicting results for (Cowan *et al.*, 1993; D. S. Williams *et al.*, 2001) and against (Nakhaee *et al.*, 2008) the effect.

As well as being used for research purposes, scan data has also been used to build anthropometric databases, including foot shape (Robinette *et al.*, 1999). The international standards ISO 7250 and ISO 20685 have been created to firstly define the anthropometric measurements taken via 3D techniques discussed, to be used as a basis for population group comparisons and secondly to ensure measurements are comparable with those taken with traditional methods. For this reason, the standards are limited to the measurement of foot length and breadth only (Telfer & Woodburn, 2010), which does not describe full foot shape itself in any level of detail.

Due to the lack of a set of standard measures for describing foot shape in adequate detail, studies carried out have used different 'self-defined' measures to characterise foot shape. Jimenez-Ormeno *et al.* (2013), Mauch *et al.* (2009) and Krauss *et al.* (2010) used only 1-Dimensional length, height, width and angular measurements to characterise foot shape. Xiong *et al.* (2009) and Hong (2011) added one and four foot cross sectional (girth) measurements respectively along with linear measurements. However, the most comprehensive foot characterisation was in a study by Witana *et al.* (2006) who employed a total of 18 measures including 6 cross sectional (Figure 2-16 and Table 2-1), defined from anatomical markers and derived from the foot alignment with the Brannock axis.

2.4.4. Dynamic Foot Morphology

As outlined, the majority of foot shape research has focussed on measuring the foot in a static position; however, the foot does not remain the same shape during movement, especially during movements that involve high loading of the lower extremity. The evolutionary function of the foot is to dissipate forces associated with locomotion, provide support and enable propulsion. Understanding how the shape of the foot changes during particular movements as a result of these functions, will potentially further improve the functionality and fit of footwear (Kimura *et al.*, 2009).

Due to the time period required to make shape measurements with existing technologies, as discussed in §2.4.2, measurement of a moving object, i.e. a dynamic measurement, is made extremely difficult. A dynamic measurement is essentially a measurement taken at a specific point during an object's movement, which is assumed to be 'stationary' for the instance of time required to complete the measurement.

A structured light approach, that has been implemented with success for feet by Kimura *et al.* (2008) using a single camera-projector method, involves moving an object through a projected 'static' light pattern, i.e. a pattern that remains stationary, whilst recording images. By imaging the surface of interest within a sufficiently short time period, the object can be assumed to be in a 'static state' and a shape measurement

can be made for that particular instance (§2.4.2). Furthermore, recording a sequence of images of the movement enables multiple dynamic measurements to be made. In Kimura *et al* (2008) work, measurements were limited to individual foot surfaces, although the method does hold potential for measuring the whole foot during dynamic movement. In this approach measurement stage resolution is determined by the frequency at which images can be recorded. Thabet (2014) employed a similar camera-projector system to measure dynamic plantar surface shape using a coded light approach, in the form of coloured stripes, which aided pattern detection in the recorded image. Measurements were made at 60Hz, limiting measurements to dynamic walking. However due to the clinical nature of the study; this was the intended locomotion speeds. Although good results were reported, measurement of the full foot using multiple synchronous measurements is difficult due to the projected pattern interactions.

In structured light methods, employment of a phase shift in projected patterns can enable a better measurement resolution, which Kimura *et al.* admitted was a drawback of their single pattern method. This approach was utilised by Zhang (2006) for facial measurements, reconstructing each individual stage measurement from three consecutive fringe images, imaged at 40Hz. Although sufficient for measuring arguably slow facial movements, the foot moves much more quickly during periods of stance, especially in running gait, and therefore a much quicker measurement would be required. This could be achieved by reducing the 'imaging duration' (capture frequency or camera shutter speed) as well as in turn increasing pattern switching speed. This was partially achieved by Schmeltzpfenning *et al.* (2010) who developed an ultra-high speed device to project the phase shifted light pattern onto the foot at potential speeds of less than 1.0ms. Using a five camera setup the authors were able to measure the whole foot shape, however, as the cameras operated in a interleaved manner (to overcome multi pattern interaction), images could only be recorded up to 49Hz, restricting measurement of foot shape to walking gait. Visual inspection of Schmeltzpfenning's results also suggests either synchronisation or measurement alignment would need to be addressed, although this was not discussed.

Liu et al (Liu *et al.*, 2011) developed a passive method for dynamic human foot shape measurement using time of flight (ToF) cameras, which uses the flight time of a light pulse to obtain three dimensional surface information at discrete stages, at a capture rate of up to 50Hz. The presented work was conducted on a platform on what appears to be a quasi-static foot movement, with a closed surface foot shape achieved. The method was also capable of measuring a basic deformation using a point set registration method, although results were only presented for 'deformation' in a single axis between two stages. Once again the synchronisation and measurement alignment was not discussed within the published work.

Stereo-photogrammetry holds probably the most potential as a dynamic measurement system as it can be employed as a passive technique and the ability for dynamic measurement is reliant solely on the imaging duration of cameras. The approach also lends itself to sequential dynamic measurements as only single

images are used for measurements, unlike phase shifted structured light methods. Kimura *et al.* (2009) used this approach to measure specific anatomical cross sections of the foot during the stance phase of gait using a twelve camera setup, which was replicated in work by Kouchi *et al.* (2009) using the same setup. This method was incapable of complete foot reconstructions as cross sectional measurements were derived from lines drawn on the surface of the foot. Furthermore the method was limited to walking gait due to hardware operating parameters. In the more detailed application by Kouchi *et al.* (2009) only linear measurements were derived from the cross sections at discrete points in stance, although a circumferential measurement, over time was presented in the previous work by Kimura *et al.* (2009) using the method.

Coudert *et al.* (2006) used a stereo-photogrammetry approach, employing three unsynchronised stereoscopic camera pairs, to measure the dorsal foot surface for up to eight quasi static positions replicating foot positions in gait. Interestingly, in addition to measurement of surface shape the authors were able to measure surface deformation between stages by measuring movement of common measured surface points between measurement stages, although a detailed description of this process was not presented.

2.5. Summary

The three dimensional shape of the foot is created from a complex set of bones and muscles that form a series of joints and structures that function to enable the support and propulsion of the human body during the stance phase of the gait cycle. Foot movement during stance is dictated by the joints of the foot and the associated ranges of motion, which function simultaneously to change the relative alignment of the underlying anatomy and enable the foot to carry out its function. It is these movements occurring in the three cardinal body planes, in addition to the forces imparted on the foot from external influences such as the floor or shoe that cause the three dimensional foot shape to change across the footstrike during stance.

Considering the three dimensional shape of the foot statically, in one position, does not represent the dynamic foot shape throughout a movement as the position/alignment of the foot and the loadings experienced are not properly represented. Measurement of the foot in a static position is in fact a practical compromise for a much more complex problem with regard to foot shape that can potentially be addressed via the capture of foot shape measurements dynamically.

The need for measurement of dynamic foot shape has been recognised in the research community, however, as a discipline it is clearly in its infancy. At the current time the focus of published work has been on creation of methodologies that are capable of providing useful measurements, which at this point is yet to be achieved. Most measurement systems being implemented are bespoke and are hindered by the use of inadequate hardware and, in addition, very few of the methods presented are truly capable of whole foot measurement at even slow locomotion speeds. Furthermore, the measurements that are made are generally

a set of individual shapes for each stage of the foot movement; there is no linking of measurements to truly describe the foot's deformation.

It is speculated that ability to capture dynamic foot shape may not enable further insight into foot function beyond what is currently possible (Telfer & Woodburn, 2010). However this is a potentially short sighted view, especially as research in this field is limited and a full understanding of its capabilities is yet to be achieved. Undoubtedly, understanding of dynamic foot shape has the potential to further improve the design of shoes for fit and function and therefore should be considered along with static foot shape (Kimura *et al.*, 2008).

3. Measurement Methodology Requirements

3.1.1. Overview

In the review of the published literature in Chapter 2, the anatomy and movements of the human foot have been discussed. Also identified and discussed are a number of methodologies that have attempted to measure the dynamic shape during locomotion, with the merits of each reviewed. In line with the objectives of this work outlined in §1.1, it was important to establish the requirements of the measurement methodology that would be developed (OBJ_2). This would outline the focus of the measurement capabilities that would feed in to decision making processes for the selection and validation of a measurement system.

3.1.2. General Parameters

In line with the foot shape measurement studies conducted in literature, the measurement of foot shape would be carried out in a barefoot condition, with three dimensional shape measurements derived from the foot surfaces. The methodology should allow measurements to be made of a subject's foot during natural running, so that the movements and loadings occurring within and on the foot are realistic.

The methodology should allow the measurement of a range of running velocities and for different running styles such as forefoot, midfoot and rearfoot runners. The methodology should also be capable of making multiple measurements of foot shape during the stance phase of a single running trial.

Measurements made through the method should be at a suitable level of accuracy, repeatability and reproducibility to support meaningful analysis and conclusions to be drawn from the measurements.

3.1.3. Foot Shape

Foot shape would be described via metrics targeted at characterising the three dimensional surface shape measured over the stance phase of gait. Metrics would be quantitative measurements, for example linear distances, surface profiles, two dimensional areas and volumes, as described in existing dynamic and static foot morphology studies (Witana *et al.*, 2004; Wunderlich & Cavanagh, 2001). In order to enable the three dimensional shape of the foot to be fully assessed, it followed that all foot surfaces should be measured to create a 'closed foot shape' from which the three dimensional shape could be characterised across the footstrike, using the appropriate metrics.

In static studies where detailed characterisation of foot shape has been attempted, the shape metrics defined have mainly focused on the foot region proximal to the MPJ (Witana et al., 2006; Wunderlich & Cavanagh, 2001), furthermore in dynamic studies where measurements have been reported (Kimura et al.,

2009; Kouchi et al., 2009), no attempt has been made to make measurements distal to the MPJ. A likely reason for this is the fact that it is widely accepted that in a shoe last design, the 'back region' of the last (i.e. proximal to the MPJ), is associated with comfort whereas the toe section (i.e. distal to the MPJ) is more related to fashion (A. Luximon & Luximon, 2009). For this reason, where attempts have been made to describe foot shape in the toe region, it has generally been conducted with very basic linear measurements of height or width, whereas more detailed shape characterisation metrics, for example cross sections, have been defined to describe foot shape proximal to the MPJ. Although the toe region is undoubtedly important in the fit of shoes in terms of shoe and last design, only the measurements made proximal to the MPJ require surface shape to be measured. Therefore, in order to allow relevant shape measurements to be made, the surface area of interest for measurement throughout the stance phase, was that proximal to the MPJ to approximately the ankle joint (as shown in Figure 3-1).
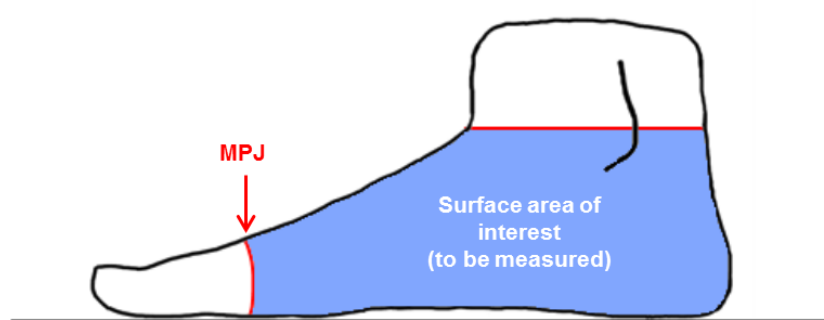
Figure 3-1 – Surface area of interest defined by the shaded region (medial view).

3.1.4. Shape Change/Deformation

Measurements of shape at discrete stages across the footstrike are useful in establishing the absolute shape of the foot at a particular point in stance, however, understanding how that particular measurement of shape changes between stages (over time) is potentially a more useful measurement when informing the design of shoes and lasts. Attempts have been made to measure the deformation (shape change) of the foot for all foot surfaces (Coudert et al., 2006; Liu et al., 2011) and for individual measurements, such as cross sections (Kimura et al., 2009), however these measurements to date have been limited.

The methodology should enable shape measurements made at individual stages during stance to be associated to one another, thus supporting the derivation of deformation measurements.

3.1.5. Kinetics and Kinematics

The primary function of the methodology was to measure the dynamic shape of the foot during the stance phase of gait. However, being able to describe the loading and movement of the lower extremity during stance was also important as they could serve as a descriptor for the drivers of foot shape and its changes, as well as enabling the definition of events during stance. The measurement of kinetics and kinematics would

give quantitative measurement of loading and limb movements that could be used in conjunction with shape and deformation measurements to characterise foot shape and its change. For meaningful measurements, kinetics and kinematics would need to be measured either simultaneously or derived from the measurements.

Linear measurements could still be made in the region; however, data points on the surface to facilitate these would have to be derived from markers located on the skin, as opposed to surface measurement data points.

3.2. Summary

This chapter has endeavoured to address OBJ_2 defined in the thesis objectives (§1.1). The requirements of the methodology have been outlined in the preceding sections, in terms of general measurement parameters and for the measurement of shape, deformation, kinematics and kinetics. These requirements will guide the measurement technology selection (OBJ_4) and validation (OBJ_5) as well as the development of the methodology for foot shape measurement (OBJ_5).

4. Measurement Technology Selection and Validation

4.1. Introduction

The selection of an appropriate measurement technology is a key objective in the success of the research work. A number of different technologies that have been successfully implemented in the measurement of dynamic human body shape have been outlined in the previous chapter.

The aim of this chapter was to select a measurement technology from those identified, understand how measurements using it are made and to ensure that it was 'fit for purpose'. The objectives of this chapter therefore were firstly, via objective means, to select a suitable technology for measurement of dynamic human foot shape (OBJ_4), and secondly, to show via appropriate means that a system, within which the technology was embodied, was suitable for the desired application (OBJ_5). This would be based on a set of defined criteria relevant to the application and the measurement requirements outline in Chapter 3. The basic concepts of DIC are also described along with the measurement methods and associated terminology.

4.2. Selection of Measurement Technology

Table 4-1 presents a comparison of four measurement technologies/methods for body morphology measurement outlined in §2.2.4; laser scanning, structured light, photogrammetry and time of flight, using a set of criteria, around which a discussion of suitability can be made.

	Laser Scan	Structured Light	Photogrammetry (DIC)	Time of Flight
Active/Passive	Active	Active	Passive	Active
Individual measurement duration	seconds	millisecs	microsecs	millisecs
N^o of images per individual measurement	Multiple	Multiple/Single	Single	N/A
Full foot shape measurement	Yes	Yes	Yes	Yes
Integrated deformation measurements	No	No	Yes	No
Specialised hardware	Yes	Yes	No	Yes/No
Point cloud density	High	High/Med	Med	High
Surface preparation	Sometimes	Sometimes	Always	Sometimes
Accuracy	-	0.4 mm Static (1)	-	0.25 mm Dynamic (2)

(1.) Jezeršek (2009) (2.) Liu *et al.* (2011).

Table 4-1 –Shape measurement technology comparison (Accuracy values based on published data for body shape measurement where available)

The key consideration in dynamic shape measurement is enabling a measurement to be made in a sufficiently short amount of time, so that the moving body (in this case the foot) can essentially be assumed 'stationary'. The shorter the time period, over which a measurement is made, the more accurate the measurement is in terms of recreating the actual foot shape. In laser scanning approaches and time of flight methods, the minimum measurement duration is governed by the time it takes to scan the laser over the foot surface, in structured light using phase shifted patterns; the constraint is the time over which the fringe patterns are projected. In photogrammetry, the only limit, due to its passive nature, is the duration over which an image is captured which is also the case for structured light methods that use a single pattern; however, measurement resolutions are generally sacrificed in this latter approach.

Achieving a short enough measurement duration has been the limiting factor in published measurements to date, with measurements limited to walking speeds. In investigative work carried out in this research, it has been observed that during running some foot surface areas can move by as much as 5 mm in only 10ms, meaning short measurement durations are needed to ensure shapes are not distorted. Photogrammetry as a method is capable of easily achieving these sorts of speeds via the adaption of imaging hardware, whereas other methods require changes to more than one hardware component.

A second consideration is the capability to measure the full foot shape, which is generally accomplished by the employment of multiple scanning/imaging devices that can view all foot surfaces. This adds a complication with active systems, as mutual interference between multiple measurement modules can occur. This can be overcome via the use of different wavelength light (Jezeršek & Možina, 2009) or operating the scanning modules slightly consecutively (Schmeltzpfenning *et al.*, 2010) in a series approach, however the latter further compromises the measurement duration, already discussed. The passive nature of photogrammetry means employment of multiple systems does not create the same problems, however in all measurement approaches alignment of surfaces made from separate devices is required to form a measurement.

A further consideration is the hardware required to enable measurements. Laser scanning and structured light techniques for dynamic shape measurements generally require specialised equipment, with published literature usually developing bespoke hardware. Photogrammetry however, by comparison, requires only a means to capture digital images from which shape measurements are made. Although some imaging hardware and peripheral components may be considered 'specialised', these are commercially available and 'turn-key' solutions for dynamic shape measurements exist.

One additional advantage of photogrammetry over other technologies was the capability to measure deformation, which was highlighted in the methodology requirements (§3.1.4). Although other techniques

claim the ability to assess this parameter, the reality is deformation measurements are unrepresentative and limited.

Digital image correlation (DIC), a form of photogrammetry is capable of measuring actual deformation by measuring the surface shape of an object undergoing a change in shape, over a period of time. Discrete surface shapes are created from sets of data points measured on the surface. These data points are created using a pattern applied to the object's surface that then allows the point to be tracked between images. As DIC is able to accurately associate the data points between stages, measurements derived from the data points (e.g. cross sections or discrete lengths) can also be 'tracked' across stages as the shape changes. Thus, relative shape measurements can be made. Furthermore, the association of surface data points to one another allows the full field surface shape change (i.e. surface deformation) to also be derived.

DIC was conceived in early 1980's to measure 2D surface shape and deformation (Sutton et al., 1983) and has since evolved to be capable of 3D measurements, driven by improvements in digital imaging technology and hardware in recent years, which have enabled more diverse applications to be developed. Although not explicitly described, DIC appears to be the technique used in foot shape measurements by Coudert et al. (2006), however, as already outlined, this work was extremely limited when related to dynamic foot shape. Meaningful deformation measurements provide a way to describe the dynamic foot shape during movement, as well as capturing absolute foot shape.

It was clear that photogrammetry, in its embodiment in DIC, had advantages over existing technologies for the measurement of dynamic shape. The relative low complexity and availability of associated hardware allowed method and measurement flexibility, in addition to the fact commercial measurement systems (encompassing hardware and software) were readily available (e.g. GOM, Braunschweig, Germany/LaVision Goettingen, Germany). Furthermore, there was potential to measure complex shapes with ease through a multi system approach, potentially enabling the integration of other measurements associated with running gait (e.g. kinematics).

For this reason, photogrammetry, and more specifically, its embodiment in digital image correlation, was selected as the preferred technology for use in the research work. To confirm DIC suitability as a measurement tool for the application, a DIC system needed to be validated against a set of requirements (which will be carried out later in this chapter). Prior to this however, it was important to appreciate the underlying principles of DIC and to understand how surface shape and deformation measurements are made.

4.3. Digital Image Correlation (DIC)

4.3.1. Overview

"Digital image correlation" (DIC) refers to a non-contact method where digital images of an object are captured and analysed to extract full field shape, deformation and/or motion measurements, (Sutton et al., 2009). The methodology is based on the comparison of images between a non-deformed and succession of deformed states in order to obtain shape from which relative deformation measurements can be derived.

DIC is grounded in photogrammetry; the science of making measurements from images. Through the use of pictures, photogrammetry allows the reconstruction and comprehensive analysis of an object's characteristics, without the requirement of physical contact. Traditionally, photogrammetry was conducted using images obtained via a photochemical means, however, advances in digital photography have created a new form of photogrammetry, whereby human vision and perception used in traditional methodologies are emulated by the computer, allowing the entire analysis process to take place via computational means (Kraus, 2007).

Measurements are made by creating and then tracking a number of points, in a sequence of digital images, on the surface of an object as it moves or/and undergoes some form of deformation. Points on the surface of an object (object points) are reconstructed from the digital image data either in two dimensions (2D) using images from a single sensor, or in three dimensions (3D) using images from a synchronised stereo camera system. Establishing the inter-relationship of the surface data points with respect to one another over time, in two/three dimensional space, allows surface deformation measurements to be derived. Measured deformations are limited to 2D strains tangential to the surface of interest; it is not possible therefore to measure a complete 3D strain value.

4.3.2. Basic DIC Concepts

DIC techniques rely upon the acquisition of digital images, captured using an image sensor, for example a charged couple device (CCD), a rectangular array of sensors (pixels) that convert the continuous intensity field reflected from the surface of interest, into a discrete array of integer intensity values. These intensity levels, otherwise known as a 'greyscale' value are usually defined via an 8bit integer value between 0 and 255; 0 being purely black and 255 being purely white, from which a monochrome image is created.
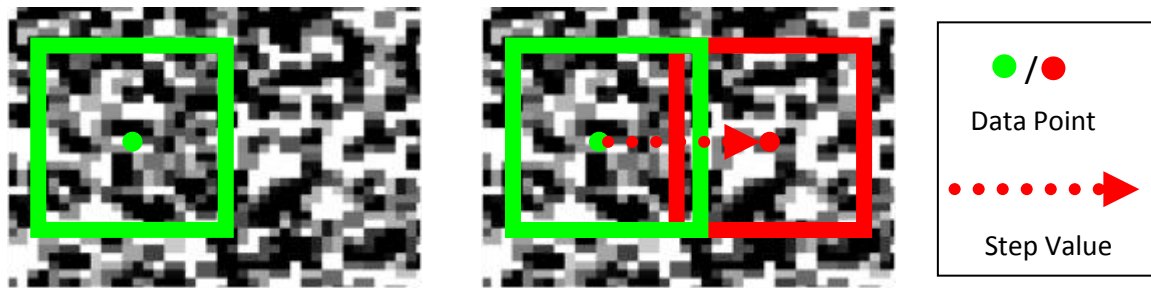
Figure 4-1 - (a) A data point created from a facet (b) Using a step to creating multiple data points

It is impossible to match a single pixel between two images by grayscale value alone, as there are likely to be thousands of pixels in the second image that will match with the greyscale value of the reference image pixel. For this reason, instead of using individual pixels, a neighbourhood of pixels are considered in order to obtain a unique correspondence between the two images, allowing an object point on the surface to be created (Figure 4-1). This collection of pixels is commonly referred to as a subset or facet, which enables the same object point on the surface to be tracked over sequential images. The final displacement result is expressed at the centre point of the subset and is an average of the displacements of a number or all of the pixels inside the subset (Lecompte et al., 2006).
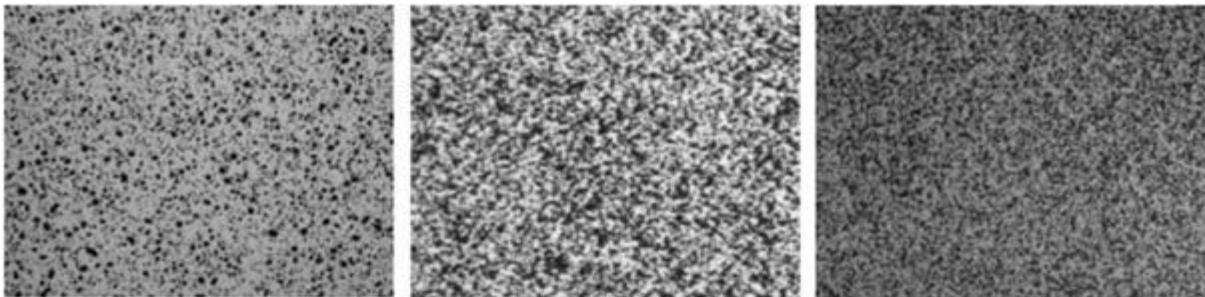
Figure 4-2 - Speckle pattern examples (from Sutton et al. 2009)

To create a suitable continuous intensity field that will aid the matching of subsets between images, a contrasting random stochastic pattern, as shown in Figure 4-2, must be applied to the object surface of interest that adheres and deforms with the surface. In order to ensure a unique correspondence of a subset between images the pattern should be isotropic and non-periodic (Sutton et al., 2009). The naturally occurring pattern of the surface is sometimes sufficient so long as it is contrasting and fulfils the conditions mentioned.

When comparing subsets between images it is likely that during deformation, an object point imaged onto the centre of an integer pixel location, in the undeformed image, will be imaged to locations between pixels of the stationary CCD (Sutton et al., 2000). Therefore in order to enable accurate estimation of surface deformation between images, an interpolation scheme is used to reconstruct the continuous intensity pattern using the discretely sampled pattern, as shown in Figure 4-3. For accurate measurement of the

surface and its deformations it is important to oversample the continuous intensity pattern (Sutton et al., 2000), i.e. using a number of sensor pixels to sample each feature of the surface pattern, thus allowing the original intensity pattern to be reconstructed with the most accuracy. The surface pattern should be adapted to the measuring volume, camera resolution and facet sizes in order to enable the surface shape and associated displacement field to be suitably measured.
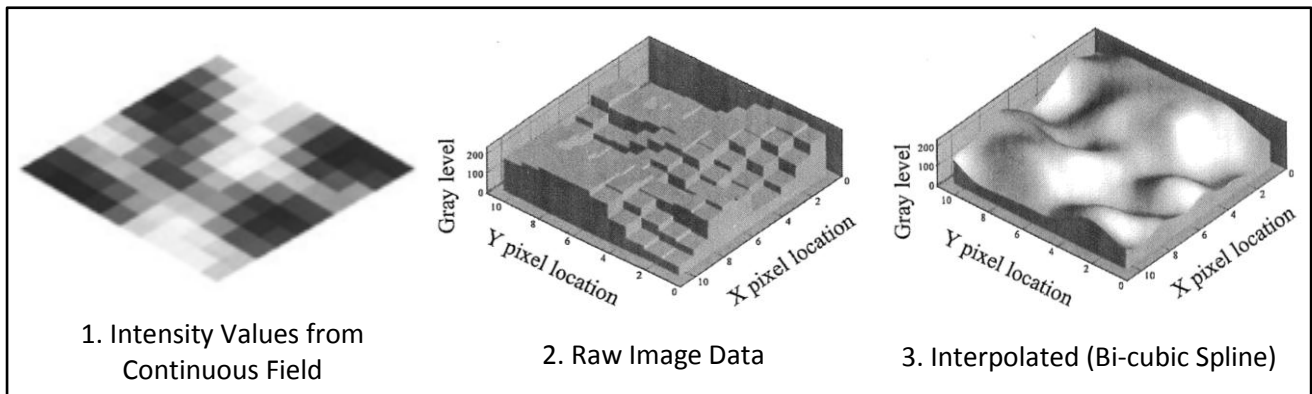
Figure 4-3 - Reconstruction of the Continuous Field Using Interpolation (adapted from Sutton et al. (2000))

Assuming that after movement (due to rigid body motion or deformation) the intensity pattern is related to the intensity pattern imaged before, parameters describing the movement of the subset can be determined by matching the intensity values of the points in the subset from the interpolation function between the two images. This 'matching' function can be achieved using one of several intensity pattern correspondence measures (correlation functions).

The number and separation of object points created across a measured surface (resolution) is dependent upon the 'computational step' parameter; the distance, in pixels, that a subset is translated within the image before another data point is created, as shown in Figure 4-1b. For the same sensor, a small computational step size applied in a large field of view will result in a larger data point separation than when applied in a comparatively smaller field of view. As the step influences number and density of data points it in turn affects the computation time of the measurement and the influence of measurement noise on results. Large separation between data points can also introduce averaging of deformation measurements as well as omitting the measurement of deformations occurring in a localised area. Thus, selection of computational step size is made with dependency on those parameters mentioned.

4.3.3. DIC-2D

An optical 2D-DIC technique was first outlined by Sutton et al. (1983), to measure the two dimensional shape and thus the in-plane surface displacements and deformations of an object surface; since then DIC-2D has been employed extensively in literature due to the appeal of its non-contact approach and potential to return detailed full field measurements.

The measurement of surface displacements using DIC-2D is implemented using a single camera to image the surface of interest, as shown in Figure 4-4. Sequential images of a surface during a deformation are captured, from which the two dimensional position and displacement of a discrete number of data points across the surface are collected using DIC techniques discussed, from which planar deformations can be derived.
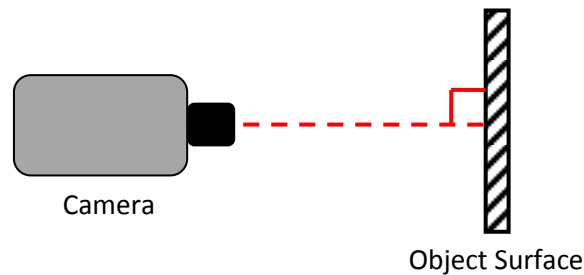
Figure 4-4 - Schematic of DIC-2D (plan view)

The 2D computer vision associated with 2D-DIC uses a pinhole camera model that performs a basic perspective projection: transforming a 3D object point, the point on the surface of interest, into a 2D image point, a pixel location on the image sensor. In doing this the third dimension is irrevocably lost and hence, for one point (p) on the image plane there are an infinite number of corresponding three dimensional points, as shown in Figure 4-5, meaning it is not possible to recover 3D object surface geometry information from the 2D approach.
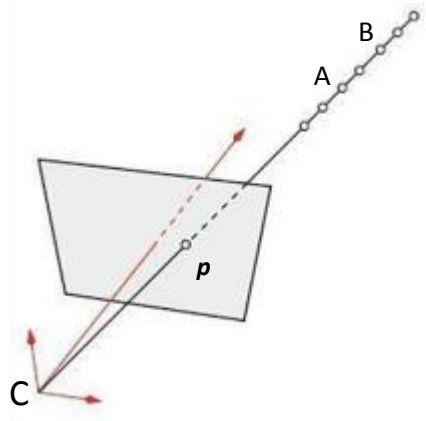
Figure 4-5 - 2D Perspective Projection (from Sutton *et al.* (2009))

As a result, only measurement of point displacements that occur parallel with the image plane are possible, generally for simple planar or pseudo planar surfaces; the accuracy of which is dependent upon the relative positions of the camera and object-surface planes. Relatively small out of plane movements during the measurement can cause changes in image magnification that introduces significant measurement errors (Sutton et al., 2000). Although this effect can be minimised for small out of plane movement by using a

longer focal length lens to increase the camera to object surface distance (Sutton et al., 1991), attempts to correct for larger out of plane movements have achieved minimal success (Sutton et al., 2000).

It is due to the inherent disadvantages of DIC-2D measurements and methodologies that approaches which enable measurement of full three dimensional shape and surface deformations have been developed.

4.3.4. DIC-3D
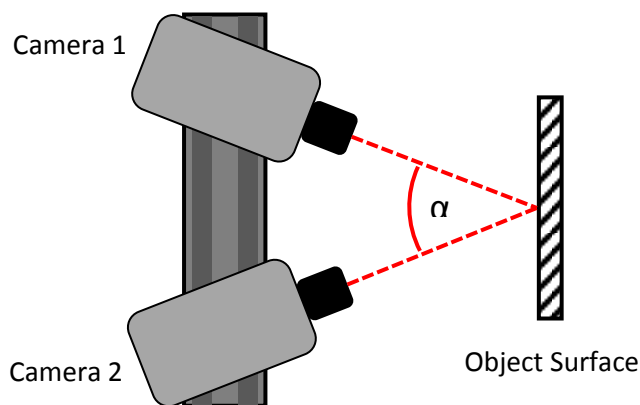
Figure 4-6 - Schematic of DIC-3D (plan view)

3D-DIC, as shown in Figure 4-6, is based on a combination of stereoscopic (stereo) computer vision and conventional DIC techniques already discussed. Information related to the 3D morphology of an object's surface can be obtained by establishing the position of subsets in images from the two simultaneous camera images from two different views.
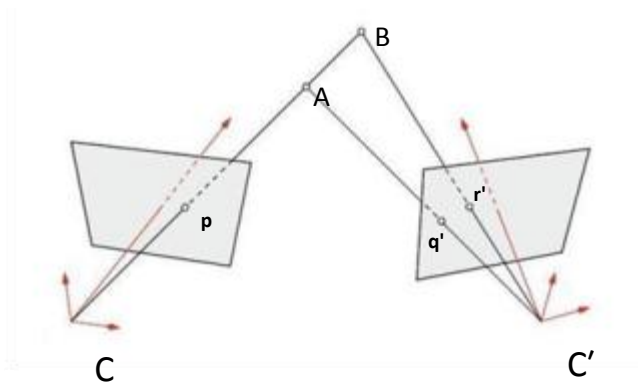
Figure 4-7 - Recovering the third dimension using two cameras (adapted from Sutton at al. (2009))

3D-DIC allows the recovery of the third dimension that is lost in 2D-DIC techniques. By imaging the surface of interest from two views, each object point on the surface of interest will have a unique combination of image points (p, q' and r') on the sensor plane, as shown in Figure 4-7. This enables each point to be distinguished and identified in 3D space.
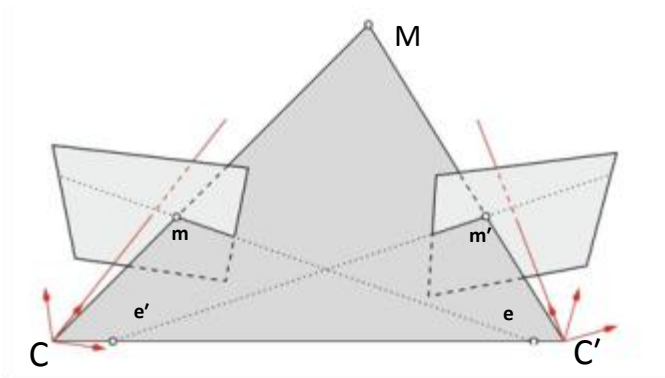
Figure 4-8 - Epipolar geometry (from Sutton et al. (2009))

Identification of common object points between camera images is facilitated by the image correlation techniques used to track data points through sequential images. This is aided by the use of epipolar lines; a geometric constraint between two image points in two different camera image planes that uniquely locate an object point in the real world co-ordinate system. These three points (M, m and m') lie in a common plane which intersects each image plane: the lines created by this intersection are the epipolar lines (e, e') (Figure 4-8). In application, when one image point is known, the epipolar line in the second image plane can be defined from mathematical formula (when certain setup and imaging parameters are known), thus reducing the matching of subsets between camera images to a single scan along the epipolar line in the second image.

The point cloud created from the three dimensional data points, in a first instance can be used to create a surface at each stage of the measurement using mathematical surface reconstruction methods e.g. such as bilinear interpolation (Buss, 2003) or Poisson surface reconstruction (Kazhdan & Hoppe, 2013). In line with the DIC technique, by comparing a set of reference images with subsequent recorded images, the changes in 3D object point position can be ascertained, thus allowing full field, three dimensional displacements to be measured for a discrete number of data points across a surface of interest from which deformations of the surface can be derived. In order for measurements to be made throughout a deformation, the surface area from which a data point is created must remain in the view of the camera pair for the duration of the measurement period.

4.3.5. DIC-3D System Calibration

Information relating to the positioning (extrinsic) and imaging (intrinsic) parameters of the cameras being used must be known in order for DIC measurements to be made. This information is used to reconstruct the two dimensional points on the camera sensor (from images) into positions in three dimensional space. Some information can be obtained with knowledge of the imaging hardware, such as sensor size and pixel dimensions, however, other parameters such as camera positioning and imaging properties have to be defined using an applied approach, usually known as a system calibration.
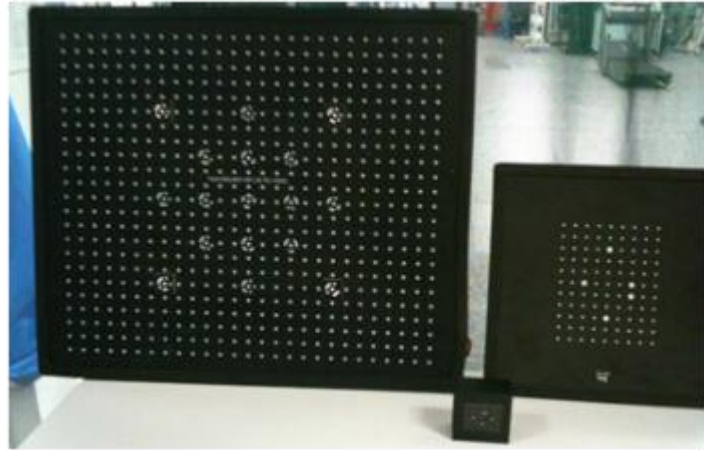
Figure 4-9 – Examples of calibration artefacts, embodied in panel form.

The system calibration defines the 'measurement volume'; this is the three dimensional real world space in which object points can be accurately reconstructed from the two dimensional location of points on the image sensor. System calibration is usually facilitated by a calibration artefact, an object providing features with known dimensions or separations. The calibration artefact serves to define a global co-ordinate system (determining relative camera position) as well as aiding in the definition of intrinsic camera parameters such as focus, lens distortion and image aspect ratio. Different calibration artefacts are used to calibrate different measurement volumes (Figure 4-9), which is ultimately governed by camera imaging properties and hardware arrangements (§4.4.3).

A system calibration is generally conducted prior to a measurement being made, returning a value relating to the level of error in reconstruction of object points (in this case features on the calibration panel) in three dimensional space. Acceptable limits for this error are generally defined by the manufacturer, or can be established via experimental work. A system will remain 'calibrated' until a change is made that alters one or more of the parameters contributing to the system calibration, for example, relative camera position or lens focus.

4.3.6. Measurement Duration Definition

The number of individual measurement stages made within a DIC measurement is defined by the capture frequency of the imaging device, usually expressed in frames per second (fps), whilst the duration of a measurement is controlled by the time period over which an image is captured; this is defined by the 'shutter speed'. The shutter speed controls the exposure time, the time over which the camera sensor samples light: the shorter the shutter speed the shorter the measurement duration. The shortest shutter duration is equal to one over the capture frequency of the imaging device.

Short shutter speeds can be paired with greater capture frequencies to enable short measurement durations, whilst controlling the number of individual measurements made over a time period, which is an advantage when processing data.

4.4. GOM ARAMIS

4.4.1. Overview

The DIC-3D measurement system that is proposed for use in this work is the ARAMIS system from GOM (Braunschweig, Germany). So as to obtain an understanding of the system and its potential capabilities, an overview of the ARAMIS system is presented in the following sections. This will cover the primary hardware components and the workflow associated with measurement as well as the terminology specific to ARAMIS which will be used herein. The ARAMIS 'system' in this work is defined as the measurement software and any imaging hardware employed, even when the latter operates independently from the software.

4.4.2. Hardware

Images used for analysis with ARAMIS can be obtained using integrated cameras which record images directly into the software, with a number of different camera systems available which have varying sensor resolutions and recording frequencies. Alternatively it is possible to capture images from an independent camera system and import images into the software for analysis; enabling more specialist imaging equipment suited to the application to be used. Images used for measurements must be in 8bit monochrome format.

Cameras are attached to a mount that primarily allows the cameras to be mechanically fixed into a position to prevent any movements that would cause a computed system calibration to become invalid. The mount also allows adjustment of camera separation and camera angle to tailor measurement volume (§4.4.3). Fixed focal length (FFL) lenses are used in conjunction with the cameras so as to ensure lens focal length can be defined accurately. GOM define setup parameters for lenses with focal lengths between 12 mm to 100 mm, however, with adjustment in setup (§4.4.3), lenses with longer focal lengths could potentially be used.

Two types of calibration artefact are available for system calibration, panels for small measuring volumes (Figure 4-9) and calibrated crosses for larger volumes. Sizes of each vary, which are matched to measurement the volume desired. Both types have coded markers at known separations, as well as uncoded markers which aid in definition of other camera parameters, which are recognised in the ARAMIS software.

4.4.3. Measurement Volume Definition

The parameters and definitions associated with the ARAMIS system measurement volume are outlined in Figure 4-10.
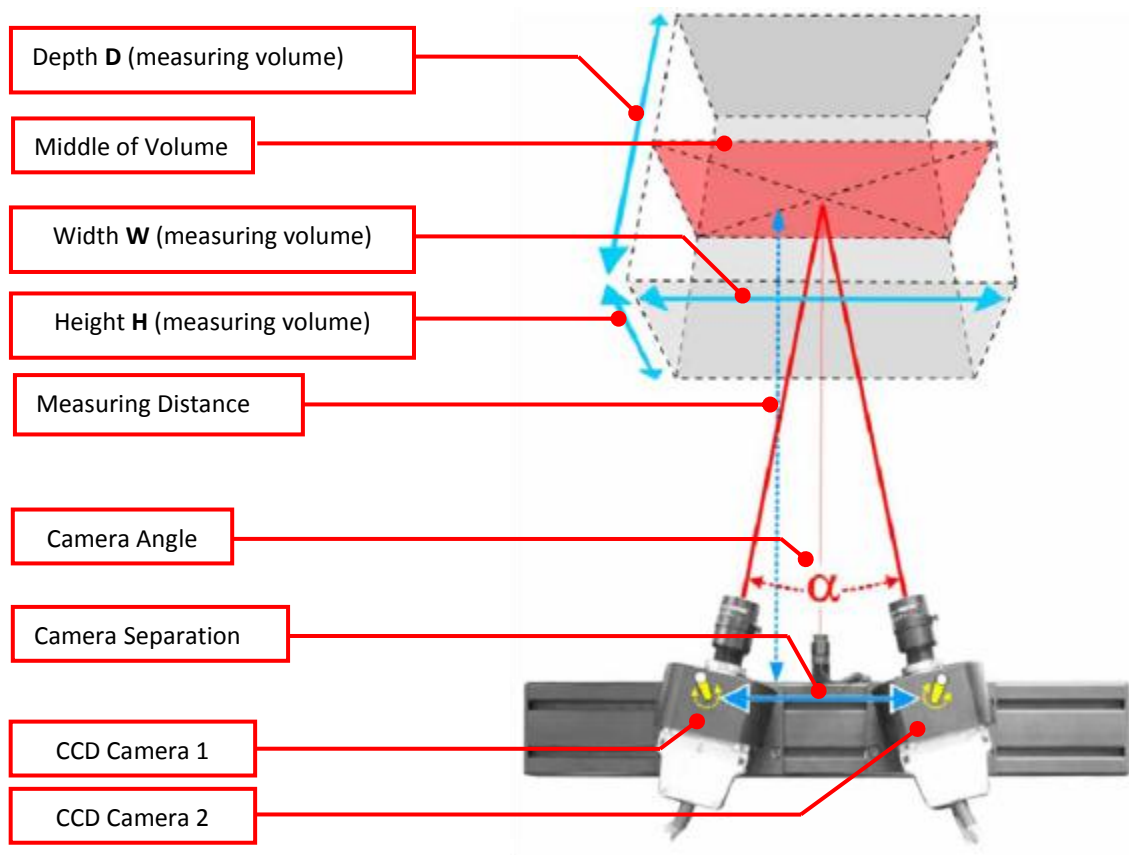
Figure 4-10 - Set up of ARAMIS DIC-3D and key parameter definitions (adapted from GOM (2009a))

In line with basic photographic principles each camera has a field of view, the size of which is a function of the sensor dimensions, lens focal length and distance to the focal plane. If the sensor parameters remain constant then the field of view can be altered by changing the distance from the sensor to the plane as shown in Figure 4-11.
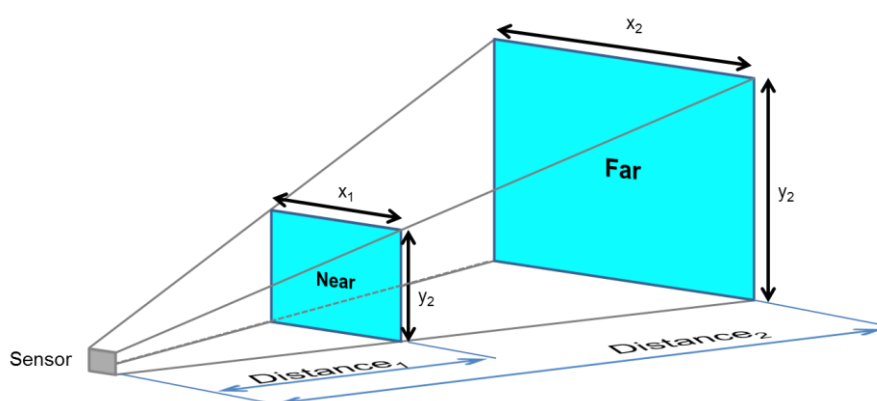
Figure 4-11 – Changing camera field of view based on distance from sensor

The three dimensional 'calibrated measurement volume' is constructed from the fields of view from each camera. Measurement volume is adjusted by increasing the measuring distance and the camera separation to ensure the camera views converge at the desired point (Figure 4-12) although a larger volume can be

attained by altering sensor parameters. The lens aperture is used to create a suitable depth of field: a distance range, in front of and behind the focused plane, within which the difference in focus is imperceptible, enabling sharp images of three dimensional moving objects in this space to be obtained.
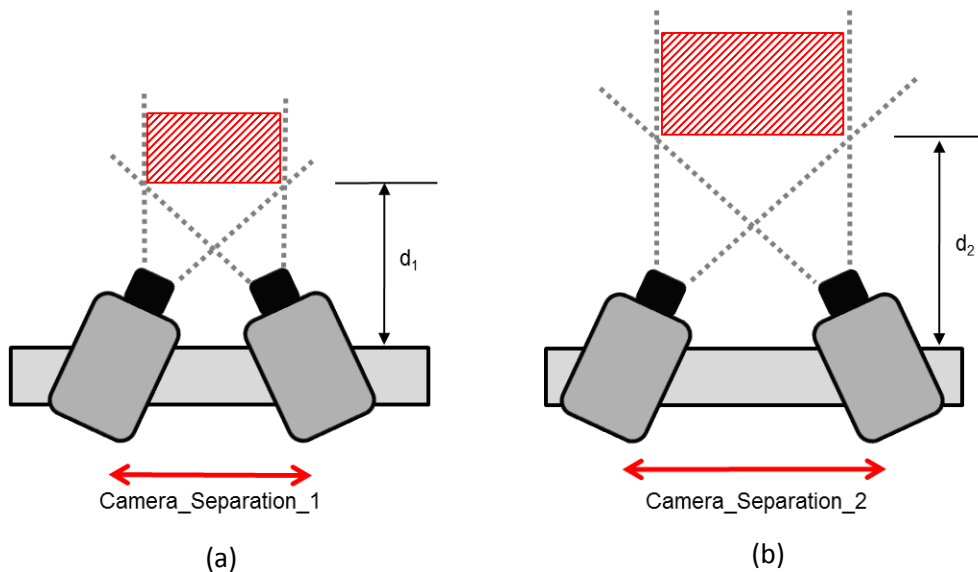
Figure 4-12 - Creating different sized measurement volumes (a) small volume (b) larger volume (Plan view). Hatched areas indicate the measurement volume created by the camera set ups .

4.4.4. System Calibration

The calibration procedure involves placing the artefact at positions around the volume in order for the markers on the surface of the artefact to be recorded. The markers are recognised in the ARAMIS software through the recorded images and are used to calculate the different parameters as well as a base for calculating the calibration error.

The GOM ARAMIS system presents the calibration error as an 'intersection deviation' value (measured in pixels) by taking the calculated 3D points, defined on the calibration artefact, and calculating them back to 2D image points. With prior knowledge of the positions of reference points the deviation can be determined. For the ARAMIS system to compute measurements for shape and deformation, average deviation across the volume must be between 0.01 and 0.04 pixels.

4.4.5. Measurement Process

A basic flow diagram for DIC-3D measurements is shown in Figure 4-13 outlining the basic set up and measurement steps involving a single camera pair.
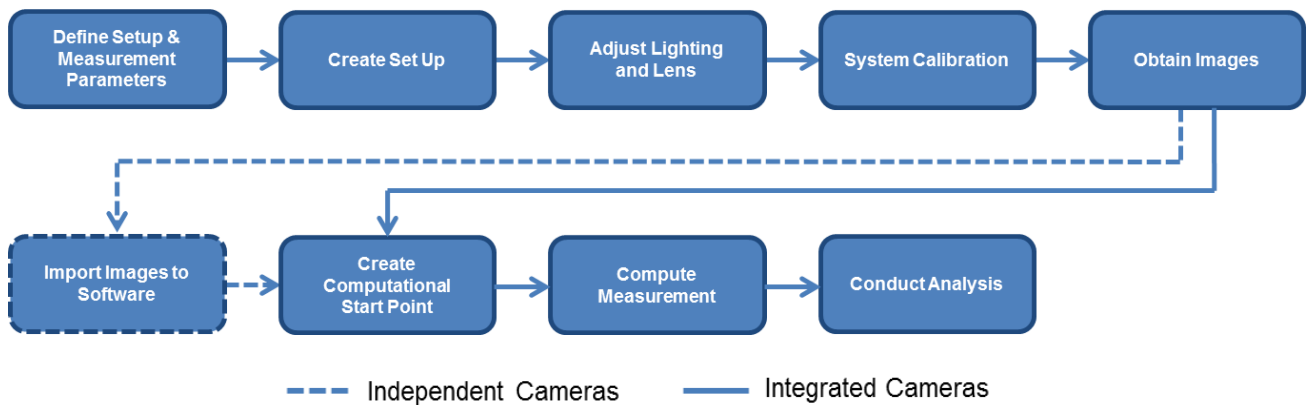
Figure 4-13 - Flow diagram for DIC-3D measurements

When independent cameras are used, recorded images must be loaded into a project in the software along with a valid calibration file (created through system calibration). The user must define in pixels the facet (subset) dimensions and computational step size that will be used for the computation. These can be changed at any point, but the project must be recomputed for changes to take effect in the measurements.

A computational 'start point' must be defined in the software, which defines the first facet in the reference stage (1st image) from which the creation of data points will begin. More than one start point is sometimes needed in measurements where boundaries or breaks on the surface of interest and/or pattern occur. Once defined, the project can be computed and shape and deformation measurements are made, which can be further analysed in a different mode of the same software.

4.5. Validation of GOM ARAMIS

4.5.1. Overview

Validation is the "provision of objective evidence that a given item is adequate for an intended use" (International Organization for Standardization, 2007). Validation was more than just considering the accuracy of measurements via a calibration, although this could form a part of the validation, it would establish the suitability of GOM ARAMIS for use in the application of dynamic foot shape and deformation measurements i.e. the fitness for purpose and was based on the application and the measurement requirements outlined in Chapter 3.

The validation was divided into two separate areas: firstly, whether the system is capable of capturing data appropriately (data capture) and secondly related to the quality of the measurement made. As an outline, in terms of data capture, for the proposed application, the measurement system should be capable of:

DC1 - *Making measurements from the skin surface*

DC2 - *Measuring foot surfaces of interest for the entire of the foot strike for any running style*

50

DC3 - Making a suitable number of measurements over the footstrike to represent foot shape temporally

DC4 - Achieving individual measurement duration short enough to assume the foot is stationary

DC5 - Making measurements at a rate that deformation rate is suitably measured

In terms of measurements, the system should be capable of:

M1 - Measuring three dimensional shape

M2 - Measuring full field surface deformation to a suitable resolution

M3 - Measuring magnitude of deformation to a level expected to be experienced

M4 - Measuring surface shape accurately

M5 - Measuring deformation accurately

M6 - Measuring surface shape repeatably

M7 - Measuring deformation repeatably

The validation was conducted using the twelve defined points defined as a basis. Appropriate experimental means were employed as well as theoretical discussion where experimental application was not required, each of which will be described in the following sections. In both cases, discussions have been supported by empirical data where possible.

4.5.2. Data Capture Validation

Data capture validation is discussed by sequentially working through points DC 1-5.

DC1. <u>*Making measurements directly from the skin*</u>

To enable the most accurate measurements, it was imperative that measurements were made directly from the foot surface, i.e. from the skin. Covering the foot (with a sock for example), would potentially cause errors in shape measurements through the material 'bridging' across contours of the foot. More importantly, it was likely that the foot surfaces would move independently beneath a material covering, introducing error in deformation measurements. Furthermore a covering may even support the foot, preventing the adoption of natural shapes, creating further errors.

The ability to make measurements directly from the skin was dependent upon a suitable pattern being applied. As a validation activity, a monochrome pattern was applied to the medial foot surface; using non-toxic water based paints (Snazaroo, Minehead, UK) and measured using the ARAMIS system. To ensure a suitable pattern contrast a white base layer was firstly applied before 'grey' features were added; suitably

sized for the measurement volume employed (approx. 500 mm x 500 mm x 500 mm). The painted surface once applied did not inhibit movement or restrain the skin or the foot movement in any way.

ARAMIS measurement results (Figure 4-14) show that surface could be measured appropriately using this approach, meaning representative foot shape measurements could be made. It was noted that the pattern did smudge/rub off relatively easily and so the paint used would need to be adapted for areas where interactions may occur, for example on the plantar surface of the foot.

Figure 4-14 - ARAMIS surface measurement results, denoted by blue region, for painted pattern applied to surface of foot.

DC2. *Measuring foot surfaces of interest for the entire of the foot strike for any running style*

To be measured, foot surfaces needed to be imaged and remain in camera view throughout the footstrike. For the dorsal foot surfaces this could be accomplished presumably with ease no matter the running style, as surfaces are not obstructed, although optimum camera placement needed to be established to ensure that surfaces remain in the camera view throughout the movement. Measurement of plantar surfaces had been achieved in other shape measurement studies by placing cameras beneath a transparent platform (Kimura et al. 2008; Schmeltzpfenning et al., 2010) so that the surface can be imaged. This could be replicated using an ARAMIS system; however optimum camera placement would need to be established. Suitable measurement volumes can be created to contain the foot and its movements, however to measure the full foot shape, separate surface measurements would need to be made via a series of stereoscopic camera pairs positioned around the foot. In this approach, foot movements would be imaged synchronously, creating a set of individual measurements that can be collated into one, composite, shape measurement at a post processing stage.
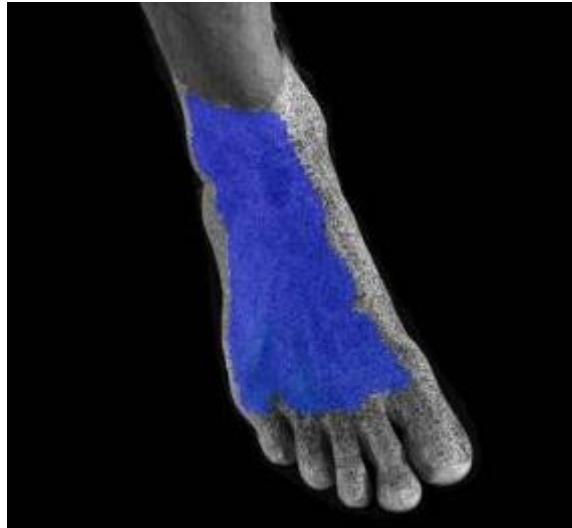
Figure 4-15 - Attempted surface measurement of toes. ARAMIS surface measurement results denoted by blue region

As shown in the ARAMIS surface measurement results in Figure 4-15 (shown in blue), it is not possible to make measurements across the toes due to the discontinuity between the surfaces; furthermore, due to the narrowness of the toes, it is not possible to create enough data points to make a surface measurement at the measurement volumes used. This was, however, acceptable as the surface of interest outlined in the requirements in chapter 3 was those approximately proximal to the MPJ.

DC3. *Making a suitable number of measurements over the footstrike to represent foot shape temporally*

The number of individual measurements should adequately describe the foot shape temporally as well as creating a resolution that ensures measurements are made at, or sufficiently close to events of interest during the foot strike, e.g. peak loading or toe off.

As runner velocity increases, the time spent in stance reduces, with a duration of approximately 0.1 seconds for elite sprinters running at 9 ms^{-1} compared to approximately 0.4 seconds when walking at 1.2 ms^{-1} (Novacheck, 1998). Hence, for different running speeds, a different imaging frequency would be required to achieve the same number of individual shape measurements. At all velocities a minimum of 50 individual measurements was deemed an appropriate number to properly represent the foot strike, which would be a measurement at 2% intervals of the whole footstrike.

Velocity	Footstrike Duration (secs)	Measurement Separation (for 50 stages) (ms)	Equivalent Capture Rate (fps)	Max Achievable Capture Rate (fps)
Walking (1.2 ms^{-1})	0.4	8.0	125	500 (integrated) 5400 (independent)
Sprinting (9 ms^{-1})	0.1	2.0	500	500 (integrated) 5400 (independent)

Table 4-2 – Parameters to achieve minimum number of individual measurements

The imaging parameters required to achieve this, for the maximum and minimum velocities, are summarised in Table 4-2, which shows that for the imaging hardware available, when using integrated or independent cameras, the desired number of measurements could be achieved.

DC4. *Achieving individual measurement duration short enough to assume the foot is stationary*

To achieve a suitable level of accuracy in the dynamic measurements, it was deemed that movements of the foot during a measurement should not exceed 0.5 mm as this would be the approximate width/height a single pixel on the CCD (based on a 1024 x 1024 resolution) would sample at the image plane for a 500 x 500 x 500 mm measurement volume. To inform the minimum required measurement duration (shutter speed), the velocity of the foot surfaces regions were measured.
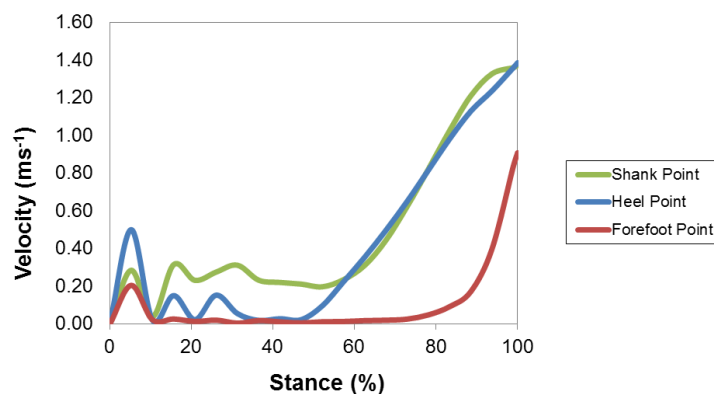
Figure 4-16 - Velocity profiles for three points located on the medial foot surface during running

Markers were placed at three locations on the medial foot surface: on the shank proximal to the ankle, on the heel and at the MPJ joint. The markers were tracked using PONTOS (GOM, Braunschweig): a three dimensional point tracking system, during steady running ($\approx$3.3 ms^{-1}) and the velocities calculated from the three dimensional displacement data, between touchdown and toe off. Ethical clearance was obtained by Loughborough University Ethical Advisory Committee and informed consent was obtained (See Appendix A).

The results showed that the proximal foot regions exhibited the highest velocities in the latter stages of stance, during heel lift as the foot unloads in preparation for the swing phase of gait. At the measured running speed, velocities did not exceed 1.5 ms^{-1} and for the majority of stance (due to the stationary position of the foot during loading) velocities were significantly lower.

At the maximum velocities measured (1.5 ms^{-1}) shutter speeds of between 0.3 and 0.4 ms would be required to ensure movement was within 0.5 mm. This was within the capabilities of both integrated and independent camera systems, each of which had capacity to reach shutter speeds as short as 0.01 ms, which equates to a foot velocity of 50 ms^{-1} to exceed the 0.5 mm movement; a velocity the foot was unlikely to reach during stance, even as an elite sprinter. The selection of shutter speed would however need to be optimised in line with the lighting needed to illuminate the foot surface, as more light is required as the exposure time decreases.

DC5. *Making measurements at a rate that deformation rate is suitably measured*

The measurement rates outlined in Table 4-2 show that the separation in measurements is less than a hundredth of a second. Due to the nature of the application, the likelihood of meaningful deformation occurring within this time region is low, due in part to the fact the foot moves such a small amount between individual measurements (DC4). Therefore for the proposed application it can be assumed with confidence, whether integrated or independent cameras are employed, that the rates of deformation will easily be covered by the ARAMIS system.

4.5.3. Measurement Validation

Validation of measurements is discussed in the following sections by discussing points M1-7 outlined in §4.5.1 sequentially.

M1. *Measuring three dimensional shape*

The ARAMIS system would be applied as a DIC-3D system, employing a stereoscopic camera pair. Therefore, with this approach, three dimensional surface shape measurements would be made from captured data. This also meant that deformations occurring in three dimensional space would be measured from the shape measurements. Sample measurements made for DC1 (§ 4.5.2) show that three dimensional surface measurements, specifically for the foot, are possible.

M2. *Measuring full field surface deformation measurement to a suitable resolution*

The resolution of deformation measurements would be determined by the separation of data points (object points) created on the surface of interest, which is a result of the computational step size, sensor resolution and the measurement volume dimension (based on camera field of view) (§ 4.3.2).

Deciding a suitable resolution was difficult without prior knowledge of exactly what deformation was likely to occur and therefore a sensible approximation was needed. Considering the approximate measurement volumes likely to be employed ($\approx$500 mm x 500 mm x 500 mm) a maximum data point separation of approximately 5 mm was deemed appropriate. ARAMIS would comfortably achieve this, for the approximate measurement volume discussed and employing a standard camera resolution of 1024px x 1024px, with a computational step size of approximately 10-pixels. At this level it also meant smaller resolutions could be achieved, if necessary, by reducing the step parameter, providing a good flexibility in measurements.

M3. *Measuring magnitude of deformation to a level expected to be experienced*

In more traditional measurement devices, prior knowledge of the magnitude of a measurement is important to ensure that it does not exceed the measurement capabilities of a device. In the case of ARAMIS, large deformations (>100%strain) can be accommodated due to the way measurements are derived, so long as

the pattern does not degrade with a deformation to a point where the pattern measured cannot be associated with pattern measurements made previously.

Measurement of the medial and lateral foot surfaces during a linear run were made to establish the approximate levels of deformation occurring (Figure 4-17), as well as to test pattern degradation. Visual inspection of results show deformations occurring within 30%strain, well within the system capabilities.
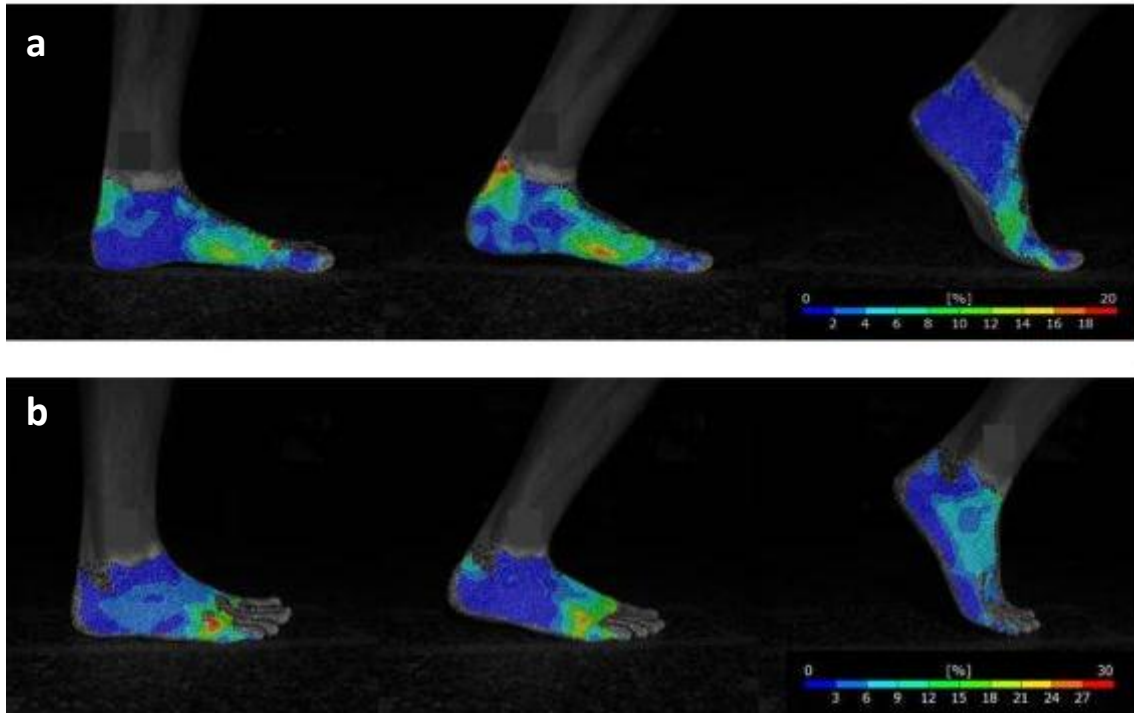
Figure 4-17 - Deformation measurements for (a) medial and (b) lateral foot surfaces at three points in the stance phase

M4. _Measuring surface shape accurately_ AND M5. _Measuring deformation accurately_

The shape and deformation measurement accuracy of the ARAMIS system is dependent upon a number of factors, due to the multi-faceted nature of the DIC measurement methodology. There is not a single overarching accuracy value that can be placed on a system, as many changes can be made to the setup, hardware and processing parameters, as well as the fact measurement accuracy is essentially a function of the size of the calibrated volume and camera resolution. Therefore some form of calibration measurement is needed to understand accuracy of the ARAMIS system for shape and deformation measurements. Due to the complexity, this falls outside the scope of this particular section of the thesis and will be discussed and investigated further in proceeding chapters.

M6. _Measuring surface shape repeatably_

To assess the repeatability of the ARAMIS system's shape measurements, six measurements were made of the medial surface of a three dimensional static foot shape (Figure 4-18): five on day one and a sixth on day two. Within day (intra-day) repeatability was assessed by comparing four of the measured surfaces to the

fifth measurement which acted as a reference, between day (inter-day) repeatability was evaluated by comparing the measured surface from day two with the same reference surface used for within day repeatability.

Figure 4-18 - Additive manufactured static foot shape used for repeatability measurements

Results from the comparison of the measured surfaces (Table 4-3) show low variability for inter- and intra-day measurements, indicating that the ARAMIS system measurements are as repeatable between days as it is within day. A portion of the error observed between measurements could have been the result of the error in the analysis, i.e. the repeatability in the processing to obtain a measurement, however, as the error between measurements was so low, it was considered unnecessary to attempt to investigate this further.

	Mean Error (mm)	Standard Deviation
Intra-Day Comparison	0.003	0.032
Inter-Day Comparison	0.004	0.030

Table 4-3 - Surface comparison results testing intra-day repeatability (Comparisons 1-4) and inter-day repeatability (Comparison 5)

M7. _Measuring deformation repeatably_

Measurement of repeatability is reliant on being able to provide the same 'input' to be measured. In the case of shape this is easily achieved as shown in M6, however creating a repeatable deformation to be measured by the ARAMIS system is a complex problem, which like M4 and M5, falls outside the scope of this particular section and will be covered in more detail in proceeding chapters of the thesis.

4.6.   Chapter Summary

This aims of this chapter were to address OBJ_4 and OBJ_5 as outlined in §1.1: objectively select a suitable measurement technology, understand how measurements are derived and to validate it as a suitable tool for the desired application.

Digital image correlation (DIC), a form of photogrammetry, was selected as the measurement technology and the system in which it was embodied was the ARAMIS system manufactured by GOM (Braunschweig, Germany). The decision was based on comparison with other measurement technologies, namely: structured light, laser scanning and time of flight technologies. The ability to derive a surface deformation measurement from shape measurements, with relative ease, was one of the key points in the decision.

To provide a base for understanding, the principles of DIC have been outlined as well as description of the ARAMIS system measurement process and associated terminology. The ARAMIS system has been validated as a measurement tool for the proposed application based upon twelve criteria: five of which relate to the capturing of measurement data and seven of which relate to the measurement results. Validation was based on both theoretical discussion and experimental means, and showed excellent capabilities for the measurement of shape and deformation of the foot in the validation criteria outlined, with flexibility to cater for changes in test parameters such as running velocity and running style.

Assessment of shape and deformation measurement accuracy and deformation measurement repeatability was not completed as part of this validation. This was due to the fact that the manufacturer does not provide calibration values for either, as there are numerous setup and hardware options for the ARAMIS system that will potentially affect the accuracy of a measurement. Conducting an 'in house' calibration would rely on the creation of shapes and deformations with known magnitudes, against which ARAMIS system measurements could be compared to establish accuracy. In addition, the repeatability of deformation measurements was not assessed due to the need for a deformation with known magnitude to be created in a repeatable way. The complexity of these tasks would require detailed explanation and discussion as well as experimental development which fell outside the remit of this chapter and therefore will be covered as a separate chapter of this thesis.

Although some further detailed assessment of system performance is required, this chapter has shown that the ARAMIS system, embodying the DIC technology, is a suitable measurement system for measurement of dynamic foot shape during running.

5. Calibration of Digital Image Correlation Measurements

5.1. Introduction

Digital image correlation (DIC) has been selected as a suitable technology for the measurement of dynamic foot shape during the support phase of running gait. The validation of the GOM ARAMIS DIC system highlighted that due to the measurement flexibility of the system, there is no set accuracy value for shape and deformation measurements. Understanding the accuracy of a measurement is imperative to facilitate meaningful analysis; without this understanding the worth of a measurement can be seriously affected. It is equally important to understand which variables affect the accuracy of a measurement, especially when components of a methodology can change; this is relevant to DIC methodology which has a number of hardware and methodology variables that can be changed to achieve a measurement.

System accuracy is determined by comparing a measured output with a known input. A shape calibration determines the system's ability to reconstruct surface points accurately and is relatively simple to assess, through the measurement of an artefact of a known shape. A deformation measurement encompasses the measurement system's ability to match and accurately track a deforming surface pattern between images. This is slightly more difficult to accomplish, as a known deformation needs to be created in order to compare against the measurement results.

Currently there are no recognised procedures for calibrating DIC systems, or any other optical instrument, for deformation measurement (Patterson et al., 2007), despite the extensive use of 2D and 3D DIC systems in industry and research. The difficulties lie in establishing a traceable calibration, calibrating measurements that record full-field, dynamic measurements (Hack, Patterson, Siebert, & Thalmann, 2010).

Attempts to fill the void in standards have been made (Patterson et al., 2007), however the reference material defined in these methods and calibration artefacts are limited to low level (μstrain), static, planar deformations, rendering them unsuitable for this application where deformations are likely to be much higher in magnitude. Without a suitable method, there is no way to, firstly, assess accuracy and secondly, understand the effect of particular methodological variables such as hardware and processing components.

The aim of the work covered in this chapter was to establish the accuracy of the DIC measurement system used for proceeding experimental work (to determine its suitability) (OBJ_5) and to understand how relevant variables of the method and measurement, which can be directly controlled by a user, affect measurement accuracy (OBJ_6). This would be achieved by developing and implementing an experimental method for calibrating deformation measurements made by a DIC system, in addition to implementing a suitable shape measurement calibration, each of which would be considered separately.

Although methods would potentially be applicable in a wider setting, the work carried out in this chapter was limited to the parameters, setups and hardware related to measurement of the human foot during the running.

5.2. System Calibration vs. Measurement Calibration

A measurement calibration is the comparison of an output from a measurement device or system against an input with a known magnitude. In this case, a known deformation or strain state.

Commercially available DIC systems have a 'system calibration' step which is typically conducted prior to a measurement. For a 3D-DIC system, system calibration enables image points on the camera's CCD to be transformed to the corresponding 3D coordinates of that point (Becker, Splitthof, Siebert, & Kletting, 2006). The discrepancy of the transformation constitutes the calibration error, which is generally derived through the measurement of a panel with a printed grid or a marker array of known dimensions. This calibration does not form a calibration of the measurement, but instead quantifies a part of the error source for the entire measurement error. Usually, this error is quantified by a value, which a system manufacturer will recommend to be within a particular range.

To prevent confusion and to distinguish between the two calibrations, 'system calibration' will refer to the calibration process for reconstruction errors, usually integrated into the measurement process chain, whereas 'measurement calibration' will refer to the error assessment of the measurements as a result of error sources introduced through the measurement process.

5.3. Calibration Outline

5.3.1. Objectives

To aid in the development of the calibration methodologies, as well as to qualify the success of the calibration measurements as a whole, it was necessary to define a calibration objective, i.e. to define a measurement calibration target error value or range.

For the consideration of a 'calibration target' a two tiered approach was adopted through the definition of a 'preferred' and an 'acceptable' calibration value. For deformation measurement calibration, in terms of percentage strain (i.e. the measured deformation value) the 'preferred' target was set to be within ±0.5% strain and the 'acceptable' target set to be within ±1.0% strain. With a view to three dimensional shape measurements, a measurement error (i.e. accuracy) of ±0.5 mm was set as the 'preferred' target and ±1mm measurement error as the 'acceptable' error range.

These values helped inform the suitability of methodology components, namely material measure design, as well as enabling a quantifiable measure of the success of a measurement calibration.

5.3.2. Measurement Ranges

It was important to ensure that the deformation calibrations would be made for deformations that are at a relevant magnitude to those expected to be observed during a footstrike. There was an obvious flaw in calibrating for micro strain, if in practice much larger deformations are to be observed. Maximum deformations in the foot region have been shown to be in the region of 25-30% strain (§4.5.3), therefore it was considered sensible to calibrate for maximum deformations of up to 50%strain.

5.3.3. Selection of Test Variables

There are a number of separate variables that can potentially influence the accuracy of a measurement via the introduction of error at points in the measurement process chain. Error sources can be grouped into two categories: errors associated with the measurement quality and errors associated with the correlation principle itself (Haddadi & Belhabib, 2008). Measurement quality is associated with the imaging parameters and the environment whereas the errors associated with correlation are parameters generally linked to the surface pattern and the way it is sampled when imaged. A list of relevant variables associated with each is presented in Table 5-1.

Associated with Measurement Quality	Associated with Correlation Principle
1. Sensor Parameters	8. Correlation functions/algorithm
2. Imaging parameters	9. *Surface pattern
3. Field of view/pixel sampling	10. *Facet Size
4. Lens focal length	11. *Subset grid pitch (step size)
5. Lens aperture	12. *Rotation of deformation
6. Lighting	13. *Position in volume
7. Environment	14. *Deformation magnitude
	*Selected as a test variable

Table 5-1 – Relevant error source variables for DIC

The system calibration manages the errors linked to equipment and working environment; measurements will only be made if the system calibration result is within the range defined by the manufacturer. If variables from this category are changed, for example lens type, then a system calibration within the acceptable range must be achieved to enable measurements to be made. If it is ensured that system calibration results are within the recommended range defined by the manufacturer, it can be presumed that the effect of changing these variables will be negligible. With this reasoning, the effects of variables associated with measurement quality were not considered for testing.

Considering the variables associated with the correlation principle (Table 5-1), as testing would be conducted using only one system (GOM ARAMIS), comparing DIC systems and their specific algorithms fell outside the scope of this work. Any settings related to the correlation principle within the software were set at manufacturer default values. The remaining seven variables, which could be controlled by a user (9, 10 and 11), or were a normal variation in a test (12, 13, 14), were selected as test variables in order to investigate their effect on measurement accuracy.

5.3.4. Control Variables

Variables that had not been selected for testing were held constant between all tests, as outlined in Table 5-2. These were selected to replicate the approximate measurement environment and parameters that would be employed in the deformation measurement of feet and footwear. Additionally, a number of these parameters would contribute to the definition and design of particular features of material measures and therefore it was important these were clearly defined at this stage.

Variable	Value
3D-DIC System	GOM ARAMIS
Camera/CCD	Photron SA1.1 (1024px x 1024px, 20µm pixel)
Camera Capture parameters	1000 fps, 1/10,000 shutter speed
Measurement volume size	360 mm x 360 mm x 360 mm (approx.)**
Lens Type	50 mm focal length (prime lens)
Lens aperture	f16
Lighting	Same source and intensity
Environment	Lab environment - not controlled (effect considered negligible)

**See Appendix B for calculation of parameters to achieve measurement volume.

Table 5-2 – Control variables and values for planar deformations tests

5.4. Material Measure: Deformation

5.4.1. Overview

As outlined in the previous chapter, deformation measurements are measured two dimensionally tangential to the surface of an object, therefore all measured deformations essentially occur in a planar manner on the surface of an object, even when an object may be deforming in three dimensions (Figure 5-1). For this reason, calibration of deformation measurements was conducted for planar deformations and to simplify a material measure design, body deformation occurring in two dimensions.
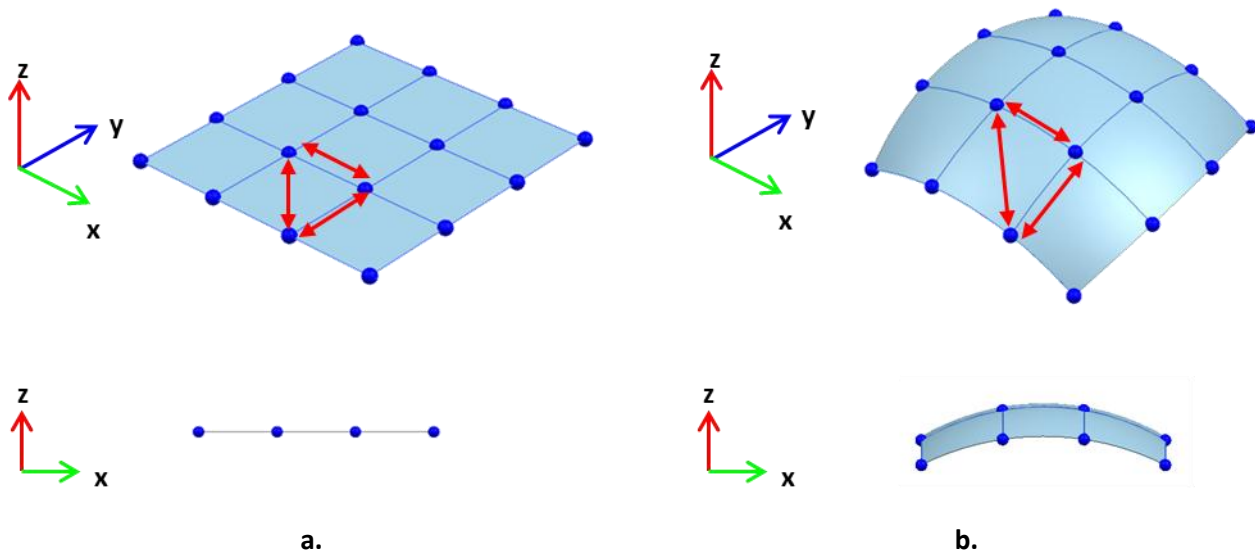
Figure 5-1 – Deformations measured by DIC tangential on a surface for an object deformation occurring (a) two dimensionally and (b) three dimensionally. Blue dots represent data points on the surface measured by DIC.

In order to establish confidence in the values delivered by the calibration methodology, the reference deformations, against which measurements are compared, must have a known accuracy. This is usually known through a traceability chain: a series of measurement standards that allow the accuracy of a measurement to be traced back, via a hierarchy of calibrations, to a national or international standard (Hack et al., 2010) (Figure 5-2).

The test equipment measurements, in this case of the 3D-DIC system, are made using a 'working standard' in the form of a 'material measure'. The material measure is 'a device intended to reproduce or supply, in a permanent manner values of a given quantity' (Hack, Burguete, & Patterson, 2005), in this case, deformation values. The material measure facilitates a meaningful measurement calibration by being traceable, via an appropriate measurement, back to a suitable standard level, i.e. the inaccuracy of the material measure is known. The final uncertainty measurement that is obtained through a calibration is the sum of the inaccuracy of the material measure, plus the uncertainty contributions that are a result of the measurement process.

Strain, which is the quantity that will be used to reflect deformation is derived from a relative change in length and DIC essentially measures length changes to compute strain; length therefore is the obvious measurement chain for traceability (Patterson et al., 2007) especially for large deformations.
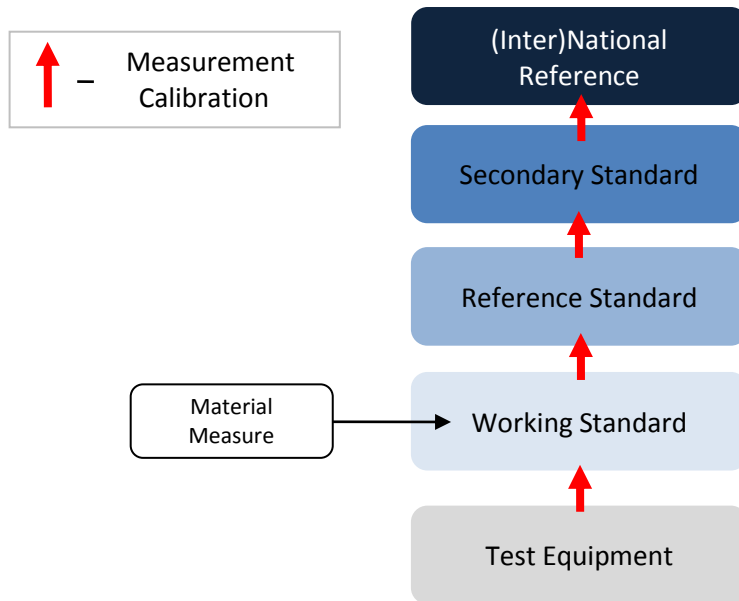
Figure 5-2 – Calibration hierarchy and traceability chain

5.4.2. Material Measure Design

A material measure for DIC deformation measurement calibration, according to Hack *et al.* (2005), should:

- Represent a strain field adapted to the imaging property of the technique.
- Reproduce in a permanent manner during use one or more known values of strain.
- Repeatedly reproduce strain states from an unstrained to a strained state.
- Create one or more strain states by a deformation that is displacement controlled.

An advantage of the material measure design in this work when compared to previous work (Patterson et al., 2007) was that the material measure need only be suitable for use in a DIC application and need not be adapted for other optical strain measurement systems.

Attempting to design a material measure from a physical material that would deform predictably to predetermined strain levels was deemed outside the scope of this research work; a more suitable, more simple solution devised was to use a simulated strain. In this approach the material component of the deformation was removed. Instead of creating a physical deformation, it was simulated by creating and 'deforming' a synthetic pattern. This approach is similar to that used by Fazzini *et al.* (2010), however, instead of capturing real images of a synthetic pattern deforming on a screen, images were captured of physical printed patterns simulating 6 discrete stages of deformation between 0 and 50% strain.

This approach enabled precise control of the deformation, through the absolute control of synthetic pattern dimensions and 'deformation' magnitudes. As the deformation was based on length measurement, through the change in pattern dimension, this enabled traceability of the material measure and due to measurement

type, calibration of full field measurements was also possible. Furthermore, use of a synthetic pattern enabled full control of the pattern properties and, because deformation was simulated, potential issues and errors associated with referencing, mounting and orienting a sample for example, were completely avoided.

5.4.2.1. Pattern creation

To determine the dimensions of the speckle pattern, its features and the print resolution, the area of the object plane sampled by each pixel on the camera sensor needed to be established; based on the optical set up parameters required to achieve the desired measurement volume. This calculation is based on the field of view at the centre of the volume divided by the number of pixels on the sensor.

Based on the camera CCD pixel resolution and the measurement volume (§5.3.4) it was determined that each pixel at the image plane (CCD) would sample approximately 0.35x0.35 mm (0.12 mm^2) at the object plane; a plane parallel to the image plane at the centre of the measurement volume. Pattern features were defined to be a minimum of four times this area (≈0.49 mm^2) so as to be oversampled to achieve accurate measurement of deformations (Sutton et al., 2000). The print resolution to print a single feature of 0.12 mm^2 was established to be approximately 72 dots per inch (dpi) (2.84 dpmm), hence a 2x2 pixel block, at this resolution, would achieve the pattern feature with an area of 0.49 mm^2.
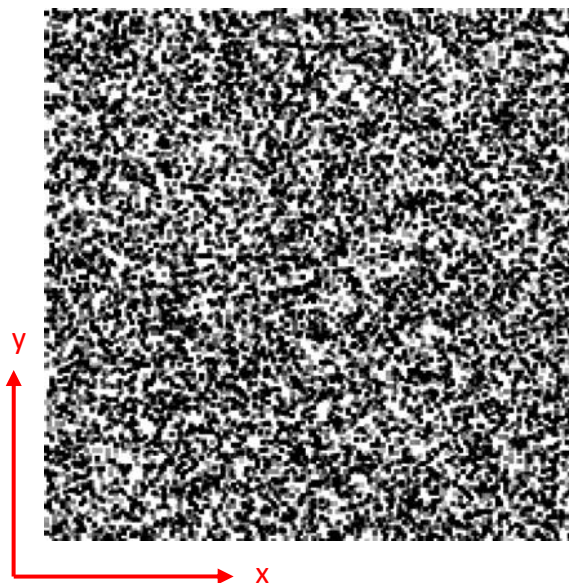
Figure 5-3 – (a) Synthetic speckle pattern example to scale (May not be to correct resolution if printed)

Speckle patterns were created using a custom Matlab (Mathworks, USA) code which allowed the definition of pattern size, number and size of pattern features and the greyscale value range of the pixels for each feature created (Appendix C). A pattern was created at a size of 200x200 pixels as shown in Figure 5-3, which at 72dpi equated to a 'test specimen' of approximately 70.55 mm x 70.55 mm at the reference stage prior to a deformation.

5.4.2.2. Pattern Characterisation

To test the influence of the pattern variable on measurement accuracy (§5.3.3), three different patterns were created for testing; each pattern varied in level of greyscale and white pixel content. For each pattern the ratio of greyscale (non-white) to white pixel content was calculated as a way of characterising each pattern. To represent the ratio across the whole pattern, the pattern was subdivided into an array of subsets, 10 x 10 pixels in size, with a 5 pixel overlap, and a ratio for each subset was calculated, the 'average subset ratio' for the whole pattern was then calculated using Equation 5-1

$$Average\ Subset\ Ratio = \frac{\sum_1^n(Ratio\ of\ white\ to\ non\ white\ in\ subset)_n}{n}$$ Equation 5-1

Patterns with an average subset ratio (non-white:white) of approximately 60:40, 70:30 ('normal') and 80:20 were created (Figure 5-4). All ratio measurements were made for the pattern in the undeformed state.
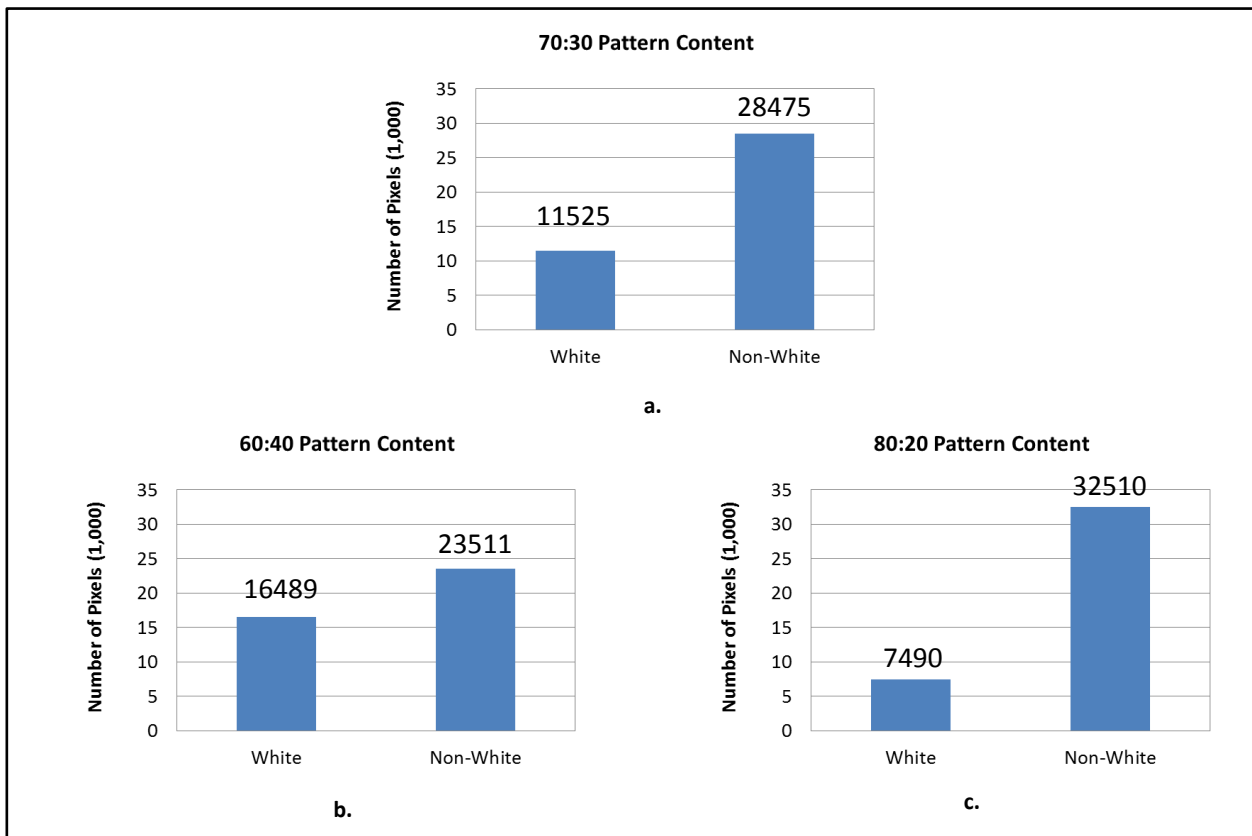
Figure 5-4 – Pattern content of non-white to white pixels for (a) 70:30 (b) 60:40 and (c) 80:20 patterns. (Total pixels in each pattern is 40000)

5.4.2.3. Pattern Deformation

To aid in accurate deformation of the pattern, once fully created, the resolution of the pattern image was increased by a factor of 10 using Adobe Photoshop (San Jose, USA) image editing software. The result was

that every original individual pixel comprised of 100 smaller pixels, each pixel with dimensions of 0.012x0.012 mm (≈0.049 mm^2), requiring a printing resolution of the image 720 dpi (28.3 dpmm).

Deformation stages of 0, 10, 20, 30, 40 and 50% strain were created by deforming the created pattern in the y-direction using the same image editing software. To induce a simulated deformation, the size of the image needed to be increased whilst maintaining the same resolution. To achieve this, the image was resampled after it had been resized. To create the 10%strain state for example, the image size was increased in the y-direction by 10% from 70.56 mm to 77.62 mm and the number of pixels was increased by 200 pixels from 2000 pixels to 2200 pixels.

Resampling was conducted using the 'nearest neighbour' interpolation algorithm within the software, meaning the cumulative effect of deforming each 10x10 pixel block by 10% created exactly one new pixel in the direction of deformation. Therefore, the exact deformation across the entire of the pattern could be maintained, whilst remaining within the acceptable limits of printing technology.

5.4.2.4.   Embodiment

The patterns for each deformation stage were incorporated into a 'speckle pattern board' (SPB) design, shown in Figure 5-5, which also integrated calibration lines, added after 'deformation' in the imaging software, to facilitate the calibration of each board (§ 5.4.3) as well as circular markers for alignment of each deformation stage. The board designs were printed on an Epson (Suwa, Japan) 11880 inkjet printer at 1440dpi; twice the new pattern resolution, so as to oversample the print resolution and attain the highest printed accuracy.
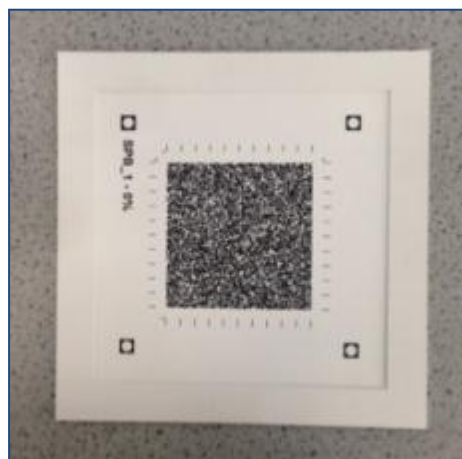
Figure 5-5 - 0% Deformation Stage Speckle Pattern Board (SPB)

5.4.3. Material Measure Calibration

The material measure SPB panels, for the three pattern types at every deformation stage, were calibrated through the measurement of the speckle pattern dimensions using a SmartScope Flash 200 multi sensor

optical measuring machine (OMM) (Rochester, USA). The measurement machine had been calibrated with traceability to the National Institute of Standards and Technology (N.I.S.T) with the length measurement error a function of the length measured (L), defined as:

$$Error\ (mm) = \left(0.002 + \frac{6L}{10^6}\right) \text{(eq. 7)}$$

	Def. Stage (%strain)	Average Measured Length (mm)	Machine Error (mm)	Corrected Length Ave (mm)	Designed Length (mm)	Average Error (mm)
SPB_1 (70:30)	0	70.706 (±0.002)	0.002	70.704	70.556	0.148 (±0.002)
	10	70.740 (±0.002)	0.002	77.738	77.611	0.127 (±0.002)
	20	84.821 (±0.002)	0.003	84.818	84.667	0.151 (±0.002)
	30	91.861 (±0.002)	0.003	91.858	91.722	0.136 (±0.002)
	40	98.930 (±0.002)	0.003	98.927	98.778	0.149 (±0.002)
	50	106.035 (±0.002)	0.003	106.032	105.833	0.199 (±0.002)
SPB_2 (80:20)	0	70.715 (±0.002)	0.002	70.713	70.556	0.157 (±0.002)
	10	77.737 (±0.001)	0.002	77.735	77.611	0.124 (±0.002)
	20	84.831 (±0.002)	0.003	84.828	84.667	0.161 (±0.002)
	30	91.950 (±0.001)	0.003	91.947	91.722	0.225 (±0.001)
	40	99.008 (±0.001)	0.003	99.005	98.778	0.227 (±0.001)
	50	106.065 (±0.001)	0.003	106.062	105.833	0.229 (±0.001)
SPB_3 (60:40)	0	70.651 (±0.002)	0.002	70.649	70.556	0.093 (±0.002)
	10	77.756 (±0.002)	0.002	77.754	77.611	0.143 (±0.002)
	20	84.866 (±0.002)	0.003	84.863	84.667	0.196 (±0.002)
	30	91.924 (±0.002)	0.003	91.921	91.722	0.199 (±0.002)
	40	98.987 (±0.002)	0.003	98.984	98.778	0.206 (±0.002)
	50	106.082 (±0.002)	0.003	106.079	105.833	0.246 (±0.002)

Table 5-3 – Length measurement results for each stage of each SPB after correction for OMM error.

Ten separate measurements of the total pattern length were made along the axis of deformation for each pattern type and deformation stage panel and an average pattern length was calculated, shown in Table 5-3. OMM measurements were corrected for the machine error, calculated using equation 7 for each stage and panel, with values between 0.001 and 0.003 observed.

The results showed that each pattern appeared to be printed slightly longer than designed by approximately 0.1 - 0.25 mm. The cause of the error could not be determined, the likelihood of it being a localised edge error was rejected as at the print resolution, the error would have equated to between 20 and 40 extra pixels. Bleeding of material on the print substrate was observed, but again not to a magnitude that would explain the error. It was assumed therefore, that the error was cumulative across the whole pattern and deformation values would need to be adjusted accordingly for the actual printed lengths.

The standard deviations for the pattern length measurements (Table 5-3) demonstrated that the metrology system was able to measure the pattern length to a high level of repeatability. However, inevitable bleeding of the printed ink on the paper substrate meant that there was error associated with the OMM defining the edge of the pattern. Determining the magnitude of this error would enable it to be allowed for in the calibration measurement.
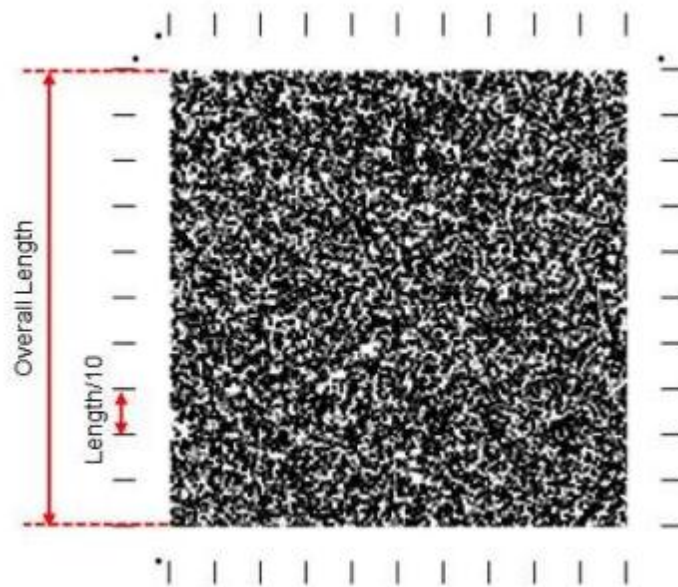
Figure 5-6 - Overall and theoretical divided length measurement definitions using pattern calibration lines

Distances between the printed calibration lines around the perimeter of the patterns were measured on each board along the deformation axis. Measurements were made for the ten divisions created by the calibration lines and compared with the theoretical separation calculated as one tenth of the total pattern length (Figure 5-6). Any edge detection error incorporated as part of the whole pattern length measurement

was divided by ten and therefore was deemed negligible in the measurements. The results for each pattern board type are shown in Table 5-4.

Pattern Board	Mean Error (mm)	s.d (mm)
SPB_1 (70:30)	0	0.013
SPB_2 (80:20)	0	0.013
SPB_3 (60:40)	0	0.010

Table 5-4 – Edge detection error mean and standard deviation for each SPB panel

An Anderson-Darling (A-D) statistical test was applied to the data for each board type in order to test whether the error measurements were drawn from a normal distribution. The null hypothesis is that the data is from a population with a normal distribution, with the null hypothesis rejected for p-values less than a significance level of 5%. The test was conducted using an inbuilt function within the Matlab software (Mathworks, USA), the results for which are shown in Table 5-5.

SPB Type	p-value	Null Hypothesis Rejection
SPB_1 (70:30)	0.93	No
SPB_2 (80:20)	0.52	No
SPB_3 (60:40)	0.07	No

Table 5-5 - Anderson-Darling statistical test results for each pattern board type

The results show that the edge measurement error for all three board types could be considered to be normally distributed and that 95% of edge detection errors would fall within two standard deviations of the mean. Consequently, with a 95% confidence, the maximum error in a length measurement as a result of the edge detection error would be ±0.026 mm for SPB_1 and SPB_2 and ±0.020 mm for SPB_3, which at the print resolution of 1440dpi, was the equivalent of approximately one 1pixel at either end of the pattern.

Detailed calibration results for each deformation stage panel for each pattern type are shown in Table 5-6, Table 5-7 and Table 5-8. The results showed a relatively consistent error across all strain states for all boards, with mean strain values within 0.15% of the designed strain. The replication of strains was comfortably within the preferred calibration target value, outlined in the objectives (§ 5.3.1) and therefore all material measures were deemed suitable for use in the calibration method for deformation measurements.

70:30 Def. Stage (%)	Measured Length (± edge detection) (mm)	Minus Edge Detection Error (mm)	Plus Edge Detection Error (mm)	Min Material Measure Deformation (%strain)	Max Material Measure Deformation (%strain)	Calibrated Deformation (%strain)
0	70.704 (±0.026)	70.678	70.730	0	0	0
10	77.737 (±0.026)	77.711	77.763	9.87	10.02	9.95 (±0.08)
20	84.818 (±0.026)	84.792	84.844	19.88	20.04	19.96 (±0.08)
30	91.858 (±0.026)	91.832	91.884	29.83	30.00	29.92 (±0.08)
40	98.927 (±0.026)	98.901	98.953	39.83	40.01	39.92 (±0.09)
50	106.032 (±0.026)	106.006	106.058	49.87	50.06	49.97 (±0.09)

Table 5-6 – Calibration Results for SPB _1 (70:30)

80:20 Def. Stage (%)	Measured Length (mm)	Minus Edge Detection Error (mm)	Plus Edge Detection Error (mm)	Min Material Measure Strain (%strain)	Max Material Measure Strain (%strain)	Mean Theoretical Strain (%strain)
0	70.713 (±0.026)	70.687	70.739	0	0	0
10	77.735 (±0.026)	77.708	77.760	9.85	10.01	9.93 (±0.08)
20	84.829 (±0.026)	84.802	84.854	19.88	20.04	19.96 (±0.08)
30	91.948 (±0.026)	91.21	91.973	29.94	30.11	30.03 (±0.08)
40	98.928 (±0.026)	98.979	99.031	39.92	40.10	40.01 (±0.09)
50	106.062 (±0.026)	105.036	106.088	49.90	50.08	49.99 (±0.09)

Table 5-7 – Calibration Results for SPB_2 (80:20)

60:40 Def. Stage (%)	Measured Length (mm)	Minus Edge Detection Error (mm)	Plus Edge Detection Error (mm)	Min Material Measure Strain (%strain)	Max Material Measure Strain (%strain)	Mean Theoretical Strain (%strain)
0	70.649 (±0.020)	70.629	70.669	0	0	0
10	77.753 (±0.020)	77.733	77.773	10.00	10.11	10.06 (±0.06)
20	84.863 (±0.020)	84.843	84.883	20.06	20.18	20.12 (±0.06)
30	91.921 (±0.020)	91.901	91.941	30.04	30.17	30.110 (±0.07)
40	98.984 (±0.020)	98.964	99.004	40.04	40.17	40.11 (±0.07)
50	106.079 (±0.020)	106.059	106.099	50.08	50.22	50.15 (±0.07)

Table 5-8 – Calibration Results for SPB_3 (60:40)

5.5. Material Measure: Shape

5.5.1. Overview

Shape artefacts are available for calibrating three dimensional shape, however, most are aimed at calibration of co-ordinate measurement machines (CMM) rather than optical systems in both shape and size. In addition, the requirement to apply a pattern to the surface of an artefact will affect the calibrated values to some extent, which may potentially need to be accounted for.

The approach in this shape calibration work was to manufacture and then calibrate a shape artefact using a separate (suitable) measurement system with a traceable calibration (§5.3.2). This artefact could then be measured with the DIC system and the two surfaces compared to establish the measurement accuracy before testing the effect of selected variables.

5.5.2. Material Measure Design and Embodiment

A sphere was selected as an appropriate three dimensional shape used for the shape calibration artefact (SCA). The SCA was designed as a dome shape as shown in the CAD images in Figure 5-7 (fully dimensioned drawings can be found in Appendix D), as it would not be possible to image the entire surface of a sphere. To aid in the accurate alignment of calibrated scan and surface measurement data, two flat surfaces were created on the domed surface at 120° separation radially, removing any rotational degrees of freedom that may introduce error during alignment.
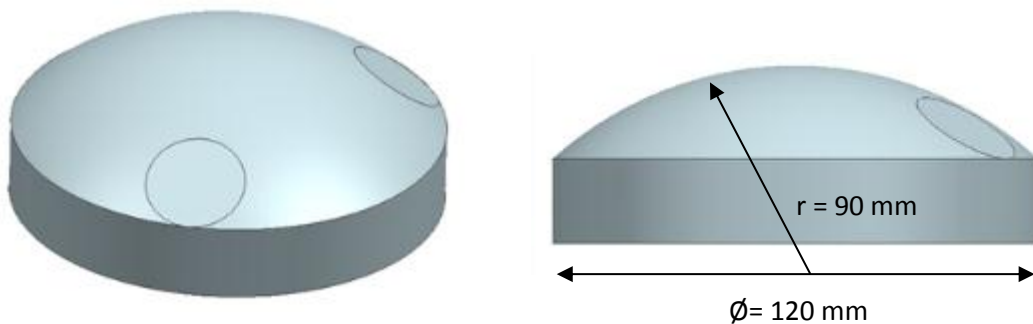
Figure 5-7 - CAD Images of shape calibrarion artefact (SCA) (Not to scale)

The radius of the SCA dome surface was set at 90 mm and manufactured on a lathe from aluminium. A layer of white paint was applied to the surface to enable a contrasting pattern to be created. Greyscale 'speckles' were applied with a permanent marker pen so as to control the size and consistency of the feature's sizes in line with the pattern parameters outlined in §5.4.2.1. A manufactured SCA with surface pattern applied, is shown in Figure 5-8

Figure 5-8 - Manufactured and surface prepared SCA

5.5.2.1. Pattern Characterisation

Two pattern types were created for testing, a low grey content pattern and a high grey content pattern; each was achieved by the size and separation of pattern features applied to the surface with marker pens. To characterise the patterns a single image was captured of each SCA when positioned such that the base was approximately parallel to the imaging plane of one camera. A circular section, at the centre of the SCA was used to characterise the pattern so as to counter any error caused by the surface curvature (Figure 5-9).
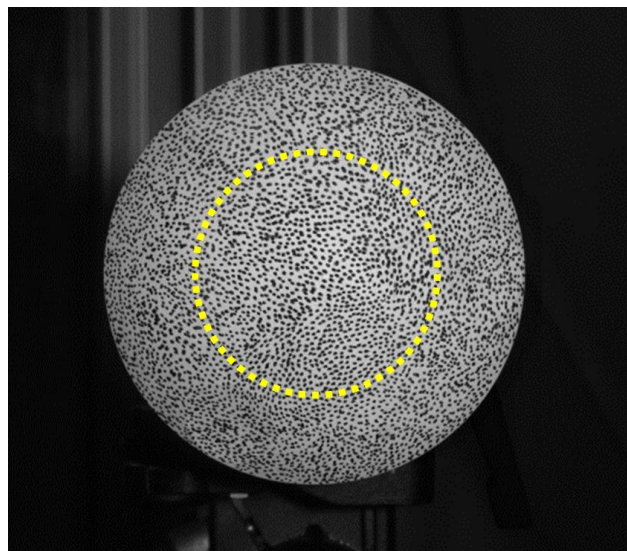
Figure 5-9 – SCA pattern characterisation area

As the white base layer on the SCA was imaged grey, a threshold greyscale value was set to define the white content of the pattern; pixels equal to or above this value were considered white. As with the characterisation of the deformation material measure (§ 5.4.2.2), the SCA pattern was characterised via an 'average subset ratio', with the pattern area divided into an array of subsets 10x10 pixels in size, with an

overlap of 5 pixels. Two pattern types were created, the first with a non-white to white ratio of approximately 40:60, representing the low grey content pattern and the second with a ratio of approximately 60:40, representing the high grey content pattern.
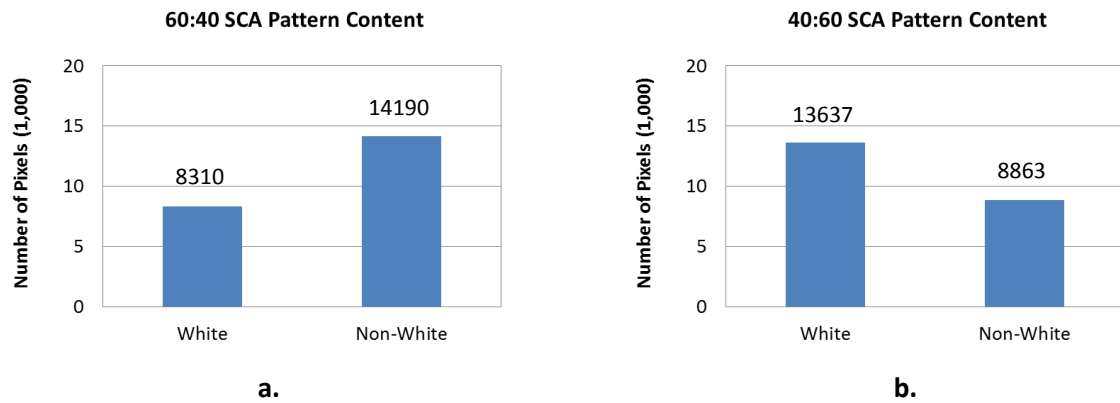
Figure 5-10 – SCA pattern content of non-white to white pixels for (a) 60:40 (b) 40:60 patterns. (Total pixels used for characterisation 22500)

5.5.3. Calibration of Material Measures

Each SCA was scanned using a 2 megapixel ATOS (GOM, Braunschweig) 3D Scanner (Figure 5-11a), which created a point cloud, containing over 35,000 points, describing the surface geometry of each artefact. A surface was created from the point cloud data (Figure 5-11b) and then exported as a g3d file, which could be used as a digital reference for comparison with ARAMIS surface measurements, forming the calibration. This surface will be referred to as the digital reference surface (DRS).
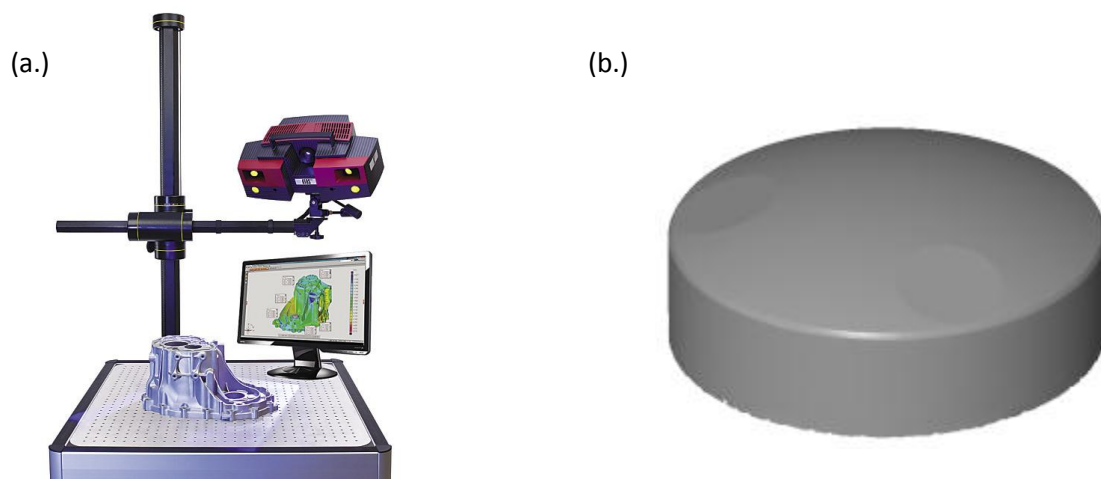
Figure 5-11 – (a) GOM ATOS 3D Scanner (from Madison (2012)) and (b) the digital reference surface

The ATOS scanner used was subject to internal, traceable calibration procedures by the owner GOM UK, who, for the setup used for scanning of the SCA's, quote a measurement error of +0.004 mm (See Appendix

E). To ensure the most accurate shape measurements for calibration, measurements were made after the white base layer had been applied to the surfaces of each SCA. Due to the shape measurements principle behind the ATOS scanner, the grey pattern features were not added until after calibration, the effect of which on the calibration measurement was deemed negligible and therefore ignored.

5.6. Measurement Calibration: Deformation

5.6.1. Overview

The following section concerns calibration of deformation measurements and investigation into the effect of selected variables on measurement accuracy, using the material measures described in §5.5 with the control variables outlined in §5.3.4.

5.6.2. Independent Variable Values

Variable	Value					Default
Deformation Magnitude (%strain)	10	20	30	40	50	50
Facet size (px)	10x10	15x15	20x20	25x25	30x30	20 x 20*
Step Size (px)	5	9	13	17	21	13**
Pattern	60:40 greyscale content (SPB_3)	70:30 greyscale content (SPB_1)		80:20 greyscale content (SPB_2)		Normal greyscale content
Orientation of deformation in plane (Orientation relative to sensor plane)	0° (parallel)	0° (angled)	45° (parallel)		45° (angled)	0° (parallel)
Position in volume	4 x corner positions at back of volume	Centre of Volume		4 x corner positions at front of volume		Centre of Volume

*Facet size of 25x25px used for step size tests. ** Step size of 9px used for facet size tests

Table 5-9 - Test variables values for planar deformation conditions

The independent variables and their associated values for the testing are summarised in Table 5-9. These values define how each variable would be altered to assess the influence on the accuracy of measurements. When not being tested, the variable was set to a default value, defined in the table, ensuring only the effect of one variable was tested.

Facet and step sizes were selected to provide a realistic range of computational parameters for the field of view and the material measure designed. Three pattern types were tested with varying grayscale content (§5.4.2.2). For other variables, attempts were made to test the best and worst case scenarios. Direction of deformation was considered rotation relative to the sensor plane. Two deformation directions were studied, in line with the pixels of the CCD sensor and at 45° to the pixels of the CCD sensor. In addition, the plane of

deformation was studied parallel to the image plane and at a 45° angle to the image plane for both directions of deformation. In a similar approach, nine positions were identified for testing of deformation location within the calibrated volume, one at the volume centre and then eight at the corner extremities as shown in Figure 5-12.
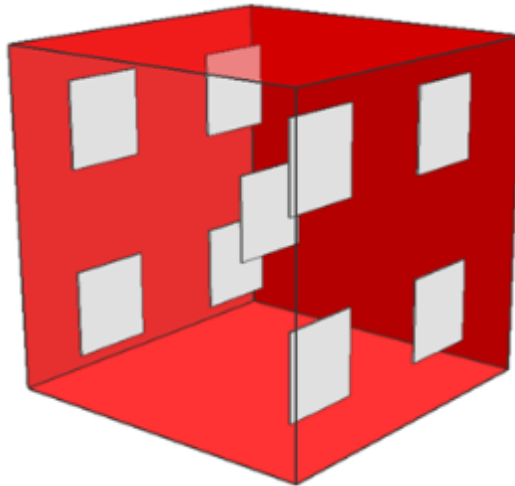
Figure 5-12 – Measurement locations across the calibrated volume for the positional variable

5.6.3. Measurement Methodology

The cameras were set up in line with manufacturer's guidelines and setup properties outlined in §5.3.4 in order to achieve the correct field of view for each camera with common field of view centre points. A system calibration was conducted prior to measurements, ensuring the error was within the range recommended by the manufacturer (§4.4.4).
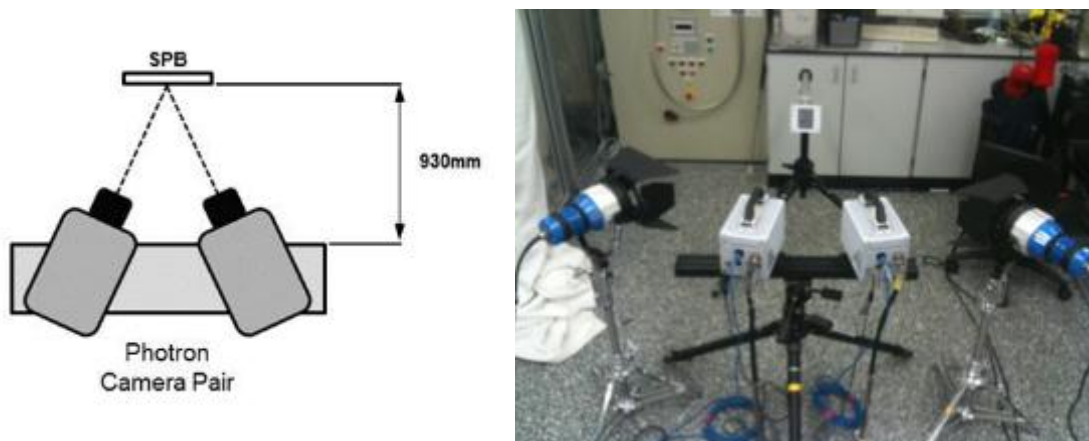
Figure 5-13 - Calibration test experimental setup schematic (left) and physical setup (right)

The SPB panels were mounted on a tripod at the centre of the camera views, as shown in Figure 5-13 and sequential images of each deformation stage were captured by changing the SPB. Additional lighting was

supplied by two ARRI (Munich, Germany) spotlights, which were set up to achieve optimum lighting of the measurement volume in conjunction with lens aperture and camera shutter speed. SPBs were only placed in front of lights for short periods of time so as to minimise any effects of heating of the pattern boards.

The same SPBs were used for all measurements (except those testing pattern type) making the results readily comparable. Sequential images of each state of deformation were captured by the Photron camera software and then imported into the ARAMIS software where analysis was made. Location and rotation of the boards in the positions around the volume was facilitated by a mount on an adjustable arm.

5.6.4. Data Analysis Methodology

The analysis approach for this work was to firstly establish a system's measurement accuracy at the default settings and then to test how this measurement accuracy was affected by changing each of the specified test variables (§5.3.3).

Hack et al. (2010) identified that DIC measurement calibration is not as simple as calibrating single measurement systems for metrics such as length or weight due to the full field nature of the measurement. Comparing individual point measurements between tests at common locations across the deformation surface is not easily achieved, as it is difficult to precisely locate the same point on a surface between measurements, due to the optical way measurements are made. Furthermore the number of data points that can be created in a measurement presents an additional challenge, as a single DIC measurement may consist of many hundreds of individual data points.

Evaluation of measurement accuracy, along with the analysis of the effect of specific variables, was therefore facilitated by considering distributions of measurements and not individual values. Measurement accuracy was defined by the distribution of measurement error: the difference between deformation measurements and the SPB calibration value (from § 5.4.3). Using suitable statistical tools, comparison of the error distributions of different measurements (e.g. changing step/facet size), allowed the effect of a selected variable on measurement accuracy to be established. A significant difference in distributions would indicate a significant difference in the accuracy of a measurement, as a result of the changing variable.

Comparison of distributions was conducted using a two sample Kolmogorov-Smirnov (two-sample K-S) test, a nonparametric test that compares the cumulative distributions of two data sets, testing the probability that the two data sets are sampled from the same distribution. A p-value is calculated from the maximum difference between the cumulative distributions (K-S statistic) and the sample size. The p-value gives the probability that if the two samples were randomly sampled from the same population the distributions would be as far apart as observed. The smaller the p-value the more likely data sets are from populations

with different distributions, conversely, the larger the p-value the more likely data sets are from populations with the same distributions.

The null hypothesis that the data sets were drawn from populations with the same distribution was rejected for p-values equal to or below a 5% level of significance 0.05. If the null hypothesis was not rejected, it could then be concluded that the measured distributions have the same underlying distribution and therefore the variable did not affect the measurement accuracy.

5.6.5. Results and Analysis

Measurements were made using the parameters outlined in section §5.3.3 and §5.3.4. Measurement data was exported from the software and analysed as detailed in §5.6.4 using Matlab (Mathworks, USA) software. The results are presented in the following sections.

5.6.5.1. Measurement Accuracy

The measurement accuracy results, presented in Table 5-10 show that the measured mean was very close to the calibrated mean for each deformation stage, with similar standard deviation values. The measurement error distribution for the 50% deformation stage, shown in Figure 5-14 as an example, shows the data appeared to be distributed in a Gaussian shape as one would expect to observe with a normal distribution.

An Anderson-Darling (A-D) statistical test was employed to test whether the data for each stage was drawn from a normal distribution, with the null hypothesis rejected at a significance level of 5%. The p-value results of the A-D tests, (Table 5-10); show that the null hypothesis was accepted for all deformation stages meaning the errors measured for each stage could be assumed to be normally distributed.

Deformation Stage (%strain)	Measured Mean (%strain)	Calibrated Deformation (SPB_1) (%strain)	Mean Measurement Error (%strain)	p-value
10	9.96 (±0.11)	9.95	0.01 (±0.11)	0.575
20	20.01 (±0.13)	19.96	0.05 (±0.13)	0.069
30	29.96 (±0.13)	29.92	0.04 (±0.13)	0.096
40	39.93 (±0.15)	39.92	0.01 (±0.15)	0.166
50	49.95 (±0.15)	49.97	-0.02 (±0.15)	0.098

Table 5-10 – Measurement accuracy results calculated for each deformation stage with p-value results for Anderson-Darling statistical test for normality.
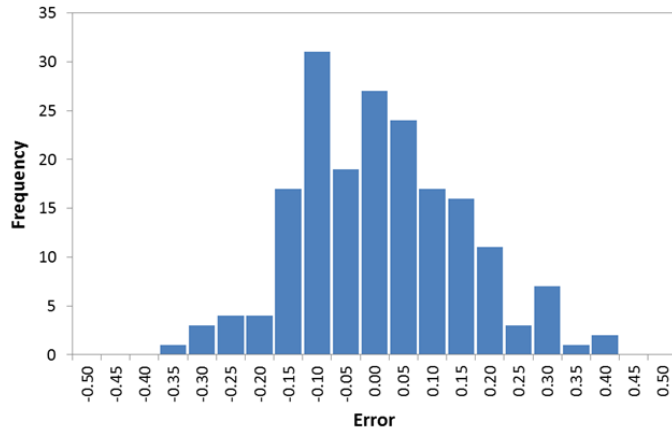
Figure 5-14 – Distribution of measurement error for 50% deformation stage

In the normal distribution 95% of the deformation error measurements at each stage would fall within two standard deviations of the mean. Using this theory, the system measurement accuracy was calculated and the results for which are shown in Table 5-11.

The results for the measurement accuracy at default settings is relatively consistent across all deformation stages, with mean error close to zero and within ±0.5%strain at a 95% confidence interval. It can be concluded from the results that the mean system measurement error at default settings, across the deformation range studied is within ±0.4%strain which is within the preferred calibration objective set out in § 5.3.1.

Deformation Stage (%strain)	Measured Mean (%strain)	Calibrated Mean (%strain)	Mean Accuracy (%strain)
0	0	0	0
10	9.96 (±0.22)	9.95 (±0.08)	0.01 (±0.30)
20	20.01 (±0.26)	19.96 (±0.08)	0.05 (±0.34)
30	29.96 (±0.26)	29.92 (±0.08)	0.04 (±0.34)
40	39.93 (±0.30)	39.92 (±0.08)	0.01 (±0.38)
50	49.95 (±0.30)	49.97 (±0.14)	-0.02 (±0.44)
Mean measurement accuracy:			0.02 (±0.34)

Table 5-11 – Measurement accuracy results for each deformation stage at a 95% confidence for measured deformations and incorporating edge detection error for calibrated deformations.

Unfortunately it is not possible to compare these calibration values to other published work as full field calibrations of large deformations have not been published to date. GOM, the manufacturer of the DIC system, quote an accuracy of strain measurement up to 0.01% strain (GOM, 2009b), but there is no disclosure of the setup and parameters to achieve this value or whether this is a best case scenario.

5.6.5.2. Deformation Magnitude

The statistical results for the two sample K-S test, comparing measurement distributions at each deformation stage to that of the 50% deformation stage are presented in Table 5-12. The results show that the null hypothesis was rejected in all but one of the deformation stages indicating that measurement accuracy is dependent upon the deformation magnitude being measured as the error distributions are significantly different.

Deformation Stage	10%	20%	30%	40%
p-value	0.011	<0.001	<0.001	0.141

Table 5-12 - p-values from a two sample K-S test comparing error distributions at each deformation stage relative to the 50% deformation stage.

Inspection of the measurement error at each deformation stage (Table 5-11) shows that similar standard deviations were observed between magnitudes and that the slightly different means may explain the rejection of the null hypothesis. To test this, the measurement error distributions for each deformation stage were 'translated' so that the mean error for each was equal to zero. The two sample K-S test was repeated, using the 50% deformation stage as a reference, the results of which show (Table 5-13) that the null hypothesis was not rejected for any comparisons. These results suggest the measurement accuracy distributions are the same, they are just translated with respect to one another. As the difference in the mean measurement errors between each deformation magnitude is so small, is can be assumed in a practical sense, that measurement accuracy is not affected significantly by the deformation magnitude.

Deformation Stage	10%	20%	30%	40%
p-value	0.459	0.886	0.780	0.499

Table 5-13 - p-values from a two sample K-S test comparing translated error distributions at each deformation stage relative to the 50% deformation stage.

5.6.5.3. Position in Volume

Measurement error distributions from the 50% deformation stage were used to compare measurements from nine positions around the calibrated measurement volume. The statistical analysis (Table 5-14) shows that for positions at the extremities of the volume, when compared with the deformation occurring at centre, the null hypothesis was not rejected. Consequently, it could be assumed that all measurements were drawn from the same distribution and that measurements made around the volume were comparable and measurement accuracy was not affected.

Position	Mean Error (%strain)	s.d. (%strain)	p value
Centre	-0.02	0.15	-
Front Top Left	-0.02	0.15	0.541
Front Top Right	0.00	0.14	0.387
Front Bottom Left	-0.03	0.13	0.502
Front Bottom Right	0.00	0.11	0.161
Back Top Left	-0.03	0.12	0.167
Back Top Right	-0.04	0.13	0.146
Back Bottom Left	-0.03	0.14	0.584
Back Bottom Right	0.00	0.132	0.522

Table 5-14 - p-values from two sample K-S tests comparing error distributions at the 50% deformation stage between measurements made at different locations within the measurement volume relative to the centre position measurement.

5.6.5.4. Deformation Type and Rotation

Error distributions were made for four rotation conditions: parallel to the image plane rotated in-plane at 0° and 45° and angled 45° to the image plane rotated in-plane at 0° and 45° (Figure 5-15), with comparisons made at the 50% deformation stage at the centre of the volume. The p-value from the two sample K-S tests, shown in Table 5-15, confirmed that the rotation of the deformation did not affect the measurement accuracy as the null hypothesis was not rejected in any test.

Deformation Type	Mean Error (%strain)	s.d. (%strain)	p value
0° parallel	-0.02	0.15	-
0° angled	0.00	0.14	0.138
45° parallel	0.01	0.12	0.165
45° angled	0.00	0.14	0.135

Table 5-15 - p-values from two sample K-S tests comparing measurement error distributions at the 50% deformation stage for different deformation rotations with comparisons made relative to the 0° parallel condition
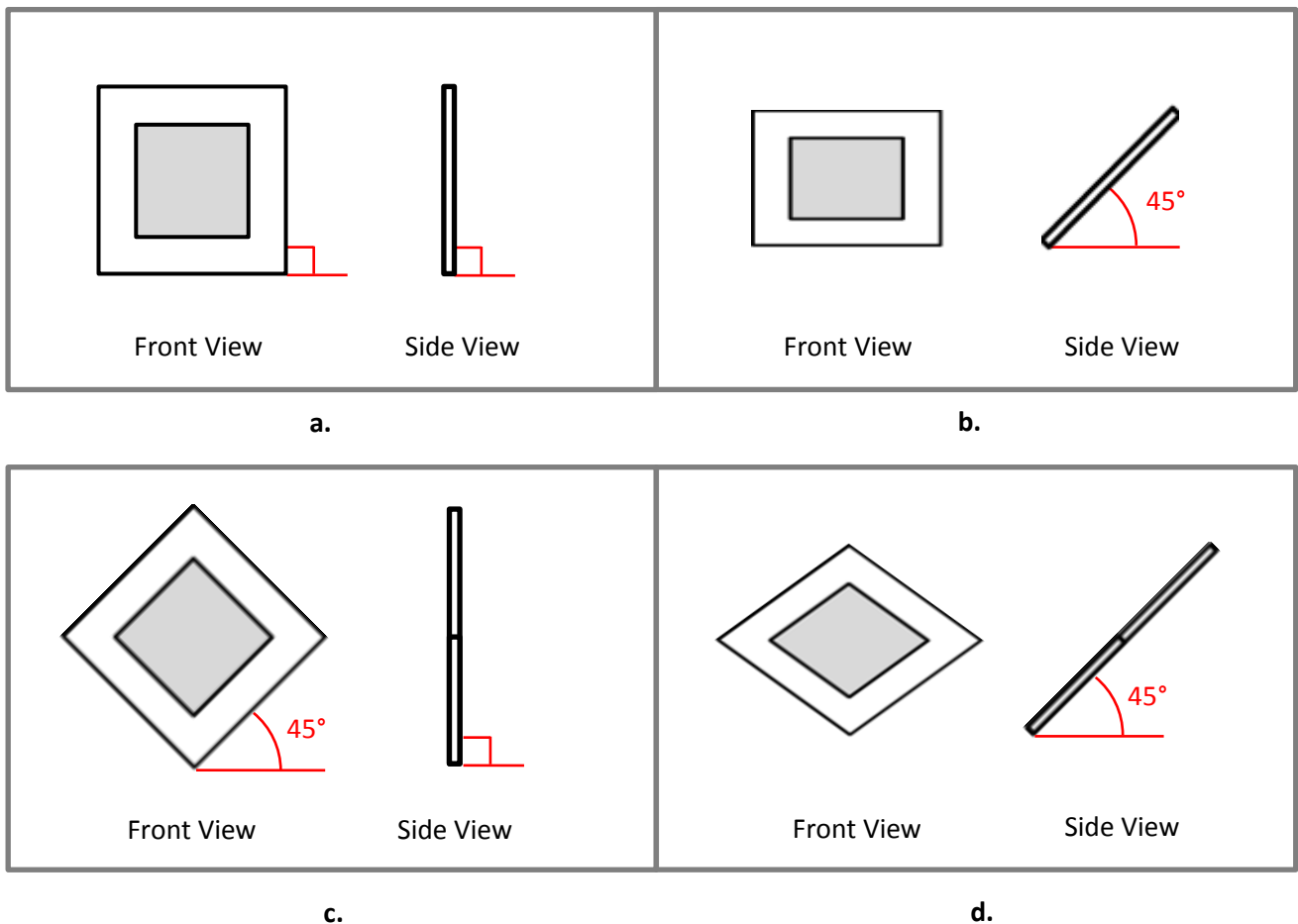
Figure 5-15 – Rotation conditions from front and side views of SPB (a) 0° parallel (b) 0° angled (c) 45° parallel (d) 45° angled

5.6.5.5. Computational Step Size

Step sizes were increased from 5 to 21 pixels in 4 pixel increments for a facet size of 25x25pixels, to assess the influence of both an increase and decrease in step size from the 13pixel default. Error measurements at each step size were computed for the 50% deformation stage, positioned at the centre of the volume. The results of the K-S tests (Table 5-16) show that measurement accuracy was not affected by increasing the computational step size, as the null hypothesis was not rejected. For the smallest computational step size, the null hypothesis was rejected signifying a significant difference in the measurement error distributions.

The mean measurement error remained consistent between tests; therefore the significant difference at the smallest step size was due to an increase in the standard deviation of the error distribution. As the step size increased, the standard deviation decreased meaning less variation and vice versa.

This changing variation in data is linked to the reconstruction of surface data points and associated errors, from which deformation measurements are derived. The closer the data points are to one another (i.e. smaller step size), the greater the effect that reconstruction errors will have on a deformation calculation, ultimately resulting in a larger standard deviation due to a greater variation in data. Conversely, the larger

the spacing, the lower the effect meaning a smaller standard deviation is observed as the data set is less varied.

Step Size (px)	Approx. Point Separation (mm)	Mean Error (%strain)	s.d. (%strain)	p value
5	1.8	-0.03	0.234	<0.001
9	3.2	-0.03	0.146	0.580
13	4.6	-0.03	0.121	-
17	6.0	-0.03	0.112	0.995
21	7.4	-0.03	0.089	0.734

Table 5-16 - p-values from two sample K-S tests comparing measurement error distributions at the 50% deformation stage for different step sizes with comparisons made relative to the 13px condition

It is likely that if the step size had been increased further, the null hypothesis from the statistical test would have been rejected as the accuracy would have improved beyond that of the reference measurement. Ultimately, the results indicate that the computational step size affects the variation in a measurement; however, measurement accuracy is not affected by computational step size when values are changed by ±4pixels.

Care should still be taken in selection of the computational step parameter; larger step sizes increase the measurement accuracy by reducing variability, but will inevitably cause averaging of steep strain gradients as well as potentially omitting locally occurring deformations. Smaller step sizes enable measurement of more complex deformations; however, measurement variability will increase resulting in less accurate measurements.

5.6.5.6. Facet Size

Facet size was increased from 10 to 30pixels at 5 pixels increments for the 50% deformation stage positioned at the centre of the measurement volume. The p-values, presented in Table 5-17, show that increasing the computational facet size did not affect measurement accuracy as the null hypothesis was not rejected, however at the smallest facet size, the variability in measurement error was increased to a point that distributions were significantly different. The mean measurement errors remained consistent between conditions, indicating that, as with the computational step parameter, facet size affects the variability in measurement error.

Facet Size (px)	Mean Error (%strain)	s.d. (%strain)	p value
10x10	-0.03	0.265	0.007
15x15	-0.03	0.197	0.091
20x20	-0.03	0.162	0.255
25x25	-0.03	0.146	-
30x30	-0.03	0.132	0.803

Table 5-17 - p-values from two sample K-S tests comparing measurement error distributions at the 50% deformation stage for different facet sizes with comparisons made relative to the 25x25px condition

Smaller facet sizes contain less grayscale image data to match and locate surface points on the two dimensional image planes, which in turn results in a less accurate reconstruction of points in three dimensional space, leading to greater variation in measurement error. These errors propagate in deformation measurement calculations resulting in greater variation in deformation measurements.

Despite significantly different distributions being observed for the 10x10px facet, the measurement error is normally distributed (AD-test: p=0.18) and therefore at a 95% confidence is still within the acceptable limits defined (±1.0%strain).

5.6.5.7. Pattern Type

Three patterns of varying grayscale content were compared using deformation measurement error distributions at the 50% deformation stage at the centre of the measurement volume. The statistical test results in Table 5-18 show that the distributions for the different pattern types were not significantly influenced by the changing grayscale content as the null hypothesis could not be rejected.

Pattern Type	Mean Error (%strain)	s.d. (%strain)	p value
SPB_1 - 70-30%	-0.01	0.14	-
SPB_2 - 80-20%	0.07	0.19	0.120
SPB-3 - 60-40%	-0.05	0.20	0.058

Table 5-18 - p-values from two sample K-S tests comparing measurement error distributions at the 50% deformation stage for different pattern types with comparisons made relative to the 70-30% pattern condition

Although the grayscale content will affect the correlation function, at the levels tested this has not been proven to be to a significant level. At increased or reduced grayscale content, however, there will come a point that measurement accuracy will begin to be significantly influenced or (more likely) that measurements will be prevented from being made in particular surface areas. Therefore, ensuring the grayscale content of a pattern applied to a surface is approximately within the range tested in this work, it can be presumed that measurement accuracy will not be affected significantly.

5.6.6. Measurement Repeatability

With known deformation inputs (SPBs), it was possible assess the single system measurement repeatability of surface deformation measurements for intra and inter test sessions, which had been identified in the system validation in Chapter 3. To assess repeatability, a total of six separate measurements were made, five within a single test session on the same day and a sixth on separate day. For the intra-session tests, setup and system calibrations remained the same for measurements, however for the inter-session test a new methodological setup, as described in 5.6.3, was created as well as a new system calibration.

Comparisons were made of measurement distributions using a two sample K-S test at the 50% deformation stage, with the panels positioned at the centre of the measurement volume. Comparisons were made relative to test 1 on day 1. The results, presented in Table 5-19, showed that there was no significant difference in intra and inter-session measurements as the null hypothesis could not be rejected, which indicated that measurements obtained from a single system could be deemed repeatable.

Day	Test	Mean (%strain)	s.d. (%strain)	p value
Day_1	Test_1	49.95	0.15	-
	Test_2	49.98	0.14	0.516
	Test_3	49.94	0.15	0.891
	Test_4	49.95	0.15	0.341
	Test_5	49.95	0.16	0.613
Day_2	Test_1	49.93	0.12	0.111

Table 5-19 - p-values from two sample K-S tests comparing measurement error distributions at the 50% deformation stage for measurements made within session and between test session with comparisons made relative to test_1 on day_1.

5.7. Measurement Calibration: Shape

5.7.1. Overview

The following section concerns calibration of shape measurements and investigation into the effect of selected variables on measurement accuracy, using the material measure described in §5.4 with the control variables outlined in §5.3.4.

5.7.2. Variable Values

Three of the six identified test variables (§5.3.3) were selected to investigate their effect on shape measurement accuracy. Shape rotation and shape size (pertaining to deformation rotation and magnitude) were deemed not applicable to the shape calibration due to the three dimensionality of the material measure used, furthermore, the position in volume test in the deformation calibration tests was not found to affect measurement error. For these reasons, these three variables were not tested.

The selected independent variables, their associated values for the testing and the default values for each variable when not being tested are summarised in Table 5-20. Subset and computational step sizes were selected in line with those used for the deformation calibration measurements and other control variable parameter settings were in line with those outlined in §5.3.4..

Variable	Values					Default
Pattern	Low Gray Content (40:60)			High Gray Content (60:40)		High Gray Content (60:40)
Subset size (px)	10x10	15x15	20x20	25x25	30x30	20x20*
Step Size (px)	5	9	13	17	21	13**

*Facet size of 25x25px used for step size tests. ** Step size of 9px used for facet size tests

Table 5-20 - Test variables and measures for static shape measurement tests

5.7.3. Methodology

The cameras were set up in accordance with manufacturer's guidelines and setup properties outlined in §5.3.4 in order to achieve the correct field of view for each camera. A system calibration was conducted prior to measurements, ensuring the error was within the range recommended by the manufacturer.

The SCA artefacts were positioned at the centre of the measurement volume using a mount, as shown in Figure 5-16. Two ARRI (Munich, Germany) spotlights were used to provide appropriate lighting in conjunction with correct lens aperture and camera shutter speeds. To minimise any effects of temperature

change, exposure to the lighting was for short periods whilst images were captured. Thermal expansion of the aluminium artefacts was deemed negligible.
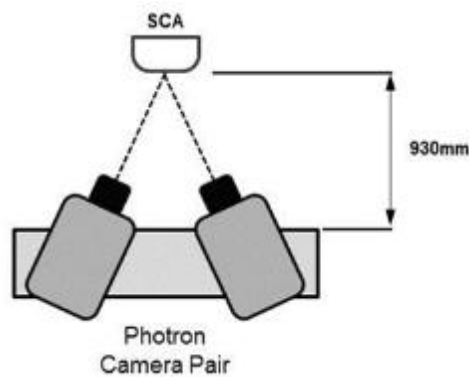
Figure 5-16 - Calibration test experimental setup schematic

Captured images were imported into the ARAMIS software for analysis. Multiple images were captured for each SCA, however, only a single image was used to obtain a shape measurement.

5.7.4. Data Analysis Methodology

The methodology for data analysis followed a similar approach to that used for the deformation calibration, modified to enable comparison of three dimensional points.

3D surface measurements made in ARAMIS were exported as an STL file, which was then imported, along with the digital reference surface (DRS) (§5.5.3), into GOM INSPECT (GOM, Braunschweig), a 3D inspection software. The two surfaces were aligned to one another using an inbuilt least squares fit function and deviations between the two surfaces were calculated.

A scalar resultant error normal to the surface, between the measured ARAMIS surface and aligned digital reference surface (DRS) was computed within the software. As data points between the measured surface and the DRS did not align, a point along the normal line on the DRS was interpolated within the software to calculate a deviation (Figure 5-17). An example visualisation of this comparison is shown in Figure 5-18.
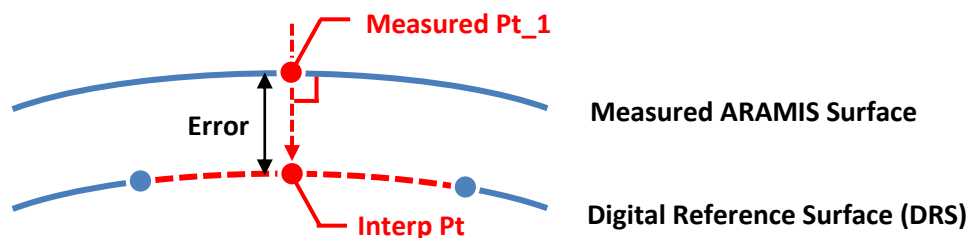
Figure 5-17 – Creation of an interpolated point on DRS surface normal to the measured point to enable the calculation of error between surfaces at that point

A set of approximately 500 deviation data points, from across the surface, were created for each measurement and exported for analysis.

As before, the distribution of the surface deviation was used to determine measurement accuracy with a two sample K-S test, at a significance level of 5%, employed to establish the effect of changing variables on measurement accuracy.
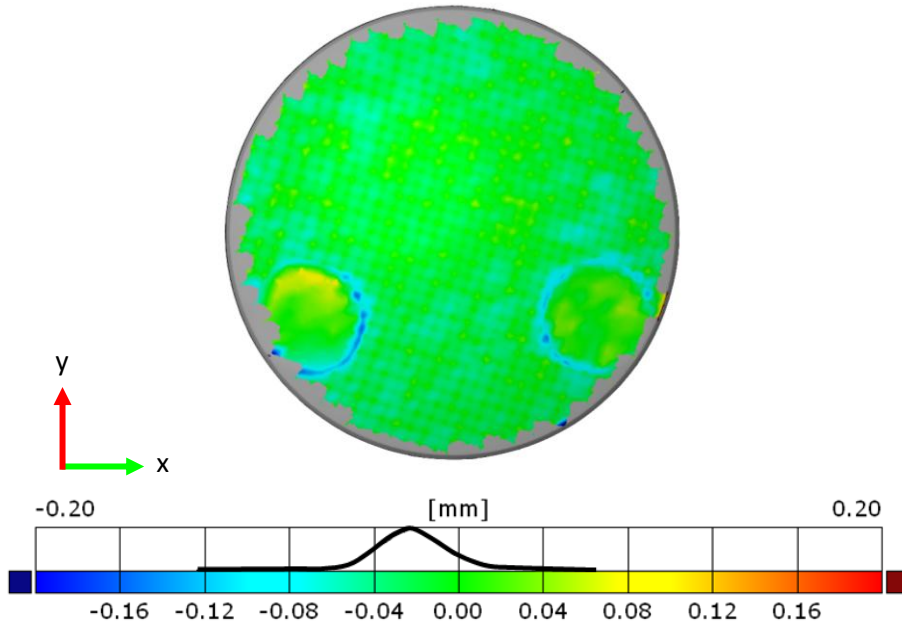
Figure 5-18 – Visualisation of measurement error results for surface comparison of the 90 mm SCA measured ARAMIS surfaces to DRS.

5.7.5. Results and Analysis

5.7.5.1. Measurement Accuracy

Shape Radius	Mean Error (mm)	s.d. (mm)
90 mm	-0.02	0.02

Table 5-21 – Shape measurement error results for 90 mm radius SCA. Mean error is corrected for calibration system error.

The shape measurement error results, presented in Table 5-21 show a mean error slightly below zero, meaning the system appears to measure the shape slightly smaller, with the standard deviation showing a low variation in error measurements around the mean. An Anderson-Darling statistical test confirmed the error data could be assumed to be normally distributed (p=0.523) and therefore 95% would fall within two standard deviations of the mean. As a result it could be concluded that shape measurement accuracy of the DIC system was ±0.04 mm at a 95% confidence, well within the preferred measurement error of ±0.5 mm outlined in §5.3.1. The error is much lower than the 0.8 mm achieved by Pan et al. (2009), although it is likely

that the measurement volume and hence the field of view used by Pan et al. was much greater than that used in this calibration.

It is worth noting that there is an error associated with the alignment of the two surfaces (measured and digital reference), however, based on the results, further investigation was deemed unnecessary.

5.7.5.2. Computational Step

Step size was again increased from 5 to 21 pixels in 4 pixel increments for a facet size of 25x25pixels, to assess both an increase and decrease in step size from the 13pixel default. Measurement error distributions were created for each condition and compared using a two sample K-S statistical test.

Step Size (px)	Approx. Point Separation (mm)	Mean Error (mm)	s.d.	p-value (A-D test)	p-value (2-sample K-S Test)
5	1.8	0.00	0.01	0.752	<0.001
9	2.8	-0.02	0.02	0.734	<0.001
13	4.0	-0.03	0.02	0.103	-
17	5.2	-0.05	0.03	0.057	<0.001
21	6.5	-0.09	0.04	0.113	<0.001

Table 5-22 - p-values from two sample K-S tests comparing shape measurement error distributions for the 9 0mm SCA for different step sizes with comparisons made relative to the 13px condition with p-value results for Anderson-Darling statistical test for normality for each step size condition.

The results (Table 5-22) show that for all step size conditions, the null hypothesis was rejected. Therefore, it can be concluded that 3D shape measurement gets less accurate as step size increases. As the step size determines the number of data points that are created to measure the three dimensional surface, it is understandable a more accurate surface will be measured when more data points are used to create that surface and the converse for fewer. Even though a significant difference in shape measurement is observed between variables, the error is still within ±0.5 mm at a 95% confidence based on the Anderson-Darling test results for each distribution which means 95% of errors will fall within two standard deviations of the mean. The impact on shape measurement accuracy is therefore deemed minimal.

Inevitably, the selection of the step size is a compromise between improved three dimensional shape measurement and the potential introduction of noise into strain measurements as the computational step size decreases, discussed in §5.6.5.5. In practice, for the parameters applied in this work, the effect of changing the step size within the range, for the shape tested, is minimal.

5.7.5.3. Facet Size

Facet size was increased from 10 to 30pixels in regular increments of 5 pixels. Table 5-23 shows the statistical test results for the comparison of error distributions for the facet size tests. In all comparisons the null hypothesis was not rejected, revealing that the accuracy of three dimensional shape measurements was not affected by the changing facet size.

Facet Size (px)	Error mean (mm)	s.d.	p-value (A-D test)	p-value (2 Sample K-S Test)
10	-0.02	0.02	0.161	0.139
15	-0.03	0.02	0.624	0.766
20	-0.03	0.02	0.394	-
25	-0.03	0.02	0.322	0.429
30	-0.02	0.02	0.686	0.669

Table 5-23 - p-values from two sample K-S tests comparing shape measurement error distributions for the 90 mm SCA for different facet sizes with comparisons made relative to the 20px condition with p-value results for Anderson-Darling statistical test for normality for each facet size condition

The statistical results from each facet size test show that interestingly, unlike with deformation measurements (which are essentially derived from shape measurement), the distribution means and standard deviations remain very consistent as the facet size changes. The shape measurements presented are a single stage measurement, whereas the deformation measurements are calculated from a comparison of two stages, a deformed state and a reference state. The changing standard deviations observed in the deformation which have not been observed in these shape measurements tests may be the result of 'error stacking'. In addition, the effect of the deforming pattern, which is not considered in this shape calibration due to the associated complications, may further introduce error, as was shown in §5.6.5.2 for deformation.

5.7.5.4. Pattern Type

Pattern Type	Mean Error (mm)	s.d.	p-value (AD test)	p-value (2 Sample K-S Test)
High (60:40)	-0.02	0.02	0.523	-
Low (40:60)	-0.01	0.02	0.498	0.254

Table 5-24 - - p-values from two sample K-S tests comparing shape measurement error distributions for the 90 mm SCA for different pattern types with comparison made relative to the 60:40 condition with p-value results for Anderson-Darling statistical test for normality for each pattern type condition.

Two different patterns with varying amounts of greyscale content were tested. Comparison of the measurement error distributions, via the two sample K-S test, show that the null hypothesis was not rejected

and therefore the two distributions were not significantly different. That is not to say that further alteration of surface pattern would not ultimately have an effect on measurement error, as the pattern is an integral part of the process to create surface point data from which all measurements are derived. However, for the setup and parameters used in this testing, accuracy of shape measurement was not affected significantly by the changing surface pattern.

5.8.   Chapter Conclusions

This chapter set out to address OBJ_5 and OBJ_6 (§1.1), through the development and implementation of a method that would enable the calibration of 3D shape and deformation measurements made by a DIC system. Furthermore, to use these methods to investigate the measurement repeatability and the effect of changing specific user controllable variables on the shape and deformation measurement accuracy.

The DIC system used in the calibration measurements was the GOM ARAMIS system, employing Photron SA1.1 high speed video cameras, with a measurement volume of approximately 360 mm^3. Preferred and acceptable calibration limit values of ±0.5% and ±1%strain were defined for deformation calibration and ±0.5 mm and ±1 mm for shape calibration. The established measurement accuracy was then used as a reference to compare measurements when selected test variables were changed.

To enable the assessment of deformation, a novel deformation material measure has been developed, consisting of a number of printed speckle patterns of five discrete deformation states that simulate a deformation via an animation style. This approach allowed full control of the pattern characteristics as well the 'deformation' which could be calibrated via the measurement of length as proposed by Patterson et al. (2007). The speckle pattern boards (SPBs) were found to be capable of reproducing a deformation state to within ±0.1%strain at a 95% confidence interval.

The measurement calibration conducted for deformation using the SPB methodology has found that deformation was being slightly overestimated, on average, by a nominal value of approximately 0.02% strain, with a typical measurement error range of ±0.34%strain at a 95% confidence interval. The measurement calibration results therefore, were well within the preferred range of ±0.5%strain defined and furthermore, differences in deformation measurements made between and within test sessions have been shown to be insignificant (p>0.05) indicating excellent measurement repeatability.

The SPB method was employed to investigate the effect of six variables; deformation magnitude, computational step, facet, deformation type and rotation, pattern type and position in volume, via the comparison of measurement error distributions using a two sample Kolmogorov-Smirnov (K-S) test. The latter three variables were found to have no significant effect on measurements, whilst the computational step and facet size only significantly affected accuracy when parameters were varied to an extreme. Even in

these cases, mean error remained consistent and accuracy range was still within the acceptable range outlined in the objectives.

Measurement accuracy was found to be significantly affected by the magnitude of a deformation; however, interrogation of results suggested the distributions were the same and that only the mean values had been translated, which may have been a result of the material measure calibration error. Even so, measurement accuracy remained within the preferred objective range and therefore the practical implications were deemed negligible.

Shape measurement calibrations were conducted using a material measure in the form of a custom manufactured three dimensional shape that was calibrated post fabrication. Shape measurement calibration results were excellent, with an accuracy range, at a 95% confidence interval, within ±0.1 mm; well inside the preferred limit outlined in the objectives.

Three relevant variables were selected to test their effect on measurement accuracy: pattern type, computational step and facet size, using the same approach of comparing error distributions as used in the deformation calibration. Pattern type and facet size were found to have no significant effect on measurement accuracy, however a significant improvement in shape measurement occurred as the step size decreased. Despite this, accuracy ranges for the step size remained within the preferred ranges defined in the objectives and as before, the practical effect was deemed negligible.

Overall the DIC system performed excellently in all calibration measurements, building on work from Chapter 4 in establishing that it is a suitable measurement device to accurately measure the dynamic shape and surface deformation of the foot during running. Furthermore, understanding the effects of user controlled and measurement variables on measurements, will build confidence in analyses made in proceeding work; this will be relevant when multiple camera systems are employed to form a single measurement. The work in this chapter has focussed on a single camera pair measurement: when multiple camera systems are used, consideration of other factors that may contribute to measurement error and variability would need to be considered. These will be discussed in the relevant section in the proceeding work.

6. Novel Dynamic Foot Shape Measurement Methodology

6.1. Introduction

Creating a method that would allow measurement of dynamic shape has the potential to be applied in multiple research activities to develop understanding of the dynamic human foot shape and inform shoe and last designs for athletic footwear.

Methodologies developed for the measurement of the dynamic human foot shape have to date been extremely limited in capabilities both in terms of accommodating locomotion speeds and possible measurements. Through validation and calibration activities for individual system measurements, preceding chapters have identified and selected digital image correlation (DIC) as a suitable technique for measuring three dimensional shape, as well as surface deformation. Although DIC is capable of individual surface measurements, it was recognised that in order to develop a methodology that would enable accurate, meaningful measurements of the human foot during dynamic movement, a multiple system measurement approach needed to be developed and applied.

In Chapter 3, the requirements of the methodology were outlined, which should be fulfilled in the developed method. Within the requirements, the measurement of kinematics and kinetics were also identified as necessary measurements (in addition to shape and deformation) and hence these were also considered in the methodology development discussed in this chapter.

The aim of this chapter was to address OBJ_7 (§1.1): to develop a methodology, using the selected technology, which would be capable of measuring dynamic foot shape during the stance phase of running gait for the requirements outlined in Chapter 3, which would also include measurement of kinetics and kinematics. The method was not intended to be definitive for a particular set of measurements or test, but instead a more generic methodology where particular components may be changed to accommodate different test parameters. This aim would be achieved through the following objectives:

- Establish a means to measure kinematics and kinetics as part of the methodology.
- Develop a multiple camera setup to measure foot surfaces using individual systems
- Develop an approach to combine individual measurements together into a single measurement.
- Devise a referencing method to allow intra and inter test comparison of relative measurements

This chapter will encompass data collection and data processing components of the method that provides a final 'composite foot shape measurement' and associated biomechanical measurements, which can be used for analysis.

6.2. Concurrent Biomechanic and DIC Measurement

Measurement of runner kinetics was straightforward through the use of an instrumented platform to measure the three components of ground reaction force, a method prevalent within the literature. However for measurement of kinematics a novel approach was required as the standard methods which have been used extensively in literature for capturing runner kinematic data involve using either a passive measurement (e.g. VICON, Oxford Metrics) or an active measurement approach (e.g. Codamotion, Charnwood Dynamics). Using one of these established systems causes a number of potential issues in both method and measurement.

The requirements for lighting, as well as imaging hardware in comparatively close proximity to the test area ruled out the use of traditional passive reflective marker measurement systems whilst the need to attach hardware to the foot and leg surface in active marker methods was clearly unsatisfactory. In theory the DIC measurements could have been used to identify the three dimensional position of points at anatomical landmarks for kinematic measurement in a similar method to (Van den Herrewegen *et al.*, 2014) . However, correct location in a DIC application is dependent upon a data point being created in the correct position, which cannot be guaranteed due to the way data points are created.

The solution was with the use of GOM PONTOS, a passive measurement system and a 'sister' system to GOM ARAMIS. Where DIC is based on creating and tracking of data points created using a subset of a surface greyscale pattern, using exactly the same hardware and setup, PONTOS is able to identify circular markers applied to a surface and then calculate their position and movement in three dimensional space, using photogrammetric principles. By adding appropriately sized, circular markers to the surface of the lower extremity at predetermined anatomical landmarks, the three dimensional position of the locations could be measured and then used to analyse the runner kinematics using the same digital images.

6.3.   Data Collection

This section details the novel method developed for capturing dynamic foot shape data alongside runner kinetic and kinematic data. This will include outlining the hardware used in each component of the method and where appropriate the development of particular elements of the methodology. Furthermore, it also discusses relevant calibrations and associated accuracy measurements.

6.3.1. Experimental Setup

A multiple camera approach was selected as the preferred methodology as described in §4.5.2. A plurality of cameras, imaging simultaneously, positioned around the foot during stance, would enable the measurement of the full foot surface for shape and deformation measurements and the 3D position of points at anatomical landmarks on the foot surface, to enable kinematic measurements of the lower extremity.

The foot, being a relatively complex shape with irregular surfaces and sharp contours meant careful consideration of camera positions was needed. In addition, the movement of the foot would need consideration to ensure surfaces would remain in view of an imaging camera pair for the entire stance phase, enabling measured data points on the surface to be tracked.

A limitation of the approach in this application is the need for multiple high speed cameras; due to the cost, hardware availability can be an issue. Furthermore, increasing the number of camera pairs inevitably increases the data processing time and data storage requirements. It was therefore necessary to optimise the positioning of the cameras to enable an acceptable amount of the foot surface to be measured for the duration of the stance. The synchronisation and spatial co-ordination of camera measurements to form a composite foot shape measurement, which are presented in this section, are described in more detail in later sections of this chapter.

6.3.1.1.   Camera Position Development

The foot surface area of interest for DIC measurements was a plane cutting through the shank approximately above the medial malleolus to a plane cutting through the foot at the MPJ. Near complete coverage of the foot surfaces in this region was required to create a full foot shape from which measurements could be derived. Kinematic marker points were located within this defined surface area and therefore the refinement of camera positioning for kinematic measurements did not need to be considered separately.

The refinement of camera positioning was divided in to two tasks, firstly measurement of plantar foot surfaces and secondly measurement of dorsal foot surfaces.

Plantar Foot Surfaces

In order to achieve the most reliable foot shape measurement, the key decisions made was to measure the surface as opposed to developing an alternative interpolation technique or method to create the surface which would ultimately reduce the reliability of shape measurements.
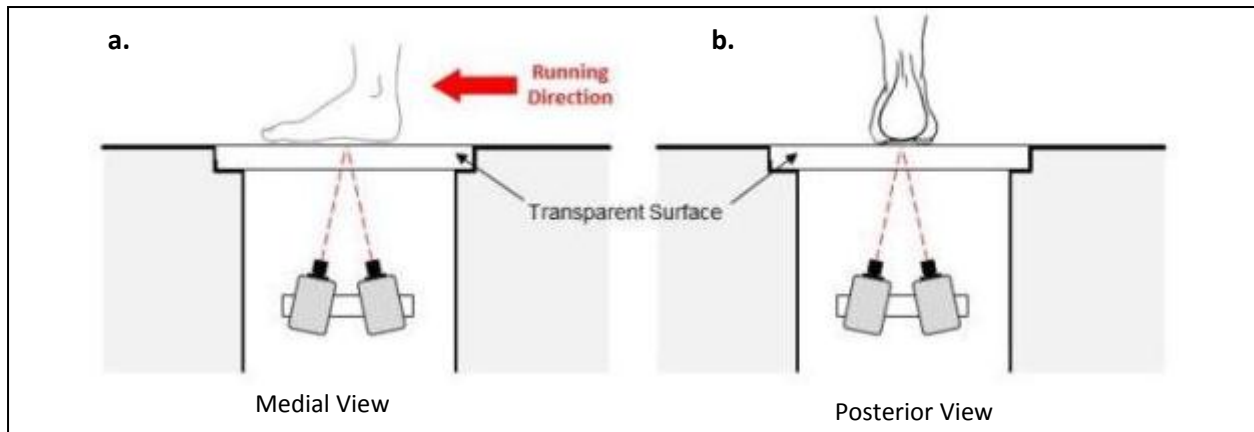
Figure 6-1 – Alternative plantar surface camera positions investigated (not to scale) (a) parallel position (b) perpendicular

As a result, there was a requirement to position cameras beneath the foot so that the plantar surface of a subject's foot could be imaged. This was facilitated by a transparent force plate underneath which was a cavity for hardware placement. A number of different camera pair orientations were trialled, with cameras orientated both parallel and perpendicular to the running direction as shown in Figure 6-1.

In the 'parallel' camera position, good surface coverage was achieved until the heel lift through to toe off stage of stance. As the heel of the foot lifts, the angle between the plantar surface of the foot and the anterior camera increases to a point that the surface can no longer be imaged in sufficient detail by that camera, resulting in poor measurement coverage of the plantar surface as shown in Figure 6-3a. This same effect was also observed in the perpendicular position, but occurred slightly later as the cameras both have the same angle to the running direction.
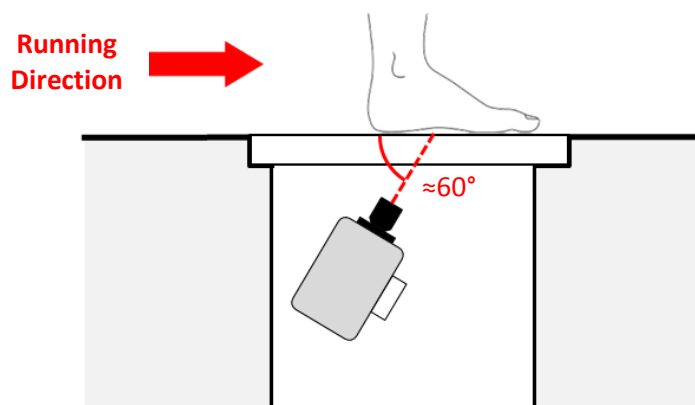
Figure 6-2 - Angled perpendicular camera position medial view (Not to Scale)

In order to improve the measurement coverage, the cameras needed to be able to image the plantar surface better during the latter stages of stance. To achieve this, using the perpendicular positioning approach, the cameras were then angled to the running direction, as depicted in Figure 6-2. In this arrangement, as the heel of the foot lifts, the plantar surface becomes more parallel with the camera imaging planes. Thus, the angle between plantar foot surface and the imaging plane of one or both of the cameras does not increase to a point where the surface can no longer be imaged. The improvement in measurement surface coverage is clearly demonstrated in Figure 6-3 using a static foot model angled at approximately 45° to glass platform.
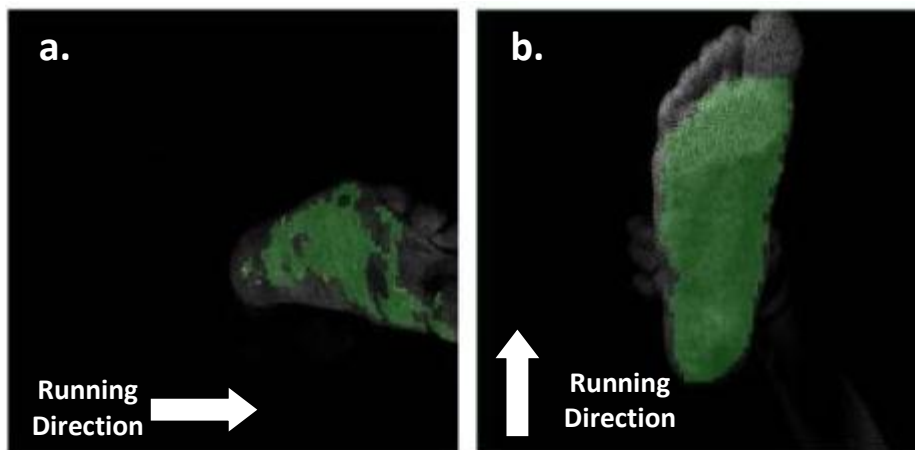
Figure 6-3 - Measurement coverage comparison for (a) parallel position (b) angled perpendicular position

Dorsal Foot Surfaces

Two camera pairs were initially positioned at 'floor level' medially and laterally, parallel to the running direction approximately 1.2m from the foot (Figure 6-4), meaning the camera image plane is normal to the floor. Measurement surface coverage for the lateral and medial sides of the foot at three stages of the stance phase are shown in Figure 6-5a and b respectively.
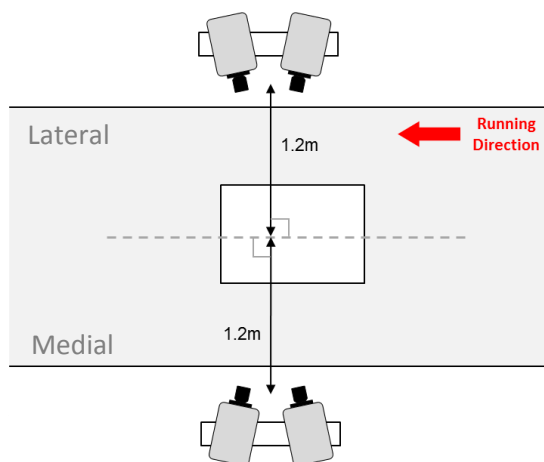
Figure 6-4 – Schematic showing position of camera pairs medially and laterally for dorsal foot surface measurement (not to scale)
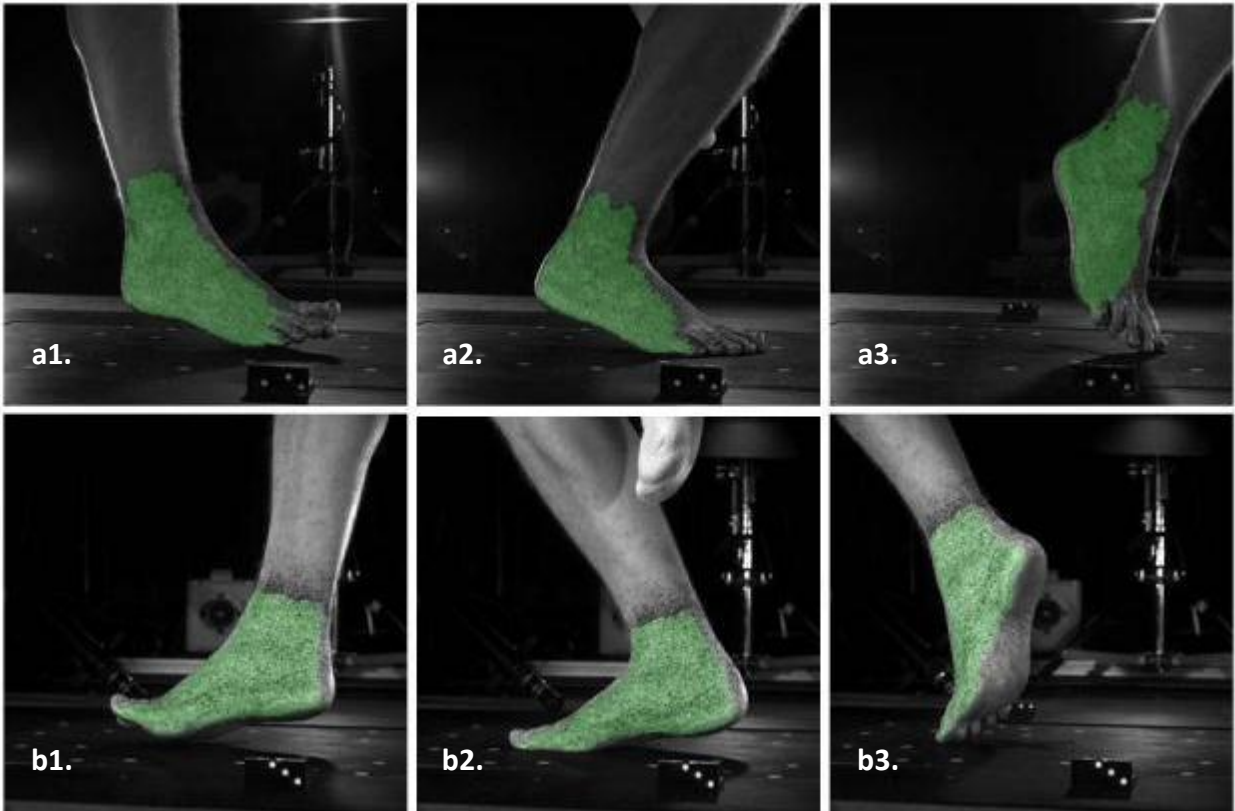
Figure 6-5 - Measurement surface coverage at (1) touchdown (2) midstance (3) toe off during stance for (a) lateral side (b) medial side

A composite measurement is shown in Figure 6-6 which illustrates that the camera positioning did not enable the 'central area' of the dorsal foot surface to be imaged; an area running from the front of the shank down to the metatarsals. This was mainly due to the shape of the foot that meant the 'top' surface is angled to the camera imaging plane, especially in the latter stages of the stance phase (as shown in Figure 6-5a1-3).
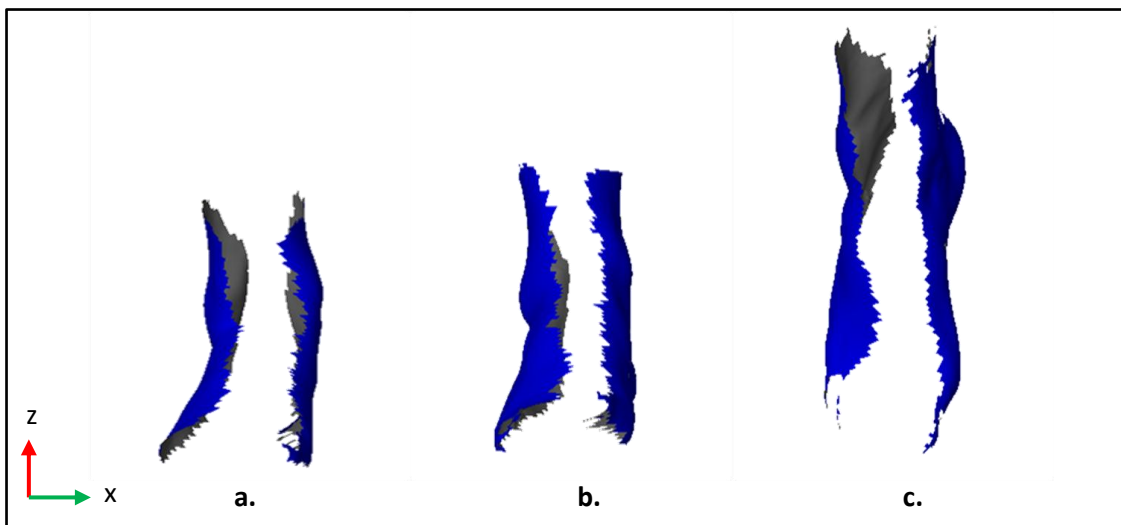
Figure 6-6 – Composite measurement for dorsal surface coverage for dual cameras at three (a) touchdown (b) midstance and (c) toe off stages of stance (anterior views)

To enable measurement of this region, an additional camera pair was introduced on the lateral side, elevated and angled down towards the foot at approximately 45°, positioned in an advanced position of where the foot would impact, facing towards the oncoming runner (Figure 6-7). The improved measurement coverage for this camera position, at three separate stages of the stance, is shown in Figure 6-8a-c.
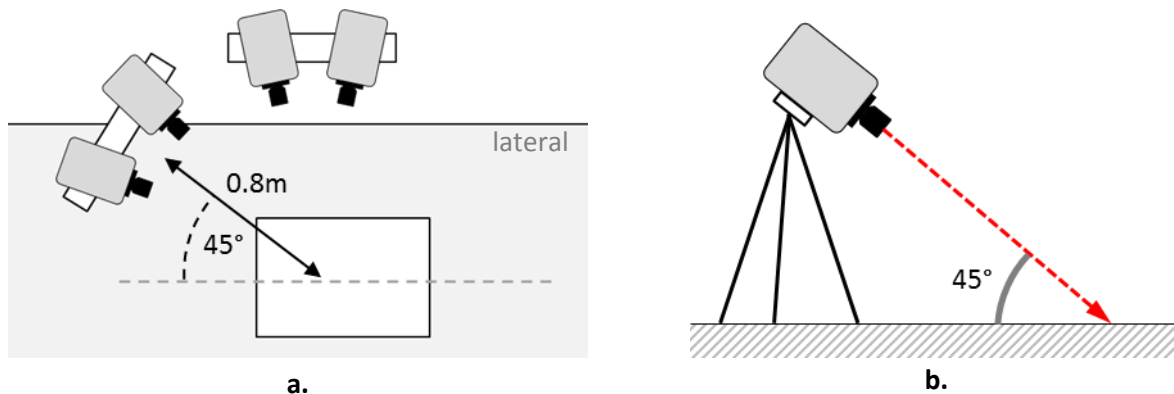
Figure 6-7 – Schematic showing (a) plan and (b) side view of elevated angled camera for dorsal surface measurement
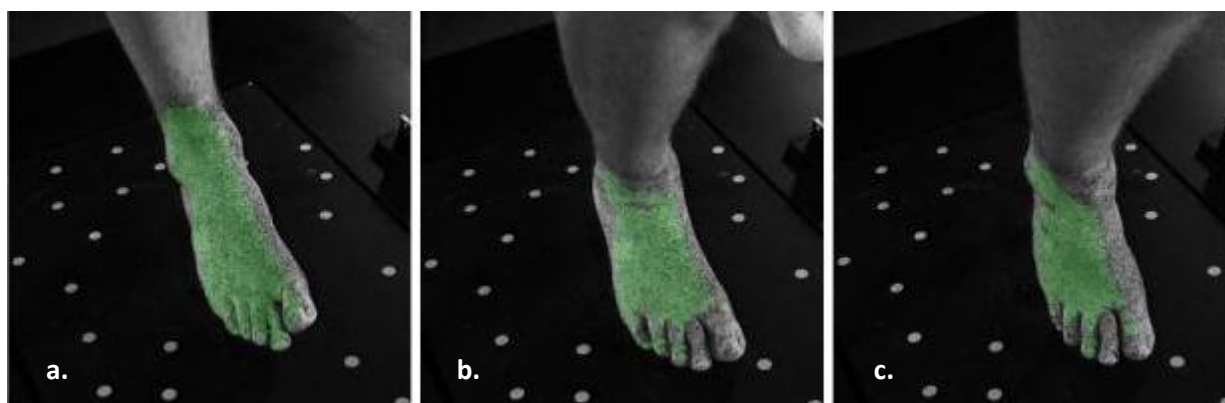
Figure 6-8 - Measurement surface coverage at (a) touchdown (b) midstance (c) toe off during stance for elevated and angled camera capturing dorsal foot surface

The composite surface measurement results (Figure 6-6), also highlighted the Achilles region of the foot as an area for improved measurement coverage. Due to the sharp contour of the heel of the foot, it was deemed necessary to add two camera pairs, positioned medially and laterally to the foot and angled at approximately 60° and 30° respectively, to the running direction. The lateral camera pair was elevated and angled down to the foot in a vertical orientation to ensure consistent imaging of the Achilles region as the foot moved through stance. The medial camera pair however, was orientated horizontally as the swing phase of the opposite limb would obscure the cameras view for a large percentage of stance if the cameras were orientated vertically.

A full composite measurement for the dorsal foot surfaces using the five camera method is presented in Figure 6-9. Although a small gap still exists between the medial and lateral measurements, as well as in the Achilles region, the gaps had been greatly reduced to a point where the measurement gaps could be

interpolated with an adequate level of confidence. This proposed approach was preferred over adding further camera pairs to the setup for the reasons discussed at the beginning of this section.
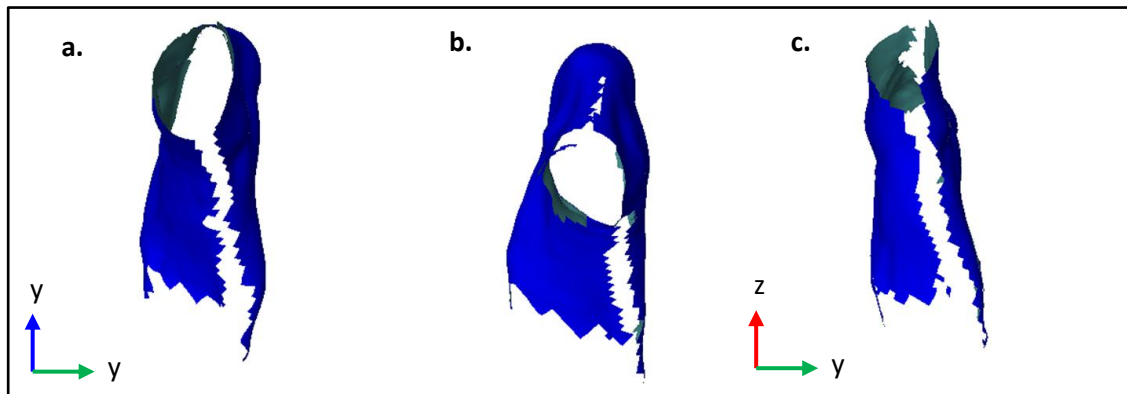
Figure 6-9 - Composite measurement for dorsal surface coverage for the five camera method at (a) touchdown (b) heel lift and (c) toe off

There was potential for a small percentage of the stance phase where the foot of the opposite limb, as it swings through during midstance, obstructs the parts of the foot surface viewed by the medial cameras. A measurement of these obstructed surfaces was therefore not possible. Due to the proximity of the swinging foot to the loaded foot, there would be no way to position a camera pair so that these obscured surfaces could be measured throughout the footstrike. Instead, as this issue may only arise with some runners and the fact the length of the obstruction is relatively short (<0.03s) and only affects the rear surfaces on the medial side, it was deemed an acceptable flaw. Where appropriate, runners would be asked to raise the trailing foot during the swing phase, to reduce/remove the obstruction, so long as their running gait was not affected.

6.3.1.2.   Final Experimental Setup

Figure 6-10 shows a schematic of the fully developed experimental setup employing six separate high speed video (HSV) camera pairs to capture foot surfaces. Figure 6-11 shows images of the physical setup. The identification of each camera pair and its position is summarised as part of Table 6-1.

All cameras and associated fixtures, mounts and wiring were arranged so that a clear path existed for a subject to run through without any part of their body being affected. This was to ensure that a natural running style could be adopted and that the running gait of each subject would not be affected in any way.

The setup required a running lane in excess of 20m in length within an indoor laboratory to enable sufficient space for subjects to reach and then maintain a desired velocity and not be accelerating or decelerating at the point of measurement. A transparent glass force platform was located within the running lane, positioned flush with the floor so as to allow a person to run over its surface without having to alter their gait and enabling the capture of plantar foot surfaces.
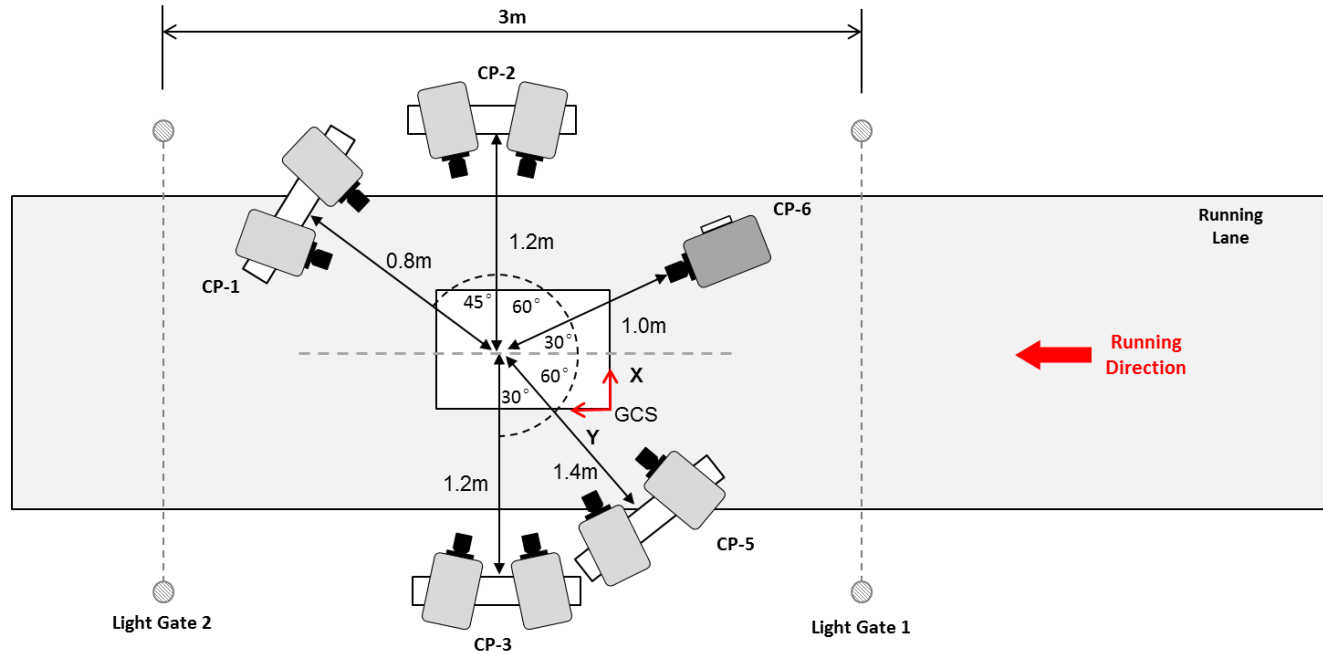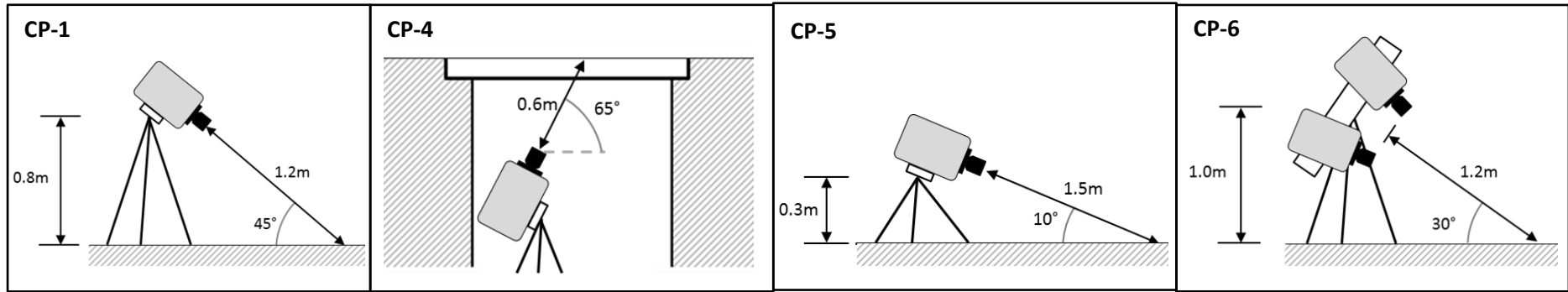
Figure 6-10 – Schematic showing the developed experimental setup employing 6 camera pairs from (a) plan view (excluding CP-4) with individual side views of (b) CP-1 (c) CP4 (d) CP-5 and (e) CP-6 showing inclined angles and measuring distances (GCS=Global Co-ordinate System)
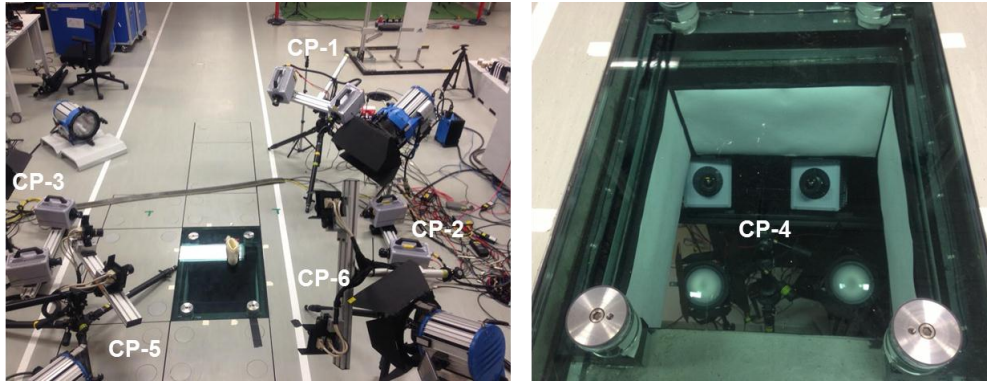
Figure 6-11 - Experimental Setup. Dorsal surface measurement camera pairs (left), plantar surface measurement camera pair (right)

6.3.1.3. Hardware

In the proposed setup two camera types were used, monochrome SA 1.1 HSV cameras from Photron (Tokyo, Japan) with a resolution of 1024 x 1024px and monochrome HXC13 cameras from Baumer (Shanghai, China) with a resolution of 1280 x 1024px. However, any HSV camera could be used with appropriate capture parameter capabilities. A total of eight Photron cameras were used to form CP-1 through to CP-4 and four Baumer cameras were used to create CP-5 and CP-6.

Camera Names	ID	Position Description	Lens Focal Length	Measurement Volume (approx.)	Frame Rate	Shutter Speed
Camera Pair 1	CP-1	Lateral elevated and angled	50 mm	450 x 450 x 450 mm	500Hz	0.13 ms
Camera Pair 2	CP-2	Lateral	50 mm	400 x 400 x 400 mm	500Hz	0.14 ms
Camera Pair 3	CP-3	Medial	50 mm	450 x 450 x 450 mm	500Hz	0.13 ms
Camera Pair 4	CP-4	Plantar	24 mm	600 x 600 x 600 mm	500Hz	0.20 ms
Camera Pair 5	CP-5	Medial Achilles	24 mm	550 x 550 x 550 mm	500Hz	0.25 ms
Camera Pair 6	CP-6	Lateral Achilles	50 mm	400 x 400 x 400 mm	500Hz	0.20 ms

Table 6-1 – Camera identification and operating parameters for each camera pair in the developed setup

Camera pairs were set up in line with recommendations outlined by GOM (GOM, 2009a, 2009b) for separation, angle and measurement distance to achieve a suitable measurement volume to capture the foot movements during the stance phase. The focal length of the lenses used and the measurement volume created for each camera pair is outlined in Table 6-1. Shorter focal length lenses were used where it was required to place the cameras closer to the foot as a result of the position of other camera hardware or space constraints. Slightly different measurement volumes were created between camera pairs, and therefore computational parameters were adjusted to achieve the same resolution of data points.

Illumination was provided from a selection of ARRI (Munich, Germany) daylight, non-flicker lights between 400W and 1200W power ratings. The lights were positioned around the test area in positions that would not encroach on camera views, create glare in any cameras or reflections on the surface of the foot or test area.

6.3.1.4. Operating Parameters

All twelve HSV cameras operated with an image sampling frequency (frame rate) of 500Hz. Lens apertures were set to an f-number of f/8 or greater (for a smaller aperture) and camera shutter speed for each camera pair was adjusted to fine tune the desired image greyscale values, these parameters are summarised in Table 6-1. Different greyscale values were observed between camera pairs due to differences in lighting intensity from different views as well as differences in sensitivity of camera sensors.

Each camera pair was individually calibrated prior to collecting measurements in line with the manufacturer procedures outlined in the user manual (GOM, 2009b). A system calibration was accepted when the calibration deviation value fell within the acceptable range recommended by the manufacturer.

6.3.1.5. Global Co-ordinate System Definition

Measurements made from each camera pair (DIC and kinematics), are each orientated in a 'measurement co-ordinate system' defined during the system calibration of each individual camera pair. To create a composite measurement aligning measurements from each camera pair, each individual measurement needs to be transformed from their measurement co-ordinate systems, to a single, common global co-ordinate system.
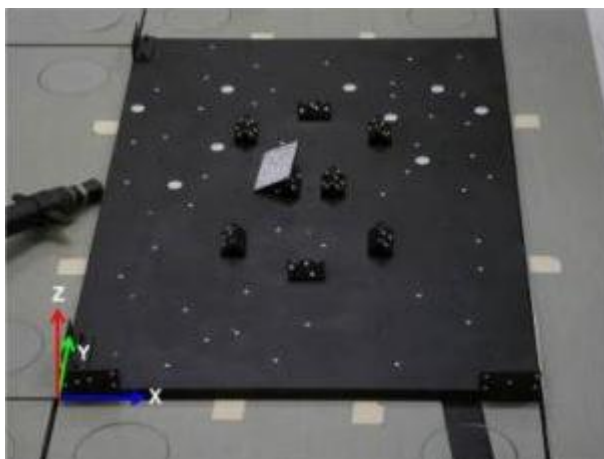
Figure 6-12 - Global co-ordinate system definition object aligned on top of force plate with GCS displayed at the posterior medial corner of force plate

The global co-ordinate system origin (GCS) was located at the medial, posterior corner of the force plate, with x running medially-laterally, y running posterior to anterior and z in the vertical direction. To facilitate the definition of the GCS position, a definition object was created, shown in Figure 6-12; this was a plate

which could be placed on top of the force plate and aligned to its four corners and on which a number of circular markers, which could be imaged by the cameras, were placed.

The position of the circular markers on the definition object surfaces were measured using GOM TRITOP, an optical co-ordinate measurement system that could accurately locate the three dimensional position of the markers. These points were used to create a point cloud, from which a co-ordinate system was defined, at the corner of the object. When aligned on the force plate as shown in Figure 6-12, the position of the co-ordinate system on the definition object defined the origin of the global co-ordinate system at the posterior, medial corner of the force plate.

When placed on the force plate, the camera pairs of the measurement system imaged a number of the markers on the definition object. Markers were placed on all surfaces, including the base of the object, so that all camera pairs could measure points using the ARAMIS and PONTOS software. These measured points were then fitted to the point cloud created from the TRITOP measurement, which created a co-ordinate transformation for each camera pair to the global co-ordinate system. The accuracy to which the points could be fitted affected the accuracy of the alignment with the GCS.

A transformation 'instruction file' was saved from the software for each camera pair, so that it could be applied to each measurement for the respective camera pair. If the camera positions moved in any way, the transformations needed to be redefined by replacing the definition object on the force plate, measuring marker point positions and fitting them to the point cloud again.

Alignment Error

As well as individual system measurement error, the additional error source associated with aligning each individual measurement to a global co-ordinate system needed to be considered to properly assess the accuracy of measurements derived from the multi camera method.

Alignment errors would ultimately affect length and angle accuracy in three dimensional point measurements and any measurements derived from the composite surfaces from DIC. DIC deformation measurements would be unaffected as these measurements are not derived from the composite measurement. The accuracy of DIC measurements ascertained in Chapter 5 for deformations therefore remained unchanged. The following section will explore the absolute alignment error for a multiple camera measurement, i.e. the inaccuracy of a measurement made from aligning multiple different measurements to form one single composite measurement.

Aligning measurements in three dimensions means that misalignment can occur in a combination of the six degrees of freedom. Rather than describing the measurement misalignment in terms of the translational and rotational components when the measurement co-ordinate system was transformed to the global co-

ordinate system, the effect of alignment differences on the end measurements, i.e. surfaces and angles was instead used.

A three dimensional foot shape object, used previously (§4.5.3, Figure 4-18), was measured using the multi camera set setup described in this chapter. The foot shape object was moved across the force platform dynamically in view of the cameras, in a direction parallel to CP-2 and CP-3. A single image was captured by each of the six camera pairs at the parameters outlined in §6.3.1.3, from which individual surface measurements were made. Each separate surface measurements was transformed to the global co-ordinate system using transformation files defined before the test using the GCS definition object and approach described previously in this section. Measured surfaces were limited to those proximal to the toes and distal to the ankle joint. A composite surface measurement was created in GOM S-VIEW (a sister software to ARAMIS) and a comparison made within the software to a virtual surface created from a scan of the foot shape object, obtained using a GOM ATOS scanner (see §5.5.3) (error = +0.01, REF). Surfaces were aligned using a least squares fitting method.
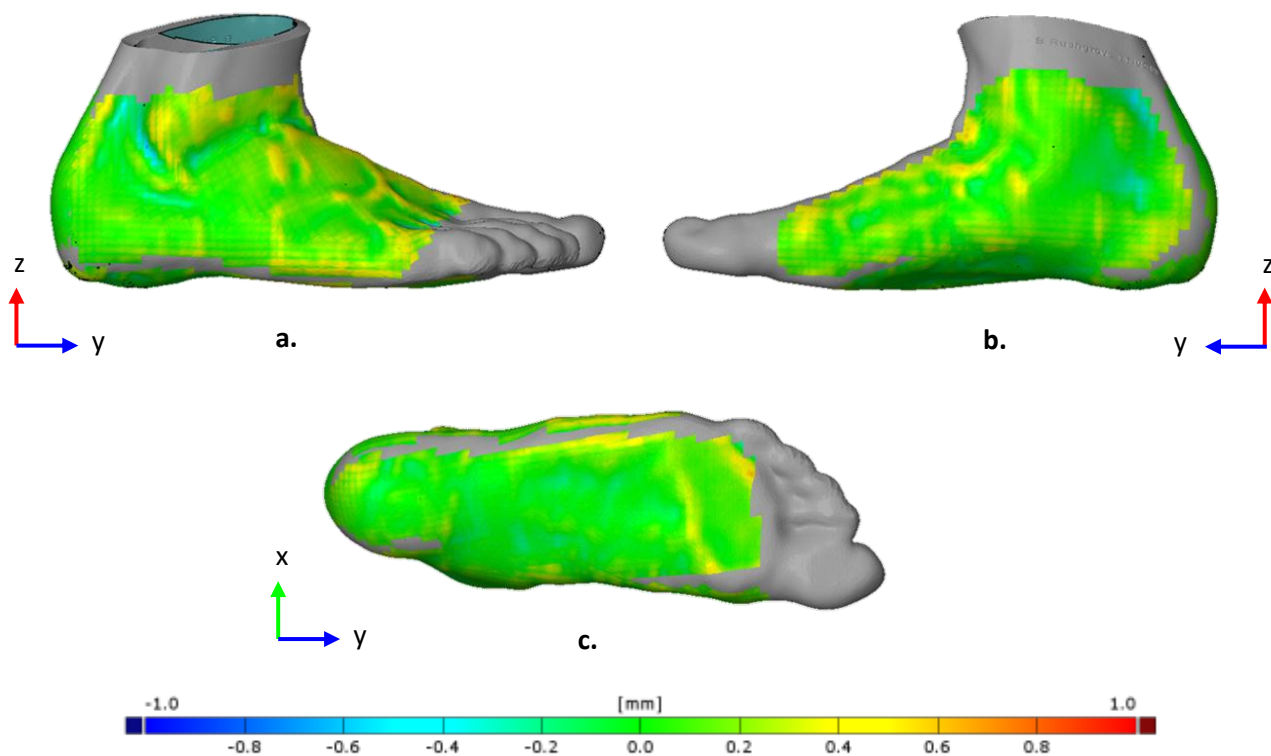
Figure 6-13 – Surface deviation results for the comparison of measured surfaces to digital reference surfaces of the foot artefact

The surface deviation plots from three views are shown in Figure 6-13. The results show that deviation of the composite, aligned surface measurements relative to the calibrated surface scan are generally well within 1 mm, with a mean error of 0.16 mm (±0.21) observed. The fact that areas of 'larger' deviations are localised suggest that these errors are a result of smoothing of some foot surface detail e.g. veins under the skin, due to the computational step size selected, which were measured by the much more detailed ATOS surface

scan, as opposed to an alignment error. One would expect to see more consistent deviations across the foot surface for alignment error, which indicates this effect is low.

With regard to measurements derived from GOM PONTOS, two measures were used for calibration, a length and an angle measurement, in line with work by Richards (1999) who presented a calibration for a number of different kinematic measurement systems. A system calibration panel was used as the reference against which measurement errors as a result of the alignment could be determined. The length and angle measurements were defined using markers on the surface of the calibration panel as shown in Figure 6-14a and b respectively. The distance between marker points A and B was calibrated by the manufacturer to 215.010 ±0.001 mm (Figure 6-14a), with the angle created by C, D and E, for the purpose of this calibration, assumed to be 90° (Figure 6-14b).

a.

b.
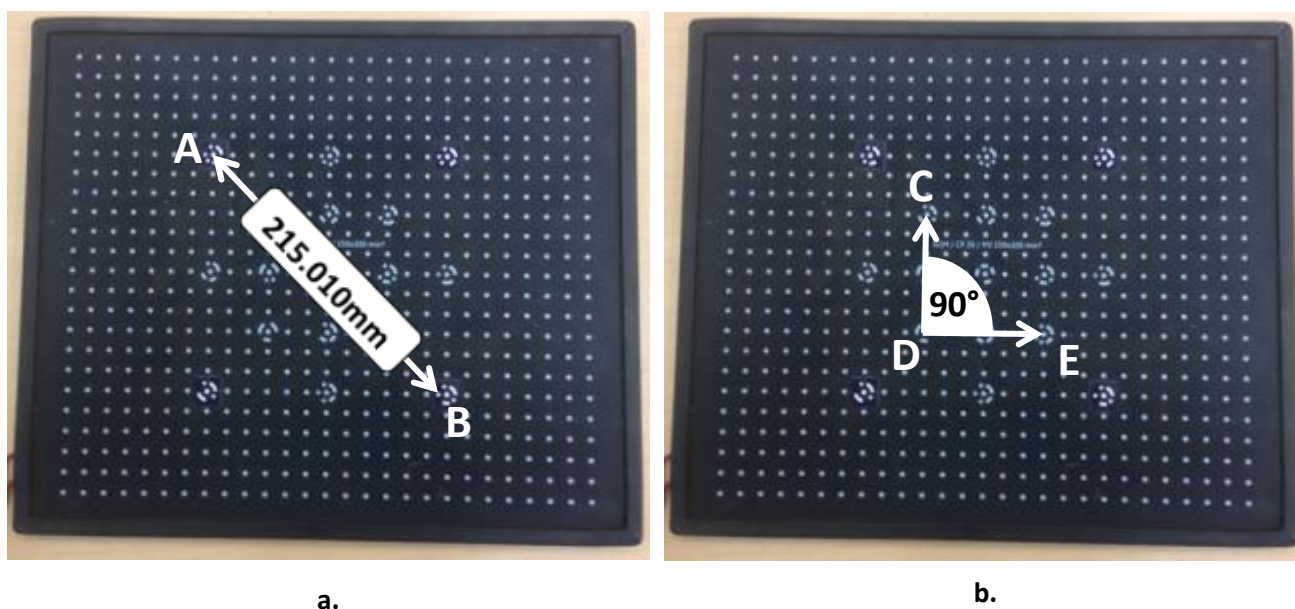
Figure 6-14 - Definition of measurements on GOM calibration panel. Distance defined between markers A and B (a) and angle defined between markers C, D and E (b)

Two camera pairs, CP-1 and CP-2, from within the described multi camera set up were used to obtain three dimensional point data from the calibration panel. Point positions were measured as the panel was rotated dynamically, so as to move the panel around the measurement volume. Camera operating parameters were as outlined in §6.3.1.3 with images captured over 3 seconds. Individual measurements, made by each camera pair, were transformed to the global co-ordinate system using predefined transformation files and merged to form a single composite measurement. Angle and length measurements were then comprised from data points drawn from each camera pair measurement within the composite.

Test	Mean Measured	Max Error	Mean Error
Length (mm)	215.11 (±0.01)	0.11	0.10 (+0.01)
Angle (°)	89.69 (±0.01)	-0.33	0.31 (+0.01)

Table 6-2 – Mean measurement error results for composite kinematic measurements.

The results (Table 6-2) show that the average error was within 0.15 mm for length and 0.35° for angle resulting from error in the alignment but also encompassing the error associated with measuring the three dimensional point marker positions. These values are markedly lower than those observed by Richards (1999) for calibration of a VICON system; who measured maximum errors of 2 mm for length and 4.6° for angle, although these results were for a measurement volume of approximately 2mx2mx2m.

6.3.2. Dynamic Foot Shape Measurement

6.3.2.1. Foot Surface Pattern

To ensure DIC measurements could be made, it was necessary to apply a pattern to the surface of the foot. A white 'background' base layer was required, in order to achieve an appropriate level of contrast with pattern features (speckles), which would not be possible with all skin types. A number of different options were trialled, however, the interaction of the barefoot plantar surface with the floor caused the pattern to smudge and rub off very quickly.

To overcome this, a harder wearing 'paint-adhesive' was employed. This type of paint, used extensively in film special effects makeup, is a 1:1 mix of water based adhesive (e.g. Pros-Aide®, ADM Tronics, NJ, USA) and non-toxic acrylic paint (e.g. Liquitex, NJ, USA) which, when applied to the skin, provides a thin but durable coating. Although the paint creates a thin second skin, it does not significantly alter the properties of the skin which would affect deformations.
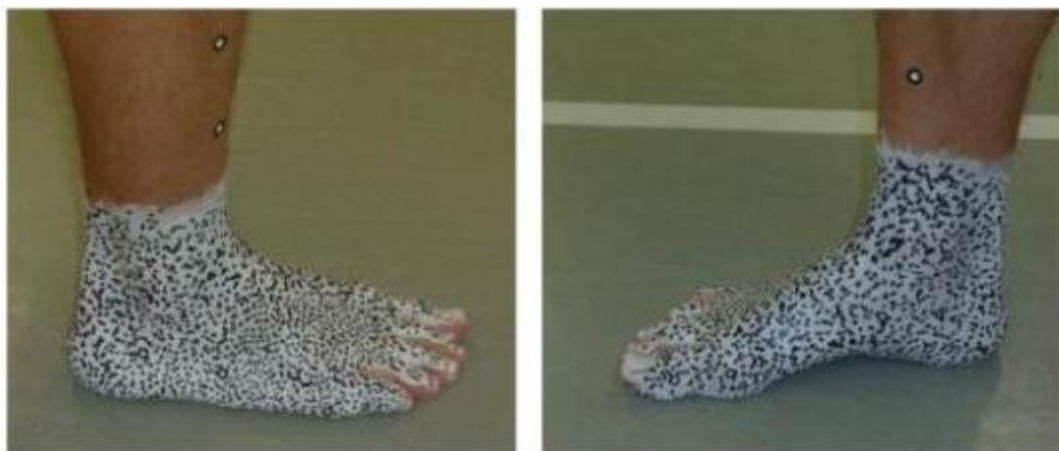
Figure 6-15 – A fully prepared 'speckled' foot lateral (left) medial (right)

A white base layer was applied using the 'paint-adhesive' with black 'speckles' applied using a basic acrylic paint pen, enabling the size and density of black features to be controlled. An example of a fully prepared foot is shown in Figure 6-15.

6.3.3. Kinematic Measurement

Kinematics were measured for the whole body and the lower extremity of a runner. Whole body kinematics in the form of average runner velocity were measured using light gates placed either side of the force platform at a 3m separation, as shown in Figure 6-10. Light gates were positioned at a height to ensure the beams would be broken by the upper body of a runner and not moving limbs which may affect measurement accuracy. Lower extremity kinematics was measured via optical measurement of markers placed on the runner, which will be discussed fully in this section.

6.3.3.1. Kinematic Marker Set
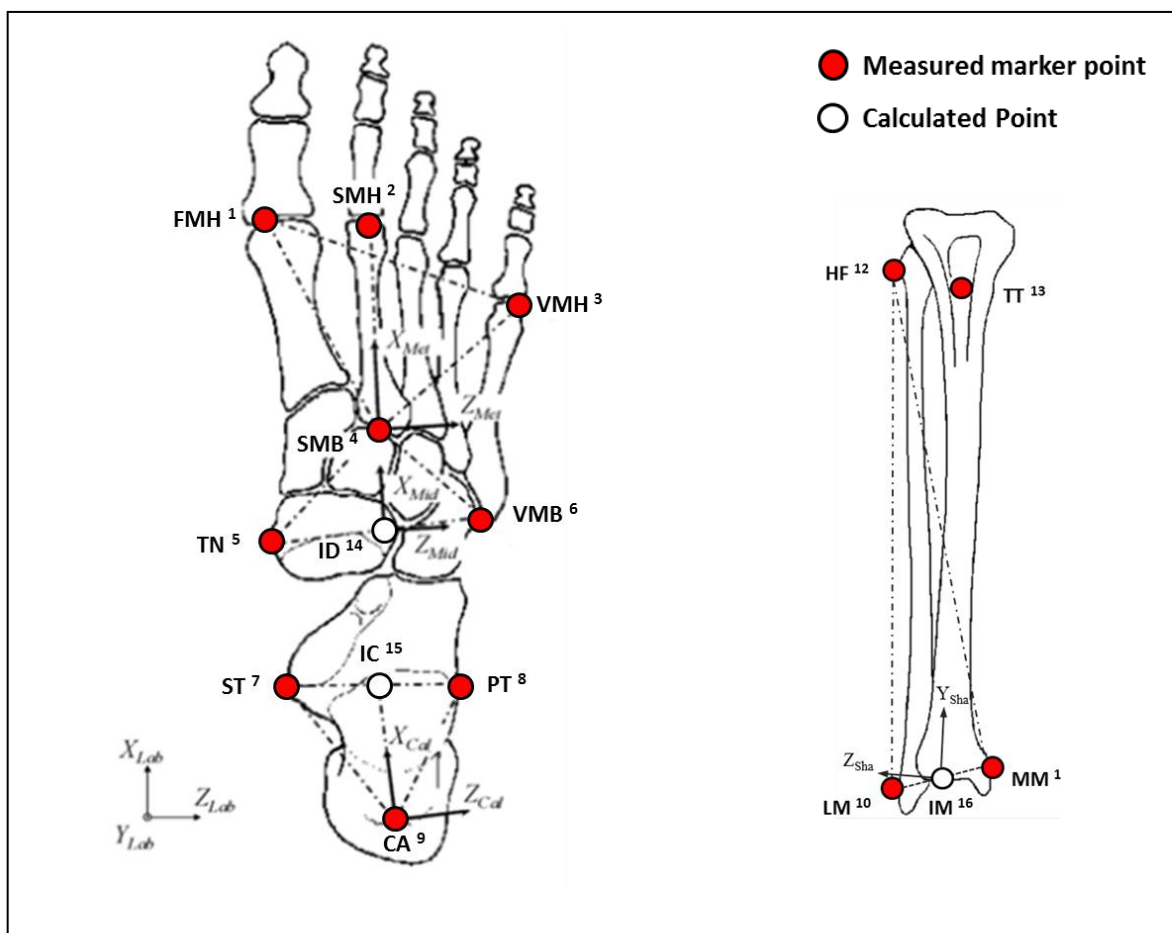
Figure 6-16 - Lower extremity kinematic marker set for foot (left) and shank (right). Adapted from Leardini (2007).

Kinematic marker sets have been presented by a number of authors with varying levels of complexity for lower limb kinematic analysis (Bruening, Cooney, & Buczek, 2012; Carson et al., 2001; Fukuchi & Duarte, 2008; Kadaba et al., 1989; Simon et al., 2006). Due to the need to measure the movement of joints within

the foot, the multi-segment foot model presented by Leardini (2007) was selected for analysing lower extremity kinematics. This model, which has been employed in a number of studies (e.g. Monaghan et al. 2013; Deschamps et al. 2012), divides the lower extremity into 4 segments; the shank, comprising of the tibia and fibula, the calcaneus, the midfoot, comprising of the navicular, lateral, middle and medial cuneiforms and the cuboid and finally the metatarsus, comprising of the five metatarsal bones, each of which were assumed to behave as rigid elements.

The four segments of the foot model were created from of a total of 13 markers placed on a runner's lower extremity at specific anatomical locations, shown in Figure 6-16 and defined fully in Table 6-3. The marker set created 13 measured points and 3 calculated points for kinematic analysis.

Variation in the positioning of skin mounted markers has been shown to be a source of error in the repeatability of kinematic measurements (Ferber, Davis, III, & Laughton, 2002) specifically when different testers apply markers (Deschamps *et al.*, 2012; Smith, *et al.*, 2010). Therefore in an attempt to ensure consistency the same tester was used to apply kinematic markers to all subjects for kinematic measurements carried out in this thesis.

	N°	Marker	Anatomical Placement
Measured	1	FMH	Head of the first metatarsal, dorso-medial aspect of the first metatarso-phalangeal joint
	2	SMH	Head of the second metatarsal, dorso-medial aspect of the second metatarso-cuneiform joint
	3	VMH	Head of the second metatarsal dorso-lateral aspect of the fifth metatarso-phalangeal joint
	4	SMB	Base of the second metatarsal, dorso-medial aspect of the second metatarso-cuneiform joint
	5	TN	Most medial apex of the tuberosity of the navicular
	6	VMB	Base of the fifth metatarsal, dorso-lateral aspect of the fifth metatarso-cuboid joint.
	7	ST	Most medial apex of the sustentaculum tali.
	8	PT	Lateral apex of the peroneal tubercle
	9	CA	Upper central ridge of the calcaneus posterior surface, i.e. Achilles' tendon attachment
	10	LM	distal apex of the lateral malleolus
	11	MM	Distal apex of the medial malleolus.
	12	HF	Most proximal apex of the head of the fibula
	13	TT	Most anterior prominence of the tibial tuberosity
Calculated	14	ID	Intermedius mid-foot, midpoint between TN and TC
	15	IC	Intermedius calcaneus, midpoint between ST and PT
	16	IM	Intermedius malleoli, midpoint between LM and MM

Table 6-3 - Lower extremity marker set definitions

Markers with a circular diameter of 3 mm were used for all foot and distal tibia and fibula anatomical locations. At the approximate measurement volumes created by each camera pair (Table 6-1) and camera resolutions, at the centre of the measurement volume, each marker would be sampled by between approximately 5 and 13pixels across its diameter. This is in agreement with manufacturer recommendations (GOM, 2011). As the markers were two dimensional, their addition to the surface did not affect DIC measurements as they essentially become a part of the pattern applied to the foot, as shown in Figure 6-12. Slightly larger markers with a 5 mm circular diameter were used for points at the knee joint, as they were in a location that was not measured by DIC and therefore did not need to 'blend in' with the surface pattern.

Figure 6-17 – Kinematic markers on the foot, ARAMIS surface measurement (left), PONTOS point measurement (right)

6.3.3.2. Kinematic Adapter

Figure 6-18 - Kinematic adapter reference cluster on anterior tibia surface

A kinematic adapter was used to specify the three dimensional position of markers out of camera views at the knee; markers 12 (HF) and 13 (TT). The 3D positions of these distal shank markers was defined prior to testing using a co-ordinate system created from three 'adapter reference points' located on the same rigid

body (or assumed rigid), i.e. three other points located on the shank segment. In order for the adapter to be implemented, these reference points had to be imaged throughout the stance.

Kinematic points 8 (ST) and 9 (PT) were used as 'adapter reference points' with a third from a marker located on the anterior surface of the tibia just above the ankle joint. As the points needed to be viewed throughout the stance, rather than relying on one marker, a cluster of markers were positioned in the area, as shown in Figure 6-18, to ensure at least one would be imaged throughout the stance phase.

The adapter was defined prior to testing by imaging the whole lower extremity with dorsal surface camera pairs whilst the subject was in a seated position with the leg flat on the ground, establishing relative marker positions. The adapter could then be applied through an automated process during the analysis of test data within the PONTOS software.

6.3.4. Kinetics Measurement

Ground reaction forces for the measured foot were collected using a 0.6m x 0.9m glass force plate (Kistler, Switzerland). The force plate has sensors at the four corners of the plate, each with three layers of piezoelectric crystals within, which deform when force is applied to the force plate. This deformation causes a change in electrical charge that is used to calculate force in three directions. In this setup medial-lateral, anterior-posterior and vertical forces were defined in the x, y and z–direction respectively, with the force plate origin defined at the medial, posterior corner of the force plate, as shown in Figure 6-11.

Using the Kistler Bioware software the GRFs were sampled at 5 kHz, ten times the HSV cameras sample rate. The force plate sensors are calibrated by the manufacture and the known sensitivity values for each sensor are inputted into the software as part of the force plate installation.

6.3.5. Measurement Referencing

A reference state was required for both kinematic and shape measurements. For kinematic measurements, a 'standing reference' (normal weight bearing standing position) was required to create the foot model in the biomechanical analysis software; furthermore it also served as a reference, from which relative foot segment movements could be calculated.

For the foot shape measurements a relevant reference was required, from which shape change (deformation) measurements could be made. For this, it was desirable to measure the foot in an 'undeformed state'. It was necessary for the reference state measurement to be reproducible to enable comparisons of test data within-day and between day. For the work carried out in this thesis the 'undeformed reference' for the foot was defined as an unloaded standing position, i.e. the foot in the same reference position for a standing position, but the foot raised from the ground so that it was not weight bearing.

111

To enable a subject to place their foot in these two reference states, in a reproducible manner, a reference fixture was created, shown in Figure 6-19. This allowed a subject to raise the left limb into a position that would not obstruct any camera views of the right foot, also allowing the subject to place their weight onto the raised limb, so that the foot being measured could be unloaded, whilst remaining balanced.
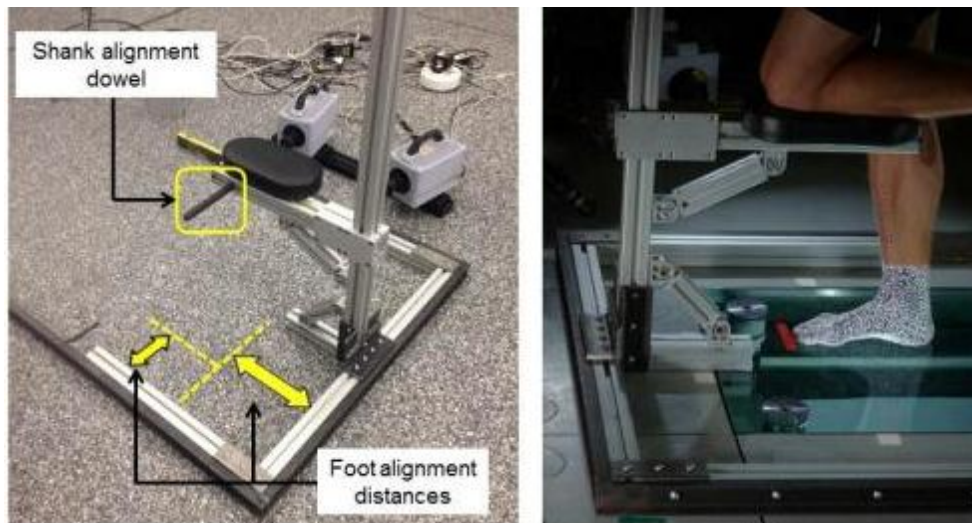
Figure 6-19 - Measurement reference fixture in use (right) and with measure definitions (left)

Two reference measurements were made for each subject prior to testing, a loaded reference and an unloaded reference. For the loaded reference, the body weight of the subject was evenly distributed between lower extremity limbs, in the unloaded reference; the body weight was placed on the raised limb only, with the foot of interest lifted so that it was just touching the floor but with no weight being placed on it.

The lower extremity of the right leg was aligned within the fixture, using three datums. Firstly the subject placed their 'shin' up against a dowel to align the shank. The front and lateral border of the subject's foot was then aligned with two datums at set distances measured from the jig supports. These three measures ensured the angle between the foot and shank as well as the location and rotation of the foot relative to the fixture was set in a reproducible position. All three measures, as well as the height of the fixture were adjustable to suit each subject; however, a definitive definition of foot position across different subjects has not been attempted in this work. The purpose of the fixture was to create a repeatable reference state for each individual subject and not a reference to enable inter subject comparisons, as the basic biological differences in the human lower extremity makes this impossible.

6.3.6. Measurement synchronisation

The separate components of the measurement systems were triggered from a TTL trigger provided from a dedicated trigger box, ensuring all acquisition hardware commenced at exactly the same time. This was

important for matching of force data to DIC and 3D point measurements, as well as to ensure temporal alignment of the DIC measurements in each stage.

6.4. Data Processing

Vertical (F_z) ground reaction force data, measured by the force platform, was used to define the touchdown and toe off stages of the stance phase, from which image data was selected and analysed for DIC and kinematic measurements.

6.4.1. ARAMIS Measurement Data

6.4.1.1. Individual Project Computation

Image data was processed for deformation and shape measurements in the GOM ARAMIS DIC software (Braunschweig, Germany). Due to slight differences in the calibrated measurement volumes, as a result of varying measuring distances and lens focal lengths (shown in Table 6-1), the processing parameters were adjusted to ensure a typical data point separation of between 4 and 5 mm over the measurement surface. This separation of adjacent points, defined by the computational step size, also specified the length over which deformation measurements were derived.

The irregular shape of the foot meant that the separation of data points varied across the measured surface; therefore in order to enable meaningful comparison between camera pairs, the average of 20 separate measurements across the reference stage surface was made. The results, shown in Table 6-4, show an average separation of between 4 and 5 mm for all camera pairs. All other 'project' and 'stage' parameter settings, within the software, were kept at default values.

Camera Pair	Facet Size (px)	Step Size (px)	Data Point Separation (average)
CP-1	18	10	5.0 mm (± 0.8)
CP-2	19	12	5.0 mm (± 0.7)
CP-3	18	10	4.6 mm (± 0.4)
CP-4	14	7	4.3 mm (± 0.3)
CP-5	15	8	4.5 mm (± 0.1)
CP-6	20	8	4.1 mm (± 0.4)

Table 6-4 - Computation parameters and resultant data point separation for each camera pair

Images from each camera pair were processed in individual ARAMIS projects using the parameters outlined in Table 6-4, which were then transformed to the global co-ordinate system using the saved transformation instruction file, as described in §6.3.1.5. Each individual measurement project was then imported into GOM

S-VIEW software (Braunschweig, Germany), a sister software to GOM ARAMIS, enabling the collation of multiple surface and deformation measurements in to one composite measurement.

6.4.1.2. Combining Foot Surfaces and Interpolation

The initial composite foot measurement contained areas where the measurements from different camera pairs overlapped, as shown in Figure 6-20a and Figure 6-21a. It was necessary therefore to remove one of the measurements in the areas where duplication occurred. For deformation, this was completed in the GOM S-VIEW software; however, as data points from each measurement did not directly align, to prevent creation of gaps in measurement data a small area of overlap, consisting of one or two data points, was left. For surface measurements, within Geomagics (Raleigh, North Carolina, USA) Studio software, all areas of duplication were deleted and surfaces interpolated, using in built functions within the software, where gaps in the surface data were created, yielding a single, continuous surface (Figure 6-20).

a.

b.

c.

d.
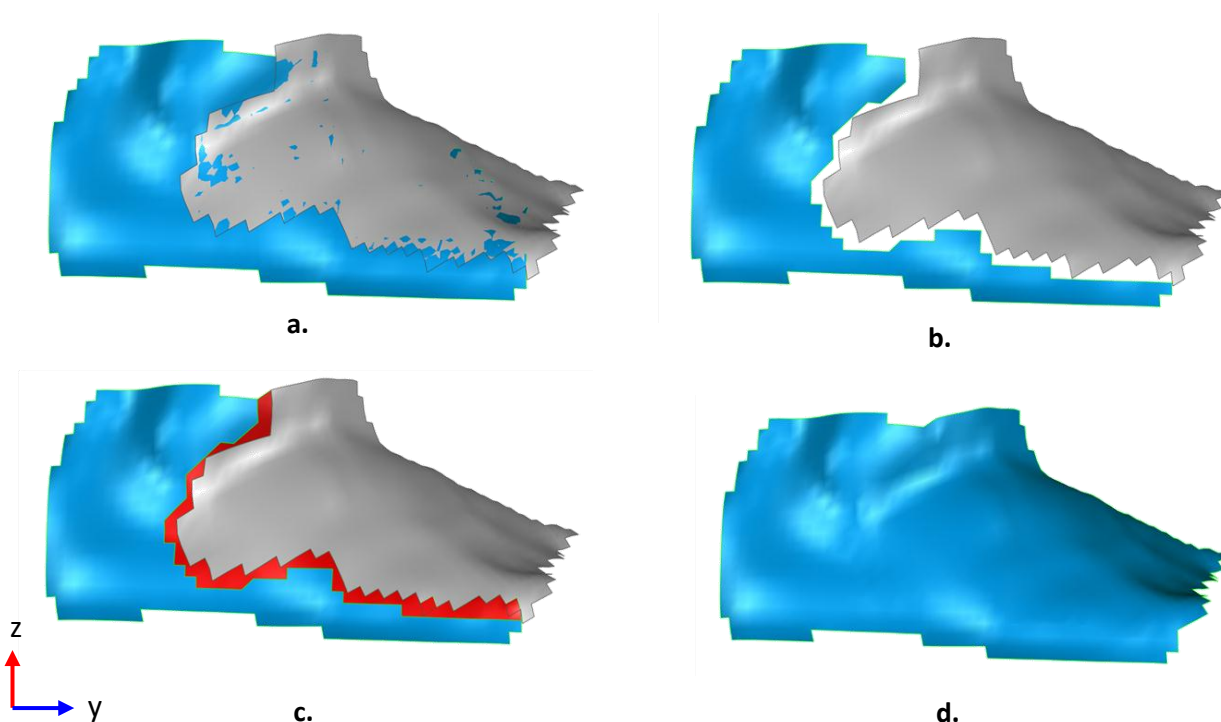
Figure 6-20 – Removal of duplicated surfaces (a and b) and interpolation of gaps in surface measurement (c and d) for the lateral foot surfaces measured by CP-1 (grey surface) and CP-2 (blue surface). Red surface shows interpolated area.

To enable certain measurements of the foot to be made, such as cross sections and volumes, a fully 'closed' foot surface was required for foot surfaces within the area of interest: proximal to the MPJ and distal to the ankle joint. To facilitate these measurements, it was necessary to interpolate gaps that occurred as a result of surface areas not being measured by any of the camera pairs within the setup. Measurements gaps were filled using the inbuilt Geomagic fill functions to bridge gaps and fill holes in the surface data to leave a final

full foot shape, as shown in Figure 6-21. As a deformation measurement is made relative to the reference stage, it was not possible to interpolate gaps in deformation measurements and therefore surface deformation analysis was limited to the surfaces measured in the first instance.

a.   b.
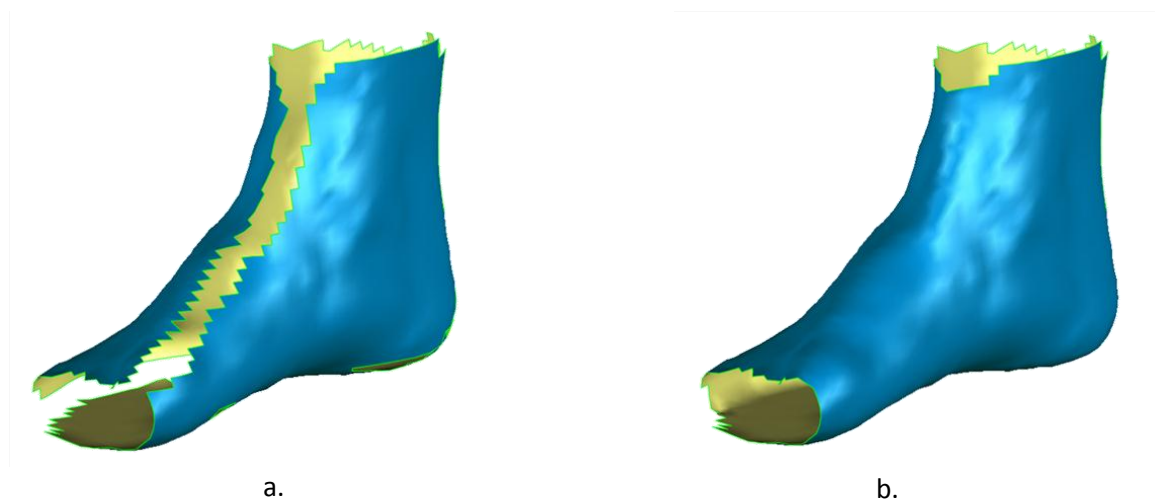
Figure 6-21 – (a) Example of gaps in surface data in the composite foot surface in the touchdown stage of stance and (b) the foot shape surface after interpolation of data gaps

The algorithms used to interpolate the surface data gaps were not readily available from the software manufacturer. It was not possible, therefore, to theoretically assess the accuracy of this process. In order to assess the error in surface interpolation the surface measurement results from the foot shape object measured in §6.3.1.5 was used with gaps in the measurement data interpolated using the 'tangent' interpolation function within the Geomagics software. This fully interpolated surface was then compared to the virtual calibration surface obtained from a GOM ATOS scan, to enable the error in the interpolated regions to be ascertained. The results of which are shown in Figure 6-22.

The results show that interpolation functions within the software approximated the missing surfaces extremely well with levels of error within that observed for alignment error (<1 mm). It was concluded therefore, for a method that was relatively simple to implement, the level of error achieved was acceptable and attempts for improvement were not required.

The accuracy of the interpolation would be dependent upon the size of the gap across which the surface interpolation was required, therefore wherever possible the unmeasured areas needed to be kept to a minimum. Additional surface data could be obtained from the DIC software when the individual stage was considered individually instead of being 'tethered' to a reference. This additional surface data, where appropriate, could reduce gaps in measurement data for a specific stage and thus keep interpolation error to a minimum.
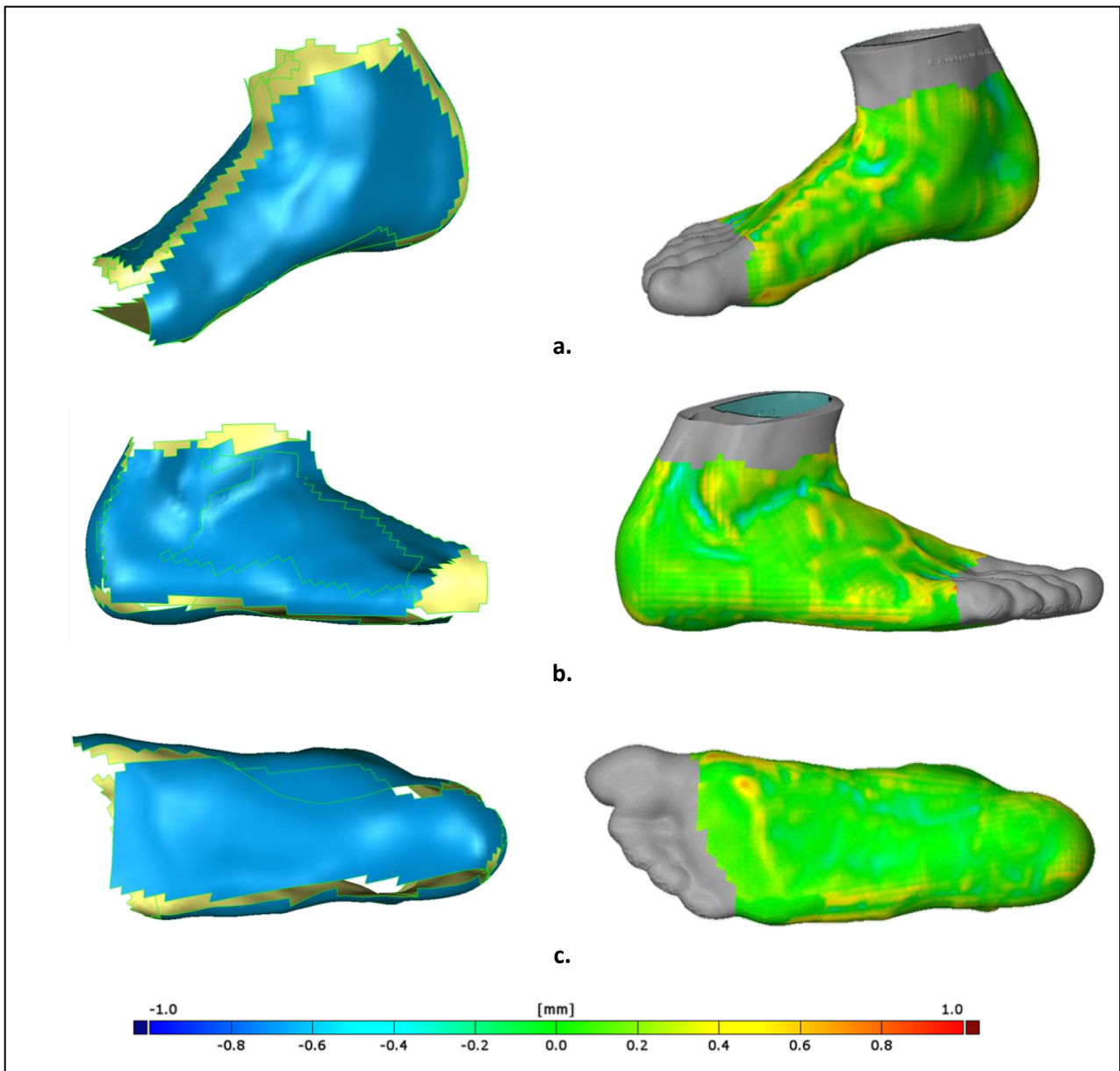
Figure 6-22 – Evaluation of foot models from three views (a) anterior/medial isometric (b) lateral and (c) plantar. Left hand images shows measured surface data with gaps, right hand image shows deviation of fully interpolated surfaces relative to the virtual calibration surface measured by GOM ATOS scan.

6.4.2. Biomechanical Data

6.4.2.1. Kinetic Data

Kinetic data was saved directly from the Kistler Bioware software and imported into Microsoft Excel (Redmond, WA, USA) where the data was 'cropped' to the touchdown and toe off events. Additional events during the stance could also be identified at this stage, for example, peak propulsive and braking forces in F_y and active and passive force peaks in F_z.

6.4.2.2. Kinematic Point Cloud

As with DIC measurements with ARAMIS, images from each camera pair were processed in individual PONTOS projects to identify the three dimensional position of the kinematic markers located on the foot surface. Each individual measurement was imported into a single PONTOS project to form a composite point cloud with kinematic points measurement attributed to a particular camera pair, as outlined in Table 6-5. Where a point was measured by an additional camera pair, the duplicated point was deleted.

Camera Pair	Kinematic Points Measured
CP-1	2_{SMH}, 4_{SMB}
CP-2	3_{VMH}, 6_{VMB}, 8_{PT}, 10_{LM}
CP-3	1_{FMH}, 5_{TN},
CP-5	7_{ST}, 11_{MM}
CP-6	9_{CA}

Table 6-5 – Definition of camera pairs for kinematic point measurements

Proximal shank markers HF and TT were created and added to the point cloud for each stage of the measurement using the kinematic adapter. This was completed using an automated function within the PONTOS software that identifies the position of relevant points in the composite point cloud and adds 'adapter points' in the predefined, relative, three dimensional locations.

The completed point cloud data was exported from the software as a generic data file, containing the three dimensional position of each marker point for each measurement stage.

6.4.2.3. Creation of C3D file

For each trial, exported data for the three dimensional position of each kinematic marker for each measurement stage along with GRF data was collated into a single Microsoft Excel spread sheet. To enable the kinetic and kinematic data to be evaluated in biomechanical analysis software, this raw data needed to be placed into a suitable file format, as it could not be imported directly. The open source, binary C3D file format was selected due to its extensive use in biomechanics and gait analysis applications meaning it was supported by most software providers.

An empty C3D file was created using 'C3D server' software from Motion Lab Systems (Baton Rouge, LA); this was then populated using the collated spread sheet data via a custom written Matlab code (The Mathworks, Natick, MA), which exported a C3D file containing biomechanical data for a trial that could then be opened in a biomechanical analysis software (see Appendix F). Two C3D files were created, one containing data from the static loaded trial and a second from the dynamic foot impact trial.

6.4.2.4.   Lower Extremity Segment Definitions

The loaded static trial C3D file with was imported into Visual 3D (C-Motion, USA) and used to build a four segment lower extremity foot model which could then be applied to dynamic trial data. The software assumes that segments are rigid, implicitly linked (i.e. not constrained) and each is defined by a right handed, Cartesian local co-ordinate system (LCS) (Robertson *et al.* 2013) defined by Leardini (2007) and summarised in Table 6-6. The foot could also be defined as a single segment as outlined in Table 6-6. The LCS of the lab was taken as the global co-ordinate system position from GOM measurements, i.e. at the back medial corner of the force plate.

Segment	Origin	Axis	Direction	Definition
Shank	IM	X_{sha}	ant-post	Orthogonal to YZ plane
		Y_{sha}	plant-dors	Projection of line joining origin and TT on the frontal plane passing through origin, LM and HF
		Z_{sha}	med-lat	Orthogonal to the y-axis lying on the frontal plane
Calcaneus	CA	X_{cal}	ant-post	Line joining origin and IC
		Y_{cal}	plant-dors	Orthogonal to XZ plane
		Z_{cal}	med-lat	Orthogonal to x-axis on transverse plane defined by x-axis and ST
Midfoot	ID	X_{mid}	ant-post	Line joining origin with MC
		Y_{mid}	plant-dors	Orthogonal to XZ plane
		Z_{mid}	med-lat	Orthogonal to x-axis on transverse plane defined by x axis and TN
Metatarsals	SMB	X_{met}	ant-post	Projection of line joining SMB and SMH on the transverse plane through origin, FMH and VMH
		Y_{met}	plant-dors	Orthogonal to XZ plane
		Z_{met}	med-lat	Orthogonal to x-axis in the transverse plane
Foot	CA	X_{foot}	ant-post	Projection of line joining origin and SMH on the transverse plane passing through origin, FMH and VMH
		Y_{foot}	plant-dors	Orthogonal to the XZ plane
		Z_{foot}	med-lat	Orthogonal to x-axis in the transverseplane

Table 6-6 - Segment Local Co-ordinate System Definitions

Three dimensional kinematic angles were calculated as the transformation between the co-ordinate systems of two selected segments; a reference segment (usually proximal) and a 'moving segment'. Angles of rotation were represented as Cardan angles calculated according to the ISB recommendations in the ZYX order (Sinclair et al., 2012; Wu et al., 2002), defining dorsi/plantar flexion around the z-axis, abduction/adduction about the y-axis and inversion/eversion about the x-axis.

6.4.2.5. Lower Extremity Segment Tracking

Position and orientation of the lower extremity segments were computed using a six degree of freedom method (Spoor & Veldpaus, 1980) within the Visual3D software, also known as the segmental optimisation approach. This method assumes all segments move independently and that the position and orientation of a segment is determined by the set of tracking markers attached to the segment, which in this model were the markers used to define each of the segments.

6.5. Measurement Capabilities

The method, outlined in the previous sections, has intentionally been presented in a relatively generic form to enable application in the measurement of human foot shape dynamically in a number of scenarios as opposed for a specific. As such, explicit measurements for describing the dynamic foot shape and its movement have not been defined, as the measurement that is required will be determined by the research question or hypothesis (related to the dynamic foot shape) posed. Understanding the measurement capabilities of the method was however important and therefore a discussion of the possible measurements that can be attained will be made here.

6.5.1. Surface Shape and Deformation

The methodology is capable of measuring the foot surfaces, from which a 'closed' foot surface model can be created via the aggregation of multiple individual surface measurements. These three dimensional foot shapes can be created at every stage of a measurement, depending on the number of images captured, and from which the foot shape can be characterised via a set of measurements; for example sections cutting across the foot shape, between two points (linear) or a volume contained by the surfaces in a region or across the whole foot. As the data points from which the surface is created can be associated between each stage, shape measurements can be 'tracked' across the whole footstrike (in subsequent surface models) and the relative change (or deformation) in that measurement calculated. Shape measurements can be defined from the surface data points or from markers, such as those used to define landmarks for kinematics, on the foot surface.

As well as shape metrics, the full field surface deformations are derived via a similar means to relative shape; measuring and tracking surface data points over time that enables a relative change in surface shape to be computed. Deformation values at a point, along a line or over an area can be extracted using the data points on the measurement surface.

6.5.2. Kinematics and Kinetics

The kinematic marker set defined in this method can be changed in order to create a different foot model or to measure specific foot segments or joints, for example the addition of the hallux or a reduction/increase in the number of segments. This would once again be dependent upon the measurement of interest linked to a research question or hypothesis. The key capability is that measurements can be made simultaneously with the surface measurements, without the need for additional hardware, so that lower extremity movements can be analysed in conjunction with surface shape and deformation measurements.

The kinetic measurements have been used primarily in the methodology to define events in the stance phase, for example touchdown and toe off. However, additional analyses such as centre of pressure could be derived from the force data as well as linking the kinetic and kinematic data to calculate joint moments and torques using inverse dynamics.

6.6. Chapter Summary

The aim of this chapter was to address OBJ_7 (§1.1): to establish a novel methodology to measure runner foot shape and biomechanics during the stance phase of gait, based on the requirements outlined in Chapter 3. The use of a digital image correlation combining measurements from multiple camera pairs has been presented, including hardware and operating parameters, along with the general data collection and processing activities required to create a foot model ready for analysis and the creation of a suitable surface pattern to facilitate measurements.

The alignment of multiple individual measurements to form a single composite measurement was achieved using an artefact to define a global co-ordinate system to which all measurements could be transformed. The error in the composite surface measurement, as a result of the alignment was shown to be within an acceptable range of ±1 mm, with the majority of error across the surfaces closer to zero. The multiple camera approach would not completely measure all foot surfaces, for this reason interpolation of measurement gaps was required. The interpolation was possible for surface measurements only (not deformation) and was completed in third party software with measurement error from interpolation shown to be within a similar range to error observed for alignment.

To measure runners kinematics, the measurement of markers placed on the skin surface using GOM PONTOS software was proposed, kinetic measurements would be measured from an instrumented force platform separately. This allowed the same images used to measure surface to be used to measure kinematics and negated the need for extra hardware that may affect DIC measurements. A preferred marker set was suggested which creates a four segment foot model as well as giving the option to model the foot as a single segment. Alternative models however, could be implemented using different marker positions.

Markers out of camera view were created via an adapter within the software, defined prior to a measurement, which positions the markers that cannot be measured relative to the position of other markers in view which are measured. The PONTOS software only served to measure three dimensional position of markers, from which a biomechanical c3d file could be created (incorporating the kinetic data) and analysed in appropriate biomechanical analysis software (e.g. Visual3D). The mean error in composite kinematic measurements (i.e. drawn from multiple systems) was shown to be 0.1 mm and 0.3° for length and angular measurements respectively. This error was the incorporation of system measurement error and alignment error, however as the levels were low and the measurement of kinematics was arguably a secondary purpose of the method further investigation of the error composition was deemed unnecessary.

To define a suitable reference state, which would enable the foot to be placed in approximately the same position between test sessions and thus enable meaningful comparison of relative measurement, a reference fixture was designed that attempted to align the foot in a set position, whilst allowing all individual cameras pairs to view foot surfaces. This would serve to provide a reference for both surface and shape measurements as well kinematics.

The developed methodology has the potential to be applied to achieve a diverse set of measurements which have previously been unobtainable, most notably the capability to make measurements during running gait and also measurement of actual shape change (deformation) both of the surface and of discrete measurements across the footstrike. The work covered in this chapter during the development regarding measurement accuracy has built upon the work in Chapter 4 and Chapter 5 which was concerned for individual system measurement.

To complete assessment of the methodology so that measurements made are useful and can be trusted, it is necessary to understand the repeatability and reproducibility of measurements made using the method, in relation to the variables associated with the employment of multiple camera pairs to obtain measurements. This assessment will give an understanding of the variations within and between test sessions. However, before that can be conducted, it is important that the developed methodology is demonstrated in an application of dynamic foot shape measurement, which will be conducted in the following chapter.

7. Dynamic Shape Measurement of the Human Foot

7.1. Introduction

In Chapter 6 a novel methodology has been presented that enables the measurement of foot shape and deformation during dynamic movement using a multiple DIC system approach. The method describes the processes required to obtain a surface model for stages across the foot strike, for a defined foot region. This includes procedures not only for data capture but also those associated with the processing of measured data. Furthermore the developed method encompasses capability to measure the runner's lower extremity kinematics concurrently, as well as capturing ground reaction forces from an instrumented running platform.

The method has been outlined in a generic form, allowing its application in a multitude of tests involving the measurement of foot surfaces and biomechanics during gait rather than a specific test. However, the aim of this thesis is to measure the foot shape during running, therefore the first objective of the work in this chapter was to demonstrate the novel methodology in tests for running speeds addressing OBJ_8 from §1.1.

Both surface and biomechanical measurements made using the methodology have the capability to support numerous analyses, to bring meaning to measurement data and allow conclusions to be drawn. However, the methodology described does not provide a definitive set of metrics for the analysis of surface or biomechanical measurements, the selection of which would be dependent upon the objective of a test or study. Without any analysis however, quantitative description of measured data is impossible. Therefore the second objective of this chapter was to define and present example measurement results for the method elements: namely, shape, surface deformation and runner biomechanics. These analyses were not intended to test a hypothesis or the intervention of a particular variable, but instead to provide a means of communicating the measurement results quantitatively.

Measurements were made of a single subject's right foot, during the stance phase of the gait cycle, during linear running. The methods, results, analysis and discussions will be described in the following sections.

7.2. Methodology

7.2.1. Overview

Methodology for data capture and analysis for both foot morphology and biomechanical measurements followed that described in detail in Chapter 6. A brief outline of the methodology, including additional elements and parameters specific to the measurement application has been outlined in the following sections.

Testing took place at an indoor laboratory with a running lane in excess of 20m in length. This enabled sufficient space to enable the subject to reach and then maintain the desired velocity and not be accelerating or decelerating at the point of measurement. A transparent glass force platform was located within the running lane, positioned flush with the floor so as to allow the subject to run over its surface without having to alter their gait in any way.

Camera pairs were positioned in line with the experimental setup outlined in 6.3.1.2 with system calibrations and global co-ordinate system definitions for each camera pair conducted prior to data collection. An injury free male subject (25yr, 78 kg) was selected for testing. The subject gave their informed consent and ethical clearance was obtained from Loughborough University Ethical Advisory Committee (see Appendix A).

7.2.2. Data Collection

Following application of a surface pattern to the subject's right foot for DIC measurements (§ 6.3.2.1), kinematic markers were attached to the foot as described in § 6.3.3.1 including markers to define an adapter for the proximal shank markers at the knee. Subsequently, reference images were obtained for DIC in a loaded and unloaded state (§ 6.3.5) along with reference images for definition of the kinematic point adapter (§ 6.3.3.2).

The subject was asked to run at a velocity of 3.5 ms^{-1} with the stance phase of gait (touchdown to toe off) occurring, for their right foot, on the force plate in a location that was within the virtual measurement volumes created by the camera pairs. Images were captured in line with the parameters outlined in Table 6-1 (§ 6.3.1.3) with the average running velocity measured using light gates spaced approximately three metres apart, on either side of the impact location. Three measurements were made, with trials accepted when the average velocity of the subject was within ±5% of the intended. The subject was given time before testing to warm up and practice running over the force platform with their right foot landing in the correct location. The subject was also given adequate time between measurements to rest to prevent fatigue.

7.2.3. Data Processing

7.2.3.1. DIC Measurements

For each test, individual shape and deformation measurements from each stereo camera pair were processed using ARAMIS software with parameters defined in Table 6-4, before being transformed to the global co-ordinate system via predefined transformation files (§ 6.3.1.5). Each individual measurement from each camera pair was imported into GOM S-VIEW software to create a composite foot shape and deformation measurement.

The foot shape for each individual stage of the measurement was exported as an STL file and individually processed in Geomagic's Studio software to interpolate gaps in the surface measurement data as well as removing duplicated surface data (§ 6.4.1.2), these 'complete' foot shapes were used to support the analysis of the dynamic foot shape.

7.2.3.2. Kinetic Measurements

Kinetic data measured from the force plate for each test was exported directly from the operating software, and processed in Microsoft Excel, from which the touchdown and toe off events were identified from the vertical GRF data, allowing identification of the first and last images of the optical measurements.

7.2.3.3. Kinematic Measurements

For each test, three dimensional kinematic point data was processed from the image data as individual measurements using the GOM PONTOS software. A 'composite point cloud' was created within the same software by importing measurements into a single measurement 'project'. The point cloud positional data was exported to create a c3d file that enabled evaluation in Visual 3D biomechanical analysis software. Lower extremity segment definitions and parameters used in processing were as described in § 6.4.2.

Filtering of kinematic data was necessary to remove noise in data introduced during the measurement. It was important not to apply a filter that may over-smooth data. A zero lag Butterworth fourth order low pass filter was applied to the kinematic data with a cut of off frequency of 12 Hz. This filter type has been used in other studies measuring kinematics at ranges between 10Hz and 30Hz (Fukuchi & Duarte, 2008; Morio et al., 2009; Queen, Gross, & Liu, 2006) the comparison between measurements derived from unfiltered and filtered data are shown in Figure 7-1, which shows measurements derived from the filtered data were not over-smoothed and therefore the cut off frequency was deemed acceptable.

Filtering would be important when calculating derivatives from displacement data such as velocities and accelerations. Even though these would not be calculated in subsequent analysis of data in this particular work, it was considered appropriate to complete the process.
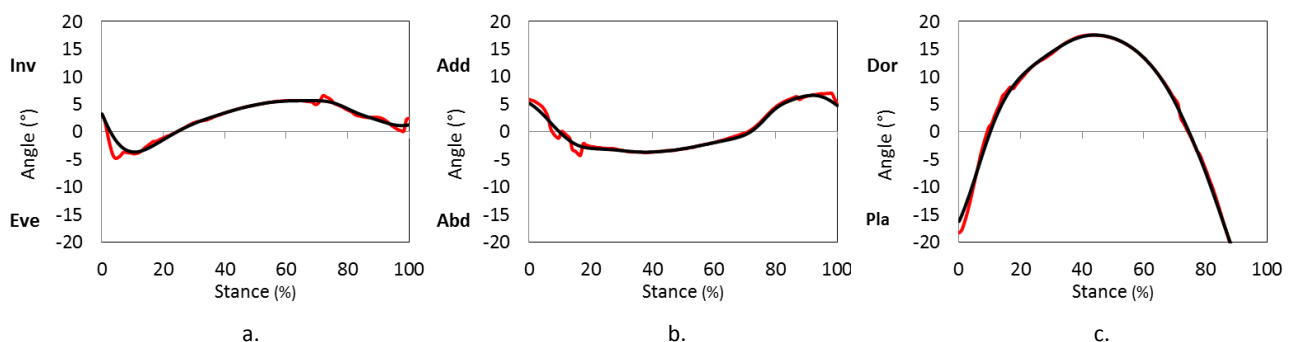
Figure 7-1 – Angular displacement measurements for the foot segment with respect for the shank about the three joint axes (a) inversion/eversion (b) adduction/abduction (c) dorsiflexion/plantarflexion. Unfiltered data: red line, filtered data: black line.

7.2.4. Data Analysis

7.2.4.1. Kinetics

The mean GRF data across the three tests was derived from individual measurement in its three components (F_x, F_y, F_z), with the timing and magnitude of four specific events within the GRF data identified and recorded: braking and propulsion peaks in F_Y and active and passive peaks in F_Z.

7.2.4.2. Kinematics

For the kinematic assessment, in line with Leardini *et al.* (2007), four joints defined from the segments of the foot model were assessed; the calcaneus with respect to the shank, the midfoot with respect to the calcaneus, the metatarsal segment with respect to the midfoot and the foot with respect to the shank. Measurements were made relative to a standing reference (§ 6.3.5) following the angle definitions outlined in § 6.4.2.4.

7.2.4.3. Foot Shape

To assess foot morphology via discrete measures, a number of separate foot shape metrics were defined, a summary of which is presented in Table 7-1. Shape metrics were defined from points on the surface of the foot, in the loaded reference stage and then tracked throughout the footstrike. A total of 7 shape metrics were defined: 5 cross sections, 1 width/length and 1 volumetric. For each cross sectional metric, two measurements were made, the cross sectional area and the circumference of the cross section.

No.	Shape Metric	Measurement	Reference
1.	Foot Breadth	Length	
2.	MPJ Cross Section	Area	Wunderlich *et al.* (2001), Witana *et al.* (2006), Kouchi et al. (2009), Wang (2010)
		Circumference	
3.	Instep Cross Section	Area	Wunderlich *et al.* (2001), Witana *et al.* (2006), Kouchi et al. (2009), Wang (2010), Hong *et al.* (2011)
		Circumference	
4.	Waist Cross Section	Area	Wang (2010)
		Circumference	
5.	Short-Heel Cross Section	Area	Wunderlich *et al.* (2001), Witana *et al.* (2006), Hong *et al.* (2011)
		Circumference	
6.	Ankle Cross Section	Area	Wunderlich (2001), Witana *et al.* (2006), Hong *et al.* (2011)
		Circumference	
7..	3D Foot Shape	Volume	

Table 7-1 - Summary of metrics for describing the foot shapeand and the measurements types from each.

The foot shape metrics defined were based on those used in previous static (Hong *et al.*, 2011; Wang, 2010; Witana *et al.*, 2006; Wunderlich *et al.*, 2001) and dynamic studies (Kouchi et al., 2009), these were not however a definitive set of measurements aimed at fully characterising the foot shape dynamically, but instead intended to facilitate demonstration of the methodology as a foot shape measurement tool. Absolute measurements were made, along with relative measurements, referenced to the value at the unloaded reference stage, which essentially formed a deformation measurement.

Foot Co-ordinate System

To aid the definition of the metrics, a foot co-ordinate system (FCS) was defined in the loaded reference stage. Its purpose was to remove the potential errors that may occur in the measurement definitions as a result of the orientation of the foot in relation to the global co-ordinate system. The origin of the FCS was located at CA, the Y axis the projection of the line joining the origin (CA) and SMH on the plane perpendicular to the XY plane passing through the origin (CA) and SMH, as shown in Figure 7-2.
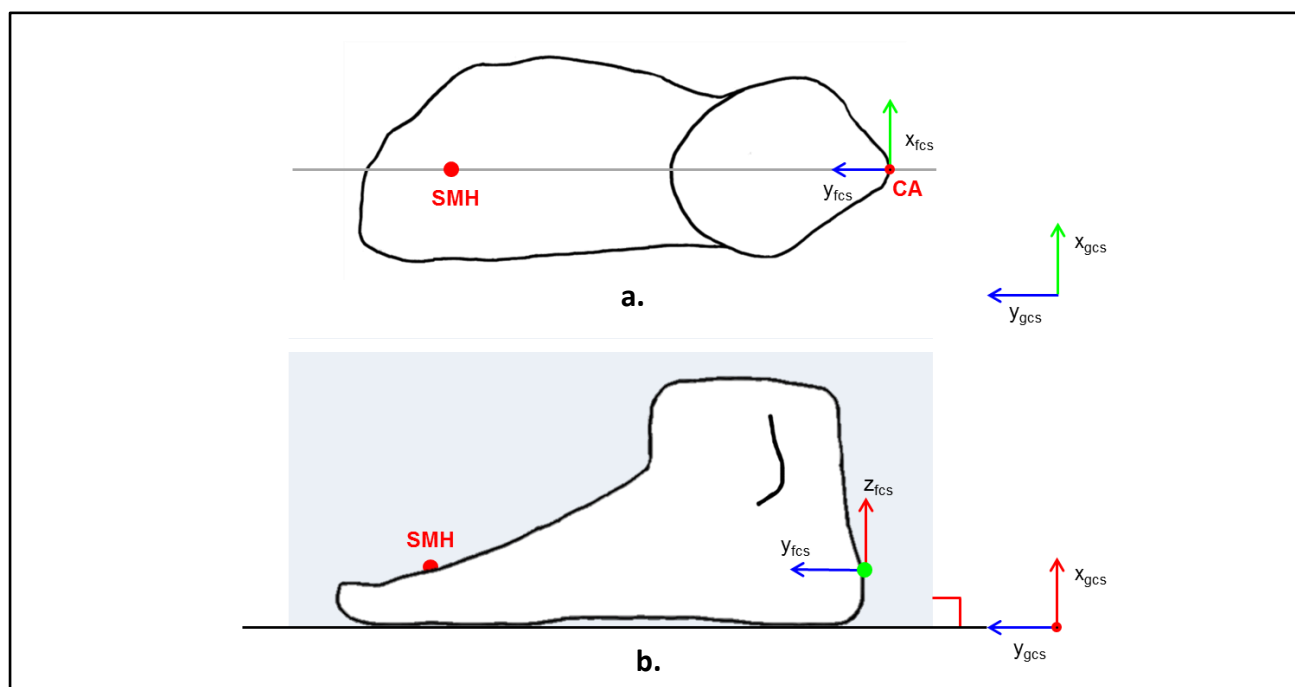
Figure 7-2 - Schematic of the foot co-ordinate system (FCS) definition on a right foot along with the global coordinate system (GCS) orientation (a) Transverse View (b) sagittal view

Foot Cross Sections

The MPJ cross section was defined from the plane intersecting the foot perpendicular to the XY_{FCS} plane, passing through marker points FMH and VMH (Figure 7-3a). The instep cross section was defined from the plane intersecting the foot perpendicular to the XY_{FCS} plane at the SMB marker point (Figure 7-3a). The waist cross section was defined from the plane intersecting the foot perpendicular to the XY_{FCS} plane, at point W_1: the midpoint between SMB and VMH marker points (Figure 7-3b). The short heel cross section was

defined from the plane intersecting the foot perpendicular to the ZY_{FCS} plane through points SH_1: the most proximal point on the foot surface along the Y_{FCS} axis on the ankle plane and SH_2: the point created from the projection of CA onto the XY_{GCS} plane along the Z_{FCS} axis (Figure 7-3c). The ankle cross section was defined in the loaded reference stage from the plane intersecting the foot parallel to the XY_{GCS} plane at the HF marker point (Figure 7-3c).
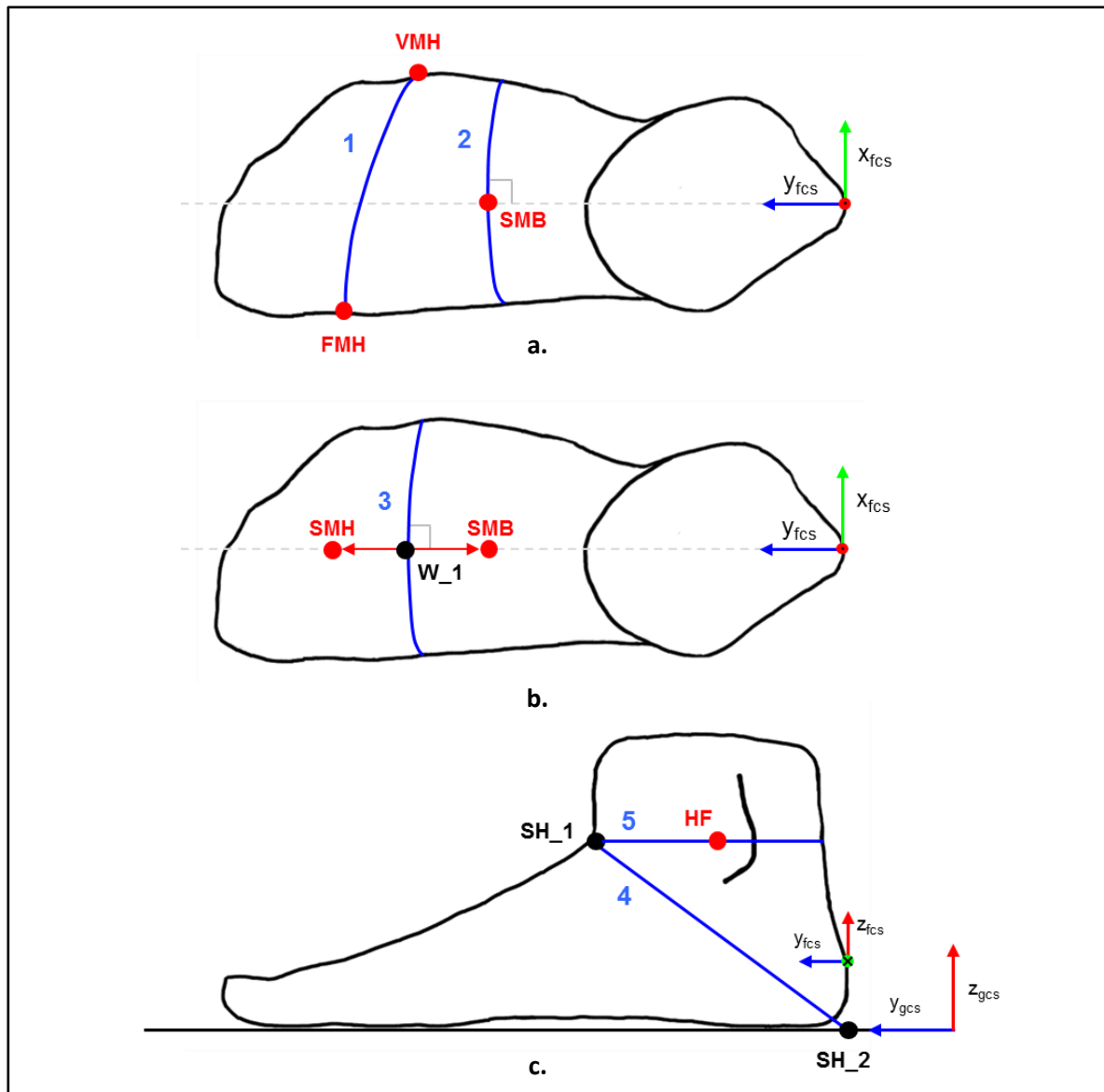
Figure 7-3 – Foot cross section definitions (1) MPJ (2) Instep (3) Waist (4) Short Heel (5) Ankle

After each plane was defined, three points on the foot surface on the plane were defined which could be tracked throughout the footstrike. These points were either points measured from the pattern by DIC or the kinematic marker points. Where DIC measured points were used, these were selected in areas where low surface deformation was observed. Figure 7-4 shows examples of the measured cross sectional shapes of the foot in the global coordinate system from two views.
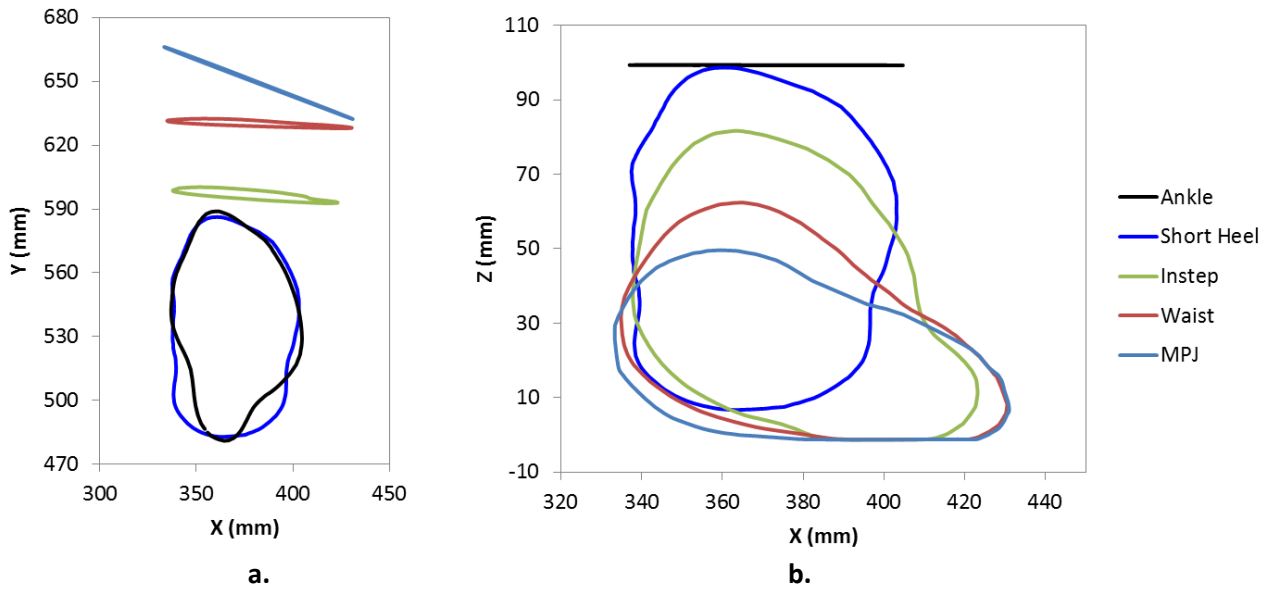
Figure 7-4 – Measured cross sectional shapes of the right foot in the reference stage in the global coordinate system (a) plan view (b) anterior view

Foot Volume

The foot volume was defined as the three dimensional foot geometry contained distally by the MPJ cross section and proximally by the ankle cross section as described previously. (Figure 7-5).
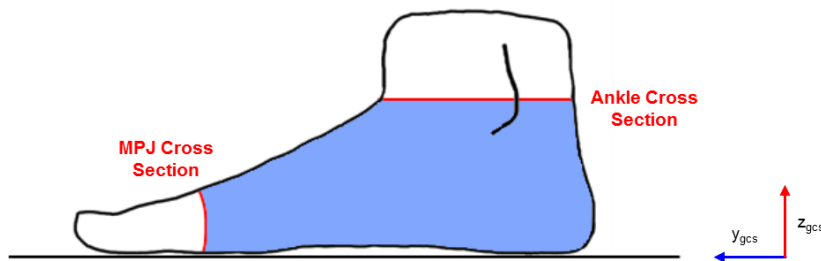
Figure 7-5 –Definition of foot volume (shaded area) contained by MPJ and ankle cross sections

Foot Breadth

Foot breadth was the linear distance between the first and fifth metatarsal heads defined by kinematic markers FMH and VMH respectively (Figure 7-6).
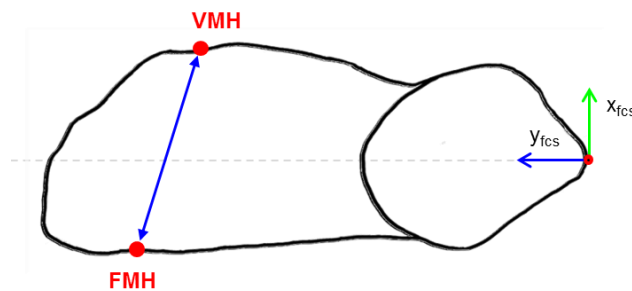
Figure 7-6 – Definition of ball width on the right foot from first and fifth metatarsal heads defined by markers FMH and VMH

7.2.4.4. Foot Surface Deformation Measurements

Surface deformation results were presented as a major strain colour plot, on a composite surface model created from individual measurements aligned in the GOM S-View software. In addition, the local direction of surface deformations were displayed via arrows overlaid on the contour plot.

Results were presented from three views: medial, lateral and plantar so as to enable inspection of the deformation occurring around the whole foot. Due to the number of stages contained in a full footstrike measurement, rather than attempting to present every stage, six discrete points in the stance, defined from the force data, were selected. They were: initial contact, passive force peak (in F_z), braking force peak (in F_y), active force peak (in F_z), propulsion force peak (in F_y) and toe off.

7.3. Results and Discussion

7.3.1. Runner Kinetics

The ground reaction forces, presented in Figure 7-7 show curve shapes and magnitudes consistent with those measured by Cavanagh and Lafortune (1980) for a midfoot running style. Notably in the vertical (F_z) GRFs (Figure 7-7c) when compared to a heel impact running style, the high frequency passive peak was less prominent and in the anterior-posterior (F_y) GRF (Figure 7-7b) where a double peak was observed in the first 20% of the stance phase.
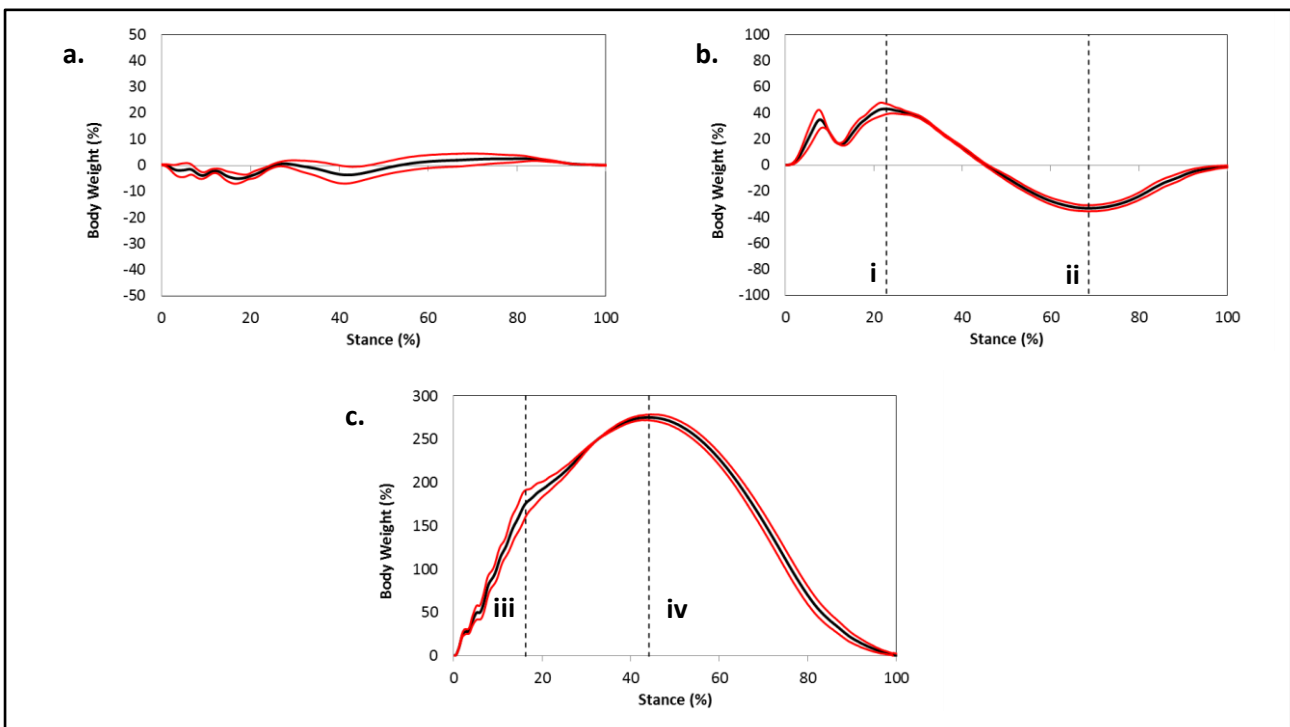
Figure 7-7 – Graphs showing mean GRF for runner: (a) medio lateral, Fx, (b) anterior-posterior, Fy and (c) vertical, Fz. Dashed lines depict (i) 16%-peak breaking. (ii) 23%-peak propulsive (iii) 44%-peak active and (iv) 69%-peak passive force events. Red lines denote +s.d.

For this particular test, the subject was not asked to run in a particular style, however the adoption of a midfoot technique (as defined by Cavanagh and Lafortune) is likely a result of running in a barefoot condition as opposed to shod; which is supported by observations in other studies (Lieberman et al., 2010).

7.3.2. Runner Kinematics

Mean kinematic results for the four foot joints are presented in Figure 7-8 with maximum mean joint excursions and timings shown in Table 7-2.

	Max Inversion (°)	Max Eversion (°)	Max Adduction (°)	Max Abduction (°)	Max Dorsiflexion (°)	Max Plantarflexion (°)
Foot wrt shank	6.3 (67%)	3.4 (11%)	7.0 (96%)	5.3 (41%)	17.0 (45%)	30.5 (100%)
Calcaneus wrt Shank	1.2 (87%)	0.9 (15%)	3.0 (0%)	2.6 (47%)	11.8 (48%)	18.1 (100%)
Midfoot wrt Calcaneus	9.8 (100%)	3.5 (22%)	3.4 (100%)	2.1 (24%)	10.6 (48%)	8.1 (100%)
Metatarsals wrt Midfoot	1.2 (64%)	3.7 (6%)	1.4 (9%)	1.8 (73%)	2.7 (25%)	8.4 (100%)

Table 7-2 – Maximum mean joint excursions and timings (% stance in brackets) in each plane for each defined foot joint

The results show the 'foot' was slightly inverted, adducted and plantarflexed at touchdown with respect to the shank (Figure 7-8a, b, c), after which the foot experienced rapid eversion followed by a steady inversion movement reaching a maximum around the peak propulsive force (F_y). This is accompanied by plantarflexion and abduction during loading response through to midstance, both of which attain a maximum at the peak active force (F_z). In terminal stance through to toe off, the foot begins to plantarflex, adduct and evert with respect to the shank, in a classic 'supination' movement.

The movement of the calcaneus segment with respect to the shank (Figure 7-8d, e ,f) compared well with those observed for the foot with respect to the shank, except for slightly reduced magnitudes which could potentially be accounted for in the motion at the mid and forefoot. As expected the greatest motion was observed in the sagittal plane (dorsiflexion-plantarflexion) for the midfoot (Figure 7-8g, h, i) and forefoot (Figure 7-8j, k, l) segments with relatively low excursions measured in the transverse and frontal planes of each. The only exception to this was the inversion of the midfoot with respect to the calcaneus during the terminal stance phase (80-100% stance).

To date, published studies employing this kinematic model have been limited to walking gait and therefore direct comparison with a running trial was not possible for all segments, most notably for the midfoot and metatarsal. However, angular displacement patterns for the calcaneus showed good agreement with those measured by Pohl et al. (2008), who defined calcaneus and shank segments in a similar way to the Leardini model used in this work, for a midfoot running style in a barefoot condition.
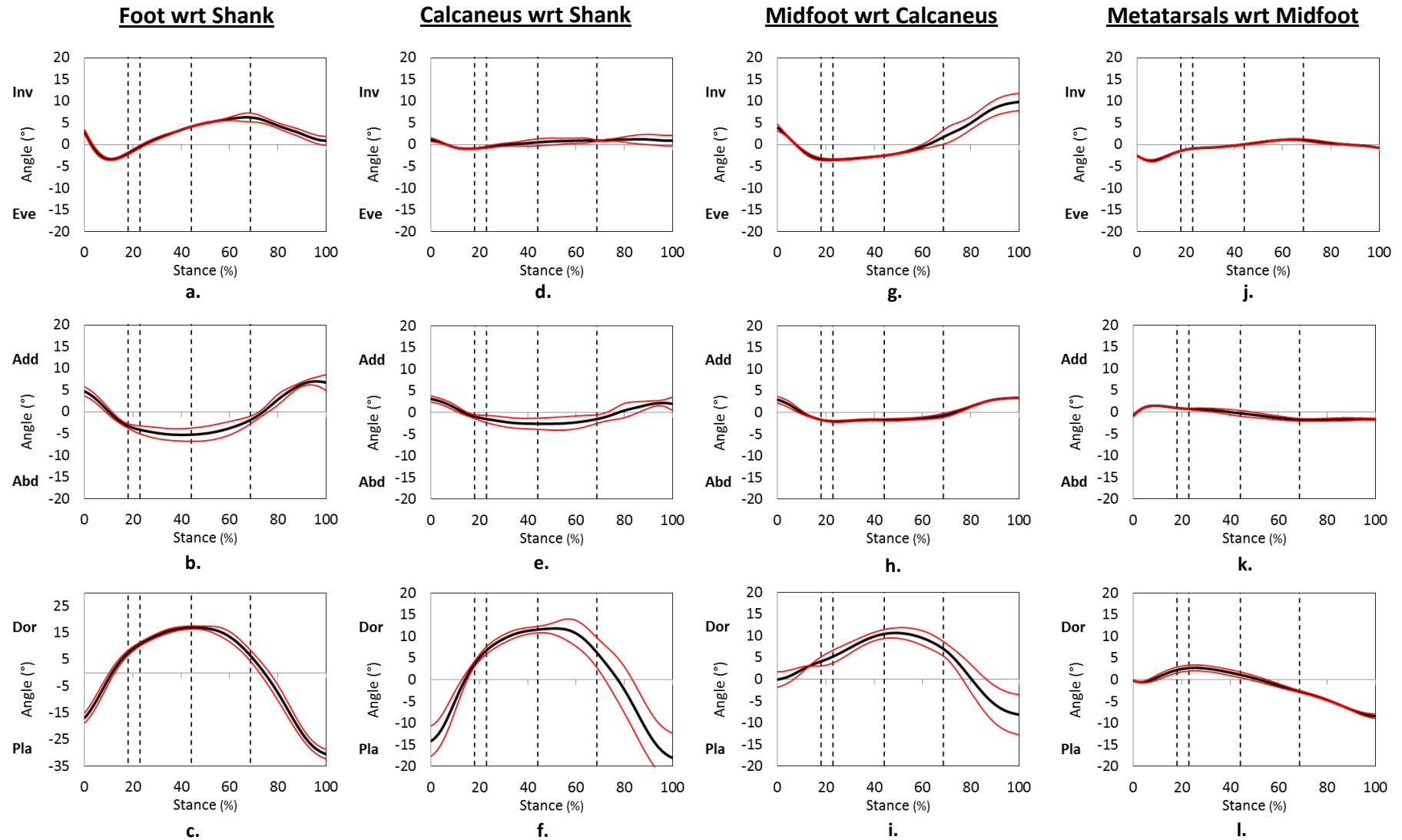
Figure 7-8 – Mean rotations about the three joint axes, over the three rows, for the four joints; foot wrt shank (a, b, c) calcaneus wrt to shank (d, e, f), midfoot wrt calcaneus (g, h, i) and metatarsals wrt to midfoot (j, k, l). Red lines denote ±s.d. and dashed lines indicate mean GRF events in stance: peak passive force in F_z (16%), peak braking force in F_y (23%), peak active force in F_z (44%) and peak propulsion force in F_y (69%).

The results show the potential for full kinematic measurement of a runner during the stance of gait that would be extremely difficult to achieve with any other methodology, due in part to the fact DIC is passive and that kinematic marker measurements can be made from the same images without affecting surface measurement coverage. Furthermore, there is no reason to believe that changing parameters such as footstrike or velocity would affect the ability to make these measurements.

The kinematic analysis presented is intentionally generic, as the results are intended to demonstrate the method. More detailed analysis would be possible with the same kinematic marker set and foot model, or alternatively a simplified analysis, dependent upon the requirements of a study. It is also important to note that the kinematic foot model could potentially be changed or substituted for a different model to suit the analysis needs of a study using the method.

7.3.3. Shape Measurements
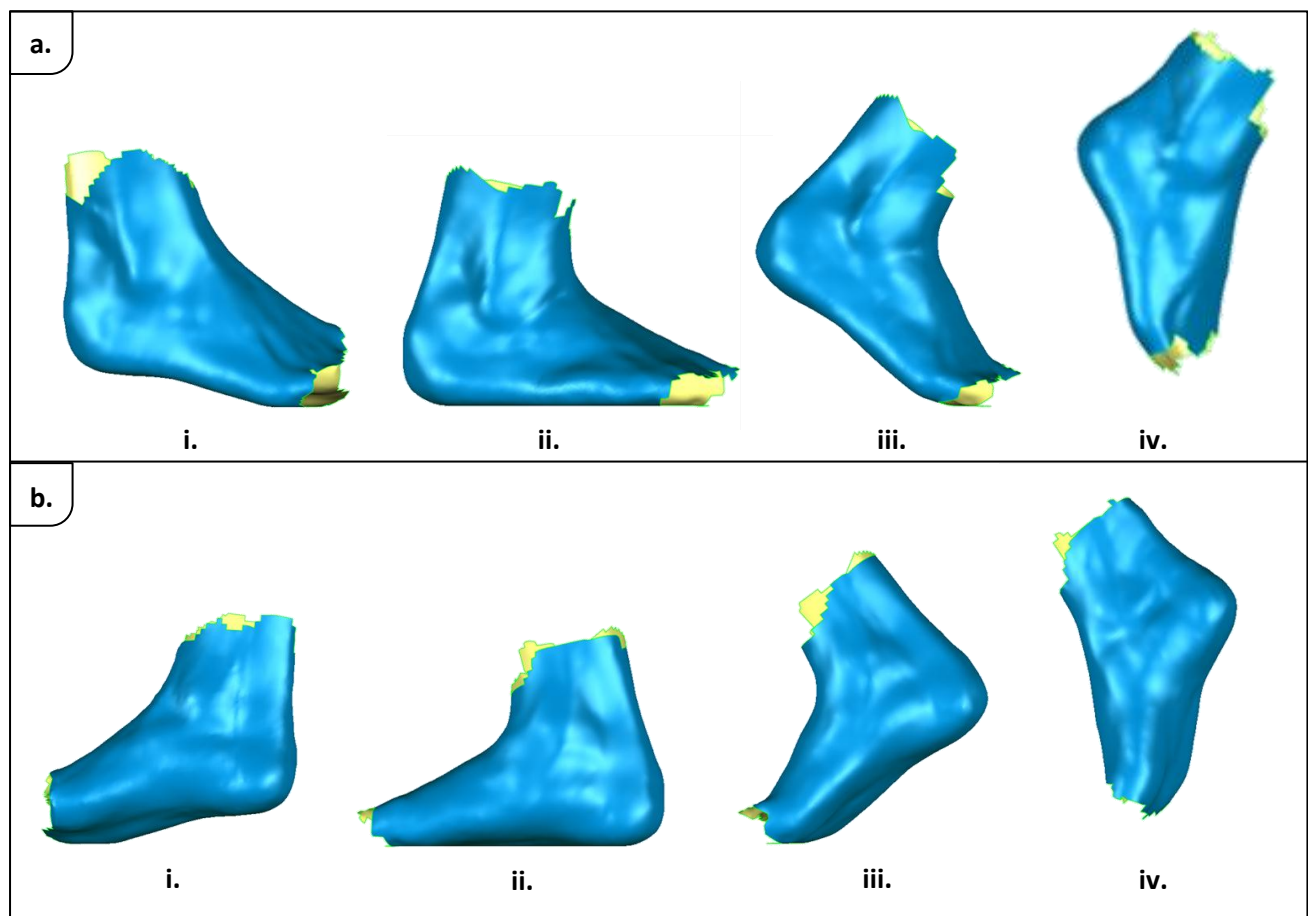
Figure 7-9 - Post processed measured surfaces from a single test from (a) lateral and (b) medial views at four stages across stance (i) touchdown (ii) peak braking (iii) peak propulsive (iv) toe off.

A sample of the measured surfaces from a number of stages from a single test across the stance, from which shape measurements were derived, are presented in Figure 7-9.

7.3.3.1. Foot Breadth Results

The mean absolute and relative foot breadth measurement across the foot strike are shown in Figure 7-10, with relative measurements made to the loaded reference stage. The curve shows a rapid increase in breadth after initial foot contact through to the point of peak braking force with a total breadth change of approximately 7.5 mm. Once the peak active force in F_z is attained, the foot breadth slowly decreases through to toe off, as the foot unloads. Across the whole footstrike, a total breadth difference of approximately 7% is observed relative to the unloaded reference, equating to approximately 9 mm.
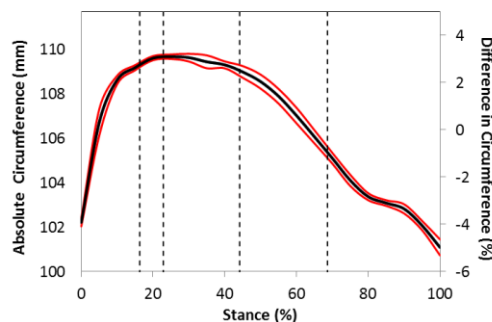
Figure 7-10 – Mean foot breadth over footstrike, absolute measurement (left y-axis) and percentage difference referenced to unloaded reference (right y-axis). Red lines denote ±s.d. and dashed lines denote GRF events in stance: peak passive force in F_z (16%), peak braking force in F_Y (23%), peak active force in F_Z (44%) and peak propulsion force in F_Z (69%).

The expansion at the foot breadth is another example of movement of the intrinsic foot structures as the foot is loaded, which acts as a mechanism for dissipating forces related to support and propulsion. One would potentially see a slightly different change in ball breadth profile when the footstrike style changes; for example where initial contact occurs at the heel of the foot, as timing and magnitudes change as a result of different foot movements and associated forces acting on the foot.

7.3.3.2. MPJ Cross Section Results

The results for the mean MPJ cross sectional area (Figure 7-11a) show that the foot's cross sectional area decreases rapidly under loading after foot contact through to the active force peak. This was followed by a period of slower reduction up to the active force peak, after which a slow increase was observed through to toe off, as the foot unloads. A maximum of around 5% reduction relative to the unloaded reference was measured and over the entire footstrike the cross sectional area changed by approximately 13%. The cross sectional circumference (Figure 7-11b) did not show such a distinct change over the footstrike, with a moderate 2% relative to the loaded reference by comparison. The graphs show, understandably, that a small change in the circumferential length was required to impart the changes in the cross sectional area. Furthermore, the increase in the circumference was observed with a decrease in cross sectional area, which was likely to be the result of areas of the cross sectional perimeter extending inwards rather than outwards (i.e. expansion).

Figure 7-11 – Mean MPJ cross sectional (a) area (b) circumference over footstrike. Left y-axis shows absolute value, right y-axis shows percentage change relative to unloaded reference. Red lines denote ±s.d. and dashed lines denote GRF events in stance: peak passive force in F_Z (16%), peak braking force in F_Y (23%), peak active force in F_Z (44%) and peak propulsion force in F_Z

7.3.3.3. Waist Cross Section Results

The mean cross sectional area results for the waist cross section (Figure 7-12a) showed a similar profile to that observed for the MPJ. An initial rapid decrease in cross sectional area was observed in the first 10-15% of stance followed by a more gentle decrease, reaching a minimum around the peak active force at midstance. A steady increase was then seen before a steep rise instigated around the peak propulsive force event through to toe off. Over the footstrike the cross sectional area varied by around 5 cm^2, equating to around 14% relative to the unloaded reference. The mean circumference (Figure 7-12b) had a different profile to that observed before, namely the increase during the latter stages of stance as the foot dorsiflexes and unloads, in line with the increasing cross sectional area. The mean circumference varied across the footstrike by approximately 10 mm, equating to around 4% relative to unloaded reference.

Figure 7-12 – Mean waist cross sectional (a) area (b) circumference over footstrike. Left y-axis shows absolute value, right y-axis shows percentage change relative to unloaded reference. Red lines denote ±s.d. and dashed lines denote GRF events in stance: peak passive force in F_Z (16%), peak braking force in F_Y (23%), peak active force in F_Z (44%) and peak propulsion force in F_Z (69%).

7.3.3.4. Instep Cross Section Results

The mean area and circumference results for the instep cross section (Figure 7-13) followed similar profiles observed for the waist and MPJ, as one would expect, due to its location. For cross sectional area a rapid initial decrease in area followed by a midstance plateau was evident, before an increase during the terminal stance stages, as the foot unloaded. Across stance the mean area varied by 10% relative to the loaded

134

reference equating to around 5 cm², with the maximum area observed at toe off. For circumference, the measurement steadily decreased from touchdown through midstance to the onset of unloading of the foot following the peak propulsive force, at which point circumference rapidly increased to toe off, as observed in the cross sectional area measurements. Across the footstrike the circumference changed by 9 mm; approximately 3.5% relative to the unloaded reference.
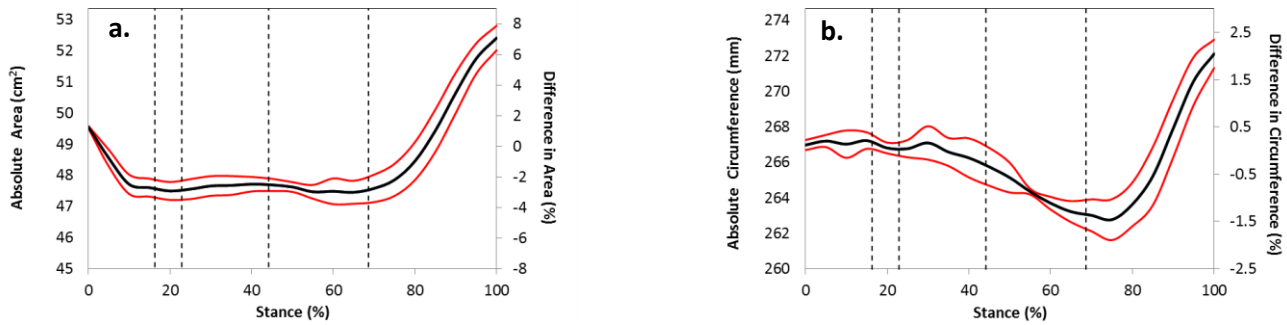
Figure 7-13 – Mean instep cross sectional (a) area (b) circumference over footstrike. Left y-axis shows absolute value, right y-axis shows percentage change relative to unloaded reference. Red lines denote ±s.d. and dashed lines denote GRF events in stance: peak passive force in F_Z (16%), peak braking force in F_Y (23%), peak active force in F_Z (44%) and peak propulsion force in F_Z (69%).

7.3.3.5.   Short Heel Cross Section Results

The mean results for short heel cross sectional area and circumference, presented in Figure 7-14, show very different measurement profiles, as one might expect, to the cross sections measured more distally along the foot. The cross sectional area increased steadily after initial contact at the beginning of stance reaching a maximum around the peak active force event. An equally steady decrease in cross sectional area was observed through to toe off, where the cross sectional area was approximately equal to that at touchdown. The range over which cross sectional area changes was 8 cm² which was approximately 11% relative to the unloaded reference. The circumference followed an almost identical profile shape with a range across the whole footstrike of 21 mm: 6% relative to the unloaded reference.
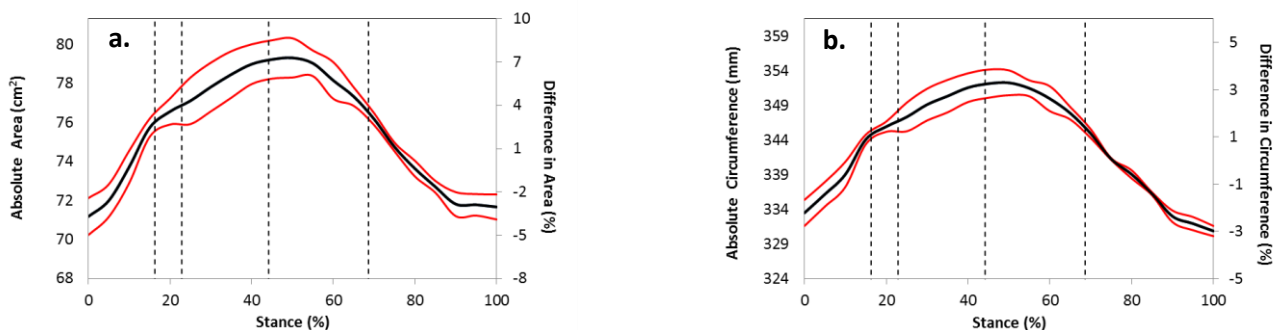
Figure 7-14 - Mean short heel cross sectional (a) area (b) circumference over footstrike. Left y-axis shows absolute value, right y-axis shows percentage change relative to unloaded reference. Red lines denote ±s.d. &dashed lines denote GRF events in stance: peak passive force in F_Z (16%), peak braking force in F_Y (23%), peak active force in F_Z (44%) & peak propulsion force in F_Z (69%).

7.3.3.6. Ankle Cross Section Results

The mean ankle cross sectional area results (Figure 7-15a), like the short heel cross section, followed a different profile to the MPJ, waist and instep cross sections as the movement and function of the foot in this region is completely different. For this reason perhaps, there does not appear to be any clear correlation between timing of force events (dashed lines) and the ankle cross sectional measurements, as was seen with previous cross sectional results.
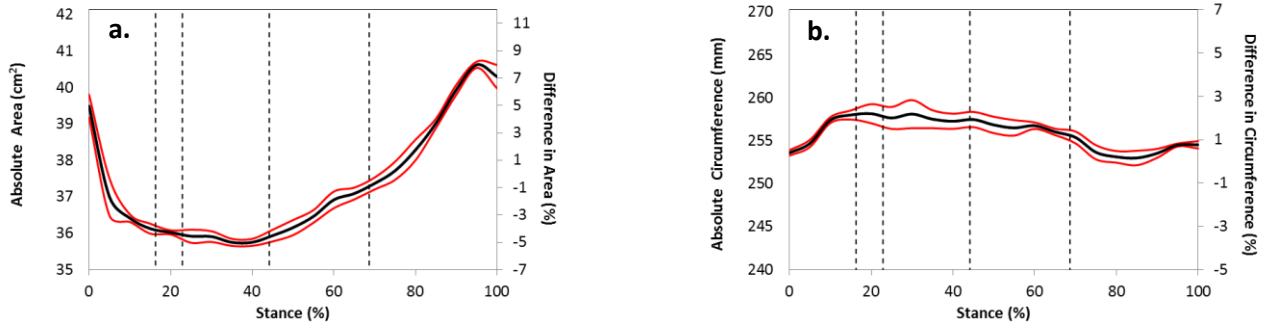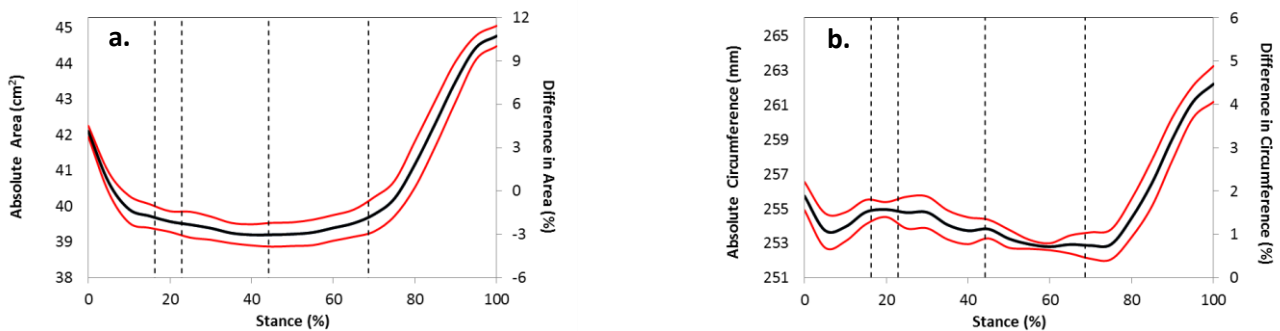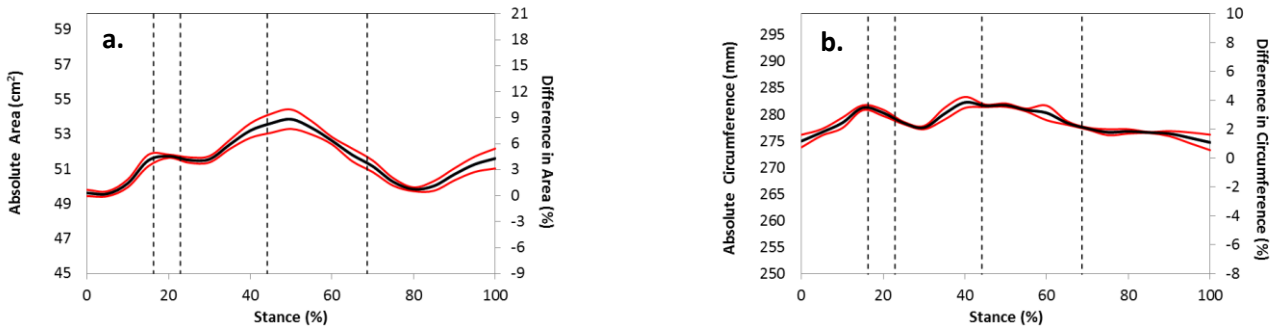

Figure 7-15 –Mean ankle cross sectional (a) area (b) circumference over footstrike. Left y-axis shows absolute value, right y-axis shows percentage change relative to unloaded reference. Red lines denote ±s.d. and dashed lines denote GRF events in stance: peak passive force in F_Z (16%), peak braking force in F_Y (23%), peak active force in F_Z (44%) and peak propulsion force in F_Z (69%).

Over the whole foot strike, a cross sectional change of around 4 cm^2 was observed equating to a 9% change relative to the unloaded reference. The greatest change was seen in midstance as the leg moved forward over the foot ready to begin heel lift and toe off movements. It is this movement, that is most likely to explain the changes measured. As with the MPJ and midfoot sections, the ankle circumference (Figure 7-15b) appears to remain relatively consistent with relative changes within 2% of the reference.

7.3.3.7. Foot Volume Results
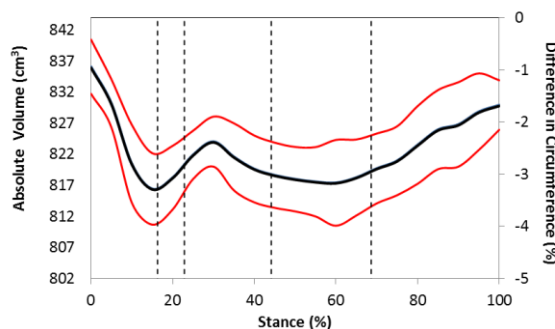
Figure 7-16 –Mean Foot volume over footstrike. Left y-axis shows absolute value, right y-axis shows percentage change relative to unloaded reference. Red lines denote ±s.d. and dashed lines denote GRF events in stance: peak passive force in F_Z (16%), peak braking force in F_Y (23%), peak active force in F_Z (44%) and peak propulsion force in F_Z (69%).

Figure 7-16 shows that across the footstrike the mean foot volume of the foot changes by approximately 2.5% (20 cm^3) compared to the unloaded reference. The foot was at its largest at initial contact, reducing in volume to a minimum at the passive force peak event (≈-3%), before experiencing a short period of volume

increase. This was followed by a slow reduction through midstance before increasing slowly up to toe off as the foot unloads during terminal stance. The standard deviation curves on the graph indicate that compared to the cross sectional measurements, the foot volume measurement was much more variable as a result of the subject.

7.3.3.8. Discussion

The decrease in the area of the MPJ, midfoot and instep cross sections demonstrate that the foot compresses/deforms relative to both the foot shape at touchdown and to the unloaded reference state with a similar pattern observed for the foot breadth. The deformations over the footstrike reveal the effect of intrinsic foot structures dissipating the external forces related to support and propulsion exerted during the stance phase. These patterns were not observed in the short heel and ankle cross sections as the function of the foot in this region is completely different. One would potentially see different cross sectional profiles when the footstrike style changes; for example where initial contact occurs at the heel of the foot, as timing and magnitudes of measurements would change as a result of foot movements and associated forces acting on the foot.

Wang (2010) suggested that the most important foot measurements related to fit and comfort of a shoe were the MPJ, waist and instep cross sections. With a relative increase in area of 10-14% in all three of these distal cross sections, it is clear there is a potential need to consider the dynamic foot shape in a shoe's design (for running). No published studies to date have reported results for the measurement of the cross sectional area of the foot during the stance phase of gait with only one study measuring dynamic circumference measurement been reported: for a version of the MPJ cross section (Kimura et al., 2009). Although this was for walking gait, the pattern of change was in general agreement with the measurements observed in this testing.

7.3.4. Surface Deformation

The foot surface deformations at six discrete stages of stance, viewed medially, laterally and from the plantar aspect are presented in Figure 7-17, Figure 7-18 and Figure 7-19 respectively, with local direction of deformation shown by arrows overlaid on the plots. As it was not possible to create plots of the average deformation (from the multiple tests), results and discussions are made around the results from a single test. Furthermore, as deformation measurements could not be interpolated like with shape, data gaps between the surfaces from each individual shape measurement can be observed.

The deformation (major strain) plots show that on the dorsal foot surfaces (Figure 7-17 and Figure 7-18), deformations are more widespread on the medial side of the foot in comparison to the lateral, especially in the midstance stages, potentially driven by the 'pronation' movement of the foot during this period.
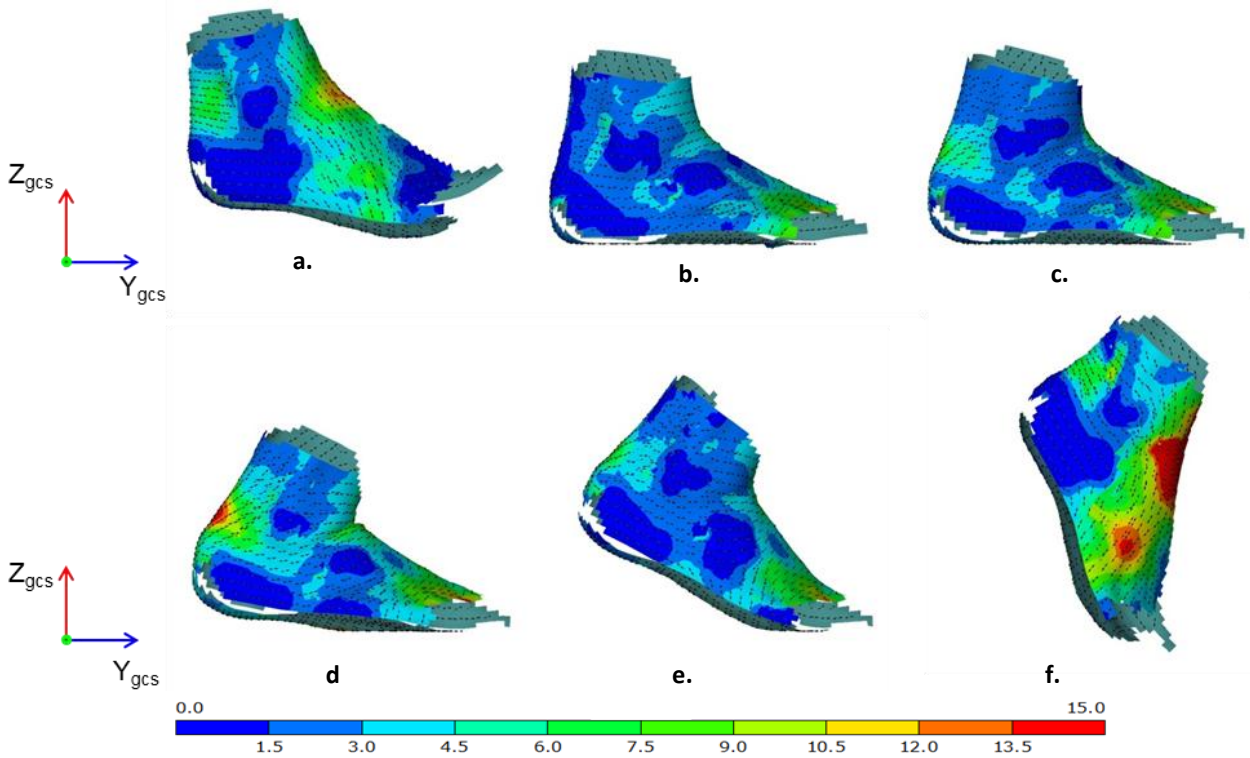
Figure 7-17 – Medial view of foot deformation measured as major strain (%) relative to unloaded reference stage at touchdown (a), passive force peak in F_z (b), braking force peak in F_y (c), active force peak in F_z (d), propulsion force peak in F_y (e) and at toe off (f). Overlaid arrows indicate local deformation direction.
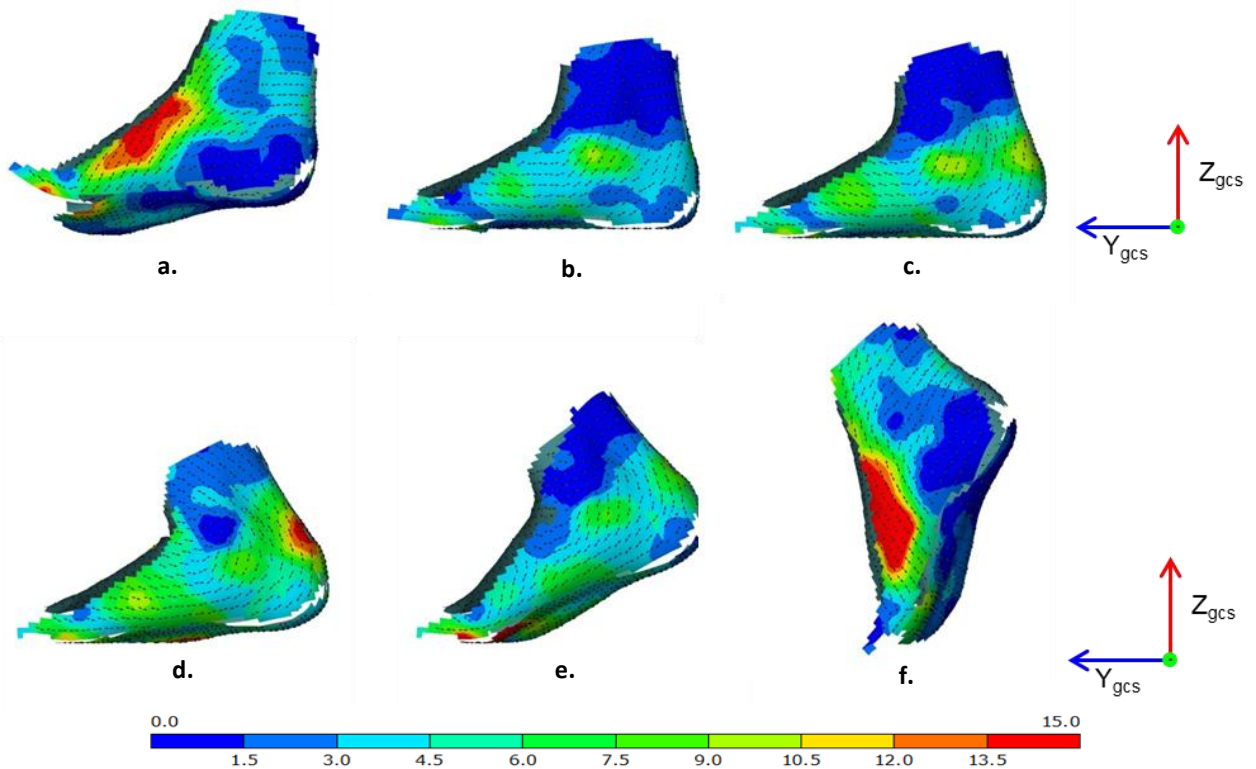
Figure 7-18 – Lateral view of foot deformation measured as major strain (%) relative to unloaded reference stage at touchdown (a), passive force peak in F_z (b), braking force peak in F_y (c), active force peak in F_z (d), propulsion force peak in F_y (e) and at toe off (f). Overlaid arrows indicate local deformation direction.
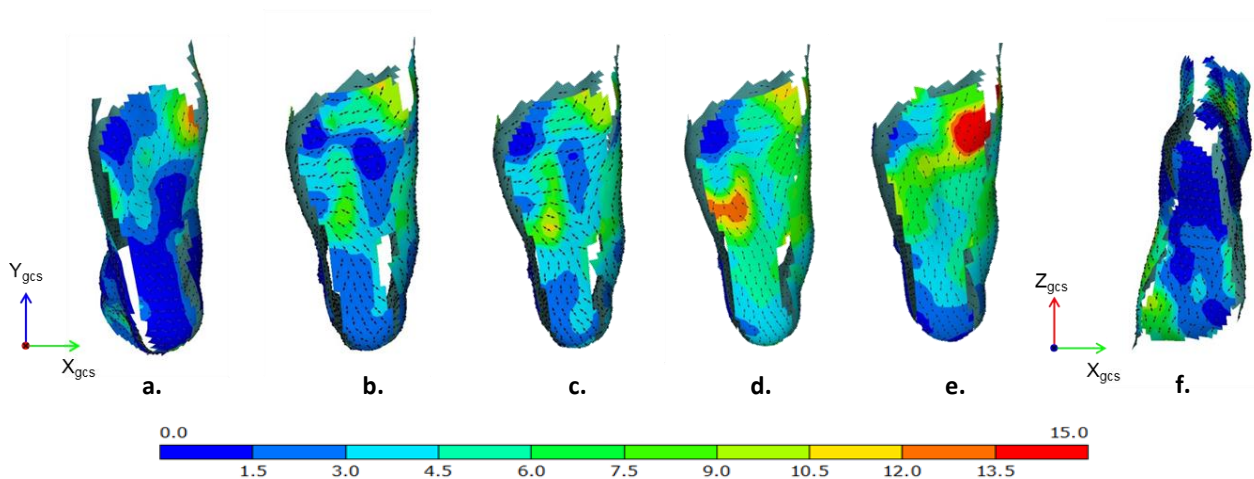
Figure 7-19 – Plantar view of foot deformation measured as major strain (%) relative to unloaded reference stage at touchdown (a), passive force peak in F_z (b), braking force peak in F_y (c), active force peak in F_z (d), propulsion force peak in F_y (e) and at toe off (f). Overlaid arrows indicate local deformation direction.

Medially, deformation is directed across the forefoot during midstance, undoubtedly due to the foot expansion in this region observed in previous measurements. As the foot plantarflexes to toe off, the direction of local deformation becomes more aligned with the shank. This is also observed at initial contact due to the comparative plantarflexion in the unloaded reference. On the lateral foot surface, at the mid and forefoot, during the loading phases, the deformations align with those occurring on the foot's medial surfaces, across the foot. As with the medial deformations, when the foot plantarflexes the deformations rotate to align to the shank. The largest deformations on the dorsal foot surfaces occur in the surfaces above the medial cuneiform and along the first metatarsal at toe off, indicating the area greatest effected by plantarflexion of the foot.

At the rearfoot, deformations were observed along the Achilles tendon during loading, occurring in the region proximal to the attachment of the tendon to the calcaneus, essentially where the foot is less rigid. At the rearfoot, both medially and laterally, deformations occur around the bony protrusions of the tibia and fibula indicating areas in the heel of the foot which are more flexible.

The deformation contour plots for the plantar foot surface (Figure 7-19) show that deformations occur due to the foot surfaces contacting the ground, anchoring the foot in position, with directions indicating the 'spreading' of the surface under loading. Plantar surfaces which are not in contact with the ground, move relative to the anchored surfaces during the footstrike to cause deformation, especially during heel lift, with deformation directions aligned along the length of the foot.

7.4. Further Application

The measurements and analysis in the previous sections were created from a single subject on a single day of testing. To demonstrate the further application of the methodology, measurements were carried out for

two additional subjects on a different day for each, with measurements made under the methodological conditions described in §7.2.

Rather than presenting a full analysis for the additional subjects (as already presented for the first subject), for demonstrative purposes, only the surface measurement results, from which shape measurements would be made are presented in Figure 7-20 and Figure 7-21. In addition, the three dimensional position of the kinematic marker positions on the foot surface were also measured (also shown in the figures) however, kinematic measurements were not derived.

The purpose of the results presented in Figure 7-20 and Figure 7-21 is to illustrate that the methodology is capable of measuring different feet and that the developed methodology has not been refined for one particular subject. While the results show that different running styles can be accommodated (Figure 7-21), it is not claimed that the developed methodology is a definitive method. Due to the variation of the population (whose feet could potentially be measured), there is likely to be different running styles, foot shape etc. that may need to be accommodated. In these cases certain elements of the method may need to be altered, the most likely being camera positioning. Nevertheless, the overall principles of the measurement methodology would remain the same.
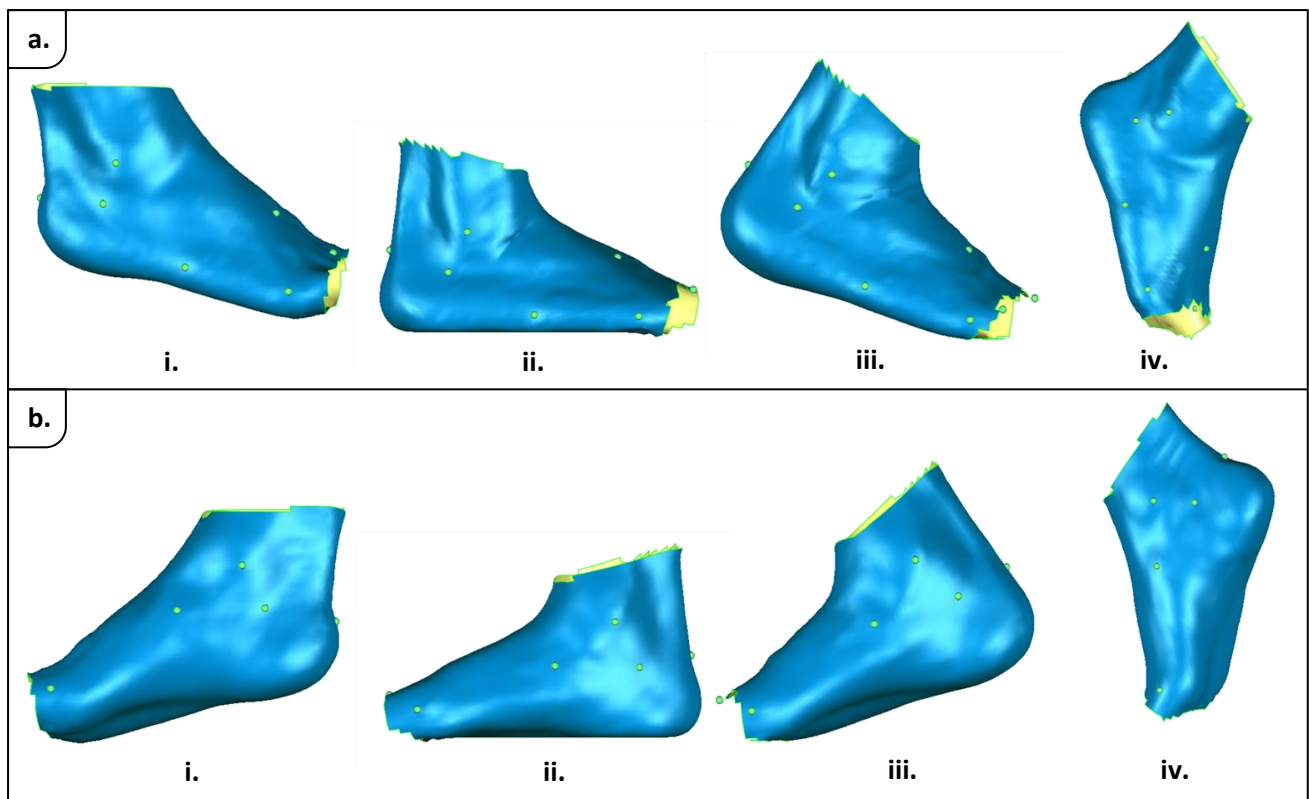
Figure 7-20 – Post processed full foot surface measurements for subject 2, from (a) lateral and (b) medial views at four stages across stance (i) touchdown (ii) peak braking (iii) peak propulsive (iv) toe off.
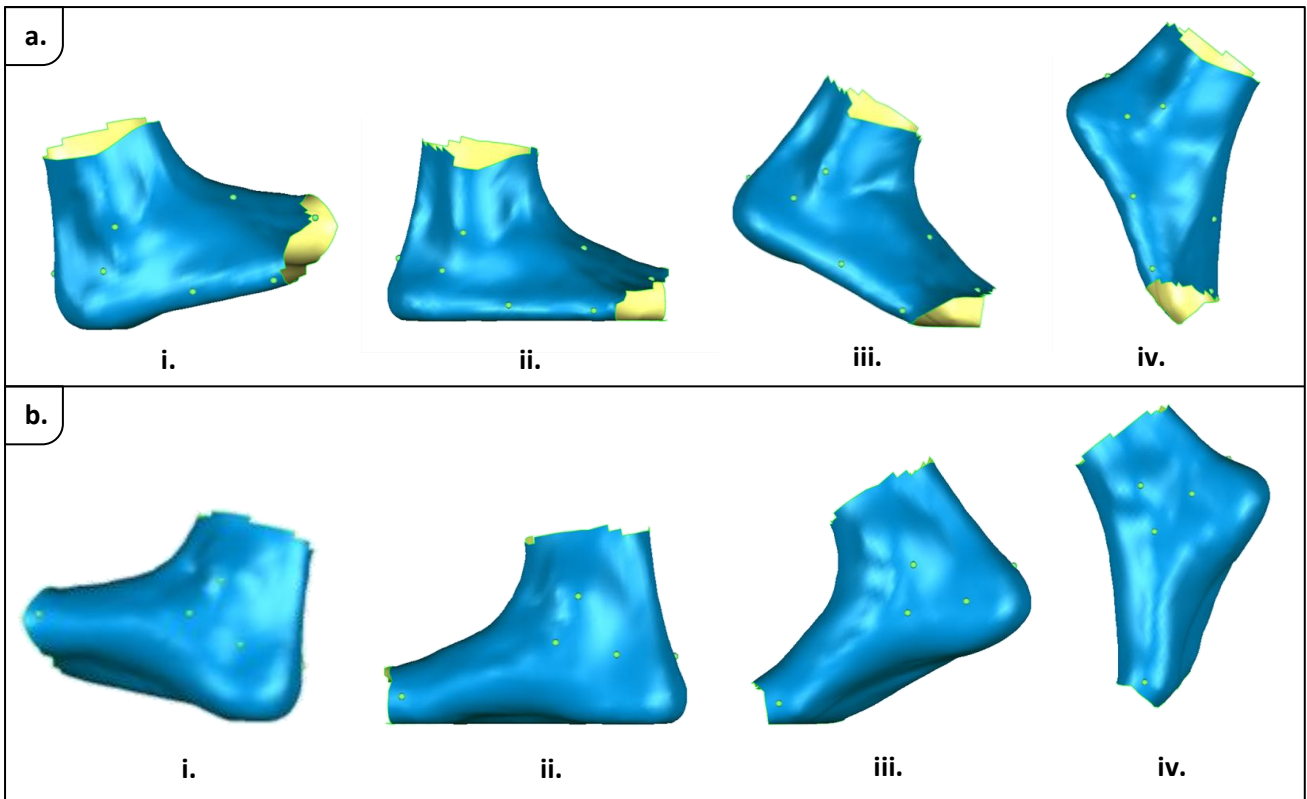
Figure 7-21 – Post processed full foot surface measurements for subject 2, from (a) lateral and (b) medial views at four stages across stance (i) touchdown (ii) peak braking (iii) peak propulsive (iv) toe off.

7.5. Chapter Conclusions

The novel methodology developed in Chapter 5 was presented in a generic form, allowing a user to reach a point where shape and deformation measurements, along with biomechanical data, could be attained for the full foot strike. The purpose of this chapter was to demonstrate the novel method and conduct relevant analysis for shape, deformation and biomechanics. The analysis conducted did not attempt to answer a particular research question or test a hypothesis; instead it was intended to provide a means of communicating measurement data as well as illustrating the capabilities for foot morphology and biomechanical measurements using the outlined method.

Employing the method, the foot of a subject was successfully measured during a multiple of footstrikes during running gait, enabling a set of surface shape models to be created and analysed. Analysis of the foot shape was made via seven metrics supporting twelve analyses defined from markers on the foot. The results have demonstrated the methodology is capable of making absolute shape measurements at discrete stages throughout the stance, as well as being capable of describing the change in the measurements over the footstrike, essentially forming a deformation measurement.

The measurement of surface deformation was also completed successfully, although as there is no way of averaging deformation measurements between tests, each measurement from each test, at present should

be considered individually. This was the first time full field surface deformation had been successfully measured on the foot and the understanding and application of the measurement needs to be investigated further. Surface deformation measurements may be capable of supporting the previously described shape analyses (e.g. cross sections), however, it would be necessary to differentiate between the two dimensional deformations (planar) occurring on the foot surface and the three dimensional deformations (non-planar). As DIC measures deformations locally tangential on the surface for both, interpretation of deformation data should be carried out with care.

Runner kinetics and kinematics were successfully measured simultaneously, and employed to support the shape measurement analysis. Although only a generic kinematic analysis was completed, a more detailed analysis specific to application could be conducted using the same marker set and segment definitions. It would also be possible to employ a different kinematic model if required, to enable a more simple or detailed kinematic analysis of foot movements during stance. This would be achieved by simply altering the positioning of kinematic markers on the foot surface to reflect a different foot model.

Though measurements employed in this chapter were not intended to be definitive, the results have surpassed all known attempts to measure dynamic foot shape reported in literature (Kimura et al., 2009; Kouchi et al., 2009; Liu et al., 2011; Schmeltzpfenning et al., 2010; Thabet et al., 2014), where locomotion speeds have been restricted to walking or quasi-static foot movements and measurements reported extremely limited. In contrast, for the developed method, full foot shape measurement in the region of interest has been demonstrated, supporting numerous quantitative measurements of foot shape, as well full field surface deformation measurement. This chapter has shown that concurrent shape measurement with kinetics and multi segment kinematics was possible, something that has not been attempted, with or without success, in any published shape measurement literature to date.

8. Methodology Repeatability and Reproducibility Assessment

8.1. Introduction

As part of the preceding work, calibration of the measurement system was conducted in order to establish the levels of measurement error and the effects of particular user controlled variables on that error. The work endeavoured to establish confidence in measurements made from a single system. However, as multiple systems were employed to assess full foot morphology, the contribution of particular measurement process chain components were considered during methodology development in chapter 6, namely, the effect of alignment error and surface interpolation on absolute shape and kinematic measurement accuracy.

The work conducted in the development of the method has shown that the individual measurement results are sufficiently accurate and that although the methodology has been demonstrated, it would only be deemed a useful measurement tool if the levels of measurement repeatability and reproducibility obtained via its use are understood. The assessment of repeatability and reproducibility focussed on the method itself and therefore variation of measurements as a result of the subject was not considered.

The repeatability of the method was concerned with establishing intra-session measurement variation: the variation, as a result of the methodology, of measurements made on the same day when the same experimental setup and process components (references, camera calibrations, alignments, data processing methods etc.) were used. The method reproducibility was concerned with establishing inter-session measurement variation; the variation, as a result of the methodology, of measurements made between different test sessions, potentially on different days in different labs, which would therefore result in changing experimental setup (camera positions) and process components that are employed to make a measurement.

Establishing the repeatability and reproducibility of the method developed will not only establish a level of competency, but also guide how results are analysed and direct refinement of particular measurement process components in any future method development. The aim of this chapter therefore was to assess the repeatability and reproducibility of the developed method in line with OBJ_9 outlined in §1.1. This will be achieved by completing the following objectives:

- Outline the measurement metrics for analysis
- Define an analysis protocol to describe measurement variation
- Conduct a repeatability analysis using constant measurement process variables
- Identify and select methodology process variables relevant to reproducibility
- Conduct a reproducibility analysis for selected methodology process variables

8.2. Measurement Method Variables

Measurement method variables were identified within the three general stages of the method: preparation, testing and data analysis, with the examiner variable overarching all stages of the method, as shown in Figure 8-1. Due to the multifaceted nature of the methodology, the identified variables would not necessarily affect all three measurement types made directly. Repeatability analysis would consider the measurement variation when method variables were constant, reproducibility would consider the effect of method variables changing.
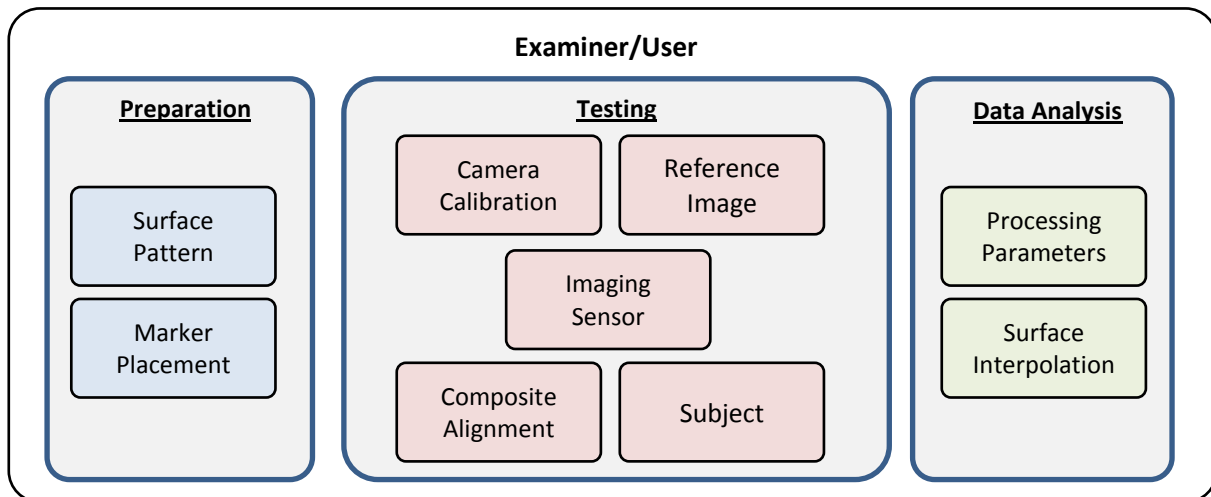
Figure 8-1 – Identification of measurement process variables across methodology stages.

8.3. Methodology

8.3.1. Data Capture and Processing

Data capture and data processing related to foot shape and runner kinematics were captured in line with the methodology described in Chapter 6, using a single subject running barefoot at a self-selected running speed of approximately 3.5 ms^{-1} in an indoor laboratory. Runner kinetics, although not analysed as part of the repeatability and reproducibility investigation, were also simultaneously captured to aid data analysis activities, in particular to enable the definition of the stance phase of gait. DIC, kinematic and kinetic data was processed as outlined in § 6.4.

8.3.2. Data Analysis

8.3.2.1. Measurement Metrics

Shape

The metrics used for shape measurement assessment were the same as those defined in Chapter 7 (§ 7.2.4.3), namely, cross sectional area and circumference at the foot MPJ, instep, waist, short heel and ankle (Figure 8-2), in addition to foot breadth and foot volume. Any relative measurements, using the metrics, were made relative to the unloaded reference stage.
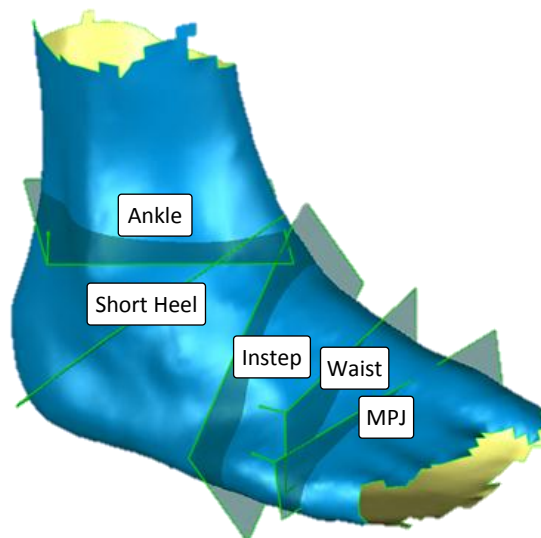
Figure 8-2 - Foot cross sections

Deformation measurements

Deformation measurements were computed as major strain, and results presented in strain plots, overlaid onto the three dimensional foot surface with measurements obtained for all stages of the footstrike. Deformation measurements were referenced in all cases to the unloaded reference stage.

Kinematics

Lower extremity kinematics were assessed via four measurements of relative segment rotation: foot with respect to the shank, calcaneus with respect to the shank, midfoot with respect to the calcaneus and metatarsals with respect to the midfoot. Rotation angles were calculated around the three axis pertaining to abduction/adduction, eversion/inversion and dorsiflexion/plantarflexion as discussed in §6.3.3. Kinematic measurements were presented as angular measurements made relative to the foot position in the loaded reference stage.

8.3.2.2. Characterising Measurement Variation

Shape and Kinematics
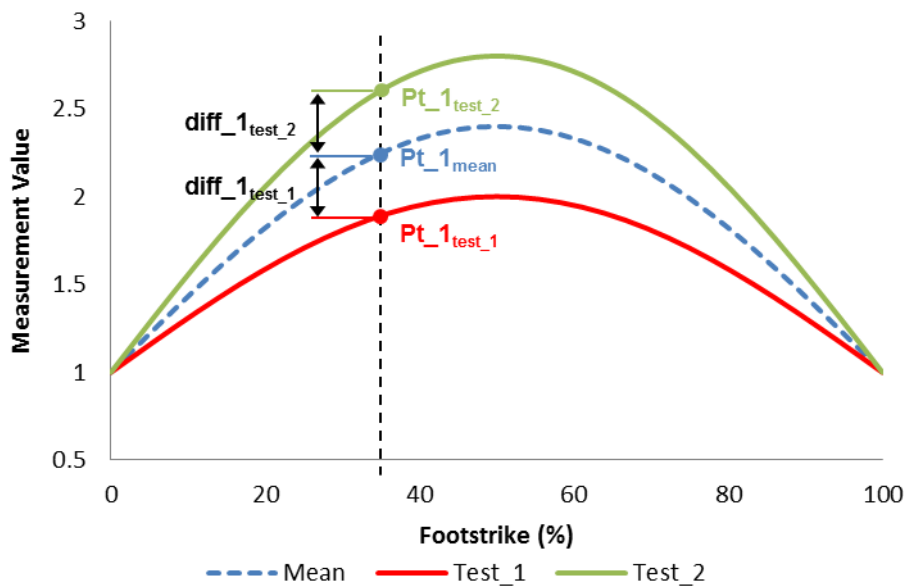
Figure 8-3 – Calculation of measurement difference for each test stage relative to the mean

The standard deviations described the absolute variation of each particular metric. To enable comparison of variation in shape measurements, where different metric types were employed meaning standard deviations were not directly comparable, coefficient of variation (CV) was used. The CV, expressed as a percentage, normalises the standard deviation, usually to the mean, to give a description of relative variability.

Individual stage CV used standard deviation and mean values calculated from the measured values at a discrete stage (Figure 8-3, Equation 8-1). For the entire footstrike, the CV was expressed via the mean CV, calculated from the CVs from all measurement stages (Equation 8-2).

$$CV_{stage\_n}(\%) = \frac{\sigma_{stage\_n}}{\mu_{stage\_n}} \times 100 \qquad \text{Equation 8-1}$$

$$Mean\ CV\ (\%) = \frac{\sum_1^n (CV_{stage_1}\ CV_{Stage_2} \ldots CV_{stage_n})}{n} \qquad \text{Equation 8-2}$$

Deformation

Comparison of deformation measurements between tests will be discussed individually in the relevant sections.

146

8.4. Repeatability of Measurement Methodology

8.4.1. Overview

The purpose of the investigation in this section was to establish the intra-test variation in measurements obtained under the same methodological conditions. Essentially determining the variability of measurements as a result of the method and its components, i.e. the measurement variation if exactly the same footstrike event was measured twice.

The inherent variability associated with human testing meant that it was impossible to obtain identical running movements which would allow the variability of measurements, resulting from the method, to be determined. In an attempt to overcome this issue, the analysis was conducted using the same raw image data from a single test, to derive measurements. This meant that the effect of differences in the raw image data (due to the imaging sensor) was not considered in the repeatability analysis. The variation in measurements would therefore be the result of the effect of the other process variables outlined in §8.2. However, within a test session the surface pattern, placement of kinematic markers, camera calibrations, reference images, alignment transformations and individual measurement processing parameters would all remain constant between tests. This meant that only the surface interpolation variable would affect the measurement repeatability and only for shape measurements; surface deformation, kinematics and kinetics would not vary (when the same raw images are used). This analysis was conducted therefore only on shape measurements.

Three separate full foot shapes were created using the same initial composite foot surface data of the unloaded reference stage, exported from GOM S-VIEW software. Shape metrics were defined in all three tests using the same marker set point positions with interpolations completed in Geomagics Studio as outlined in §6.4.1.2. As foot breadth was a linear measurement and not created from interpolated surfaces, it was ignored in the analysis as its repeatability would be in line with kinematic measurement variation, i.e. none.

8.4.2. Results and Discussion

Measurement comparison were made as outlined in §8.3.2.2 and results for shape measurement comparison shown in Table 8-1.

The results show that the variation in shape measurements was extremely low across all metrics. Standard deviations for area measurements were within 0.05 cm^2 and circumferences within 0.1 mm. Considering measurements relative to the mean, the CV results showed that all shape measurements varied within 0.1%.

	MPJ X-section		Instep X-Section		Waist X-Section		Short Heel X-Section		Ankle X-Section		Foot Volume (cm^3)
	Area (cm^2)	Circumference (mm)	Area (cm^2)	Circumference (mm)	Area (cm^2)	Circumference (mm)	Area (cm^2)	Circumference (mm)	Area (cm^2)	Circumference (mm)	
μ (measured)	37.4	255.2	48.7	265.4	40.6	254.4	75.9	343.9	51.8	278.5	821.2
σ	0.02	0.04	0.04	0.06	0.03	0.04	0.05	0.03	0.03	0.03	0.11
Mean CV (%)	0.05	0.02	0.08	0.02	0.07	0.02	0.07	0.01	0.06	0.01	0.01

Table 8-1 - Mean maximum and minimum measurement values, standard deviation and coefficient of variation results for foot shape measurements at the unloaded reference from three repeatability tests

The results show that measurement repeatability was excellent. This was in part due to the fact that the only source of error when the same raw images were used was surface interpolation, as most measurement parameters remain constant within intra test measurements, meaning kinematics and deformation measurements would be unaffected. Changing raw image data, occurring due to the fluctuations in imaging sensor sensitivity or subtle changes in illumination, may contribute to measurement variation; however, differences are unlikely to be at a level that would affect measurements significantly. This is supported by individual system measurement repeatability investigations, conducted in Chapter 4 for shape and in Chapter 5 for surface deformation, where low levels of variation were observed when image data was changed.

There is potential for levels of repeatability to be significantly affected by the operator (user), which has not been considered in this analysis. Measurements made by one user may be more repeatable than another and therefore this would need to be assessed by comparing measurements made by different operators trained in the use of the method, which at this point in the methodology development was not possible.

It is important for the measurement methodology to be repeatable, in order for measurements made using it to be trusted. The repeatability of the developed method is at a level that means when two different measurements are made within the same session, variation observed will be due to an intervention only, for example, the subject and not variation introduced from the method. This fact was important in the ensuing investigations regarding the measurement reproducibility, as differences observed between tests when process variables are changed would be the direct result of that change alone, allowing meaningful conclusions to be drawn.

8.5. Reproducibility of Measurement Methodology

8.5.1. Overview

The purpose of the investigation in this section was to establish the reproducibility of measurements obtained using the developed methodology. The reproducibility is the level of variation introduced to the measurement as a result of changes made to the methodology process variables, with the overall reproducibility the summation of the variations from each component.

Understanding measurement reproducibility in this context is important as it allows meaningful comparison of measurements made between test sessions, when method variables (§8.2) will have changed. Understanding the contributions of relevant process variables to the overall measurement variability will establish the importance of particular variables and direct the development of particular components of the methodology to improve measurement reproducibility.

The overall approach of the reproducibility analysis therefore, was to isolate and test individual measurement process variables to understand how changes, that may potentially occur when the methodology is employed, will influence a measurement result. As already discussed, the analysis was concerned with the methodology only and therefore variability of the subject was omitted. To facilitate this, the same footstrike image data was used for each test to ensure exactly the same event was being measured; changes were then made to process variables involved with deriving a measurement. This approach meant that measurements variations would be a direct result of the change in variable and not a combination with subject variability.

Due to the multifaceted nature of the methodology, the identified measurement process variables outlined in §8.2 would not necessarily affect all three measurements types made directly. Figure 8-4, shows which process variables affected shape/surface deformation, kinematic and kinetic measurements respectively.

Measurement variability as a result of the subject, as already discussed, was not considered as part of the analysis; in addition, the examiner/user was not considered. As these were the only components to influence kinetic measurements (Figure 8-4), the variability analysis was therefore made for shape, surface deformation and kinematic measurements only, with the assumption, based on the kinetic repeatability results, that kinetic measurements would be reproducible as long as measurements were made in line with the method outlined.

Experimental work in Chapter 5 (§5.7.5.4) indicated that changing a surface pattern does not influence measurement accuracy (i.e. variability) significantly, within outlined parameters, for shape or surface deformation measurements and therefore was not considered in the investigations in this chapter. The effect of processing parameters within the DIC software have already been investigated in Chapter 5

(§5.6.5.5 and §5.6.5.6) in relation to measurement of shape and deformation, and were therefore not considered in this analysis. Likewise, the influence of camera calibration on measurements was previously deemed negligible, so long as system calibrations were within the constraints specified by the manufacturer (GOM, 2009b) and so on this basis, was also not considered.

Shape/Deformation	Kinematics	Kinetics
1. Surface Pattern		
2. Marker Placement*		
3. Camera calibration		
4. Composite Alignment*		
5. Reference Image**		
6. Subject		
7. Processing Parameters		
8. Surface Interpolation*		
9. Examiner/User		
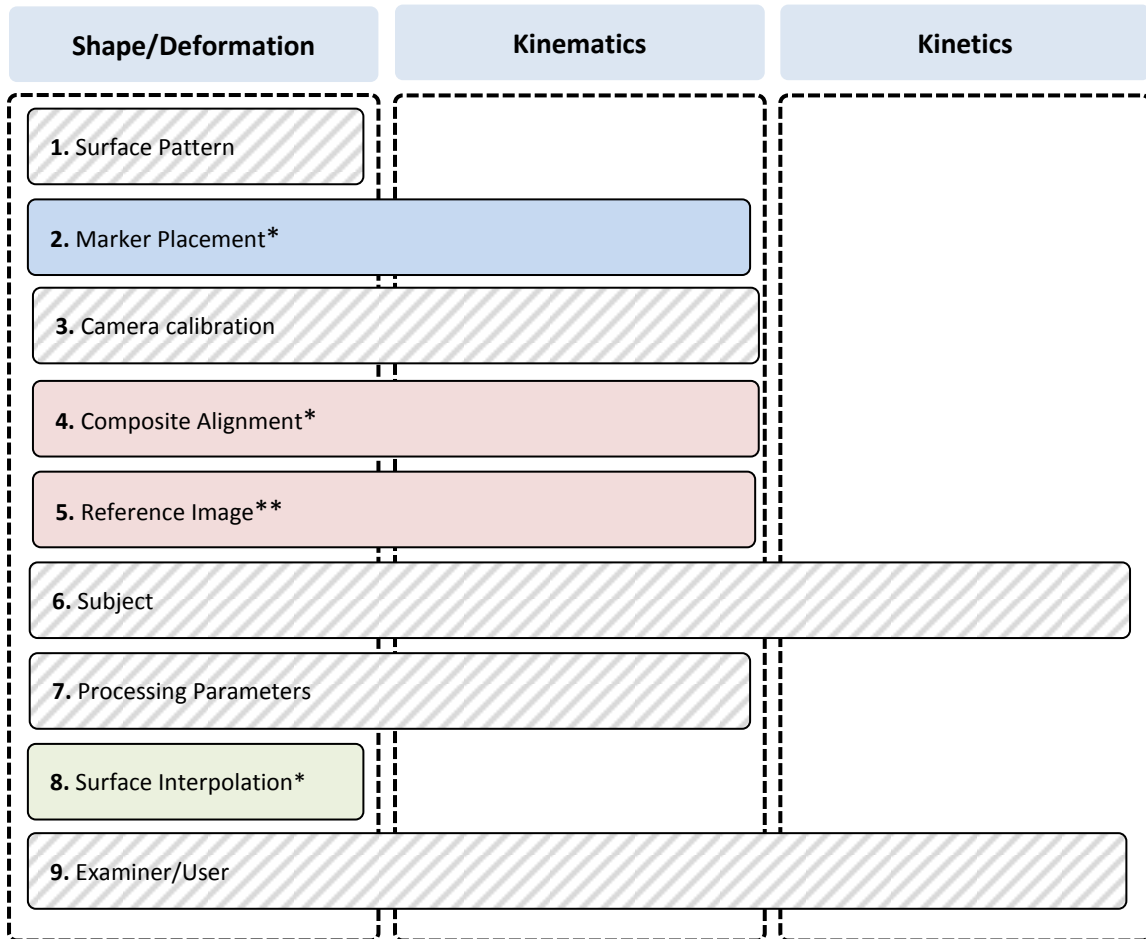
* Does not affect deformation measurements   ** Affects relative measurements only

Figure 8-4 –Effect of measurement process variables on the three measurement types obtained via the method. Hatched variables are those not considered in the investigations in this chapter.

Evaluation of surface measurement would have been a repetition of the repeatability test from the previous section, as all other variables would be constant, therefore this left three process variables for assessment: the reference stage, marker placement and composite alignment. These variables were related directly to the method and the effects were tested individually, before the cumulative effect was considered, in which results for shape measurements from §8.4.2 for surface interpolation would be used.

Surface interpolation was required in all tests to create a closed foot shape that would then enable shape measurements to be made. It was not possible therefore, to remove the effect of this variable when assessing the shape measurement variation as a result of another. However, as the variation had been

shown to be so low, it was deemed negligible unless similar levels were observed in the analysis for any of the other three variables identified.

8.5.2. Foot Reference

The purpose of this particular analysis was to establish the effect that different reference stages, from which measurements are made, may have on measurements. The 'foot reference' provides the datum from which all relative shape/deformation and kinematic measurements are made and is, therefore, an important component of the methodology. It is important to be able to recreate the same reference stage, which would be required every time a new pattern or kinematic marker set is applied to the foot, so that useful comparative measurements can be made.

Ultimately the variability is a result of the inconsistency in which a person can be place their foot in the reference position. Efforts have been made within the methodology to reduce the variation in the reference, via the use of a reference fixture (§ 6.3.5), which attempts to standardise the foot and lower extremity positions and orientations when reference images are captured. However, variation in posture, although reduced, will still occur and will cause a change in the reference measurement values, which define 'zero'. These changes do not affect the pattern of a subsequent (individual) measurement across the footstrike, but instead causes a constant shift in measurement magnitudes in line with the difference between the references. For this reason, only comparison of reference measurements to one another was required, as opposed to analysis of the same footstrike data using each reference stage.

Once a suitable pattern had been applied to the foot along with the kinematic marker set, five separate reference measurements were made as outlined in (§ 6.3.5) for shape and kinematics. From these images, shape, surface deformation and absolute kinematic values were retrieved for analysis, with shape measurements made in the unloaded reference and kinematic measurements made in the loaded reference.

8.5.2.1. Results

Shape and Kinematics

The analysis results for kinematic and shape measurements, calculated as outlined in §8.3.2, are presented in Table 8-2 and Table 8-3 respectively.

The standard deviation results for kinematics show the variation in measurements was relatively consistent across all twelve measurement metrics, range: between 0.3 and 1.2°. The greatest (1.2°) occurring in the Y-component (adduction/abduction) of the foot segment relative to the shank, with a similar level observed in the same component for the calcaneus relative to the shank, which suggests improved alignment of the shank and the rotation of the foot in the reference jig would reduce the variation. In the current method the foot is positioned by measured distances from the reference jig frame. As the position is only defined by

markings on the floor surface, there is potential for the foot position to vary easily as there is no definitive boundary to align to repeatably.

For shape measurements (Table 8-3), there was a similar variation when considering the standard deviations within a common metric type (e.g. cross sectional areas or circumferences), with a range of between 0.2 and 0.7 cm^2 for area and 0.4 and 2.5 mm for circumference. The coefficient of variation (CV) revealed similar, low variations between all metrics, meaning no one measurement was more variable than another (in a relative sense) with the low CV values indicating the effect on the overall measurement was small (CV≤1% approx.).

	Shank-Foot			Shank-Calc			Calc-Midfoot			Midfoot-Met		
	X (°) (Inv/Eve)	Y (°) (Add/Abd)	Z (°) (Dor/Pla)	X (°) (Inv/Eve)	Y (°) (Add/Abd)	Z (°) (Dor/Pla)	X (°) (Inv/Eve)	Y (°) (Add/Abd)	Z (°) (Dor/Pla)	X (°) (Inv/Eve)	Y (°) (Add/Abd)	Z (°) (Dor/Pla)
μ (Measured)	6.5	9.1	21.4	13.3	25.5	2.7	6.7	4.0	35.6	21.6	24.4	74.3
σ	0.7	1.2	0.8	0.3	1.1	0.8	0.5	0.3	0.3	1.0	0.4	0.3

Table 8-2 – Mean measured and standard deviation results for lower extremity kinematics at the loaded reference stage, from five reference stage tests.

	MPJ X-section			Instep X-Section		Waist X-Section		Short Heel X-Section		Ankle X-Section		Foot Volume (Cm^3)
	Area (cm^2)	Circumference (mm)	Foot Breadth (mm)	Area (cm^2)	Circumference (mm)	Area (cm^2)	Circumference (mm)	Area (cm^2)	Circumference (mm)	Area (cm^2)	Circumference (mm)	
μ (Measured)	38.0	254.2	106.4	49.4	268.0	40.2	251.2	73.9	343.6	49.8	272.0	844.4
σ	0.3	1.5	0.3	0.6	2.0	0.3	0.4	0.7	2.5	0.2	2.2	3.4
CV (%)	0.7	0.6	0.3	1.1	0.7	0.6	0.2	0.9	0.7	0.4	0.8	0.4

Table 8-3 – Mean measured, standard deviation and coefficient of variation results for shape measurements at the unloaded reference stage, from five reference stage tests.

In practical terms, as the reference serves as the zero datum, the effect would be a constant offset on measurements made relative to it. Making an assumption that the 'difference measurements' are normally distributed, then the variation offset as a result of the reference stage will be within ±2.5° for kinematics, ±1.3 cm^2 for cross sectional area, ±5 mm for cross sectional circumference and 7 cm^3 for foot volume (at a 95% confidence).

Viewing the results, it may be appropriate to take the average of a number of reference tests to obtain reference values for shape and kinematics, thus reducing the potential for introduction of larger variations in

reference measurements; ultimately creating a more reproducible reference 'state' than is achieved with a single reference stage. However, in the first instance, improving the reference jig, particularly in the areas discussed, would be in the first instance the most sensible approach.

Deformation

In the repeatability analysis, it was possible to easily compare all points of the full field strain due to the fact that, between tests, each measurement was the same shape, which meant that measurements could be aligned for comparisons. When comparing between different reference stages, the shape of the foot in each test was different meaning it was not possible to align surfaces and make direct comparisons of strain values. Instead, a visual assessment of the separate reference tests was conducted.

Surface deformation results are shown in Table 8-4, with surfaces from four separate tests (test_2 to test_5) compared relative to 'test_1' which acts as the zero datum. The results, presented from three views, show that there are obvious differences in the strain maps between reference states, predominantly on the medial and plantar surfaces.

In the most part, the differences are small, in the region of 0-2%strain, larger differences (up to 5%strain) are observed in localised areas in the medial surface and toward the anterior of the plantar surface. This is likely a result of the variation in the way the foot is positioned in the reference state; as it is unloaded it makes it more difficult to repeatably position the foot in the same way. As part of the method the participant is asked to place their foot on the floor, but not to place any load on the foot. Results from the plantar surface comparisons suggest that some level of load is potentially being applied inconsistently, or/and the orientation of the foot is causing differences in the foot shape in these areas. The latter also potentially explains the differences on the medial surface measurements, as the small changes in the orientation and position of the foot relative to the shank (i.e. 'ankle' rotation) could affect the surface.

The differences between references ultimately offsets the measured values across the foot surface over the footstrike, potentially altering the patterns of surface deformation at stages of the footstrike. There is no way of averaging multiple reference measurements for deformation, as suggested for shape and kinematics, due to the way deformation measurements are derived. Therefore the only way to reduce the variability would be to have a more repeatable reference state, which could be achieved by improving the definition of the foot positioning.

	Test_2	Test_3	Test_4	Test_5
Medial				
Lateral				
Plantar				

0.0 [%] 5.0

0.5 1.0 1.5 2.0 2.5 3.0 3.5 4.0 4.5
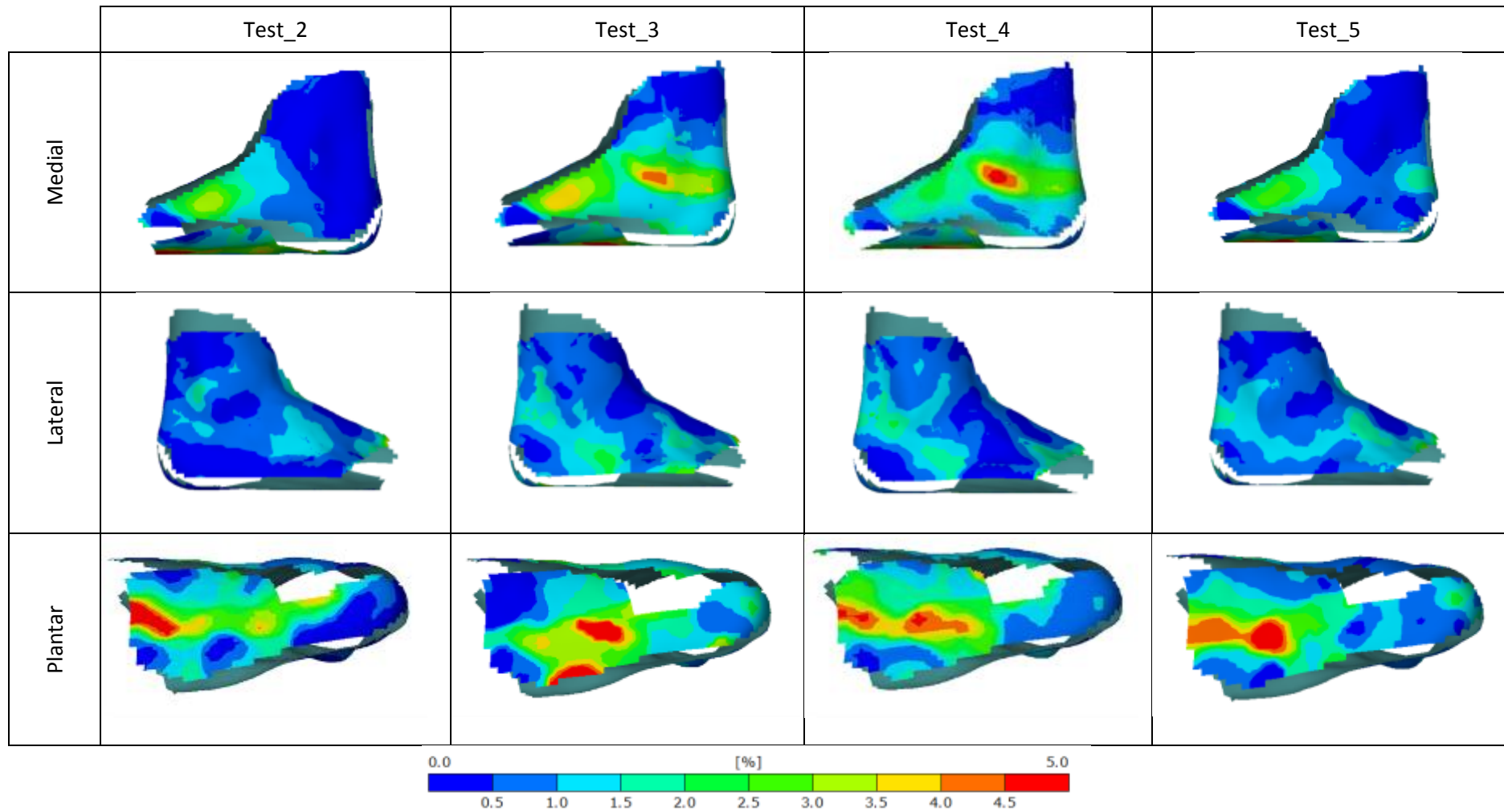
Table 8-4 - Surface deformation measurement comparison results from medial, lateral and plantar views. Tests referenced to Test_1 (Not shown) with deformation presented as major strain. Individual measurements are made in the unloaded reference state.

8.5.3. Composite Alignment

The purpose of this analysis was to assess the effect that changing the co-ordinate system alignments of each camera may have on measurements. As discussed in §6.4.1.2, separate measurements made from individual camera pairs are transformed from their measurement co-ordinate systems to a common, global co-ordinate system (GCS) using a co-ordinate system definition object. Each camera pair measures the location of markers on the definition object and the transformation is based on the fitting of the measured point cloud to a reference point cloud (via a best fit approach). This 'goodness of fit' will vary based on the relative difference between the reference point cloud and the measured point cloud.

The variability associated with the fitting of respective point clouds, will ultimately affect the alignment of individual measurements to one another; potentially affecting measurements as the relative alignment of surfaces and marker points change. Deformation measurements are not formed from a composite measurement and, therefore, these values are unaffected by alignment. The investigation in this section was concerned, therefore, with the effect of alignment of the individual measurements to the GCS on kinematic and shape measurement.

Three different alignments in the form of a set of transformation instruction files, defining the transformation for each camera pair, were created using the definition object. Each set of instruction files was created using the same global co-ordinate system definition object, but each time a new reference point cloud was created (using GOM TRITOP) and a different measured point cloud was computed, by repositioning the definition object each time.

These three sets of instruction files were then applied to the same measurement data for a full foot strike and shape and kinematic measurements were made as outlined in §8.3.2..

8.5.3.1. Results

The results for variation in kinematics and shape across the footstrike as a result of changing alignments are presented in Table 8-5 and Table 8-6 respectively

Results show that there was essentially no measurable difference in kinematic measurements across the footstrike as a result of variation in measurement alignment to the global co-ordinate system. Shape measurements however, did show more measureable variation, although these were small both in an absolute sense and relative, highlighted by the coefficient of variation results which show variation of less than 0.5% when normalised to the mean range. Interestingly, the foot breadth metric, which was defined from the position of two kinematic markers, showed similar variability levels to those observed in kinematics, suggesting linear measurements have similar variability to kinematics.

	Shank-Foot			Shank-Calc			Calc-Midfoot			Midfoot-Met		
	X (°) (Inv/Eve)	Y (°) (Add/Abd)	Z (°) (Dor/Pla)	X (°) (Inv/Eve)	Y (°) (Add/Abd)	Z (°) (Dor/Pla)	X (°) (Inv/Eve)	Y (°) (Add/Abd)	Z (°) (Dor/Pla)	X (°) (Inv/Eve)	Y (°) (Add/Abd)	Z (°) (Dor/Pla)
μ max	5.7	6.5	17.6	1.4	3.3	12.1	9.1	3.4	11.1	1.3	1.5	2.6
μ min	-3.6	-3.7	-31.4	-1.0	-1.2	-20.4	-3.7	-1.9	-6.4	-3.8	-1.9	-8.6
Mean s.d.	0.03 ±0.02	0.03 ±0.03	0.01 ±0.01	0.03 ±0.02	0.03 ±0.02	0.03 ±0.00	0.02 ±0.01	0.03 ±0.02	0.04 ±0.03	0.02 ±0.01	0.04 ±0.03	0.03 ±0.02

Table 8-5 – Maximum and minimum measured mean values and mean standard deviation results for lower extremity kinematics across the whole footstrike, from three composite alignment tests.

	MPJ X-section			Instep X-Section		Waist X-Section		Short Heel X-Section		Ankle X-Section		Foot Volume (Cm^3)
	Area (cm^2)	Circumference (mm)	Foot Breadth (mm)	Area (cm^2)	Circumference (mm)	Area (cm^2)	Circumference (mm)	Area (cm^2)	Circumference (mm)	Area (cm^2)	Circumference (mm)	
μ max	35.9	255.9	109.6	52.6	271.9	44.7	262.4	79.8	353.6	51.7	283.7	837.6
μ min	40.7	252.5	101.2	47.7	262.3	39.4	252.8	71.5	330.3	49.6	275.4	817.4
Mean s.d.	0.2 ±0.08	0.6 ±0.26	0.1 ±0.02	0.1 ±0.01	0.4 ±0.27	0.2 ±0.04	0.9 ±0.25	0.1 ±0.10	0.4 ±0.24	0.1 ±0.06	0.3 ±0.19	1.2 ±0.66
Mean CV (%)	0.6	0.2	0.0	0.2	0.1	0.4	0.3	0.2	0.1	0.1	0.1	0.2

Table 8-6 - Maximum and minimum measured mean values, standard deviation and coefficient of variation results for foot shape measurements across the whole footstrike, from three composite alignment tests.

The results show that the reproducibility of measurements with changing alignments is very good for shape and especially so for kinematics, where very small levels of variation were measured. The shape is understandably more susceptible to variation, due to the nature of the measurement and the effect small changes in position and orientation in the composite measurement of one surface relative to another surface can have on a measurement, particularly for volume and cross sectional area. Nevertheless, if the measured differences across the footstrike are assumed to be normally distributed, shape measurements will still only vary at worst within 1.5% relative to the measured mean (at 95%confidence), and in most cases much less.

Overall the results show that the reproducibility of a measurement is affected very little by changing the alignment process variable, when performed as described in the method.

8.5.4. Marker Placement

Markers placed on the foot serve to define the lower extremity kinematic segments as well as aiding in the definition of foot shape metrics. The variation in the positioning of the markers on the foot will therefore affect any measurements utilising their position.

The variability in kinematic measurement of human gait, as a result of marker positioning, has been investigated in walking for the multi segment foot model used in this work by Deschamps et al. (2012) who showed mean variability of relative angles of between 0.9 and 4.2° which was similar to levels measured by Carson et al. (2001) who employed a different multi-segment model and reported a variation of between 1 and 6°. Carson et al. (2001) also noted that variations are generally represented as a shift in the absolute value of inter-segment angles as opposed to changing angular movement patterns.

Previous studies related to variation due to marker placement have been conducted for multiple tests meaning measured variations are combined with variability of the runner, even if attempts are made to remove that component (Carson et al., 2001) variations are not solely the result of the new marker positions. To isolate the marker locations as the only variable, the same movement needs to be used and a different marker set applied to it. This could be achieved in theory by translating marker positions to different foot locations to replicate potential variation in marker placement, however this is difficult with traditional kinematic measurement techniques, as there is no knowledge of the foot surface as only marker positions (usually prominent from the foot surface) are known, meaning movement of marker positions is not possible with any level of confidence.

With the methodology developed in this work, the foot surface is known and therefore marker locations can be translated to new positions on the surface of the foot, thus forming a different marker set that can be used with the same movement data and reference states. Three marker sets were created by translating each marker on the lower extremity in a proximal and distal direction from the original marker position to create two new positions for each point. This included the proximal shank markers, where the natural occurring skin pattern enabled the 'knee' surface to be measured in one image, from which two new marker positions could be derived from the initial marker placement. For the purposes of this assessment, it was assumed that an experienced practitioner could locate markers to within 5 mm and therefore marker positions were translated by this limit.

Kinematic and shape measurements were derived using each marker set, once again, as deformation measurements were not affected they were not considered.

8.5.4.1. Results

Analysis of measurement variation across the footstrike for marker placement changes was completed as described in §8.3.2. The results of which for kinematic and shape measurement across the footstrike are presented in Table 8-7 and Table 8-8 respectively.

	Shank-Foot			Shank-Calc			Calc-Midfoot			Midfoot-Met		
	X (°) (Inv/Eve)	Y (°) (Add/Abd)	Z (°) (Dor/Pla)	X (°) (Inv/Eve)	Y (°) (Add/Abd)	Z (°) (Dor/Pla)	X (°) (Inv/Eve)	Y (°) (Add/Abd)	Z (°) (Dor/Pla)	X (°) (Inv/Eve)	Y (°) (Add/Abd)	Z (°) (Dor/Pla)
μ max	2.3	6.8	17.7	1.7	3.3	12.1	9.0	3.3	10.9	1.0	1.3	2.6
μ min	-3.6	-3.6	-31.4	-1.1	-1.1	-20.4	-3.6	-1.9	-6.4	-3.6	-1.8	-8.7
Mean s.d.	0.4 ±0.21	0.2 ±0.13	0.2 ±0.11	0.3 ±0.17	0.3 ±0.11	0.2 ±0.11	0.2 ±0.07	0.2 ±0.17	0.4 ±0.3	0.2 ±0.09	0.4 ±0.13	0.4 ±0.36

Table 8-7 – Maximum and minimum measured mean values and average standard deviation results for lower extremity kinematics across the whole footstrike, from three marker placement tests.

	MPJ X-section			Instep X-Section		Waist X-Section		Short Heel X-Section		Ankle X-Section		Foot Volume (Cm³)
	Area (cm²)	Circumference (mm)	Foot Breadth (mm)	Area (cm²)	Circumference (mm)	Area (cm²)	Circumference (mm)	Area (cm²)	Circumference (mm)	Area (cm²)	Circumference (mm)	
μ max	40.7	257.5	109.3	52.34	270.8	44.7	261.5	80.2	354.2	53.0	282.4	843.6
μ min	35.7	252.1	101.4	47.4	261.4	39.1	252.6	71.0	329.9	49.3	276.1	820.9
σ	1.6 ±0.22	2.5 ±1.04	0.4 ±0.12	0.7 ±0.06	1.4 ±0.27	0.8 ±0.06	1.5 ±0.14	0.3 ±0.21	1.0 ±0.6	1.3 ±0.33	0.7 ±0.67	25.3 ±0.77
Mean CV (%)	4.4	1.0	0.4	1.4	0.5	2.0	0.6	0.4	0.3	2.4	0.3	3.1

Table 8-8 - Maximum and minimum measured mean values, average standard deviation and coefficient of variation results for foot shape measurements across the whole footstrike, from three marker placement tests.

The results for kinematics show that a relatively consistent absolute variation was observed between measurements when marker placements were changed. For all metrics, across the whole footstrike average standard deviations are less than 0.5°. The shape results also showed fairly consistent variation between metric types, with cross sectional area and circumference standard deviations between 0.3 and 1.6 cm² and 0.7 and 2.5 mm respectively. Relative to the measured mean, variations were within 5% although over half were within 1% indicating a good level of reproducibility with changing marker placement.

If a normal distribution is assumed for measurement difference across the footstrike, at a 95% confidence, at worst kinematic metrics would vary within $\pm1°$, cross sectional areas within ±3.2 cm^2, circumferences within ±5 mm and foot volume approximately ±50 cm^3 as a result of marker placement.

8.5.5. Overall Reproducibility

The investigations in the previous sections have shown the contribution to measurement variation of individual process variables. However, the overall reproducibility of any measurement will ultimately be the aggregation of these individual differences introduced via each independent process variable.

The overall variation as a result of the cumulative effect of the identified variables was described via the average standard deviation, calculated from the sum of the average variances from each of the four tested variables (Birch, 2003). To calculate the mean coefficient of variation for shape measurements, stage CVs were calculated using the cumulative standard deviation, divided by the measured values (at each stage) obtained from a single test when the identified method variables were at a 'default'; i.e. before any changes were made for an analysis. The results for shape and kinematic measurements are summarised in Table 8-9 and Table 8-10 respectively. Analysis was not required for surface deformation as the measurements were only affected by one of the selected variables: the reference stage.

The results for shape show standard deviations for the cross sectional area and circumference were relatively consistent with a range between 0.8 to 1.4 cm^2 and 2.3 to 2.8 mm respectively. Relative to the measured mean, all shape measurements were within 4%, with consistency observed between CV values for metric types. Generally speaking, the CV results indicated cross sectional areas and foot volume were more variable in comparison to cross sectional circumferences and foot breadth, although difference were still small (<2%).

	MPJ X-section			Instep X-Section		Waist X-Section		Short Heel X-Section		Ankle X-Section		Foot Volume (Cm^3)
	Area (cm^2)	Circumference (mm)	Foot Breadth (mm)	Area (cm^2)	Circumference (mm)	Area (cm^2)	Circumference (mm)	Area (cm^2)	Circumference (mm)	Area (cm^2)	Circumference (mm)	
Σ Var (ave)	2.69	8.86	0.26	0.86	6.12	0.77	3.22	0.59	7.41	1.74	5.42	653.1
s.d (ave)	1.6	3.0	0.5	0.9	2.5	0.9	1.8	0.8	2.7	1.3	2.3	25.6
Mean CV (%)	4.4	1.2	0.5	1.9	0.9	2.2	0.7	1.0	0.8	2.5	0.8	3.9

Table 8-9 – Cumulative shape measurement variations and mean CV values, derived from identified process variables; surface interpolation, reference, alignment and marker placement.

	Shank-Foot			Shank-Calc			Calc-Midfoot			Midfoot-Met		
	X (°) (Inv/Eve)	Y (°) (Add/Abd)	Z (°) (Dor/Pla)	X (°) (Inv/Eve)	Y (°) (Add/Abd)	Z (°) (Dor/Pla)	X (°) (Inv/Eve)	Y (°) (Add/Abd)	Z (°) (Dor/Pla)	X (°) (Inv/Eve)	Y (°) (Add/Abd)	Z (°) (Dor/Pla)
Σ Var	0.65	1.48	0.68	0.18	1.30	0.68	0.29	0.13	0.25	1.04	0.32	0.25
σ	0.8	1.2	0.8	0.4	1.1	0.8	0.5	0.4	0.5	1.0	0.6	0.5

Table 8-10 – Cumulative lower extremity kinematic measurement variations derived from identified process variables; reference, alignment and marker placement.

The absolute variation described by the standard deviations for kinematics was also relatively consistent with a range of 0.8° between 0.4 and 1.2°, with the greatest contribution in variation coming from the definition of the reference stage. If it is assumed that the measurement differences as a result of measurement process variable changes would be normally distributed, then at a 95% confidence, the reproducibility of kinematic measurements in will be within ±2.5°. Care should be taken when comparing measurements with low ranges of motion where the effect of the variation will be greatest. For shape, relative to the measured means, measurements will vary within ±9% for cross sectional areas, within ±2.5% for circumferences, within ±1% for foot breadth and approximately ±5% for foot volume. Although when the MPJ cross section is ignored the variation in area decreases to ±4.5%.

8.5.6. Discussion

The work in the preceding sections has endeavoured to establish the reproducibility of a measurement using the methodology developed in its current form. When variations are considered as an aggregate of individual inconsistencies, introduced by changing individual process variables, the method shows good levels of reproducibility with kinematic measurement variation ±0.8-2.5° and shape measurements at within ±1-8% of the measured mean, both at a 95% confidence. The kinematic results are better than those observed for a VICON motion capture system by Carson *et al.* (2001), who measured variations, for a multi segment foot model with similar segment definitions, between 1.5° and 5°.

Considering the variations as a result of changing individual process parameters, the greatest difference in respective measurements was introduced by the reference stage and by marker placement with surface interpolation and composite alignment both having an arguably negligible effect. It is understandable that the two process variables with the greatest contribution to measurement variation are as a result of human inconsistencies; in the case of the reference stage, it is the variability of the subject to place their foot in a repeatable position, for marker placement it is the variability in attempts by the examiner to place markers

in the same places on the foot. For interpolation and composite alignment process variables however, the human involvement is reduced to such a level that any influence is removed and thus, measurement variations are small to negligible.

The variability as a result of the reference stage affects relative measurements for all three measurement types: shape, surface deformation and kinematics. As it serves as a zero datum only, the effect of variation is a constant offset on relative footstrike measurements; absolute shape and kinematic measurements are unaffected by reference stage variation. Surface deformation measurements are reliant on the reference stage, with the current definition of the foot position in the reference allowing for localised variations in deformation of up to 5%strain, particularly on the medial and plantar surfaces in comparison to the lateral foot surfaces. These localised differences have the potential to alter deformation values as well as patterns in the full field strain plots over the footstrike. Improvement of the definition of the foot position in the reference is the most likely way to improve the reproducibility of the reference measurements for surface deformation. For shape and kinematics, an approach of averaging of multiple reference tests, which is not possible with surface deformation references, will reduce the influence of larger variations and therefore increase reproducibility across different test sessions.

Marker placement influences both shape and kinematic measurements. Reducing measurement variation due to marker placement will be very much dependent upon the skill level of the examiner. It is inevitable that there will be variation due to the nature of the method from which measurements are derived. The tests in this work have assumed a skilled examiner would essentially be repeatable to within a 5 mm radius on the surface; however this could theoretically be improved by marking the locations of markers on the skin as reference between test sessions for example, but variation will always occur.

There is no hard and fast rule to decide if the reproducibility of the method is acceptable, although at the levels identified in these investigations, even without any further development, an arguably good level of measurement reproducibility has been achieved. The ultimate goal is the measurement variation as a result of the method is considerably less than the measurement variation as a result of an intervention. In this scenario differences between measurements can then be attributed to the intervention/variable change and not potentially be solely a result of the variability in the method, thus allowing meaningful analysis to be made.

8.6.   Chapter Conclusions

The aim of this chapter was to assess the repeatability and reproducibility of the dynamic foot shape measurement methodology created in this work as outlined in OBJ_9 in §1.1. The motivation was to build confidence in the measurements that are obtained from the method and guide the analysis of results and the future development of components of the method process. The assessment of repeatability and

reproducibility was intentionally limited to the variation as a result of the methodology itself and therefore the variation of the human footstrike was excluded from the test.

The measurement metrics as defined in previous chapters were used to allow comparison between tests, with methodologies for comparison of measurements at individual stages and across the footstrike devised. The measurement repeatability was shown to be excellent, with extremely small variations observed only in shape measurements (CV<0.1%) introduced by the surface interpolation process; a result of all other variables remaining constant between measurements within the same test session meaning surface deformations and kinematics were not affected (i.e. would be identical) when test images were not changed.

For measurement reproducibility, the greatest contributions to measurement variation were from the differences between tests of the marker placement and the reference stage with the greatest variation generally occurring in the cross sectional area measurements in each. The effect on measurement reproducibility as a result of surface interpolation and composite alignment was small to negligible for both shape measurements and kinematics. Aggregated variations results showed shape measurements would vary by a maximum of ±9% at a 95% confidence (assuming a normal distribution), but less than ±5% for all other metrics (excluding foot volume) and within ±2.5° for all kinematic metrics.

The conclusions that can be drawn is that when measurement comparisons are made for measurements made on the same day under the same conditions i.e. the same test parameters, all variations between measurements will be the result of a variable intervention as the contribution to measurement variation as a result of the method will be negligible.

Reproducibility served to assess the level to which a measurement would differ when made under different conditions in relation to the methodology. To this end good levels of reproducibility have been measured, although understanding the level of the variation as a result of a studied variable e.g. subject, needs to be established before the reproducibility reported can be deemed acceptable.

The method reproducibility has the potential to be improved through further refinement of particular elements of the measurement process. The results from the testing in this work suggest that marker placement and the reference stage process variables, which contribute greatest to measurement variation, should be the focus of future methodological refinement to this end. Overall in the current form, due to the better measurement repeatability versus reproducibility the method holds the most potential as a tool for within-day/session measurement comparisons over between day/session until subject variability is known.

9. Conclusions and Future Work

9.1 Research Summary

The aim of the work in this thesis was to develop a methodology that was capable of measuring the shape of the human foot at multiple stages throughout the stance phase of running gait; this has been achieved by completing research objectives outlined in §1.1 through the work carried out in each chapter.

Review of current research revealed that foot shape measurement methodologies were almost exclusively focussed on the static foot shape, usually in a basic weight bearing, standing position. However, the loadings and movements of the human foot throughout the footstrike would cause changes to the three dimensional shape of the foot, which should be potentially be considered in the design and manufacture of shoes and shoe lasts. Methodologies for the measurement of dynamic foot shape are limited, and those developed by researchers were mainly hindered by hardware capabilities or measurement technology employed, which meant that only measurements of walking gait were made. Even then, reported measurements were also extremely limited with the focus generally on the method.

The basic requirements for the methodology were outlined: defining the measurement types a developed method should be capable of making and defining the foot regions of interest for shape measurements which excluded the surfaces of the toes distal to the MPJ (approx.). The measurement of runner biomechanics through the measurement of kinematics and kinetics was identified as an additional requirement within the methodology capabilities, in order to support shape and deformation measurement analysis.

Comparison of existing shape measurement technologies that had been identified previously was conducted from which digital image correlation (DIC), a passive optical metrology system, which makes measurements from images using photogrammetric principles, was objectively selected as a suitable technology for application within the methodology. DIC was able to associate discrete measurements (from individual stages) which would allow both absolute shape and relative deformation measurements to be derived. The embodiment of the technology was within the ARAMIS system manufactured by GOM, on which a validation was conducted to ensure fitness for purpose. The validation demonstrated that the ARAMIS system was capable of making measurements of the foot shape in dynamic movements associated with running gait in terms of both data capture and measurement quality. A multiple system methodology was identified as a necessary approach, in order to capture all surfaces of the foot during movement.

It was highlighted as part of the measurement system validation that there was no means to calibrate the surface deformation measurements to establish accuracy of the systems. Furthermore, as a result, there was

no way to understand the influence of the multiple hardware and software parameters, associated with DIC, on surface deformation measurement accuracies, which would be important when developing a method. A novel methodology was therefore devised for the calibration of deformation measurements, using material measures that allowed a deformation to be simulated. Results found that surface deformation measurement accuracy was within 0.5%strain and within day variability insignificant, both at a 95% confidence. 3D surface measurement calibration was also conducted, with accuracy found to be within 0.04 mm at a 95% confidence. Insignificant variation in surface deformation measurements was observed for pattern type, position in the measurement volume and type and rotation of deformation, with computational facet size and pattern type having no significant effect on three dimensional shape measurement variations. In conditions where significant differences were observed, the variations were at a level that meant the practical implications were negligible.

A method employing the validated GOM ARAMIS system was developed for the measurement of foot shape. The setup comprised six pairs of high speed video cameras located to capture images of both the dorsal and plantar foot surfaces of the right foot, during the stance phase of a person's gait cycle. The measurement of runner kinematics was facilitated using GOM PONTOS: a software capable of measuring the three dimensional marker positions of circular markers from images. By placing markers on the foot surface, three dimensional marker positions could be derived from the same images used for surface measurements, which could then be evaluated in appropriate biomechanical analysis software. Kinetic measurements were captured simultaneously using a transparent, instrumented force platform. Individual surface and kinematic point data measurements could be combined into a single composite measurement respectively, using a definition object which defined a global co-ordinate system that all measurements could be aligned to before gaps in measurement data interpolated for surface. The output of the described method was a full foot shape, for the surface region of interest, from which foot shape measurements could then be derived. A means to reference shape and deformation measurements as well as kinematic measurements was also discussed as part of the method using a rig, which would allow comparison of data between test sessions.

Measurements of multiple trials of a single subject running were completed to demonstrate the developed methodology, with shape characterised via five cross sectional measurements, linear length and volume as well as measuring surface deformation. Kinetics and multi segment kinematics were also measured and results presented, which served to inform the shape and deformation analysis. The results provided actual deformation measurements of the separate metrics as well as absolute shape values at discrete stages throughout the stance phase. Basic measurement results were also presented for two different subjects during linear running, in an attempt to demonstrate that the method was capable of measuring different feet within different test sessions. Although only basic surface and point data results were presented, if desired, complete analysis could be conducted in line with the fully presented results of the first subject.

Finally, the repeatability and reproducibility of the measurements derived from the developed method were investigated in an attempt to assess the intra and inter test session measurement variability as a result of the method and to identify the methodological contributors to shape, surface deformation and kinematic measurement variation. Excellent measurement repeatability was observed due to the fact within a test session, most methodological variables remained constant and that variability was introduced by the interpolation process, affecting shape measurements only, with negligible levels observed (CV<0.1%). For reproducibility the greatest contributor for both shape and kinematics to measurement variation was the reference stage and the kinematic marker placements. The aggregate variation from all error sources stemming from methodology process variables tested were found to be within ±8% for shape measurement (relative to the mean measured values) and ±2.5° for angular kinematic measurements. The results showed that improvements in referencing and the placement of kinematic markers would increase the reproducibility levels of measurements.

9.2 Novelty of Research

The work documented in this thesis has added novel research in two areas: firstly, in the calibration of optical systems measuring large surface deformations and secondly, in developing a method for the measurement of foot shape during dynamic movement, specifically in running.

Prior to this work there was no method reported in literature to obtain a traceable calibration of DIC system measurements for large surface deformations (>μstrain). Although attempts had been made for micro strain (Patterson et al., 2007) these were not suitable for larger deformations. The method applied developed in this work gives full control of the deformation and its magnitude and can be calibrated via the measurement of length, as recommended by Patterson *et al.* (2007). The method also gives the user control of the pattern and its features which is difficult to achieve with manual application of a pattern. The method has potential to be applied to calibrate any deformation magnitude or measurement volume, as long as the correct printing parameters can be achieved.

The key area of novelty in this research is the creation of the method using DIC, that is capable of making shape measurements of the foot during the stance phase of running gait. Methods presented in literature to data have speculated the capability to measure shape at running velocities, however, developed systems within their work have generally fallen short due to hardware and selected technology issues and measurements are yet to be presented. The work carried out in this thesis has developed and demonstrated, successfully, measurements of the dynamic shape of the foot during running for a selection of different people.

Unlike almost all methods reported in literature that are only capable of making absolute shape measurements, using DIC the method developed is capable of making the same absolute shape

measurements as well as measuring actual deformations, both of the surface and of discrete shape measurements derived from the measured surfaces which can be associated between measurements. Furthermore, as part of the method, measurement of runner kinetics and kinematics has also been facilitated, through the use of an instrumented force platform and application of GOM PONTOS software respectively. The latter allows the measurement of kinematics from the same images without the need for additional hardware. These comprehensive measurement capabilities within the developed method created in this thesis are yet to be reported in any published research to date.

9.3 Implications of Research

The method overall greatly improves the capabilities for the measurement of foot shape during gait, particularly where locomotion velocity exceeds that associated with walking. The methodology has the potential to be applied in a number of research areas related to the measurement of dynamic foot morphology and understanding the change in foot shape during the stance phase of gait. The most obvious area is in the design of shoes and shoes lasts, particularly in the athletic footwear field, where changes in the foot shape are likely to be the most distinct due to the nature of the movements and the benefits to athlete and product performance will yield the greatest results. Furthermore, the capability for the measurement of kinetics and kinematics also allows the potential for wider applications in understanding the drivers for human foot shape change and potential relationships to injury.

9.4 Recommendations for Future Work

Future work should potentially look to refine the methodology in terms of hardware used to capture images. The cost and availability of the multiple high speed imaging cameras used in the work in this thesis could prohibit the recreation of the measurement method and inhibit its application in future research activities. As the measurement principles remain the same no matter the imaging device, finding a cheaper imaging alternative that is capable of the short shutter speeds to make a dynamic measurement would enable application of the measurement method within the research community. Furthermore, the use of higher resolution imaging hardware may also serve to improve measurement quality. In addition, the processes within the method are currently labour intensive; automation of certain processes related to analysis would also promote improved measurements. This would be especially important when considering application of the method for large numbers of subjects or measurements.

In its current form, the methodology has the potential to be applied in a number of research fields related to the measurement of the human foot shape where currently the consideration of dynamic shape is limited. The ability to link kinetic and kinematic measurements to shape and deformation measurements could potentially allow more detailed understanding of foot behaviour during the stance phase of gait when allied

with shape and deformation measurements. Efforts should be made to implement dynamic foot shape measurements into shoe last design and to investigate if improvements in dynamic fit are achieved.

Outside of the obvious applications in research to support the investigation of hypotheses and research questions relating to the human foot shape, the dynamic foot shape surface measurements have the potential to be used to provide boundary conditions for finite element (FE) modelling, which would improve the realism of models involved in the virtual engineering of shoes. Measurements could also be used to validate FE models of human foot shape. At a more basic level, the surface models created from measurements could be manufactured in a discrete physical form, with instrumentation, potentially, to serve as a tool to predict fit of shoes in a dynamic condition, thus informing shoe design within the development process.

10. References

Azernikov, S., & Fischer, A. (2008). Emerging non-contact 3D measurement technologies for shape retrieval and processing. *Virtual and Physical Prototyping*, *3*(2), 85–91. doi:10.1080/17452750802048808

Barr, A., & Backus, S. (2001). Biomechanics of Gait. In M. Nordin & V. Frankel (Eds.), *Basic Biomechanics of the Musculoskeletal System* (pp. 438–457). Phillidelphia: Lippincott Williams & Wilkins.

Bates, B., Osternig, L., Mason, B., & James, S. (1978). Lower Extremity Function during the Support Phase of Running. In E. Asmussen & K. Jorgensen (Eds.), *Biomechanics VI-B* (pp. 30–39). Copenhagen, Denmark.

Becker, T., Splitthof, K., Siebert, T., & Kletting, P. (2006). Error Estimations of 3D Digital Image Correlation Measurements. *Speckle06: Speckles, From Grains to Flowers*, *6341*(May 2011), 63410F–1 – 63410F–6. doi:10.1117/12.695277

Birch, K. (2003). Good Practice Guide: Estimating Uncertainties in Testing. *British Measurement and Testing Association*, *36*.

Brown, L., & Yavarsky, P. (1987). Locomotor Biomechanics and Pathomechanics: a Review. *Journal of Orthopaedic and Sports Physical Therapy*, *9*, 3–10.

Bruening, D. A., Cooney, K. M., & Buczek, F. L. (2012). Analysis of a kinetic multi-segment foot model. Part I: Model repeatability and kinematic validity. *Gait & Posture*, *35*(4), 529–534. doi:http://dx.doi.org/10.1016/j.gaitpost.2011.10.363

Buss, S. R. (2003). 3D Computer Graphics: A Mathematical Introduction with OpenGL.

Butler, R. J., Davis, I. S., & Hamill, J. (2006). Interaction of arch type and footwear on running mechanics. *American Journal of Sports Medicine*, *34*(12), 1998–2005. doi:10.1177/0363546506290401

Carson, M. C., Harrington, M. E., Thompson, N., O'Connor, J. J., & Theologis, T. N. (2001). Kinematic analysis of a multi-segment foot model for research and clinical applications: a repeatability analysis. *Journal of Biomechanics*, *34*(10), 1299–307. Retrieved from http://www.ncbi.nlm.nih.gov/pubmed/11522309

Cavanagh, P. (1987). The biomechanics of lower extremity action in distance running. *Foot and Ankle*, *7*(4), 197–217. Retrieved from http://www.ncbi.nlm.nih.gov/pubmed/3817667

Cavanagh, P., & Kram, R. (1990). Stride Length in Distance Running: Velocity, Body Dimensions and Mass Effects. In P. Cavanagh (Ed.), *Biomechanics of Distance Running* (pp. 35–64). Champaign: Human Kinetics.

Cavanagh, P., & Lafortune, M. (1980). Ground reaction forces in distance running. *Journal of Biomechanics*, *13*(5), 397–406. Retrieved from http://www.sciencedirect.com/science/article/pii/0021929080900330

Clarke, T., Frederick, E., & Cooper, L. (1983a). Biomechanical measurement of running shoe cushioning properties. In B. M. Nigg & B. Kerr (Eds.), *Biomechanical aspects of sport shoes and playing surfaces* (pp. 25–33). Calgary: University Press.

Clarke, T., Frederick, E., & Cooper, L. (1983b). Effects of Shoe Cushioning Upon Ground Reaction Forces in Running. *International Journal of Sports Medicine*, *4*(4), 247–251.

Clarke, T., Frederick, E., & Hamill, C. (1983a). The effect of shoe design paramaters on rearfoot control in running. *Medicine & Science in Sports & Exercise*, *15*(5), 376–381.

Clarke, T., Frederick, E., & Hamill, C. (1983b). The effects of shoe design parameters on rearfoot control in running. *Medicine & Science in Sports & Exercise*, *15*(5), 376–381. Retrieved from http://www.ncbi.nlm.nih.gov/pubmed/6645865

Coudert, T., Vacher, P., Smits, C., & Van der Zande, M. (2006). A method to obtain 3D foot shape deformation during the gait cycle. *9th International Symposium on the 3D Analysis of Human Movement*, 3–6. Retrieved from http://www.univ-valenciennes.fr/congres/3D2006/Abstracts/117-Coudert.pdf

Cowan, D. N., Jones, B. H., Robinson, J. R., & Reed, W. (1993). Foot Morphologic Characteristics and Risk of Exercise-Related Injury. *Archives of Family Medicine*, *2*(7), 773–777.

Daanen, H. A. M., & Ter Haar, F. B. (2013). 3D whole body scanners revisited. *Displays*, *34*(4), 270–275. doi:10.1016/j.displa.2013.08.011

De Wit, B., De Clercq, D., & Aerts, P. (2000). Biomechanical analysis of the stance phase during barefoot and shod running. *Journal of Biomechanics*, *33*(3), 269–78. Retrieved from http://www.ncbi.nlm.nih.gov/pubmed/10673110

Deschamps, K., Staes, F., Bruyninckx, H., Busschots, E., Jaspers, E., Atre, A., & Desloovere, K. (2012). Repeatability in the assessment of multi-segment foot kinematics. *Gait & Posture*, *35*(2), 255–260. doi:http://dx.doi.org/10.1016/j.gaitpost.2011.09.016

Dillman, C. (1975). Kinematic Analyses of Running. *Exercise and Sports Science Reviews*, *3*, 193–218.

Divert, C., Mornieux, G., Baur, H., Mayer, F., & Belli, A. (2005). Mechanical comparison of barefoot and shod running. *International Journal of Sports Medicine*, *26*(7), 593–8. doi:10.1055/s-2004-821327

Donatelli, R. (1987). Abnormal biomechanics of the foot and ankle. *The Journal of Orthopaedic and Sports Physical Therapy*, *9*(1), 11–16.

Dugan, S. A., & Bhat, K. P. (2005). Biomechanics and Analysis of Running Gait. *Physical Medicine and Rehabilitation Clinics of North America*, *16*(3), 603–621. doi:http://dx.doi.org/10.1016/j.pmr.2005.02.007

Edington, C., Frederick, E., & Cavanagh, P. (1990). Rearfoot Motion in Distance Running. In P. Cavanagh (Ed.), *Biomechanics of Distance Running* (pp. 135–164). Champaign: Human Kinetics.

Elftman, H. (1960). The transverse talar joint and its control. *Clinical Orthopaedics*, *16*, 41–45.

Eslami, M., Begon, M., Farahpour, N., & Allard, P. (2007). Forefoot-rearfoot coupling patterns and tibial internal rotation during stance phase of barefoot versus shod running. *Clinical Biomechanics*, *22*(1), 74–80. doi:10.1016/j.clinbiomech.2006.08.002

Fazzini, M., Mistou, S., & Dalverny, O. (2010). Error assessment in Image Stereo-correlation. *EPJ Web of Conferences*, *6*, 31009–p1–8. doi:10.1051/epjconf/20100631009

Ferber, R., Davis, I. M., III, D. S. W., & Laughton, C. (2002). A comparison of within- and between-day reliability of discrete 3D lower extremity variables in runners. *Journal of Orthopaedic Research*, *20*(6), 1139–1145. doi:http://dx.doi.org/10.1016/S0736-0266(02)00077-3

Ferrandis, R. (1994). Rearfoot motion and torsion in running: the effects of upper vamp stabilizers. *Journal of Applied Biomechanics*, *10*, 28–42. Retrieved from http://scholar.google.com/scholar?hl=en&btnG=Search&q=intitle:Rearfoot+Motion+and+Torsion+in+Running+:+The+Effects+of+Upper+Vamp+Stabilizers#0

Ferrandis, R., García, A., Ramiro, J., Hoyos, J., & Vera, P. (1994). Rearfoot Motion and Torsion in Running - The Effects of Upper Vamp Stablilizers. *Journal of Applied Biomechanics*, *10*(1), 28–42.

Floyd, R. (2006). *Manual of Structural Kinesiology*. Boston: McGraw Hill.

Fukuchi, R. K., & Duarte, M. (2008). Comparison of three-dimensional lower extremity running kinematics of young adult and elderly runners. *Journal of Sports Sciences*, *26*(13), 1447–1454. doi:10.1080/02640410802209018

GOM. (2009a). *ARAMIS SA1 Sensor Configuration*. Braunschweig, Germany: GOM.

GOM. (2009b). *ARAMIS User Manual RevA - Software*. Braunschweig, Germany: GOM.

GOM. (2011). *PONTOS User Manual RevA- Software*. Braunschweig, Germany: GOM.

Gray, H. (2004). *Gray's Anatomy: the anatomical basis of clinical practice*. Edinburgh: Elsevier Churchill.

Hack, E., Burguete, R., & Patterson, E. (2005). Traceability of Optical Techniques for Strain Measurement. *Applied Mechanics and Materials*, *3-4*(2005), 391–396. doi:10.4028/www.scientific.net/AMM.3-4.391

Hack, E., Patterson, E., Siebert, T., & Thalmann, R. (2010). Calibration and validation of full-field techniques. In F. Bremand (Ed.), *ICEM 14: 14th International Conference on Experimental Mechanics, Vol 6* (Vol. 6). Les Ulis: E D P Sciences. doi:10.1051/epjconf/20100646003

Haddadi, H., & Belhabib, S. (2008). Use of rigid-body motion for the investigation and estimation of the measurement errors related to digital image correlation technique. *Optics and Lasers in Engineering*, *46*(2), 185–196. doi:10.1016/j.optlaseng.2007.05.008

Hamill, J., Bates, B., & Holt, K. (1992). Timing of lower-extremity joint actions during treadmill running. *Medicine & Science in Sports & Exercise*, *24*(7), 807–813.

Hamill, J., & Knutzen, K. (2003). *Biomechanical Basis of Human Movement*. Baltimore: Lippincott Williams & Wilkins.

Hasegawa, H., Yamauchi, T., & Kraemew, W. J. (2007). Foot strike patterns of runners at the 15-km point during an elite-level half marathon. *JOURNAL OF STRENGTH AND CONDITIONING RESEARCH*, *21*(3), 888–893. doi:10.1519/R-22096.1

Hawes, M., Sovak, D., Miyashita, M., Kang, S., Yoshihuku, Y., & Tanaka, S. (1994). Ethnic-differences in forefoot shape and the determination of shoe comfort. *Ergonomics*, *37*(1), 187–196. doi:10.1080/00140139408963637

Hicks, J. (1953). The Mechanics of the Foot - 1. The Joints. *Journal of Anatomy*, *87*(4), 345–357.

Hong, Y., Wang, L., Xu, D. Q., & Li, J. X. (2011). Gender differences in foot shape: a study of Chinese young adults. *SPORTS BIOMECHANICS*, *10*(2), 85–97. doi:10.1080/14763141.2011.569567

Hreljac, A., Marshall, R., & Hume, P. (2000). Evaluation of lower extremity overuse injury potential in runners. *Medicine & Science in Sports & Exercise*, *32*(9), 1635–1641. Retrieved from http://www.hhs.csus.edu/homepages/khs/biomechanics/manuscripts/hreljac.runninginjuries.pdf

International Organization for Standardization. (2007). International vocabulary of metrology - Basic and general concepts and associated terms.

James, S., Bates, B., & Osternig, L. (1978). Injuries to Runners. *The American Journal of Sports Medicine*, *6*(2), 40–50.

Jezeršek, M., & Možina, J. (2009). High-speed measurement of foot shape based on multiple-laser-plane triangulation. *Optical Engineering*, *48*(11), 113604. doi:10.1117/1.3265522

Ji, Z., & Leu, M. C. (1989). Design of optical triangulation devices. *Optics & Laser Technology*, *21*(5), 339–341. doi:http://dx.doi.org/10.1016/0030-3992(89)90068-6

Jimenez-Ormeno, E., Aguado, X., Delgado-Abellan, L., Mecerreyes, L., & Alegre, L. M. (2013). Foot morphology in normal-weight, overweight, and obese schoolchildren. *EUROPEAN JOURNAL OF PEDIATRICS*, *172*(5), 645–652. doi:10.1007/s00431-013-1944-4

Kadaba, M. P., Ramakrishnan, H. K., Wootten, M. E., Gainey, J., Gorton, G., & Cochran, G. V. B. (1989). Repeatability Of Kinematic, Kinetic, and Electromyographic Data in Normal Adult Gait. *Journal of Orthopaedic Research*, *7*(6), 849–860. doi:10.1002/jor.1100070611

Kapanji, I. (1970). *The physiology of the joints. Volume 2: Lower Limb*. Edinburgh: Churchill Livingstone.

Kazhdan, M., & Hoppe, H. (2013). Screened Poisson Surface Reconstruction, *32*(3), 1–13.

Kimura, M., Mochimaru, M., & Kanade, T. (2008). Measurement of 3D foot shape deformation in motion. *Proceedings of the 5th ACM/IEEE International Workshop on Projector Camera Systems*, *1*(212). Retrieved from http://dl.acm.org/citation.cfm?id=1394636

Kimura, M., Mochimaru, M., & Kanade, T. (2009). 3D measurement of feature cross-sections of foot while walking. *Machine Vision and Applications*, *22*(2), 377–388. doi:10.1007/s00138-009-0238-3

Komi, P., Gollhofer, A., Schmidtbleicher, D., & Frick, U. (1987). Interaction between man and shoe in running - considerations for a more comprehensive measurement approach. *International Journal of Sports Medicine*, *8*(3), 196–202. doi:10.1055/s-2008-1025655

Kouchi, M., Kimura, M., & Mochimaru, M. (2009). Deformation of foot cross-section shapes during walking. *Gait & Posture*, *30*(4), 482–6. doi:10.1016/j.gaitpost.2009.07.113

Kraus, K. (2007). *Photogrammetry: Geometry from Images and Laser Scans*. Walter de Gruyter.

Krauss, I., Grau, S., Mauch, M., Maiwald, C., & Horstmann, T. (2008). Sex-related differences in foot shape. *ERGONOMICS*, *51*(11), 1693–1709. doi:10.1080/00140130802376026

Krauss, I., Valiant, G., Horstmann, T., & Grau, S. (2010). Comparison of female foot morphology and last design in athletic footwear - are men's lasts appropriate for women? *Research in Sports Medicine*, *18*(2), 140–56. doi:10.1080/15438621003627216

Leardini, A., Benedetti, M., Berti, L., Bettinelli, D., Nativo, R., & Giannini, S. (2007). Rear-foot, mid-foot and fore-foot motion during the stance phase of gait. *Gait & Posture*, *25*(3), 453–62. doi:10.1016/j.gaitpost.2006.05.017

Lecompte, D., Smits, A., Bossuyt, S., Sol, H., Vantomme, J., Van Hemelrijck, D., & Habraken, A. (2006). Quality assessment of speckle patterns for digital image correlation. *Optics and Lasers in Engineering*, *44*(11), 1132–1145. doi:10.1016/j.optlaseng.2005.10.004

Lieberman, D. E. (2012). What We Can Learn About Running from Barefoot Running: An Evolutionary Medical Perspective. *Exercise and Sports Science Reviews*, *40*(2), 63–72. doi:10.1097/JES.0b013e31824ab210

Lieberman, D. E., Venkadesan, M., Werbel, W. a, Daoud, A. I., D'Andrea, S., Davis, I. S., … Pitsiladis, Y. (2010). Foot strike patterns and collision forces in habitually barefoot versus shod runners. *Nature*, *463*(7280), 531–5. doi:10.1038/nature08723

Liu, S., Cui, Y., Sanchez, S., & Stricker, D. (2011). Foot scanning and deformation estimation using time-of-flight cameras. *Footwear Science*, *3*(sup1), S98–S99. doi:10.1080/19424280.2011.575862

Lucintel. (2012). *Global Retail Sporting Goods Market Analysis 2012–2017: Industry Trends, Profit, and Forecast Analysis*.

Luo, G., Houston, V. L., Mussman, M., Garbarini, M., Beattie, A. C., & Thongpop, C. (2009). Comparison of Male and Female Foot Shape. *JOURNAL OF THE AMERICAN PODIATRIC MEDICAL ASSOCIATION*, *99*(5), 383–390.

Luthanen, P., & Komi, P. (1977). Mechanical factors influencing running speed. In E. Amussen & K. Jorgensen (Eds.), *Biomechanics V-B* (pp. 23–29). Baltimore: University Park.

Luximon, A., & Luximon, Y. (2009). Shoe-last design innovation for better shoe fitting. *Computers in Industry*, *60*(8), 621–628. doi:10.1016/j.compind.2009.05.015

Luximon, A., & Luximon, Y. (2013). Shoe-Last Design and Development. In *The Science of Footwear* (pp. 193–212). Boca Raton, FL: Taylor & Francis Ltd.

Luximon, Y., & Luximon, A. (2013). Sizing and Grading of Shoe Lasts. In A. Luximon (Ed.), *Handbook of Footwear Design and Manufacture* (pp. 197–215). Woodhead Publishing Limited.

Maclean, C., Davis, I., & Hamill, J. (2009). Influence of running shoe midsole composition and custom foot orthotic intervention on lower extremity dynamics during running. *Journal of Applied Biomechanics*, *25*(1), 54–63. Retrieved from http://www.ncbi.nlm.nih.gov/pubmed/19299830

Madison, A. (2012, October). Seeing the Light. *Cutting Tool Engineering*.

Mann, R. (1993). Biomechanics of the Foot and Ankle. In *Surgery of the Foot and Ankle* (pp. 3–43). St Louis: Mosby.

Manter, J. (1941). Movements of the subtalar and transverse tarsal joints. *The Anatomical Record*, *80*, 397–410.

Mauch, M., Grau, S., Krauss, I., Maiwald, C., & Horstmann, T. (2009). A new approach to children's footwear based on foot type classification. *Ergonomics*, *52*(8), 999–1008. doi:10.1080/00140130902803549

McGinnis, P. M. (2005). *Biomechanics of Sport and Exercise* (2nd ed.). Champaign: Human Kinetics.

McNair, P. J., & Marshall, R. N. (1994). Kinematic and Kinetic-Parameters Associated With Running in Different Shoes. *British Journal of Sports Medicine*, *28*(4), 256–260.

Milner, S. (2010). Common disorders of the foot and ankle. *Surgery (Oxford)*, *28*(10), 514–517. doi:http://dx.doi.org/10.1016/j.mpsur.2010.07.007

Mitchell, S. R., Jones, R., & Newman, S. T. (1995). A Structured Approach to the Design of Shoe Lasts. *Journal of Engineering Design*, *6*(2), 149–166. doi:10.1080/09544829508907910

Monaghan, G. M., Lewis, C. L., Hsu, W.-H., Saltzman, E., Hamill, J., & Holt, K. G. (2013). Forefoot angle determines duration and amplitude of pronation during walking. *Gait & Posture*, *38*(1), 8–13. doi:http://dx.doi.org/10.1016/j.gaitpost.2012.10.003

Morio, C., Lake, M., Gueguen, N., Rao, G., & Baly, L. (2009). The influence of footwear on foot motion during walking and running. *Journal of Biomechanics*, *42*(13), 2081–8. doi:10.1016/j.jbiomech.2009.06.015

Morley, J., Decker, L., Dierks, T., Blanke, D., French, J., & Stergiou, N. (2010). Effects of varying amounts of pronation on the mediolaterla ground reaction forces during barefoot versus shod running. *Journal of Applied Biomechanics*, *26*(2), 205–214.

Murphy, D. F., Connolly, D. A. J., & Beynnon, B. D. (2003). Risk factors for lower extremity injury: a review of the literature. *BRITISH JOURNAL OF SPORTS MEDICINE*, *37*(1), 13–29. doi:10.1136/bjsm.37.1.13

Nakhaee, Z., Rahimi, A., Abaee, M., Rezasoltani, A., & Kalantari, K. K. (2008). The relationship between the height of the medial longitudinal arch (MLA) and the ankle and knee injuries in professional runners. *The Foot*, *18*(2), 84–90. doi:http://dx.doi.org/10.1016/j.foot.2008.01.004

Nigg, B., & Hintermann, B. (2002). Biomechanics of the Ankle Joint Complex and the Shoe. In M. Nyska & G. Mann (Eds.), *The Unstable Ankle* (pp. 17–26). Champaign: Human Kinetics.

Nigg, B. M., Herzog, W., & Read, L. J. (1988). Effect of Viscoelastic Shoe Insoles on Vertical Impact Forces in Heel-Toe Running. *American Journal of Sports Medicine*, *16*(1), 70–76. doi:10.1177/036354658801600113

Nigg, B., & Morlock, M. (1987). The influence of lateral heel flare of running shoes on pronation and impact forces. *Medicine & Science in Sports & Exercise*, *19*(3), 294–302.

Nigg, B., & Segesser, B. (1992). Biomechanical and orthopaedic concepts in sports shoe construction. *Medicine & Science in Sports & Exercise*, *24*(5), 595–602.

Nilsson, J., Thorstensson, A., & Halbertsma, J. (1985). Changes in leg movements and muscle-activity with speed of locomotion and mode of progression in humans. *Acta Physiologica Scandinavica*, *123*(4), 457–475. doi:10.1111/j.1748-1716.1985.tb07612.x

Novacheck, T. (1998). The biomechanics of running. *Gait & Posture*, *7*(1), 77–95. Retrieved from http://www.ncbi.nlm.nih.gov/pubmed/10200378

Ouzounian, T., & Shereff, M. (1989). Invitro determination of midfoot motion. *Foot and Ankle*, *10*(3), 140–146.

Pan, B., Xie, H., Yang, L., & Wang, Z. (2009). Accurate Measurement of Satellite Antenna Surface Using 3D Digital Image Correlation Technique. *Strain*, *45*(2), 194–200. doi:10.1111/j.1475-1305.2008.00450.x

Patterson, E., Hack, E., Brailly, P., Burguete, R., Saleem, Q., Siebert, T., … Whelan, M. (2007). Calibration and evaluation of optical systems for full-field strain measurement. *Optics and Lasers in Engineering*, *45*(5), 550–564. doi:10.1016/j.optlaseng.2006.08.012

Perry, S., & Lafortune, M. (1995). Influences of inversion/eversion of the foot upon impact loading during locomotion. *Clinical Biomechanics*, *10*(5), 253–257. Retrieved from http://www.ncbi.nlm.nih.gov/pubmed/11415562

Pivečka, J., & Laure, S. (1995). *The Shoe Last: Practical Handbook for Shoe Designers*. Zlin, Czech Republic: International School of Modern Shoemaking.

Pohl, M., & Buckley, J. (2008). Changes in foot and shank coupling due to alterations in foot strike pattern during running. *Clinical Biomechanics*, *23*(3), 334–41. doi:10.1016/j.clinbiomech.2007.09.016

Queen, R. M., Gross, M. T., & Liu, H.-Y. (2006). Repeatability of lower extremity kinetics and kinematics for standardized and self-selected running speeds. *Gait & Posture*, *23*(3), 282–287. doi:http://dx.doi.org/10.1016/j.gaitpost.2005.03.007

Ray, S. (1988). The Geometry of Image Formation. In R. Jacobson (Ed.), *The Manual of Photography* (8th ed., pp. 28–47). London and Boston: Focal Press.

Reinschmidt, C., & Nigg, B. (2000). Current issues in the design of running and court shoes. *Sportverletzung-Sportschaden*, *14*(3), 71–81.

Reinschmidt, C., Van Den Bogert, A., Lundberg, A., Nigg, B., Murphy, N., & Alta, T. (1997). Tibiofemoral and tibiocalcaneal motion during walking : external vs skeletal markers. *Gait & Posture*, *6*(2), 98–109.

Reinschmidt, C., van Den Bogert, A., Murphy, N., Lundberg, A., & Nigg, B. (1997). Tibiocalcaneal motion during running, measured with external and bone markers. *Clinical Biomechanics*, *12*(1), 8–16. Retrieved from http://www.ncbi.nlm.nih.gov/pubmed/11415666

Richards, J. G. (1999). The measurement of human motion: A comparison of commercially available systems. *Human Movement Science*, *18*(5), 589–602. doi:http://dx.doi.org/10.1016/S0167-9457(99)00023-8

Robertson, G., Hamill, J., Kamen, G., & Whittlesey, S. (2013). *Research Methods in Biomechanics* (2nd ed.). Champaign: Human Kinetics.

Robinette, K. M., Daanen, H., & Nrc, E. P. (1999). The Caesar Project : A 3-D Surface Anthropometry Survey. In *The Second International Conference on 3D imaging and Modelling* (pp. 380–386). Ottawa.

Sammarco, G., & Hockenbury, R. (2001). Biomechanics of the Foot and Ankle. In M. Nordin & V. Frankel (Eds.), *Basic Biomechanics of the Musculoskeletal System* (pp. 222–255). Phillidelphia: Lippincott Williams & Wilkins.

Schmeltzpfenning, T., Plank, C., & Krauss, I. (2010). Dynamic foot scanning. Prospects and limitations using synchronized 3D scanners to capture complete human foot shape while walking. In *Proceedings of the 3rd International Conference on Applied Human Factors and Ergonomics*. Miami. Retrieved from http://scholar.google.com/scholar?hl=en&btnG=Search&q=intitle:Dynamic+Foot+Scanning+.+Prospects+and+Limitations+of+Using+Synchronized+3D+Scanners+to+Capture+Complete+Human+Foot+Shape+While+Walking#0

Schuette, K. H., Miles, K. C., Venter, R. E., & Van Niekerk, S.-M. (2013). Barefoot Running Causes Acute Changes in Lower Limb Kinematics in Habitually Shod Male Runners. *South African Journal for Research in Sport Physical Education and Recreation*, *35*(1), 153–164.

Scott, S., & Winter, D. (1991). Talocrural and talocalcaneal joint kinematics and kinetics during the stance phase of walking. *Journal of Biomechanics*, *24*(8), 743–752. doi:10.1016/0021-9290(91)90338-N

SGMA. (2011). *2011 State of the Industry Report*.

Simon, J., Doederlein, L., McIntosh, A., Metaxiotis, D., Bock, H., & Wolf, S. (2006). The Heidelberg foot measurement method: development, description and assessment. *Gait & Posture*, *23*(4), 411–24. doi:10.1016/j.gaitpost.2005.07.003

Sinclair, J., Taylor, P. J., Edmundson, C. J., Brooks, D., & Hobbs, S. J. (2012). Influence of the helical and six available Cardan sequences on 3D ankle joint kinematic parameters. *Sports Biomechanics*, *11*(3), 430–437. doi:10.1080/14763141.2012.656762

Smith, A., Forrester, S., & Roberts, J. (2010). Repeatability of Golf Swing Kinematics Between Day and Between Tester. In *Biomechanics Interest Group of the British Association of Sport and Exercise Sciences*.

Snel, J., Delleman, Y., Heerkins, Y., & Van Ingen Schenau, G. (1985). Shock-absorbing characteristics of running shoes during actual running. In D. Winter, R. Wells, K. Hayes, & A. Patla (Eds.), *Biomechanics IX-B* (pp. 133–138). Champaign: Human Kinetics.

Soutas-Little, R., & Beavis, G. (1987). Analysis of foot motion during running using a joint co-ordinate system. *Medicine & Science in Sports & Exercise*, *19*(3), 285–293. Retrieved from http://ukpmc.ac.uk/abstract/MED/3600243

Spoor, C. W., & Veldpaus, F. E. (1980). Rigid body motion calculated from spatial co-ordinates of markers. *Journal of Biomechanics*, *13*(4), 391–393. doi:http://dx.doi.org/10.1016/0021-9290(80)90020-2

Stacoff, A., Kälin, X., Stuessi, E., & Segesser, B. (1989). The Torsion of the Foot in Running. *International Journal of Sport Biomechanics*, *5*(4), 375–389.

Su, X., & Zhang, Q. (2010). Dynamic 3-D shape measurement method: A review. *OPTICS AND LASERS IN ENGINEERING*, *48*(2), 191–204. doi:10.1016/j.optlaseng.2009.03.012

Subotnick, S. I. (1985). The biomechanics of running - implications for the prevention of foot injuries. *Sports Medicine*, *2*(2), 144–153.

Sutton, M. A., McNeil, S. R., Helm, J. D., & Chao, Y. J. (2000). Advances in Two-Dimensional and Three-Dimensional Computer Vision. In P. K. Rastogi (Ed.), *Photomechanics* (pp. 323–372). Springer.

Sutton, M. A., Orteu, J. J., & Schreier, H. W. (2009). *Image Correlation for Shape, Motion and Deformation Measurements*. New York: Springer.

Sutton, M. A., Turner, J. L., Bruck, H. A., & Chae, T. A. (1991). Full-field representation of discretely sampled surface deformation for displacement and strain analysis. *Experimental Mechanics*, *31*(2), 168–177. doi:10.1007/BF02327571

Sutton, M. A., Walters, W. J., Peters, W. H., Ranson, W. F., & Mcneil, S. R. (1983). Determination of displacements using an improved digital correlation method. *Image and Vision Computing*, *1*(3), 133–139.

Taunton, J., Celement, D., Smart, G., Wiley, J., & McNicol, K. (1985). A triplanar electrogoniometer investigation of running mechanics in runners with compensatory overpronation. *Canadian Journal of Applied Sports Science*, *10*(3), 104–115.

Telfer, S., & Woodburn, J. (2010). The use of 3D surface scanning for the measurement and assessment of the human foot. *JOURNAL OF FOOT AND ANKLE RESEARCH*, *3*. doi:10.1186/1757-1146-3-19

Thabet, A., Trucco, E., & Salvi, J. (2014). Dynamic 3D shape of the plantar surface of the foot using coded structured light: a technical report. *Journal of Foot and Ankle Research*, *7*(5), 1–12. Retrieved from http://link.springer.com/article/10.1186/1757-1146-7-5

Van de Graaf, K. (1998). *Human Anatomy*. Boston: W.C. Brown.

Van de Graaf, K., & Fox, S. (1995). *Concepts of Human Anatomy and Physiology*. Dubuque: W.C. Brown.

Van den bogert, A., Smith, G., & Nigg, B. (1994). In-vivo determination of the anatomical axes of the ankle joint complex - an optimization approach. *Journal of Biomechanics*, *27*(12), 1477–1488. doi:10.1016/0021-9290(94)90197-X

Van den Herrewegen, I., Cuppens, K., Broeckx, M., Barisch-Fritz, B., Vander Sloten, J., Leardini, A., & Peeraer, L. (2014). Dynamic 3D scanning as a markerless method to calculate multi-segment foot kinematics during stance phase: Methodology and first application. *Journal of Biomechanics*, *47*(11), 2531–2539. doi:10.1016/j.jbiomech.2014.06.010

Wang, C.-S. (2010). An analysis and evaluation of fitness for shoe lasts and human feet. *Computers in Industry*, *61*(6), 532–540. doi:10.1016/j.compind.2010.03.003

Williams, D. S., McClay, I. S., & Hamill, J. (2001). Arch structure and injury patterns in runners. *CLINICAL BIOMECHANICS*, *16*(4), 341–347. doi:10.1016/S0268-0033(01)00005-5

Williams, K. (1980). *A biomechanical evaluation of distance running efficiency (Unpublished)*. Pennsylvania State University.

Williams, K. (2000). The Dynamics of Running. In *Biomechanics in Sport* (pp. 161–183).

Williiams, K. (1985). Biomechanics of Running. In R. L. Terjung (Ed.), *Exercise and Sport Science Reviews* (13th ed.). McMillan Publishing Company.

Witana, C., Feng, J., & Goonetilleke, R. (2004). Dimensional differences for evaluating the quality of footwear fit. *Ergonomics*, *47*(12), 1301–17. doi:10.1080/00140130410001712645

Witana, C., Xiong, S., Zhao, J., & Goonetilleke, R. (2006). Foot measurements from three-dimensional scans: A comparison and evaluation of different methods. *International Journal of Industrial Ergonomics*, *36*(9), 789–807. doi:10.1016/j.ergon.2006.06.004

Wolf, P., List, R., Ukelo, T., Maiwald, C., & Stacoff, A. (2009). Day-to-Day Consistency of Lower Extremity Kinematics During Walking And Running. *Journal of Applied Biomechanics*, *25*(4), 369–376.

Wu, G., Siegler, S., Allard, P., Kirtley, C., Leardini, A., Rosenbaum, D., … Stokes, H. (2002). ISB recommendation on definitions of joint coordinate system of various joints for the reporting of human joint motion - part 1: ankle, hip, and spine. *Journal of Biomechanics*, *35*(4), 543–548. doi:10.1016/S0021-9290(01)00222-6

Wunderlich, R., & Cavanagh, P. (2001). Gender differences in adult foot shape: implications for shoe design. *Medicine & Science in Sports & Exercise*, *33*(4), 605–611. Retrieved from http://cat.inist.fr/?aModele=afficheN&cpsidt=1001915

Xiong, S., Goonetilleke, R. S., Zhao, J., Li, W., & Witana, C. P. (2009). Foot deformations under different load-bearing conditions and their relationships to stature and body weight. *ANTHROPOLOGICAL SCIENCE*, *117*(2), 77–88. doi:10.1537/ase.070915

Zhang, S., & Huang, P. (2006). High-resolution, real-time three-dimensional shape measurement. *Optical Engineering*, *45*(12). doi:10.1117/1.2402128

Appendix

APPENDIX A – Ethics Forms
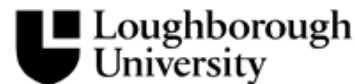
Loughborough University

Shape-Strain Measurement and Instrumentation of Human Feet & Athletic Footwear during Dynamic Real Time Human Motion

Participant Information Sheet

Main Investigator:
Rob Blenkinsopp, Sports Technology Institute, Loughborough University
Email: r.blenkinsopp@lboro.ac.uk, Tel: 01509 56 4812

Supervisors:
Dr Jon Roberts, Sports Technology Institute, Loughborough University
Email: J.R.Roberts@lboro.ac.uk, Tel: 01509 54 4803

Dr Andy Harland, Sports Technology Institute, Loughborough University
Email: A.R.Harland@lboro.ac.uk, Tel: 01509 56 4802

What is the purpose of the study?

The purpose of this study is to gain understanding of the behaviour of the human foot during dynamic sporting movements and the foot-shoe interactions as well as the influence on the human body. The aim is to use the information to improve sports footwear design.

Who is doing this research and why?

This study is a part of a student research project funded by Loughborough University

Are there any exclusion criteria?

If you are currently injured, sick or have been explicitly told not to exercise by your doctor.

Once I take part, can I change my mind?

Yes! After you have read this information and asked any questions you may have we will ask you to complete an Informed Consent Form, however if at any time, before, during or after the sessions you wish to withdraw from the study please just contact the main investigator. You can withdraw at any time, for any reason and you will not be asked to explain your reasons for withdrawing.

Will I be required to attend any sessions and where will these be?

The sessions will take place at various locations at Loughborough University dependent on the test being carried out, you will be told by the investigator where.

How long will it take?

The total expected time is approximately 2-3 hours.

Is there anything I need to do before the sessions?

No.

Is there anything I need to bring with me?

Your own training clothes (e.g. shorts, shirt, running trainers) and medication you usually need during light exercise sessions (e.g. inhaler).

What type of clothing should I wear?

See above.

What will I be asked to do?

At the testing sessions you will be required to complete sports movement whilst measurements are taken. This may be in a barefoot, or shod (with shoe) condition. The testing may involve the attachment of equipment to the body and video footage being taken, this will be outlined to you by the investigator.

Some data capture methods require a contrasting speckled pattern to be applied to the surface of interest to enable the surface to be recognised optically. In barefoot measurements this will be achieved by using water based, hypoallergenic, non-toxic face paint applied to the skin. The paint will be applied before the testing and can be removed immediately after with soap and warm water.

At the end of the testing there may be a requirement for perception questionnaires or interviews to take place, based on the trial that has just been conducted.

What personal information will be required from me?

Age, sex, weight, running history.

Are their any risks in participating?

There are no perceived risks involved in this testing. Time is provided for warm up prior to testing and rest between trials to eliminate the potential possibility of any exhaustion or overuse injuries occurring.

Will my taking part in this study be kept confidential?

Yes. All personal data will be stored in accordance with the data protection act, in a secure location and you will only be referred to as a participant number/letter. Any video footage obtained will be destroyed/erased after 3 years.

What will happen to the results of the study?

The results of this study will be used in PhD research material, including published journals, conference papers and theses. You will be not be identified by name in any.

What do I get for participating?

Any test data that is taken will be available for you once all tests have been completed.

I have some more questions who should I contact?

Please contact the principle investigator or one of the supervisors listed at the top of this document.

What if I am not happy with how the research was conducted?

The University has a policy relating to Research Misconduct and Whistle Blowing which is available online at http://www.lboro.ac.uk/admin/committees/ethical/Whistleblowing(2).htm.

Loughborough University

**Shape-Strain Measurement and Instrumentation of Human Feet &
Athletic Footwear during Dynamic Real Time Human Motion**

INFORMED CONSENT FORM
(to be completed after Participant Information Sheet has been read)

The purpose and details of this study have been explained to me. I understand that this study is designed to further scientific knowledge and that all procedures have been approved by the Loughborough University Ethical Advisory Committee.

I have read and understood the information sheet and this consent form.

I have had an opportunity to ask questions about my participation.

I understand that I am under no obligation to take part in the study.

I understand that I have the right to withdraw from this study at any stage for any reason, and that I will not be required to explain my reasons for withdrawing.

I understand that all the information I provide will be treated in strict confidence and will be kept anonymous and confidential to the researchers unless (under the statutory obligations of the agencies which the researchers are working with), it is judged that confidentiality will have to be breached for the safety of the participant or others.
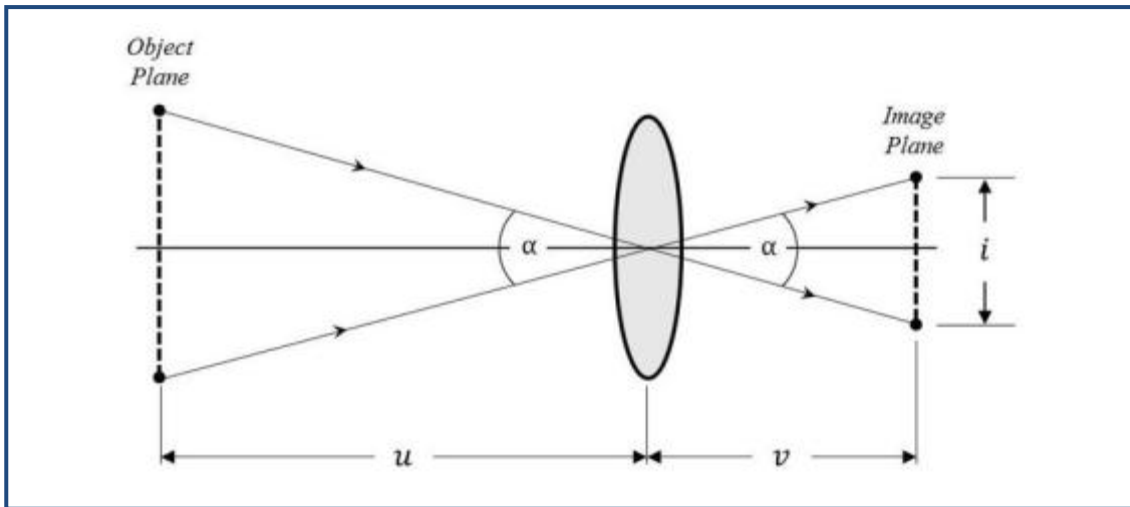
I agree to participate in this study.

Your name   _____

Your signature   _____

Signature of investigator   _____

Date   _____

APPENDIX B – Calculation of Field of View

| m = magnification factor | f = lens focal length | u = lens-object distance |
| v = lens-image distance | α = angle of view | i = image height/width |

Pinhole Camera Model for Field of View (FOV)

The lens conjugate equations for a rectilinear lens, incorporating the lens magnification factor, and assuming a square image at the CCD, equations 1-4 can be derived (Ray, 1988).

$$m = \frac{f}{u-f} \ (eq.1)$$

$$v = f\,(m+1) \ (eq.2)$$

$$\alpha = 2\left(\tan^{-1}\frac{i}{2v}\right) \ (eq.3)$$

$$FOV_h = FOV_v = 2\left[\tan\left(\frac{\alpha}{2}\right) \times u\right] \ (eq.4)$$

Known variables			Calculated Variables		
f (mm)	i (mm)	FOV(mm)	u (mm)	v (mm)	α (°)
50	20.48	360.5	930	52.84	21.93

```matlab
clc
clear all
tic;
sx=101;%defines size of image y (eventhough it says x)
sy=101;%defines size of image x (eventhough it says y)
spt(sx,sy)=0; %creates white background for everything

a=2; %square dimension width
L=4250; %Number of spots
spt(sx,sy)=0;
spt00(sx,sy)=0;
spt1(sx,sy)=0; %creates black background for spt to be added to first time
through loop
B=1;

for k=1:L;
      ctrx=randi(sx,1); %random interger for centre location
      ctry=randi(sy,1); %random interger for centre location
            Gray=randi([50 200],1,1);

for lay=1:B %number of layers for each spot % puts a spot down
    cx=ctrx;
    cy=ctry;
    for i=1:sx
        for j=1:sy
            if i>cx
                if i<=cx+a
                    if j>cy
                        if j<=cy+a
                        spt(i,j)=(Gray);%/B;%makes the maximum overlap value 255
which at this point is white
                        else
                        spt(i,j)=0; %makes areas outside the speckle black
                        end
                    end
                end
            end
        end
    end
    spt1=spt1+spt;
    spt=spt00;
    lay;
  end
end
for i=1:sx %makes spots which have a value bigger than 255 equal to 255
      for j=1:sy
            if spt1(i,j)>255; %wherever there is an overlap, renumbers it to be
255 (max)
                spt1(i,j)=255;
            end
      end
end
for i=1:sx %Inverts colours
      for j=1:sy
            if spt1(i,j)>0;
                spt1(i,j)=((spt1(i,j)-255)*(-1)); %changes scale so that values
in the lower range become high range values
            else
```
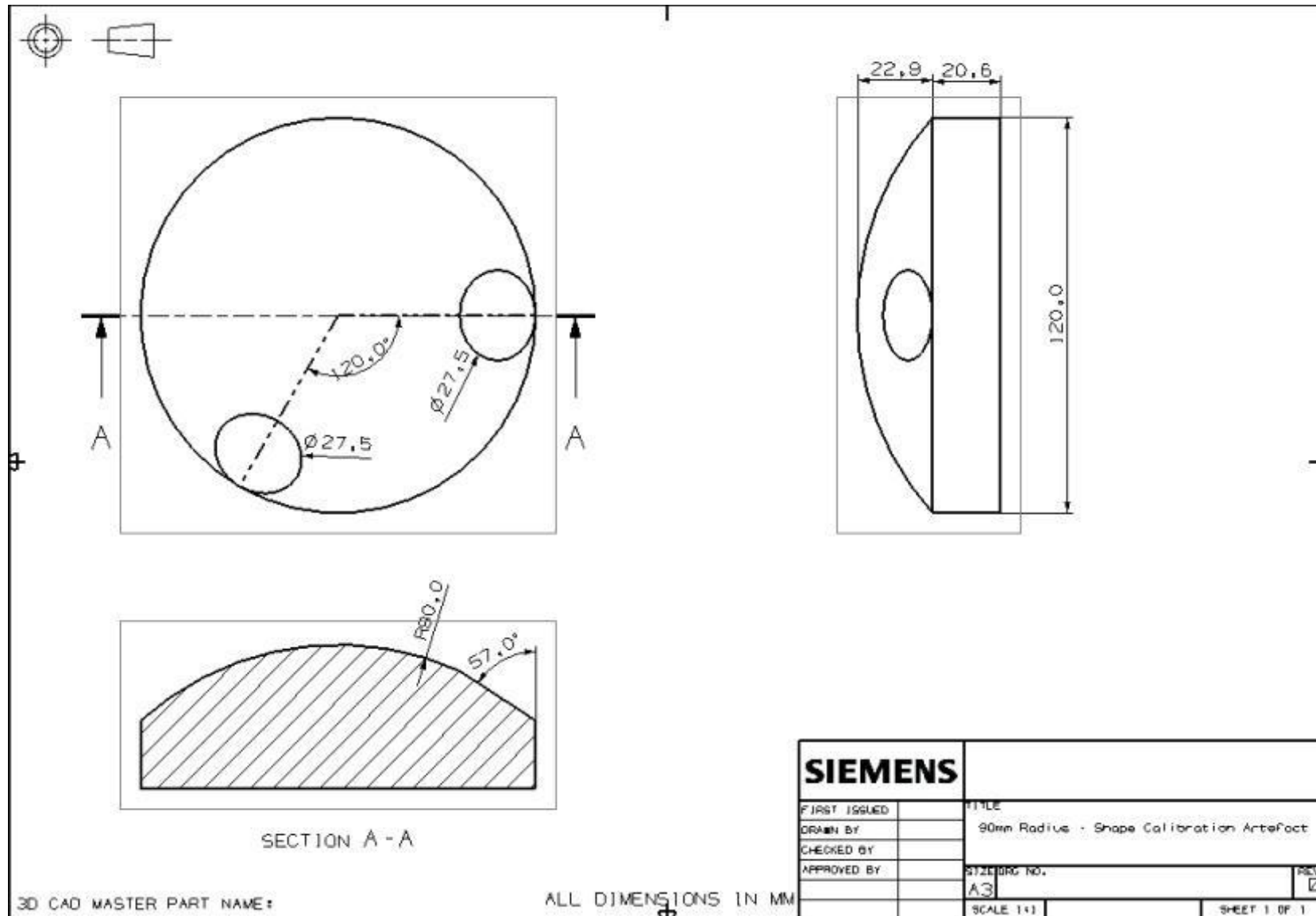
```matlab
                spt1(i,j)=(spt1(i,j)+255); % wherever there is a 0 it makes it
255
            end
        end
end

figure
imagesc(spt1)
axis square
colorbar
colormap('gray')
axis on
t=toc;
imwrite(spt1/255,'SPB.tif');
```

SECTION A-A

3D CAD MASTER PART NAME:

ALL DIMENSIONS IN MM

SIEMENS

FIRST ISSUED		TITLE		
DRAWN BY		90mm Radius - Shape Calibration Artefact		
CHECKED BY				
APPROVED BY		SIZE DRG NO.		REV
		A3		☑
		SCALE 1:1		SHEET 1 OF 1

APPENDIX E – GOM ATOS Calibration Certificate

GOM mbH
Mittelweg 7-8
38106 Braunschweig
Germany

gom Optical Measuring Techniques

GOM Acceptance Test

131104_CP40-200-100196
Certificate No.

Acceptance/Reverification According to VDI/VDE 2634, Part 3

This document may only be distributed in its entirety and without changes. Excerpts and changes require the approval of the issuing company. This document was created electronically and is valid without a signature.

General Data

System:	ATOS Core 185 SN:130993
Measuring volume:	MV185 (185x140x140) mm
Date:	04.11.2013
Inspector:	Jan Kristen
Measuring temperature:	19.8 °C

Artifact

General

Name:	PSA/400/Z0011_L6R6
Calibration date:	26.04.2013
Calibration ID:	0225-D-K-15007-02-00-2013-04
Calibration temperature:	20.0 °C
Expansion coefficient for sphere spacing:	$4.00 \cdot 10^{-6}$ K^{-1}
Expansion coefficient for diameter:	$10.50 \cdot 10^{-6}$ K^{-1}

Basic dimensions

Sphere spacing:	115 mm
Diameter left sphere:	20 mm
Diameter right sphere:	20 mm

Calibrated nominal dimensions

Sphere spacing:	115.0133 mm
Diameter left sphere:	20.0045 mm
Diameter right sphere:	20.0026 mm

GOM mbH   1./5   11/4/13 10:01 AM

Measurement Parameters

Measurement Settings

Number of exposure times:	1
Min. fringe contrast:	15 gray values
State: avoid points at strong brightness differences?:	Yes
State: avoid Triple Scan points?:	No
State: avoid Triple Scan points at strong brightness differences?:	Yes
Max. residual:	0.20 pixel
Depth limitation mode:	Automatic depth limitation
Corner mask size:	0
Measurement resolution:	Full resolution

Settings of Checks

State: check "Sensor movement"?:	Enabled
Max. sensor movement:	0.10 pixel
State: check "Lighting change"?:	Enabled

Sensor Calibration

General

Calibration date:	Mon Nov 04 09:47:22 2013
Measurement temperature:	20.0 °C

Calibration Object

Calibration object type:	Panel (Triple Scan)
Calibration object name:	CP40-200-100196
Test distances:	360.0000 / 360.0000 mm
Certification temperature:	22.0 °C
Expansion coefficient:	$3.25 \ 10^{-6} \ K^{-1}$

Calibration Settings

Focal length (camera):	23.000 mm
Focal length (projector):	12.500 mm
Light intensity:	100%
Snap mode:	Double snap
Max. ellipse quality:	0.40 pixel

Calibration Result

Calibration deviation:	0.028 pixel (Quality check: Good)
Calibration deviation (optimized):	0.014 pixel
Projector calibration deviation:	0.087 pixel (Quality check: Good)
Projector calibration deviation (optimized):	0.015 pixel
Camera angle:	31.95 deg
Height variance:	139.968 mm
Measuring volume:	180 x 142 x 142 mm

Acceptance/Reverification Test

General

Number of test positions (measurement series):	3
Nominal diameter of left sphere with temperature correction:	20.0045 mm
Nominal diameter of right sphere with temperature correction:	20.0026 mm
Nominal sphere spacing with temperature correction:	115.0132 mm

Parameter Probing Error Form, Left Sphere

Pos[2]	M[3]	P[4]	Min. deviation	Max. deviation	Range of deviation	Probing error form (sigma)
1	12	18621	-0.003 mm	0.003 mm	0.005 mm	0.001 mm
2	12	18412	-0.004 mm	0.003 mm	0.007 mm	0.001 mm
3	12	26243	-0.003 mm	0.003 mm	0.005 mm	0.001 mm

Parameter Probing Error Form, Right Sphere

Pos[2]	M[3]	P[4]	Min. deviation	Max. deviation	Range of deviation	Probing error form (sigma)
1	12	18932	-0.002 mm	0.002 mm	0.005 mm	0.001 mm
2	12	18780	-0.003 mm	0.003 mm	0.006 mm	0.001 mm
3	12	26880	-0.003 mm	0.002 mm	0.005 mm	0.001 mm

Parameter Probing Error Size, Left Sphere

Pos[2]	M[3]	P[4]	Diameter (actual)	Diameter (nominal)[1]	Probing error (size)
1	12	18621	20.004 mm	20.004 mm	-0.000 mm
2	12	18412	20.000 mm	20.004 mm	-0.004 mm
3	12	26243	20.001 mm	20.004 mm	-0.004 mm

Parameter Probing Error Size, Right Sphere

Pos[2]	M[3]	P[4]	Diameter (actual)	Diameter (nominal)[1]	Probing error (size)
1	12	18932	20.002 mm	20.003 mm	-0.000 mm
2	12	18780	19.997 mm	20.003 mm	-0.006 mm
3	12	26880	19.999 mm	20.003 mm	-0.003 mm

Sphere Spacing Error

Pos[2]	M[3]	Sphere spacing (actual)	Sphere spacing (nominal)[1]	Sphere spacing error
1	12	115.016 mm	115.013 mm	0.003 mm
2	12	115.017 mm	115.013 mm	0.004 mm
3	12	115.016 mm	115.013 mm	0.003 mm

Parameter Length Measurement Error

Pos[2]	M[3]	Length (actual)	Length (nominal)[1]	Length measurement error
1	12	135.020 mm	135.017 mm	0.003 mm
2	12	135.018 mm	135.017 mm	0.001 mm
3	12	135.017 mm	135.017 mm	0.000 mm

[1] With temperature correction
[2] Test position
[3] Number of measurements
[4] Number of points

189

Summary Acceptance/Reverification Test

Parameter	Maximum deviation
Probing error form (sigma)	0.001 mm
Sphere spacing error	0.004 mm

Restrictions to Operation Modes and Conditions

Operation Modes

- The sensor and its components are set up at the factory and must not be changed. This particularly applies to the cameras and lenses.
- The sensor has to be calibrated according to the hardware user manual. It is critical that the warm-up times and calibration limit values be maintained.
- The measurements are performed with the quality setting "High".
- The duration of image acquisition has to be selected such that the measuring images are well exposed. Overexposures are not permitted.
- The individual measurements combined to a mesh are post-processed with the polygonization setting "Standard".
- The spheres are determined using the least squares method, where 0.3% of the measured values are rejected as outliers. This value corresponds to a setting of 3 sigma. For calculating the spheres only measurement data is taken which is above a defined plane. This plane is parallel to the artifact base plate. Its position is defined by intersecting the sphere at the latitude of 10 degrees south.
- The length measurement error quality parameter is determined using Method C (see VDI/VDE 2634 Part 3, pg. 18).

Operation Conditions

- The artifact includes two spheres fixed to each other by means of a base plate. The sphere have the nominal diameters defined in section "Artifact".
- The sphere spacing approximates the nominal distance defined in section "Artifact".
- The spheres are made of steel and are coated with a titanium dioxide layer to ensure diffuse reflection.
- The sphere diameter and spacing have to be determined through a DAkkS calibration; in this case, the corresponding measuring uncertainty has to be very small compared to the corresponding limit value.
- The ambient conditions in accordance with the hardware user manual have to be maintained. In particular, the temperature must be kept constant throughout the measurement period.
- The ambient temperature and the temperature of the artifact have to be identical.
- The measuring environment must be free of mechanical vibrations.
- The ambient light should not vary extensively during the measurement.
- Avoid extremely bright external light sources.

APPENDIX F – C3D File Creation Matlab Code

```
clc
clear all

%Reads force and kinematic data in from Excel
% --> ('FILENAME.xlsx','WORKSHEET','DATA RANGE TOP LEFT CELL : DATA RANGE BOTTOM
RIGHT CELL')
[data_kinematic]=xlsread('Align_3 - Force and Kinematics for c3d.xlsx','Kinematic
Data','C4:AU4');
[data_force]=xlsread('Align_3 - Force and Kinematics for c3d.xlsx','Force
Data','B2:D11');

%import empty C3D file
% --> c3d = btkReadAcquisition('FILENAME.c3d');
c3d=btkReadAcquisition('Align_3-FF-Day_1-35-Test_3 - Reference - Empty.c3d');

%View data in C3D file%
marker_vals=btkGetMarkersValues(c3d);
force_vals=btkGetAnalogs(c3d);

%Set data to the C3D file
btkSetMarkersValues(c3d,data_kinematic);
btkSetAnalogsValues(c3d,data_force(1:10,:)); %(CHANGE VALUE TO NUMBER OF FORCE
STAGES in Data Force)

%Write data to C3D file
% --> btkWriteAcquisition(c3d, 'OUTPUT FILENAME.c3d');
btkWriteAcquisition(c3d, 'Align_3-FF-Day_1-35-Test_3 - Reference.c3d');
```